INFORMATION TO USERS

This manuscript has been reproduced from the microfilm master. UMI films the text directly from the original or copy submitted. Thus, some thesis and dissertation copies are in typewriter face, while others may be from any type of computer printer.

The quality of this reproduction is dependent upon the quality of the copy submitted. Broken or indistinct print, colored or poor quality illustrations and photographs, print bleedthrough, substandard margins, and improper alignment can adversely affect reproduction.

In the unlikely event that the author did not send UMI a complete manuscript and there are missing pages, these will be noted. Also, if unauthorized copyright material had to be removed, a note will indicate the deletion.

Oversize materials (e.g., maps, drawings, charts) are reproduced by sectioning the original, beginning at the upper left-hand corner and continuing from left to right in equal sections with small overlaps.

Photographs included in the original manuscript have been reproduced xerographically in this copy. Higher quality 6" x 9" black and white photographic prints are available for any photographs or illustrations appearing in this copy for an additional charge. Contact UMI directly to order.

ProQuest Information and Learning
300 North Zeeb Road, Ann Arbor, MI 48106-1346 USA
800-521-0600

Université d'Ottawa · University of Ottawa

AERODYNAMIC DAMPING IN LATERAL BUFFETING

by

Tashi Dwivedi

A thesis presented to the University of Ottawa
in partial fulfillment of the requirements for the degree of
Master of Applied Science
in
Civil Engineering
under the auspices of the
Ottawa-Carleton Institute for Civil Engineering

July, 2001

Department of Civil Engineering, University of Ottawa
Ottawa, Canada, 2001

Abstract

Using the balanced cantilever method of erection, the cable-stayed bridge during its critical construction phase resembles a long overhanging cantilever structure. This type of structure is particularly vulnerable to wind-induced buffeting instabilities because of its low natural frequencies and low overall stiffness.

In the past, the critical buffeting case for both vertical and horizontal excitation was assumed to occur when the wind was incident perpendicular to the bridge's axis. Recent observations in some cable-stayed bridges during construction revealing higher lateral responses at yaw angles other than perpendicular have triggered interest in the lateral vibration case.

Buffeting instabilities are affected mainly by the aerodynamic damping term. Experimental research for the vertical aerodynamic damping resulted in the cosine approximation. In the absence of available experimental data for lateral vibration, the cosine approximation is extended from the vertical case and assumed to be valid for the lateral aerodynamic term.

The experimental section of this thesis attempts to clarify the validity of the cosine approximation for the lateral aerodynamic damping case. Cantilever-type section models are triggered into vibration under various wind speeds and over a range of yaw angles, the aerodynamic damping is calculated, and the results are studied.

Acknowledgment

The author wishes to extend his deepest gratitude to his supervisor, Dr. H Tanaka, who through a perfect balance of guidance and freedom has allowed the author to complete this work.

As well, the author would like to thank the National Research Council for the use of their facilities during the experimental testing. In particular, Mike Savage is owed a special thanks because of his keen interest in the project and the technical expertise he provided throughout the testing phases.

The author would also like to thank his mother for greatly assisting in the editing stages, eventually resulting in the final copy to be produced.

Finally, the author would like to extend a special thanks to Sophie, who provided support, encouragement, and just the right amount of *push* throughout this entire period.

Table of Contents

Chapter 1
Introduction

1.1 The Cable-Stayed Bridge

From spanning shallow streams to stretching over vast and deep waterways, the bridge has always been a useful structure in our society. Whether for municipal, military, or recreational purposes, bridges have been built in a variety of configurations and using a wealth of different materials. As time passes, however, the strive is for bigger. Through the development of stronger and lighter building materials, coupled with a staggering increase in numerical computing power, the road has been paved for the rise of the long span bridge.

One particular type of long span bridge, the cable-stayed bridge, has become a common choice for the bridge designer. Aesthetically pleasing, as well as structurally sound, the cable-stayed bridge blends an equal mixture of form and function into a unique structure which can transform an ordinary sea channel into a picturesque landscape.

The interaction of the long span bridge with the natural wind has always been a subject of consideration and concern. Through the increase in span length, the wind engineer has been forced to better understand his/her technique and its application towards the creation of these longer spans. Overlooking such an integral portion is sure to lead to instabilities or even disaster.

Through to the present day, a vast amount of research has already been accomplished in the field of wind effects on long span bridges. From selecting a deck section which will remain stable in high winds, to predicting the bridge response during its construction stages, the theoretical and analytical development has been quite remarkable.

Much of the previous analysis of cable-stayed bridges have typically focused on winds incident normal to the bridge axis. Only recently have serious considerations been taken to understand the effects of the situation where the wind strikes the partially completed bridge at an angle other than normal (yawed; see Figure 1.1 for a description of yaw angle). Although in the wind tunnel phase, there have been some studies carried out to investigate the effects of the yawed case, the theoretical development has not been studied in detail. Even less common, has been the theoretical study regarding the effect of the yawed wind when the bridge is excited in a horizontal vibration mode.

1.2 Scope of Thesis

The scope of this thesis is to attempt to clarify the aerodynamic drag damping for horizontal vibration modes as it applies to cable-stayed bridges during construction phases. The first part of the thesis consists of a quite extensive review of buffeting theory combined with a review of the some of the parameters used to describe the incident wind. The buffeting theory begins with the original contributions by Davenport and leads into some of the more recent work dealing with the particular wind loading case pertinent to this thesis (i.e., the yawed wind case). As well, some wind tunnel test results from past bridge studies are discussed.

The second part of this thesis focuses on the wind tunnel experiments performed in order to measure aerodynamic drag damping of various bluff rectangular sections oscillating in smooth flow. A description of the experiment is followed by a discussion of the results with reference to their general applicability.

The final part of this thesis involves verifying the accuracy of the existing modified buffeting theory proposed by Kimura et al. (1998). Aerodynamic damping test data is used in order to calculate some typical responses of aerodynamically bluff sections in a *hypothetical* turbulent wind, and these results are compared with similar responses using the quasi-steady theoretical approach for calculating aerodynamic damping.

Chapter 2

Historical Development of Buffeting Analysis

2.1 Wind-Structure Interaction

The wind loading on a structure is indeed a complex problem with many interactive factors requiring consideration. The problem can be simplified through a basic understanding of the flow-structure interaction. When the wind hits an object, it pushes against that object, resulting in structural deflection. As most structures are sufficiently stiff to resist most of this pushing force, the flow is forced around the structure. The detailed flow field around any given structure is unique and will depend on the incident wind properties -- mean wind velocity, turbulent fluctuation intensities, etc.; the structural geometry -- width, length, location of railings, aerodynamic appendages, etc.; as well as the motion of the structure itself. The moving structure may cause the incident wind to further deflect and the flow field may be subsequently altered. It is important for the engineer to understand the types of forces which may be acting on a structure and their relative importance. Following is a brief outline of the forces which may be present as a structure interacts with the surrounding wind field.

(i) Vortex-Shedding Excitation:

When the flow passes over a structure, periodic vortices are shed downstream of the trailing edge. These alternating vortices, known from earlier aerodynamic theory as *von Karman* vortices, generate an alternating force on the structure in the cross-wind direction. For a bridge, these alternating vortices produce lift forces. As the mean wind speed of the flow is increased, the shedding frequency also increases. If the shedding frequency is well out of the range of any natural frequency of the structure, then the structure's response will not be influenced much by these types of forces. However, shedding frequencies within a certain range of a natural frequency may cause resonance effects which can lead to limited amplitude dynamic instabilities if the structural damping ratio for the resonant vibration mode is low. Suppressing vortex-induced vibrations can be accomplished at a relatively early stage of the

design often through section model testing. Vortex shedding frequencies of a deck section can be altered by changing the cross-sectional shape, adding railings or other appendages, or modifying the stiffness (although this last method tends to be more difficult).

(ii)Motion-Induced Forces:

Normally a long span bridge will be in a constant state of motion likely induced by surrounding winds or traffic loading. A deck in constant motion can be described at a particular instant by its velocity, relative deflection from its static zero position, and inertial properties due to the changing acceleration of the bridge as it oscillates in a particular vibration mode. When the deck is surrounded by moving air, the velocity, deflection, and inertia tend to change the local flow patterns around its cross-section. Changing the flow patterns will result in a change of pressure distributions around the bridge deck, which, for a given pressure distribution, will result in a net total force effectively acting at a certain point and in a certain direction. Depending on the magnitude and orientation of this force, further excitation of the bridge deck may be triggered. If this net force is acting in the same direction as the bridge motion, its effect will likely be to increase the amplitude of vibration. These motion-induced forces are commonly referred to as self-excited aerodynamic forces and can play a significant role in the stability, or lack thereof, of a particular bridge section under certain wind conditions. One of the formulations of self-excited forces acting on long span bridges was introduced by Sabzevari and Scanlan (1968). Today, it is considered important for engineers to examine the effects of self-excited forces when designing long span bridges.

(iii)Gust Buffeting:

An obstacle placed in the path of moving air is subjected to a force proportional both to the square of the relative speed at which the air is moving and to some linear dimension of the obstacle. For a non- fluctuating wind, this dynamic force is of constant value with respect to time and can be described by the following equation:

$$P = \frac{1}{2}\rho U_R^2 C_D B \tag{2.1}$$

where P is the dynamic force per unit width, ρ is the air density, U_R is the relative mean wind speed, C_D is the drag coefficient usually dependent on the overall shape (length, width, depth, support conditions) of the obstacle, and B is a linear dimension of the obstacle typically taken as the width or depth of the deck.

When the wind contains random fluctuations in its velocity, however, the dynamic force changes with time. These time-varying dynamic forces are known as buffeting forces and are always present in a natural wind, regardless of the bridge deck motion or the self-excited forces.

For any time-dependent force, if its time dependency is periodic, the corresponding response of a structure subjected to this force is also shown to be periodic. The dynamic pressure, a randomly fluctuating force, can be best described periodically through Fourier analysis as an infinite sum of various sinusoidal components. This Fourier analysis leads to a statistical approach to the problem of gust buffeting (the most common method employed today), that results in a statistical response to the incident wind.

2.2 Statistical Properties of the Incident Wind

Due to its random nature, the incident wind, for the purpose of buffeting calculations, is usually described in a statistical way. If a single point wind record is taken and averaged over an hour (common averaging time is usually anywhere from ten minutes to an hour), the average or mean wind speed can be described as

$$U = \frac{1}{T}\int_0^T U(t)\,dt \tag{2.2}$$

where $U(t)$ is the instantaneous wind velocity recorded at time t and T is the averaging time.

The mean square fluctuating component (or variance) of the wind velocity can then be calculated using the mean wind speed as follows:

$$\sigma_u^2 = \frac{1}{T}\int_0^T (U(t)-U)^2\,dt \tag{2.3}$$

The root-mean-square (RMS) or standard deviation is then the square-root of the variance:

$$\sigma_u = \sqrt{\sigma_u^2} \tag{2.4}$$

Another important parameter is the covariance. Covariance gives a measure of how two quantities are related to each other. For example, if two wind velocities recorded simultaneously over a length of time at two different points, both in the mean flow direction, are multiplied together at each time step, averaged, and divided by the product of the RMS velocity values of each of the components, the correlation will be obtained. The correlation is a normalized covariance obtained by dividing by the product of the RMS values of the two velocities (common definition). If this value is unity, the velocities are said to be perfectly correlated: i.e., *on average*, the two wind velocities are of the same magnitude and direction. If the coefficient is negative unity, the velocities are perfectly negatively correlated: on average they have the same magnitude but completely opposite directions with respect to their coordinate axes. A correlation of zero would indicate no correlation whatsoever, meaning that it would be impossible to predict the magnitude and direction of one velocity component knowing the values of the other. Two different types of covariance relationships

are important in our case:

1. Time correlation: wind velocities are recorded at the same point but at various different time lags. Mathematically, this can be described as follows:

$$R_{ij}(\tau)=\overline{u_i(t)u_j(t+\tau)} \tag{2.5}$$

where u is the instantaneous velocity and the overbar denotes the average of many different points. The *temporal* (time dependent) correlation coefficient is then calculated using

$$\rho_{ij}(\tau)=\frac{R_{ij}(\tau)}{\sigma_i\sigma_j} \tag{2.6}$$

When $i=j$, the correlation function is called the autocorrelation. When $i\neq j$, the function is called the cross-correlation.

2. Spatial correlation: Wind velocities are recorded at the same time, but separated by a distance r at two different points in space. This can be described as follows:

$$R_{ij}(r)=\overline{u_i(x)u_j(x+r)} \tag{2.7}$$

The *spatial* correlation coefficient is then

$$\rho_{ij}(r)=\frac{R_{ij}(r)}{\sigma_i\sigma_j} \tag{2.8}$$

The turbulence intensity, I_i, is another useful parameter related to the random wind. The intensity is a measure of how violent or gusty the turbulent wind is. It is best described as

$$I_i=\frac{\sigma_i}{U} \tag{2.9}$$

where the subscript i denotes a coordinate direction. Thus there are three turbulence intensities related to wind: I_u, I_v and I_w (representing the x, y, and z directions respectively). The flow is often considered to be smooth when the turbulent intensities are in the order of 1%, whereas in extremely windy conditions, the intensities are not likely to exceed about 25%.

A turbulent wind can be thought of as a combination of a number of turbulent eddies of different sizes. An approximate measure of the eddy size is usually taken roughly as the diameter. Each eddy, by its swirling nature, contributes to the dynamic force acting on an object in its path. If the flow were purely smooth, the eddies would be extremely large in diameter, corresponding to large-scale pressure systems and seasonal variations. As the flow becomes more and more turbulent (I_i increasing), eddies of a broader size range would appear. If all the eddy sizes in a one-hour sample of the velocity are averaged, the integral scales of turbulence are obtained. Mathematically, these integral scales can be obtained from the spatial correlation functions by integrating them over the entire field of separation distances:

$$L_i^j = \int_0^\infty \rho_{ii}(r_j)\,dr_j \tag{2.10}$$

In this definition, i refers to the wind direction and j refers to the coordinate direction of the separation distance. In all, there are nine different integral length scales corresponding to the three different wind directions and the three different spatial separations.

An ideal tool suitable in completing the statistical description of the turbulent wind is the energy spectrum. The energy spectrum is a measure of how much energy there is in the total flow at specific frequency ranges. The relative energy is associated with the amplitude of its cosine function, thus, if a random wind signal has a large amount of energy associated with a frequency of, say, 5 *Hz*, a plot of the energy versus frequency spectrum would reveal a peak at 5 *Hz*. If, however, a wind signal has relatively comparable amounts of energy at numerous different frequencies, there may not be a dominant peak at all.

The energy spectrum of the wind field can be described by taking the Fourier transform of the time correlation. The autospectrum is the Fourier transform of the autocorrelation function as follows:

$$S_i(n) = 2\int_{-\infty}^{\infty} R_{ii}(\tau)\mathrm{e}^{-in\tau}\,d\tau \tag{2.11}$$

Since it is known that the autocorrelation functions are even, the autospectrum can be simplified as follows:

$$S_i(n) = 4\int_0^\infty R_{ii}(\tau)\cos(n\tau)d\tau \tag{2.12}$$

There are a few important autospectrum functions which are in wide use today. As a design tool, the autospectrum of the wind velocity would be measured, plotted, and then fitted with the *best fit* spectral equation. Some of the common autospectra for atmospheric boundary layer turbulence are as follows:

(i) von Karman Spectra (see for example, Irwin [1977]):

$$S_u(n) = \frac{4\sigma_u^2 \frac{L_u^x}{U}}{\left[1+70.78\left(\frac{nL_u^x}{U}\right)^2\right]^2} \tag{2.13}$$

for the along-wind horizontal component, and

$$S_w(n) = \frac{2\sigma_w^2 L_w^x}{U} \frac{\left[1+188.8\left(n\frac{L_w^x}{U}\right)^2\right]}{\left[1+70.78\left(n\frac{L_w^x}{U}\right)^2\right]^{11/6}} \tag{2.14}$$

for the cross-wind vertical component. The von Karman forms were obtained theoretically on the basis of homogeneous isotropic turbulence. Spectral expressions can also be obtained by fitting wind data from full-scale measurements:

(ii)Kaimal Spectra (see for example, Huang [1995]):

$$S_u(n) = \frac{\sigma_u^2}{n} \frac{22f}{(1+33f)^{5/3}} \tag{2.15}$$

for the along-wind component, where $f = \frac{nZ}{U}$ is a reduced frequency variable dependent on height above ground Z.

$$S_w(n) = \frac{\sigma_w^2}{n} \frac{1.3f}{(1 + 5.3f)^{5/3}} \tag{2.16}$$

for the cross-wind component.

There are other fits for the autospectrum, and their forms may be employed, depending on the field data obtained. In some cases, in the absence of field data, one of the above forms may be assumed.

Typically, the spectrum of the transverse (along-span) component is neglected. As will be seen later, in the buffeting formulations resulting from the *strip* assumption, it is common practice to ignore the effects of this spanwise component of turbulence. For the case of a partially erected bridge deck under yawed wind, however, this spanwise flow may in fact significantly contribute to the buffeting response and should be accounted for.

Because a bridge structure tends to be long and slender, the engineer is also interested in the spatial distribution of turbulence. As a design aid, single point autospectra do not provide enough information for the bridge engineer because the vibration modes of a bridge vary along the span. What is of more interest is how the wind field correlates at a particular frequency at various points along the span. This will ultimately determine the effectiveness of the wind in exciting the bridge structure in its various natural frequencies. This concept was first introduced by Davenport (1962a) in his joint acceptance function.

A general expression for the cross-spectrum of two velocity components can be obtained by taking the Fourier transform of their general (time lag and spatial difference) cross-covariance function:

$$S_{ij}(n, r) = 2 \int_{-\infty}^{\infty} \overline{u_i(x,t) u_j(x+r, t+\tau)} e^{-i n \tau} d\tau \tag{2.17}$$

Generally, because the cross-covariance of a random turbulent field is not an even function, the cross- spectral expression will have both real and imaginary components. For long span bridges, cross-spectral expressions are used taking r in the y direction. It is quite common to

assume atmospheric boundary layer turbulence as isotropic to locally simplify cross-spectra obtained from 2.17. This results in the imaginary components of the cross-spectra S_w being reduced to zero and the cross-velocity expressions S_{uv}, S_{uw}, S_{vu}, S_{vw}, S_{wu}, S_{wv} vanishing. For actual boundary layer conditions, the cross-velocity expressions are usually small compared to the cross-spectra and can be ignored, although, if desired, expressions can be fitted from recorded field data.

In isotropic conditions, any cross-spectrum can be represented by its one-point autospectrum at a reference point multiplied by a term denoted as the root-coherence (also termed the cross-correlation of velocity fluctuations). For cross-spectra in the y separation direction, the following expressions are obtained:

$$S_{ij}(n) = S_i(n) R_{ij}(y,y';n) \quad for\ i=j \tag{2.18}$$

$$S_{ij}(n) = \sqrt{S_i(n) S_j(n)}\, R_{ij}(y,y';n) \quad for\ i \neq j \tag{2.19}$$

where the expression $R_{ij}(y,y';n)$ represents the cross-correlation, at frequency n of i and j velocity components at spanwise points y and y'.

Davenport (1961a) first suggested an exponential-type function for the spanwise cross-correlation of two parallel velocity components as

$$R_{ii}(y,y',n) = \mathrm{e}^{-c\frac{n\Delta y}{U}} \tag{2.20}$$

where $\Delta y = |y-y'|$, and the empirical constant c will take on different values depending on the direction i (for $i=u$, $c\simeq 7$). Irwin (1977) later pointed out that this function, although a good approximation, represented the case of a turbulence field with an infinite along-wind integral scale, which is not very realistic. Based on previous experimental tests, Roberts and Surry (1973) derived more theoretical spanwise cross-correlation functions for the u and w directions as follows:

$$R_{uu}(y,y',n) = \frac{2^{1/6}}{\Gamma(5/6)}\left(\eta^{5/6} K_{5/6}(\eta) - \frac{\eta^{11/6}}{2} K_{1/6}(\eta)\right) \tag{2.21}$$

where

$$\eta = \frac{\Delta y}{2L_u^y} 0.747 \sqrt{1 + 70.8\left(\frac{n2L_u^y}{U}\right)^2}$$

For the w direction:

$$R_{ww}(y,y',n) = \frac{2^{1/6}}{\Gamma(5/6)}\left(\eta^{5/6}K_{5/6}(\eta) - \frac{\eta^{11/6}K_{1/6}(\eta)}{1+\frac{8}{3}\left(\frac{2\pi}{B_1}\right)^2\left(\frac{nL_w^y}{U}\right)^2}\right) \tag{2.22}$$

where $\eta = \frac{\Delta y}{2L_w^y} 0.747 \sqrt{1 + 70.8\left(\frac{n2L_w^y}{U}\right)^2}$

For 2.21 and 2.22, $\Gamma(z)$ is the Gamma function. Also, $K_{5/6}(z)$ and $K_{1/6}(z)$ are the modified Bessel functions of the second kind of non-integer order 5/6 and 1/6, respectively.

Expressions for the spanwise cross-correlation $R_{uu}(y,y';n)$ are not readily available but, if required, can be measured either in the field or in the wind tunnel and fitted with appropriate expressions.

The necessary statistical parameters for the wind are usually obtained from meteorological records or, where records are not readily available, from site measurements. When these parameters are known, the focus then shifts to the susceptibility of the structure itself to these winds.

2.3 Historical Development of Buffeting Analysis

Early airfoil theory provided methods for predicting wind loads, motion induced loads, and subsequent responses of airfoils encountered under various flight conditions (see, for example, Milne-Thomson [1952] and Bisplinhoff et al. [1955]). Statistical concepts and buffeting analysis was merged with the aerodynamic field in detail by Liepmann (1952). In terms of civil engineering structures, theoretical development on the response of systems to random dynamic loads, in particular the application of Fourier transforms and the frequency domain approach, can be traced back to Eringen (1957), and Davenport (1961b). Davenport was the first to apply statistics to the response of civil engineering structures subjected to turbulent wind loads. His detailed theoretical analysis of turbulence buffeting on slender structures covered all aspects from the nature of the incident wind to the movements of the structure in various modes under the action of these winds. Davenport's original theory is still in widespread use and is periodically extended through ongoing research which continues to broaden its range of applicability.

The following sections detail the major contributions in the development of a theoretical framework for predicting the buffeting response of cable-stayed bridges during construction phases when subjected to turbulent winds at various yaw angles. The review commences with the original theory proposed by Davenport.

2.3.1 Davenport's Quasi-Steady Drag Response for Line-Like Structures

As a first step, Davenport (1961a) analyzed a large amount of wind climate data from which he derived statistical parameters in the form of a horizontal gust spectra as a function of the height above ground and a coherence expression as a function of the vertical separation distance.

Applying the statistical parameters of the incident wind to the response of a single-degree-of-freedom (SDOF) system, Davenport (1961b) showed that the structural response would take the same general form as the input wind -- i.e., that of a fluctuating component linearly imposed on a mean component that can be calculated by static stiffness methods. The fluctuating component, characterized through an energy versus frequency, or response spectrum relation, is multiplied by two magnification factors: the mechanical admittance and the aerodynamic admittance. Both functions are frequency dependent and describe the response magnitude to an input of unit magnitude at a particular frequency.

The mechanical admittance describes the structure's dynamic response at a particular frequency when subjected to an input force of unit magnitude with the same frequency. The equation is as follows:

$$|H_f(n)|^2 = \frac{1}{\left[\left(1-(n/n_0)^2\right)^2 + (2\xi_t)^2(n/n_0)^2\right]} \tag{2.23}$$

where n_o is the natural frequency of the structure and ξ_t is the total damping, expressed as the sum of the structural and aerodynamic damping, $\xi_t = \xi_{st} + \xi_{aero}$.

The aerodynamic admittance function relates the fluctuating wind velocity power spectrum to the corresponding fluctuating aerodynamic force power spectrum. The function gives the amplitude of the aerodynamic force at a certain frequency generated by a unit amplitude velocity signal at that same frequency. For an SDOF system, the aerodynamic admittance for drag deflections at a particular reduced frequency ζ (here $\zeta = nD/U$) can be taken as the

ratio of the drag coefficient at ζ to the drag coefficient for $\zeta=0$.

The mean component, X, of the response is equal to P/K. Here K is the stiffness and P is the mean force corresponding to the mean wind from Equation 2.1.

The most convenient way to characterize the response spectrum is by calculating the overall variance. Integrating the response spectrum over the entire frequency range gives the variance

$$\sigma^2(x) = \left(\frac{\rho U^2 C_D}{2K}\right)^2 \int_0^\infty |\chi_a|^2 |H_j|^2 \frac{S_x(n)}{U^2} dn \tag{2.24}$$

where $S_x(n)$ is the wind velocity spectrum.

Following the analysis of the SDOF system, Davenport (1962a) extended the analysis to include the case of slender line-like structures, in particular long span bridges. Unlike the SDOF system, the multiple- degree-of-freedom (MDOF) system has a spatially separated area and more than one vibration mode. Some attention must therefore be directed to the spatial properties of the incident wind, the corresponding dynamic loading, and their effects in exciting vibration of this type of structure under its various modes.
Davenport gives the overall static deflection, X, of the structure as $\sum (P_r/K_r)\mu_r(y)$.
Here $P_r = 1/N_r \int_0^l P(y)\mu_r(y)dy$, $K_r = 1/N_r \int_0^l K(y)\mu_r(y)dy$, $N_r = \int_0^l \mu_r^2(y)dy$, and
$\mu_r(y)$
is the normalized mode shape of the r^{th} vibration mode. P_r, K_r, and N_r are generalized modal quantities for the r^{th} mode with the summation taken over all the applicable mode shapes.

The autospectrum of the dynamic load is expressed as

$$S_{P_r}(n) = \frac{1}{N_r^2} \int_0^l \int_0^l S_p(y,y';n)\mu_r(y)\mu_r(y')\,dy\,dy' \tag{2.25}$$

where $S_p(y,y';n)$ is the cross-spectrum of the loads at spanwise positions y and y' at frequency n.

Equation 2.25 incorporates the cross dependance of the spanwise mode shape and the fluctuating pressure. Assuming the spatial coherence of the dynamic force takes the same form as the coherence of the wind velocity, the cross-spectrum of dynamic loading can be expressed as the product of the spatial pressure coherence and the autospectrum of pressure at an arbitrary reference point:

$$S_p(y,y';n) = S_p(n)R(y,y';n) \tag{2.26}$$

Replacing 2.26 in 2.25, Davenport defines the *joint acceptance* factor:

$$|J_r(n)|^2 = \frac{1}{N_r^2} \int_0^l \int_0^l R(y,y';n)\mu(y)\mu(y')\,dy\,dy' \tag{2.27}$$

The joint acceptance factor demonstrates the interaction between the spatial correlation of pressure along the span and the mode shape along the span, all in terms of the r^{th} mode. The response spectrum for the r^{th} mode can be obtained as follows:

$$S_{X_r}(n) = \frac{1}{K_r^2}|H_{f_r}(n)|^2|J_r(n)|^2 S_P(n) \tag{2.28}$$

The r^{th} mode variance will then be equal to $\int_0^\infty S_{X_r}(n)\,dn$ and the overall variance of the structural deflection at position y from all mode contributions, $\sigma_x^2(y)$, is given as $\sum \sigma_{x_r}^2 \mu_r^2(y)$.

When it is known how to obtain the response quantities for the structural system, attention is shifted to the the loading spectrum $S_p(n)$. Through the use of the aerodynamic admittance function, this spectrum is generated from the fluctuating velocity components as they strike the structure. To simplify this process, Davenport made the following assumptions regarding the nature of the wind loading:

1. The wind pressure on a section or strip of the slender structure is due only to the incident wind velocity on that section and is not affected by the spanwise flow of wind velocities or pressures from other adjacent sections. This assumption is commonly referred to as the *strip assumption* and it allows the analysis of the pressures to be restricted to a strip of unit width in the spanwise direction. Once the forces on this strip are calculated, integration over the entire span length results in the total force across the span.
2. The magnitude of the wind gusts is small compared to the mean wind value. This allows the dynamic gust-induced forces to be expressed as linear functions of the gust velocities, providing a simplified approach in obtaining the gust loading spectrum from the incident wind spectrum. The assumption is valid for most boundary layer wind conditions because, most often, the turbulence intensities of the wind compose only a small fraction of the mean wind.
3. The important gust wavelengths, U/n, of the velocity fluctuations in the oncoming wind are much greater than the cross sectional dimensions of the bridge deck. This is referred to as the *quasi-steady* assumption. Here, the engineer is concerned only with the significant, or energy containing waves in the oncoming flow. In a turbulent flow there is a full range of wavelengths, but the smaller wavelengths which do not contain sufficient energy to excite the structure, will not have a very great correlation over the cross-section of the deck. The quasi-steady assumption then assumes that the energy-containing waves in the flow are fully correlated around the bridge deck. This results in an assumed steady flow hitting the deck and allows the use of the steady-state force coefficients $C_D(0)$ rather than $C_D(\xi)$.

For a typical long-span bridge, the width or depth of the deck is, in fact, usually of the same order as the effective gust wavelengths of the oncoming flow. This leads to a case where the pressure is not fully correlated over the width of the bridge deck, an assumption inherent in the quasi-steady theory. The aerodynamic admittance function also corrects for this discrepancy. From the above discussions concerning the aerodynamic admittance function, it can be seen that this single function serves the following purpose: It is applied in order to convert the velocity fluctuations into corresponding pressure fluctuations on a section of the structure. It accomplishes this by compensating for the errors introduced by the use of the steady-state force coefficients. The admittance function also accounts for the fact that the pressure generated by the velocity fluctuations must occur on an area of finite size and does not simply occur at a single point on the structure. If the latter were true, the correlation would be unity. In actuality, the former is the case and so the velocity correlation must be less than unity over this area, and hence the pressure distribution.

Using the assumptions described above, the time-varying drag force on a strip will be as follows:

$$P(t) = \overline{P} + 2\overline{P}[\chi_1(n)]\frac{u}{U}\sin(2\pi n t + \Theta_1) \tag{2.29}$$

The autospectrum of this drag force is given by:

$$S_P(n) = 4\overline{P}^2|\chi_1(n)|^2\frac{S_u(n)}{U^2} \tag{2.30}$$

where $S_u(n)$ is the autospectrum of the horizontal along-wind velocity fluctuations. Notice here the appropriate introduction of the aerodynamic admittance function. Now the expression for $S_P(n)$ can be substituted into the expression for $S_{x'}(n)$ in 2.28 and the response can be obtained.

A typical long span suspension bridge will have well separated mode shapes and low overall damping ratios. The response spectrum for this type of structure generally exhibits a sharp peak located at $n=n_r$ containing most of the energy. By considering only this narrow banded portion, an accurate estimation of the true response can be given as

$$\sigma_x^2 = \frac{\pi^2 n_r}{2\xi_t} S_{x'}(n_r) \tag{2.31}$$

The aerodynamic damping for a multiple-degree-of-freedom system vibrating in a steady wind was derived theoretically by Davenport (1962a). Using the concept of conservation of energy, Davenport produced the following expression:

$$\xi_{aero} = \frac{1}{2\pi n_r} \left[\frac{\int_0^L \frac{\frac{1}{2}\rho \overline{U}_y^2 B C_D(y)}{\overline{U}_y} \mu_r^2(y)\,dy}{\int_0^L m\,\mu_r^2(y)\,dy} \right] \tag{2.32}$$

The mean wind speed $\overline{U}$ and drag coefficient C_D are shown as functions of y. By using the strip assumption, the spanwise dependance of both terms disappears, removing them from the integrand. If m is also constant along y, the expression reduces to the quasi-steady aerodynamic drag damping expression:

$$\xi_{aero} = \frac{\rho U D C_D}{4\pi n_r m} \tag{2.33}$$

This expression shows that the aerodynamic damping is linearly proportional to the mean wind speed and is taken to be valid in both smooth flow and turbulent flow conditions.

Davenport (1962b) also derived a general expression for aerodynamic admittance for drag response of a typical bridge section as a function of the reduced frequency $\zeta = nD/U$:

$$C(\zeta) = \frac{2}{(7\zeta)^2}\left(7\zeta - 1 + e^{-7\zeta}\right) \tag{2.34}$$

The expression is obtained by spatially integrating the velocity correlations around the cross-section.

The following comments can be made on the above theory:

1. The wind velocity spectra and spatial coherence functions used are taken from the results of field measurements. The exponential form of the coherence function, however, does not accurately model the situation when n is close to zero.
2. The quasi-steady drag damping resulting from the strip assumption assumes both the mean wind speed and the drag coefficient are constant over the span. Although the mean wind speed will likely be constant over the span, the drag coefficient may vary, depending on the particular structure.
2. The case of a yawed angle incident wind is not incorporated in the analysis. For a completed bridge structure, the maximum response likely occurs when the wind is perpendicular to the axis of the bridge, decreasing with an increase in yaw angle. However, the same result may not always be the case for cable-stayed bridges during construction phases.

2.3.2 Irwin's Lateral Buffeting of the Lion's Gate Bridge

In evaluating the response of the Lion's Gate bridge to turbulent wind, Irwin (1977) made some modifications to Davenport's original buffeting theory. Irwin incorporated the same step-by-step process but introduced some modified expressions.

The von Karman expressions for the along-wind and vertical gust components as well as modified expressions for the lateral coherence functions (see section 2.2) are used to describe the incident wind. In the analysis of the dynamic wind forces, the quasi-steady and strip assumptions are used as well, justifying the use of the steady state force coefficients and the neglect of any spanwise flow effects.

The buffeting response of the bridge in lateral vibration for the r^{th} sway mode, in terms of the variance of the generalized time coordinate, $\sigma^2(q_r)$, is given in simplified form:

$$\sigma^2(q_r) = \left(\frac{\rho U B C_D}{4\pi^2 n_r^2 m \sqrt{L}}\right)^2 \int_0^\infty |\chi_a(n)|^2 |H_f(n)|^2 S_u(n) C_{IUU}(n)\, dn \qquad (2.35)$$

C_D is the steady flow drag force coefficient taken on an area projected normal to the mean flow direction. It is assumed that the coefficient is not significantly changed for small variations in vertical angle of attack: i.e., $dC_D/d\alpha$ is close to zero.

$|H_f(n)|^2$ is the mechanical admittance given in 2.23 with the aerodynamic damping term given in 2.33 but using B instead of the depth D.

$|\chi_a(n)|^2$ is the aerodynamic admittance function. Irwin points out that Davenport's admittance expression 2.34 assumes an infinite longitudinal integral scale, L_u^x. Accounting for the finite value of the integral scale by using the von Karman correlation 2.21 and integrating this correlation spatially around the bridge section yields:

$$|\chi_a(n)|^2 = \frac{4}{(\eta_1\eta_3)^2}(\eta_1 - 1 + e^{-\eta_1})(\eta_3 - 1 + e^{-\eta_3}) \qquad (2.36)$$

This function more accurately models the lower frequency range, while at higher n, the 2.36 above is similar to 2.34.

Here $\eta_1 = 0.95\frac{b}{L_u^x}\left(1 + 70.78\left(\frac{nL_u^x}{U}\right)^2\right)^{1/2}$ and $\eta_3 = 0.95\frac{b}{2L_u^y}\left(1 + 70.78\left(\frac{2nL_u^y}{U}\right)^2\right)^{1/2}$.

Only a single integration is performed in order to calculate $\sigma^2(q_r)$. For lower vibration modes, the mode shape will likely be relatively constant over the spanwise distance where the wind velocity has significant correlation. Therefore, joint acceptance equations appearing in the form of

$S_u(n)\int_0^L\int_0^L R_{uu}(y,y',n)\mu_r(y)\mu_r(y')dydy'$ can be closely represented as

$2L\int_0^\infty S_{uu}(\Delta y, n)d\Delta y$, where $\Delta y = |y - y'|$ is the separation distance between two spanwise points.

This single integration can be further reduced as $S_u(n)C_{IUU}(n)$ where

$$C_{IUU}(n) = \frac{1.887 L_u^y}{\left(1+70.78\left(\frac{nL_u^y}{U}\right)^2\right)^{1/2}}.$$

If the response spectrum is narrow banded, 2.35 becomes:

$$\sigma^2(q_r) = \left(\frac{\rho U B C_D}{4\pi^2 n_r^2 m\sqrt{L}}\right)^2 S_u(n_r) C_{IUU}(n_r)\left[\frac{n_r \pi}{4(\xi_{st}+\xi_{aero})_r}\right] \tag{2.37}$$

The following comments can be made on the above theory:

1. By using 2.21, the coherence is better represented when n approaches zero. This is an improvement from the exponential form derived by Davenport, although this von Karman form leads to a more complicated integral to evaluate.
2. Again by the strip assumption, the drag coefficient is taken as constant over the span length, leading to inaccuracy when this coefficient varies along the bride length.
3. Using the similar assumption that increasing the yaw angle will decrease the overall response, predictions for changes is the yaw angle are not accounted for.

2.3.3 Xie et al.'s Attempts to Evaluate Buffeting with Yaw Winds

The first theoretical attempt at including the possible directional changes in the incident wind was undertaken by Xie et al. (1989, 1991). As a first step to approaching the problem, it was desired to convert all wind statistics from the wind axis (XY') to the bridge axis (XY) -- a conversion based on the assumption that only the components of the yawed wind oriented perpendicular to the bridge axis would be effective in exciting the structure.

The effective mean wind speed U is taken as $U'\cos(\beta)$ and the along-wind auto-spectrum, $S_u(n)$, is taken equal to $S'_u(n)\cos^2(\beta)+S'_v(n)\sin^2(\beta)$. In the absence of available data, the lateral spectrum $S_{v'}(n)$ is assumed to take the same von Karman form as $S_w(n)$ (2.14), replacing L^x_w with $L^{x'}_{v'}$, and σ^2_w with $\sigma^2_{v'}$.

The along-wind cross-spectrum $S_{uu}(y_1,y_2;n)$ is expressed in terms of auto-spectra and coherence:

$$S_{uu}(y_1, y_2, n) = R_{u'u'}(y_1, y_2; n)S_{u'}(n)\cos^2(\beta) + R_{v'v'}(y_1, y_2; n)S_{v'}(n)\sin^2(\beta) \qquad (2.38)$$

The along-wind coherence $R_{u'u'}$ is taken in von Karman form (2.21) and $R_{v'v'}$ is taken equal to the vertical coherence (2.22). In these expressions, the effective wind speed U is used. As well, the bridge axis length scales L^y_u and L^y_v are used. These scales are found by introducing the *ellipse model* which allows the calculation of bridge axis length scales from wind axis length scales for any yaw angle β. The model accounts for the fact that an along-wind scale (i.e., L^x_u) would be greater than a cross-wind scale (i.e., L^y_u). Using the model, a wind axis length scale is calculated, plotted, and then rotated through the yaw angle β to obtain the related bridge axis scale. Through rotation, the length scale is scaled according to the ellipse regularity. This leads to the following equations for the along-wind and lateral bridge axis length scales:

$$L^y_u = L^{y'}_{u'}\sqrt{\left(1+\tan^2(\beta)\right) / \left(1+(L^{y'}_{u'}/L^{x'}_{v'})^2\tan^2\beta\right)} \qquad (2.39)$$

$$L^y_v = L^{y'}_{v'}\sqrt{\left(1+\tan^2(\beta)\right) / \left(1+(L^{y'}_{v'}/L^{x'}_{v'})^2\tan^2\beta\right)} \qquad (2.40)$$

These two equations would be substituted appropriately in the expressions for $R_{u'u'}$ and $R_{v'v'}$.

With the modified form 2.38, the drag response for a yawed wind can be investigated. In terms of the bridge axis, the variance of the lateral response for the r^{th} mode generalized coordinate is obtained by integrating the response spectrum of the r^{th} mode:

$$\sigma_r^2 = \frac{1}{\left(M_r 4\pi^2 n_r^2\right)^2} \int_0^\infty |H_f(n)|^2 S_{P_r} dn \tag{2.41}$$

where M_r is the generalized mass obtained as $\int_0^L m(y)\mu_r^2(y)dy$; $|H_f(n)|^2$ is the mechanical admittance function (2.23); and S_{P_r} is the generalized drag force in the r^{th} mode due to the fluctuating wind velocity components. The generalized force is expressed as the joint effect of the spatially distributed load and the r^{th} mode shape:

$$S_{P_r}(n) = \int_0^L \int_0^L S_P(y_1, y_2; n)\mu_r(y_1)\mu_r(y_2)dy_1 dy_2 \tag{2.42}$$

In the expression, $S_P(y_1, y_2; n)$ can be expressed in terms of the cross-spectrum of the fluctuating wind velocity as

$$S_P(y_1, y_2; n) = \left(\frac{\rho U B}{2}\right)^2 |\chi_D(n)|^2 \left(\frac{2C_D}{U}\right)^2 S_{uu}(y_1, y_2; n) \tag{2.43}$$

where C_D is the steady state drag coefficient for a perpendicular incident wind. It is now required to express all the bridge axis properties in terms of the known wind axis properties. For the aerodynamic admittance, Xie et al. use an experimental technique to more accurately identify the shape of the function.

Other expressions can be used, but, regardless, 2.43 will become

$$S_P(y_1, y_2, n) = \left(\rho B U' \cos(\beta) C_D\right)^2 |\chi_D|^2 \left[R_{u'u'} S_{u'}(n)\cos^2(\beta) + R_{v'v'} S_{v'}(n)\sin^2(\beta)\right] \tag{2.44}$$

The generalized force for the rth mode then becomes:

$$\begin{aligned} S_{P_r} = \left(\rho B U' \cos(\beta) C_D\right)^2 |\chi_D|^2 \, [\, & S_{u'} \cos^2(\beta) \int_0^L \int_0^L R_{u'u'} \mu_r(y_1)\mu_r(y_2) dy_1 dy_2 \\ & + S_{v'} \sin^2(\beta) \int_0^L \int_0^L R_{v'v'} \mu_r(y_1)\mu_r(y_2) dy_1 dy_2 \,] \end{aligned} \tag{2.45}$$

Assuming a constant mode shape over the region of significant velocity correlation results in integrals in the form of $1/L\int_0^L\int_0^L R_{u_1u_2}dy_1dy_2 = J_u$ and $1/L\int_0^L\int_0^L R_{v_1v_2}dy_1dy_2 = J_v$. Using the von Karman coherence and standard integral tables, these two expressions can be solved for given length scales (1989).

Combining all the necessary terms, the variance for the r^{th} generalized coordinate can be expressed as

$$\sigma_r^2 = \left(\frac{\rho B U' \cos(\beta) C_D}{M_r}\right)^2 \int_0^\infty |\chi_D|^2 |H_f(n)|^2 \left(S_{u_1}(n)\cos^2(\beta)J_u + S_{v_1}(n)\sin^2(\beta)J_v\right)dn \quad (2.46)$$

For the case of narrow band response, the variance becomes

$$\sigma_r^2 = \left(\frac{\rho B U' \cos(\beta) C_D \pi}{2M_r n_r (\xi_{st}+\xi_{aero})_r}\right)^2 |\chi_D(n_r)|^2 \left(S_{u_1}(n_r)\cos^2(\beta)J_u + S_{v_1}(n_r)\sin^2(\beta)J_v\right) \quad (2.47)$$

The following comments can be given the above analysis:

1. The aerodynamic damping term is obtained from quasi-steady analysis with the perpendicular wind speed, U'cosβ, taken as the effective velocity component acting on the bridge.
2. The response will not predict the case where the drag coefficient may vary along the length. Also, Xie et al. point out that this analysis will only be valid for models with supported ends, a case where the drag coefficient will likely remain constant along the span.
3. This model is only valid for a limited range of yaw angles. As the yaw angle increases, the spanwise flow component may become important and should be considered.

2.3.4 Kimura's Aerodynamic Damping under Yawed Winds

Kimura (1991) followed Xie's derivation in an attempt to explain the buffeting response of a structure that had an unsupported end and, in particular, the possible formation of additional lift forces. Although the present topic is drag buffeting, Kimura's modified buffeting analysis serves as a useful introduction.

The experimental phase of the project involved studying the vertical buffeting response of flat plate cantilever models subjected to various yawed wind conditions. Kimura found that using a simplified *cosine* rule approximation, which involved using $U'\cos\beta$ as the effective wind speed while using the original wind axis length scales, tended to underestimate the observed response. He also found that for flat plate-like sections under vertical vibration, the proportionality $\xi_{aero}(\beta) = \xi_{aero}(0)\cos(\beta)$ held up quite well. It was noted that for bluff-type sections, however, the aerodynamic damping tendencies were quite complex and might not be best described using this cosine proportionality. The change of aerodynamic damping with wind speed showed linear variation for most flat plate sections, a finding which is in accordance with theoretical predictions based on the quasi-steady assumption.

The analytical study involved modifying the original buffeting theory to allow a prediction for the case of a yawed wind. To simplify the problem, Kimura identified two leading-edge cases: the spanwise edge and the endwise edge. The spanwise edge applied for yaw angles around β=0°; this case was termed the *cosine case*. The endwise leading edge applied for β close to 90°; this case was termed the *sine case*. For each case, the vertical buffeting forces were derived for an along-wind strip. The differences between the sine and cosine cases for the strip forces are as follows:

1. For the cosine case, the vertical deflection of the strip is the same along its length. As well, $dC_{LC}/d\alpha$ is taken to be the same along the entire length of the strip, an assumption which is justified because of the unchanging vertical deflection. From early airfoil theory (see for example Milne-Thomson [1952]), the total lift force was assumed to act at the quarter

chord point from the leading edge.

2. For the sine case, the vertical deflection inside a strip is of the same form as the r^{th} mode shape. This results in $dC_{LS}/d\alpha$ changing continuously along the strip. A previously defined variation (McCormick [1979]) was assumed to apply in this case.

The dependance of the lift coefficient slope on the aspect ratio (defined as the ratio of length to width, *L/B* for the cosine case and *B/L* for the sine case) was accounted for by modifying the lift coefficient slope value from its infinite aspect ratio value. Force coefficients are normally obtained from section model tests which represent sections of infinite aspect ratios. The modification accounts for the fact that for a finite length plate, some additional lift forces are generated by vortex action created as the flow passes over the end(s) of the plate.

When the buffeting force on the strip was known, the generalized strip buffeting force for the r^{th} vibration mode could then be obtained by multiplying the r^{th} mode shape by the buffeting force. For the cosine case, the generalized strip force at spanwise position y'' is given by the following expression:

$$dF_{ZC}(y'',t) = \frac{1}{2}\rho U' \cos(\beta) w(y'',t) dy'' \int_0^B \frac{dC_{LC}(x)}{d\alpha} \mu_r(y'') dx \qquad (2.48)$$

Here, $w(y'',t)$ is the fluctuating vertical component of velocity at spanwise position y'', $\mu_r(y'')$ is the value of the r^{th} mode shape at y^*, and dy'' is the strip width at y''. The mode shape and lift coefficient slope are both constant along dx, so the corresponding expressions can be removed from the integrand.

The expression for the generalized strip force at endwise position x'' for the sine case is as follows:

$$dF_{ZS}(x'',t) = \frac{1}{2}\rho U' \sin(\beta) w(x'',t) dx'' \int_0^L \frac{dC_{LS}(y)}{d\alpha} \mu_r(y) dy \qquad (2.49)$$

The integration is required in this expression because the deflection and the lift coefficient slope both vary along the length of the strip. Here dx'' is the strip width at endwise position x'', and $w(x'',t)$ is the fluctuating wind component at x''.

With these generalized strip forces, the spectrum of the overall generalized buffeting forces can be obtained. The procedure is similar to the case of drag buffeting, and for the cosine case results in

$$S_{ZC}(n) = \left(\frac{1}{2}\rho U' \cos(\beta) B \frac{dC_{LC}}{d\alpha}\right)^2 \int_e^{L+e}\int_e^{L+e} S_{ww}(y_1, y_2, n)\mu_r(y_1)\mu_r(y_2)dy_1 dy_2 \qquad (2.50)$$

To simplify the calculation, Kimura rotates the model boundaries as a parallelogram with the yaw angle so that sides of the strip always run parallel to the incident wind. In the double integration, the limit e arises from this modified shape as well as the assumption that the total strip lift force acts at the quarter chord point from the leading edge. In performing the integration, the mode shape for $y > L$ is taken to be equal to $y = L$ (e is likely to be small compared to L). $S_{ww}(y_1,y_2;n)$ is taken to be of von Karman form.

For the sine case, 2.50 will be

$$S_{ZS}(n) = \left(\frac{1}{2}\rho U' \sin(\beta)\int_0^L \frac{dC_{LS}(y)}{d\alpha}\mu_r(y)dy\right)^2 \int_0^B\int_0^B S_{ww}(x_1, x_2, n)dx_1 dx_2 \qquad (2.51)$$

Where $S_{ww}(x_1,x_2;n)$ is also assumed to be of von Karman form.

The variance of the r^{th} mode generalized coordinate for either case is

$$\sigma^2(q_r) = \frac{1}{(M_r 4\pi^2 n_r^2)^2}\int_0^\infty |X_Z(n)|^2 |H_f(n)|^2 S_F(n)dn \qquad (2.52)$$

where $S_F(n)$ is either $S_{ZC}(n)$ or $S_{ZS}(n)$.

The following comments can be given to the above theory:

1. The method predicts the response for flat plate-like sections. To extend this analysis for bluff sections, further investigation as to the possible spanwise variation of lift coefficient slope for bluff- type sections should be studied.
2. The aerodynamic admittance was assumed as unity. This usually leads to an over-estimation of the overall response.

3. The aerodynamic damping is taken from the experimental results. The quasi-steady equation tended to under-predict the experimental values.
4. The von Karman expressions for cross-spectrum and coherence were used in the calculations.
5. The results for the *cosine* case were thought to be applicable in the range of 0°, and within the range of 90° for the *sine* case. In a later paper, Scanlan (1993) proposed a *Pythagorean approximation* for intermediate yaw angles as $\sigma^2_{beta} = (\sigma_{cos}\cos\beta)^2 + (\sigma_{sin}\cos\beta)^2$. Calculations based on this equation were compared with Kimura's results and reported to be similar.

2.3.5 Huang's Aerodynamic Damping under Horizontal Vibration

Extending Kimura's modified buffeting theory, Huang (1995) presented a theoretical framework for the lateral buffeting response of free end models under yawed winds. The derivation followed Kimura's method, separating the problem into both cosine and sine cases.

The quasi-steady lateral buffeting force per unit length acting on a spanwise strip can be expressed as

$$F_X(t) = \frac{1}{2}\rho U^2 B\left(2C_D\frac{u(t)}{U}\right) \tag{2.53}$$

For the lateral vibration under a yawed wind, the important velocity fluctuating components are the along-wind $u'(t)$ and the lateral $v'(t)$ components. The vertical component, $w'(t)$, can be assumed negligible here and its effects are presently ignored.

The effective velocities for the cosine and sine cases are, respectively:

$$U_C(t) = (U'+u'(t))\cos\beta - v'(t)\sin\beta \tag{2.54}$$

$$U_S(t) = (U'+u'(t))\sin\beta + v'(t)\cos\beta \tag{2.55}$$

The corresponding buffeting forces for each case are obtained by substituting the expressions above into 2.53. In the expansion of U_C^2 and U_S^2, terms involving products of velocity fluctuations u' and v' are negligible and are ignored. The generalized buffeting force for the r^{th} vibration mode at spanwise position y'' for the cosine case is obtained by multiplying the r^{th} mode shape in the along-wind direction, and can then be expressed as

$$dF_{XC}(y'',t) = \rho U' dS'' \left[u'(y'',t)\cos^2\beta - v'(y'',t)\cos\beta\sin\beta\right] \int_0^B C_{DC}(x)\mu_r(y'',x)dx \qquad (2.56)$$

where dS'' is the strip area at y'', and $C_{DC}(x)$ is the cosine case drag coefficient as a function of the along- wind direction. The drag coefficient, taken to be constant along x, is obtained from experimental measurements (Winter [1936]). Winter's results are reported for flat plate sections but are taken to be applicable for the present case of bluff sections. Similar to the cosine case for the vertical buffeting forces, the r^{th} mode shape is also constant in the x direction. The integration therefore reduces to equal B.

For the sine case, the generalized strip buffeting force at spanwise position x'' is

$$dF_{XS}(x'',t) = \rho U' dS'' \left[u'(x'',t)\sin^2\beta - v'(x'',t)\cos\beta\sin\beta\right] \int_0^L C_{DS}(y)\mu_r(x'',y)dy \qquad (2.57)$$

where dS'' is the strip area at spanwise position x'', $C_{DS}(y)$ is the sine case drag coefficient and is constant along y and so removed from the integrand. The mode shape, however, will remain as a function of the spanwise position y.

To obtain the expressions for the spectral density functions for the cosine and sine cases, 2.56 and 2.57 are integrated in the cross-strip direction (y direction for the cosine case, x direction for the sine case). The spectral expression for the cosine case will be

$$\begin{aligned} S_{XC}(n) = &\left(\rho U' B C_{DC}\cos^2\beta\right)^2 \int_0^L \int_0^L S_{u'u'}(y_1,y_2,n)\mu_r(y_1)\mu_r(y_2)dy_1dy_2 \\ &+ \left(\rho U' B C_{DC}\cos\beta\sin\beta\right)^2 \int_0^L \int_0^L S_{v'v'}(y_1,y_2,n)\mu_r(y_1)\mu_r(y_2)dy_1dy_2 \end{aligned} \qquad (2.58)$$

and for the *sine* case,

$$S_{XS}(n) = \left(\rho U' C_{DS} \sin^2\beta \int_0^L \mu_r(y)\,dy\right)^2 \int_0^B \int_0^B S_{u'u'}(n)\,dx_1\,dx_2 + \left(\rho U' C_{DS} \cos\beta \sin\beta \int_0^L \mu_r(y)\,dy\right)^2 \int_0^B \int_0^B S_{v'v'}(n)\,dx_1\,dx_2 \tag{2.59}$$

In 2.59 the mode shape does not appear in the double integral because it is constant in the x direction, so its cross dependance at *any* two positions x_1 and x_2 is equal. The variance for the r^{th} mode response is found by substituting $S_{XC} = S_F$ (cosine case) or $S_{XS} = S_F$ (sine case) into 2.52.

The following comments can be given to the above theory:

1. Aerodynamic damping is assumed to vary with the cosine of the yaw angle. This is the same as was used for flat plate sections under vertical vibration and was used in the absence of experimental data.
2. The method still requires the validity of the strip assumption. For bluff sections with finite aspect ratios, experimental data is still needed regarding the variation of the drag coefficient in the across- strip direction.
3. The aerodynamic admittance was taken as unity and the exponential forms proposed by Davenport for the coherence were used. Also, because the spectrum and coherence of the v' component was not measured, its form was assumed to be the same as the w component.

2.3.6 Kimura et al.'s Modified Buffeting Theory for Horizontal Vibration

Following some of the earlier attempts at a theoretical treatment of buffeting response under yawed winds, Kimura et al. (1998) developed a more refined buffeting analysis applicable to horizontal vibrations of cantilever-type structures under yawed winds. The main refinement in this method was the inclusion of a drag force coefficient which varied with spanwise position y as well as with yaw angle β. This variation is necessary for free-end structures because the

presence of the free end may give rise to flow patterns which can change the spanwise drag force distribution.

The analytical development of the method accounts for the sine and cosine cases through the use of the drag coefficient, allowing a more practical single expression for the buffeting response. The quasi-steady assumption is also used. In the analysis, only the $u'(t)$ and $v'(t)$ components of the fluctuating wind velocities are considered to be effective, the vertical component, $w'(t)$, being ignored. Looking at a spanwise strip of area dS (height D and width dy), the fluctuating buffeting forces acting on this strip due to the u' and v' components can be expressed as:

$$dF_x(y,t,\beta) = \frac{1}{2}\rho U'^2 dS\left[2C_D(y,\beta)\frac{u'(y,t)}{U'} + \frac{dC_D(y,\beta)}{d\beta}\Theta(t)\right] \tag{2.60}$$

The buffeting force is now a function of time and spanwise position as well as the yaw angle β. The first term inside the brackets takes on the common form for the u' component. The second term, however, requires some further explanation. The v' velocity component can be introduced through the Θ(t) term. The instantaneous yaw angle will be due to the steady yaw angle β plus the time-dependent
yaw angle increase Θ(t). Here $\Theta(t) = \tan^{-1}[v'(t)/(U'+u'(t))] \approx v'(t)/U'$, the approximation arising from the fact that u' is small compared to the mean wind U'.
Introducing this into 2.60,

$$dF_x(y,t,\beta) = \frac{1}{2}\rho U'^2 dS\left[2C_D(y,\beta)\frac{u'(y,t)}{U'} + \frac{dC_D(y,\beta)}{d\beta}\frac{v'(y,t)}{U'}\right] \tag{2.61}$$

The generalized force for the r^{th} vibration mode can then be obtained by multiplying 2.61 with the r^{th} mode shape and integrating along the span. The resulting expression will be

$$F_{x_r}(y,t,\beta) = \rho U' D\int_0^L C_D(y,\beta)u'(y,t)\mu_r(y)dy + \frac{1}{2}\rho U' D\int_0^L \frac{dC_D(y,\beta)}{d\beta}v'(y,t)\mu_r(y)dy \tag{2.62}$$

The spectrum for the generalized force of the r^{th} mode can then be calculated by jointly integrating the mode shape along the span with the cross correlation of the fluctuating velocity components. In this expression, there will also be additional terms due to the spanwise dependence of the drag force coefficient and its slope with respect to β. Ignoring cross-spectral terms gives the spectral expression

$$S_{X_r}(n) = (\rho U' D)^2 \int_0^L \int_0^L S_{u'u'}(y_1, y_2, n) C_D(y_1, \beta) C_D(y_2, \beta) \mu_r(y_1) \mu_r(y_2) dy_1 dy_2$$
$$+ \left(\frac{1}{2} \rho U' D\right)^2 \int_0^L \int_0^L S_{vv}(y_1, y_2, n) \frac{dC_D(y_1, \beta)}{d\beta} \frac{dC_D(y_2, \beta)}{d\beta} \mu_r(y_1) \mu_r(y_2) dy_1 dy_2 \quad (2.63)$$

The variance for the r^{th} mode response can be calculated using

$$\sigma^2(q_r) = \frac{1}{M_r^2 \omega_r^2} \int_0^\infty |X_D(n)|^2 |H_f(n)|^2 S_{X_r}(n) dn \quad (2.64)$$

The spanwise drag force for a cantilever type model was assumed to vary linearly with the spanwise position as a first estimate. Simple sections were tested under smooth-flow conditions in order to obtain this drag force distribution. Although the actual distributions could not be measured, the average drag and the drag-induced moment were measured and, based on the assumed linear distribution, this drag force distribution was calculated.
The aerodynamic drag damping was assumed to follow the cosine rule
$\xi_D(\beta) = \xi_D(0)\cos(\beta)$. The value at β=0° was determined theoretically using 2.32 and taking $C_D(y)$ as $C_D(y, \beta=0°)$:

$$\xi_D(0) = \frac{\rho D U' \cos\beta}{4\pi n_r M_r} \int_0^L C_D(y, \beta=0) \mu^2(y) dy \quad (2.65)$$

The velocity spectra in the analysis were assumed to follow von Karman form with the lateral component S_{vv} assumed to be the same as the vertical component S_{ww}. The spanwise correlations and aerodynamic admittance were also taken in von Karman form.

The wind axis turbulence parameters at yaw angle β were converted to bridge axis values using the ellipse model. The bridge axis parameters could then be used to calculate the tip variance for the r^{th} lateral vibration mode.

In order to test this modified theory using actual bridges during erection phases, Kimura compared the wind tunnel test results of four bridge models with the results predicted by this theory. The bridge models examined were the Pont de Normandie, Tatara bridge, Kao Ping Hsi bridge, and the Meiko-Chuo bridge. Overall, the theory tended to under-predict the model test results, but overall shapes of the RMS response versus yaw angle graphs were similar. The notable exception was the Kao Ping Hsi bridge, the model tests of which tended to show an increase in lateral response with increasing yaw angle.

The following comments can be made regarding the above theory:

1. The validity of the theoretical aerodynamic damping equation and the cosine approximation should be investigated. As well, the effects of various bluff cross-sectional shapes should be studied.
2. The distribution of the drag force along the spanwise axis needs further attention. The assumed linear distribution seems to be a good first approximation, but this distribution may indeed be dependent on the actual cross-sectional shape.
3. The energy spectrum of the lateral velocity component, $v'(t)$, needs further study. Here it is assumed to be the same as the vertical component $w(t)$, an assumption valid only for isotropic turbulence.
4. The inclusion of the vertical fluctuating velocity component, w(t), and its effects on the lateral response might be a further area of study.
5. Kimura notes that the results from the theoretical study ignore any contributions from the stay cables. The presence of the stay cables during construction phases may tend to destabilize the structure as a whole.

2.3.7 Overview

To date, the progress towards an accurate theoretical model to predict the buffeting response of cable-stayed bridges during their construction phases has been well documented. The most important contributions are detailed in the above sections. In particular, the work of Kimura et al. (1998), has suggested a few areas of further study: the spanwise distribution of drag forces, the aerodynamic damping, and the spectrum of the lateral velocity component. This thesis focuses on the aerodynamic drag damping parameter.

In order to investigate the tendencies of the drag damping, an experimental model was set up. The objective was to observe the changes in aerodynamic damping for various bluff sections oscillating in various wind yaw angles. The results allow some insight into the applicability of quasi-steady and cosine proportionality assumptions to the aerodynamic drag damping.

Chapter 3. Bridge Response During Construction

3.1 The Nature of the Problem

A common method of erecting a cable-stayed bridge is the *balanced cantilever* method. The method involves constructing the main bridge pylons, then incrementally erecting the deck from both sides of the pylon. Supporting cables are attached at appropriate sections, and the two deck sections from adjacent pylons are finally joined to complete the span.

The partially erected structure closely resembles a cantilever type structure with frequencies of vibration in lower modes being smaller than those of the completed structure. With these lower natural frequencies, the bridge may become more susceptible to wind buffeting. At lower frequencies, the energy containing eddies in the flow may more closely coincide with a lower mode natural frequency of the bridge. A greater amount of energy is then directly converted into vibration energy acting on the partially completed structure. This, combined with a case of decreased overall stiffness, results in a structure which is more susceptible to buffeting instabilities. As spans increase, the effect is to decrease both the overall stiffness and the lower mode natural frequencies, increasing the chances of buffeting instabilities.

As with any theoretical development, it is necessary to parallel this research with experimental investigations. Experimental investigations serve to validate theory as well as allow deficiencies in the theory to be identified.

The theoretical works discussed in the previous section were usually compared against some experimental findings. Through the years, it has become quite common to test cable-stayed bridges during their erection phase behaviour in an attempt to identify instabilities and to remedy these instabilities. Through wind tunnel testing, properly scaled bridge models and turbulent wind conditions can allow for prototype response predictions. In many cases, however, it is only required to observe the bridge response in these different flow conditions rather than attempt to model the process mathematically. Experimental results are typically

compared against the quasi-steady theoretical predictions and discrepancies are noted but not necessarily explained. For a bridge model test, if a discrepancy is observed, the value obtained from the model test is usually taken to be more accurate (provided many of the necessary parameters are properly scaled).

3.2 Experimental Investigations into Erection Phase Behaviour

Paralleled with the attempts at a theoretical development of drag buffeting of cable-stayed bridges during erection phases, there have been some experimental works carried out during the testing phases of actual cable-stayed bridges.

Following is a brief recount of some of the tests which have been carried out as part of the wind tunnel testing for various cable-stayed bridges. Performing tests during erection phases with yaw winds can be traced almost as far back as Davenport's early theoretical work.

3.2.1 Northumberland Straits Bridge

The Northumberland Straits bridge is a multi-span concrete bridge with the longest main spans being 247 metres. Scale model testing of the bridge was undertaken in 1969 at the Boundary Layer Wind Tunnel in the University of Western Ontario (Davenport et al., 1969). The bridge was tested during its critical construction stage, when the concrete deck was cantilevered from the pier extending 100 metres. A 1:207 scale model of the bridge and pier was constructed and tested in smooth and turbulent flow conditions ranging from 0-240 kilometres per hour (full scale). The model was tested at wind yaw angles of 0°, 15°, 30°, 45°, and 75°. The response spectra for both drag and lift deflection were recorded. The results of the tests showed that increasing the yaw angle had the effect of decreasing the drag response, a result that serves to validate the quasi-steady theory predictions.

3.2.2 Pont de Normandie

The Pont de Normandie is a cable-stayed bridge spanning the Seine River in France. The main span is 856 metres in length and extends from both sides of two 203 metre high pylons. The Danish Maritime Institute (Larose and Livesey, 1993) carried out scale model tests for the bridge during its critical erection stage. At this critical stage, the bridge resembles a 426 metre cantilevered structure. A 1:150 scale model was constructed to carry out the wind tunnel tests. During the tests, the model was subjected to two different turbulent flow conditions to represent the two possible flow conditions at the actual site. For one of the turbulent flow conditions (termed Exposure 2), the yaw angle of the mean wind was adjusted in 5° increments from 0° – 90°. For this exposure, the mean wind speeds were set at 108, 119, 140, and 158 kilometres per hour (full scale).

Results from the tests at various yaw angles showed that the peak lateral response was maximum at a yaw angle around 35° for all wind speeds. This contradicts the conventional buffeting theory which predicts increasingly lower responses as the yaw angle increases. The vertical buffeting response, however, did show a decrease with increasing yaw angle.

3.2.3 Kao Ping Hsi Bridge

The Kao Ping Hsi bridge in Taiwan is a unique cable-stayed bridge constructed using only a single pylon to support the deck. The main span is 331 metres, which also represents the length of the critical cantilever stage of the bridge during erection. Wind tunnel tests of the critical erection phase were undertaken by the Danish Maritime Institute (Larsen and Livesey, 1997).

The scale model was constructed at 1:150 and tested in both smooth and turbulent flow conditions. For both flow conditions, the mean wind speed was adjusted from 18 – 288 kilometres per hour. The wind yaw angle for each wind speed was also adjusted from 0° to 90° in increments of 15°.

The test results for the lateral buffeting response indicated similar results to those of the Pont de Normandie; maximum buffeting responses not necessarily always occurring at the 0° yaw angle. In this case, peak lateral responses at 245 km/hr occurred both at 0° and 60°. At other wind speeds, peak responses were always observed at 0°, however, the responses did not always decrease with increasing yaw angle.

3.2.4 Introduction to Experimental Work

By only comparing the results from a few different wind tunnel studies, it appears that the existing quasi-steady buffeting theory does not accurately predict a cable-stayed bridge's lateral buffeting response over the full range of incident wind yaw angles. In some cases, the lateral buffeting response was observed to be greater at a yaw angle other than zero. This observation is in direct contradictions with the current theory.

The aerodynamic damping plays an important role in the lateral buffeting response. Increasing the damping leads to a decrease in the overall response while decreasing the aerodynamic damping leads to an increase in the overall response. Current theory assumes that the lateral aerodynamic damping is maximum when the yaw angle is 0° and will be zero when the yaw angle is 90° and follows a cosine relationship at intermediate yaw angles. A discrepancy between the theoretical and experimental aerodynamic damping values is likely the cause of the conspicuous behaviour of certain bridge models subjected to non-zero yaw angles.

The experimental work carried out in this thesis investigates the change in aerodynamic damping for various aerodynamically bluff sections subjected to yawed incident winds. As well, a portion of the analysis involves studying the effects that a changing aerodynamic damping value has on the overall lateral buffeting response. The experimental work and subsequent analysis serves as an important step towards a more complete understanding of the effects of a yawed incident wind on cable-stayed bridges during construction.

Chapter 4. Measurement of Aerodynamic Damping

4.1 Purpose

For a long span bridge during its construction phase, there has not been much research effort directed towards the effects of wind on the horizontal vibration modes. Past research seems to have focused its efforts on the effects of turbulent winds to vertical and torsional responses. As well, much of the early experiments and theoretical developments dealt mainly with incident wind normal to the axis of the bridge. Later attempts at incorporating a yawed wind were made by Kimura (1991) for the vertical mode, Huang (1995) for the horizontal mode, and more recently Kimura et al. (1998). A treatment of these studies was made in section 2.

Although there are many complex and interactive parameters involved in the response of slender structures to turbulence buffeting, one parameter, the aerodynamic damping, remains as one of the most important. The aerodynamic damping present in a flexible structure is caused by the relative velocity of the air as it flows past the moving structure. Intuitively, an object oscillating in an air flow will tend to encounter forces opposing its motion, essentially damping out this motion. The faster the air is flowing, the greater are the opposing forces, and hence the greater the value of aerodynamic damping. Wind speed is not the only factor influencing this damping; it also seems quite reasonable to factor in linear dimensions of the object (length, width, height), mass parameters (mass per unit length), as well as the frequency of motion of the object. All these parameters do in fact appear in the quasi-steady approximation.

Aerodynamic damping for a cantilever flat plate vibrating in the vertical direction was shown by Kimura (1991) to vary closely proportional to the cosine of the incident wind yaw angle. Because of these test results, it was believed that the aerodynamic damping in the horizontal vibration mode could be thought to vary in similar fashion and this approach was studied by Huang (1995) and Kimura et al. (1998).

The wind tunnel experiments carried out as part of this thesis research were designed to examine the effects of yaw angle and wind speed on the aerodynamic damping of various bluff sections in horizontal vibration. The sections were all designed as free end structures to approximate a typical cable-stayed bridge during its construction stage. All the tests were performed at the National Research Council's 0.9m closed circuit low speed wind tunnel in July of 1999. The tunnel is located in building M2 of the Montreal Road facility and is a 1/10 scale model of the facility located at the Uplands campus near the Ottawa International Airport. The cross-section of the tunnel is 0.9m x 0.9m with a working section length of 2.3m. Test section wind speeds can be adjusted from 0.3 m/s to 40 m/s with a maximum turbulence intensity of 0.5 percent (of the mean wind speed).

4.2 The Experiment

4.2.1 Test Sections

Five bluff rectangular test sections were selected to investigate their aerodynamic damping properties in smooth flow under horizontal vibration modes. The test sections were all made with acrylic glass and were 203.2 mm in length. A summary of the remaining necessary physical and dynamic properties are shown in the table below:

Section #	D x B (mm)	Cross Sectional Area (mm^2)	Mass / Length (kg/m)	Natural Frequency 1st Mode Lateral (Hz)
1	12.7 x 12.7	161.3	0.1914	3.125
2	12.7 x 25.4	322.6	0.3826	2.174
3	12.7 x 38.1	483.9	0.5740	1.852
4	25.4 x 12.7	322.6	0.3826	2.222
5	38.1 x 12.7	483.9	0.5740	1.852

Table 4.1 Test Section Properties

The mass per unit length was calculated based on a mass density of 1185 kg/m^3. The first mode natural frequencies were obtained from the free vibration test results. From the free vibration damping traces, peak readings were extracted using a Fortran77 routine. A printout of the routine can be found in Appendix A. By selecting n consecutive peaks and dividing by the time between them, the natural frequency was obtained. The process was repeated using different numbers of peaks in order to obtain an average value for the natural frequency. Appendix B presents some typical damping traces obtained during the experimental tests. The damping traces are shown for the 12.5 seconds of each run.

4.2.2 Setup

The models were rigidly connected to a stiff leaf spring at one end while the other end was free. The leaf spring was made of spring steel and had a 61.5 mm free length for vibration. The length and thickness of the leaf spring was selected such that the vibration mode for all the model sections was lateral only. Selecting a spring with a lower stiffness would have resulted in the dynamic motion to be a combination of both lateral and torsional modes. A precision strain gage (EA-06-250PD-350, made by Measurements Group, Inc.) was attached to the spring to record the data during the tests. During a test run, the strain gage would record the decaying dynamic motion of the model section as it oscillated in the wind tunnel. Readings from the strain gage were given in volt counts. The other end of the leaf spring was rigidly connected to a vertical steel post with a high bending stiffness. Steel wire was attached to the post in two positions, fixed to the plywood base plate, and sufficiently tensioned to further stiffen the post against unwanted sway during vibration. The post itself was 305 mm long and was fixed to a circular plywood base. The plywood base was inserted flush to the wind tunnel floor and was marked with 10° graduations (from -10° to 100°) to allow the incident wind yaw angle to be adjusted to various values during the tests. Diagrams of the setup can be seen in Figures 4.1. (a-c). The setup of the model and surrounding apparatus was designed to allow simple transition between model sections without having to recalibrate the strain gage each time.

A schematic of the overall test setup equipment can be seen in Figure 4.2. Following is a description of the electronic equipment used in the experiment:

1. Datametrics Barocel Pressure Sensor (Type 1400): This electronic manometer was used to obtain the time varying dynamic pressure in the wind tunnel. The dual input consisted of the static pressure out and the total pressure out from the pitot tube in the wind tunnel. The single output was the dynamic pressure which was obtained by subtracting the static pressure from the overall pressure. The output was sent to the Channel 1 input on the DAS-20 control box.
2. Amplifier / Power Supply: A 5 Volt continuos power supply was fed to the strain gage. The strain gage output was then fed through an amplifier to allow for the tolerance limits in the DAS-20 recording. If the signal was not amplified, the readings from the DAS-20 box would all likely have been zero.
3. Frequency Devices Tunable Lowpass Filter (Series 900): The output from the amplifier was passed through a lowpass filter prior to sending it to the DAS-20 box. A cut off frequency of 50 Hz was used in order to reduce instrument and background noise from the strain gage signal. This cutoff frequency was appropriate because the highest model frequency was 3.125 Hz. The output from the filter was sent to the Channel 0 input on the DAS-20 control box.
4. Data Acquisition System (DAS-20): The DAS-20 box accepted the two inputs and recorded them in data files for later analysis. The readings were all given in volt counts and could be converted to a voltage reading if the range of the DAS-20 box was known. In our case, the range was set at ± 0.5 volts. This led to the conversion from counts to volts as counts/4096 = volts.
5. Atmospheric Pressure Sensor: This sensor was permanently fixed outside of the wind tunnel and kept a reading of the atmospheric pressure which was needed to calculate the actual tunnel speed.
6. Pacer Industries Digital Thermometer (DTA 4000): This device was installed on the inside of the tunnel downstream of the test section. The readings provided an approximate value for the mean wind speed in the tunnel. This value was used as an approximate to the true

wind speed when performing the tests. Actual wind speeds were later corrected based on the dynamic pressure and atmospheric pressure. The instrument also gave a reading of the tunnel temperature.

The actual tunnel wind speed could be obtained via the following equation:

$$V = \sqrt{\left(\frac{2P_0}{T_0\rho_0}\right)\left(\frac{Tq}{P}\right)} \tag{4.1}$$

where P_0 is the standard atmospheric pressure (101.325 kPa); T_0 is the standard temperature (288^0 Kelvin); ρ_0 is the standard density of air (0.002378 slug/ft^2); T is the temperature in the wind tunnel (in ^{0} Kelvin); q is the dynamic pressure; and P is the actual atmospheric pressure.

4.2.3 Experimental Procedure

4.2.3.1 Strain Gage calibration

The first step, prior to any dynamic runs, was to calibrate the strain gage. If we were only interested in the dynamic traces of the data, it would not be necessary to calibrate the strain gage. In fact, since the conversion from counts to volts to deflection is linear, the damping ratio calculated based on peak to peak values using any of these data sets would lead to the same damping ratio. The strain gage calibration is necessary, however, since we wish to know the static deflection of the models in the various wind conditions. Dynamic oscillations occur about a static mean deflection point, and the degree of static deflection alters the incident yaw wind angle.

The strain gage was calibrated by applying successive deflections to the spring, holding this deflection thus allowing the strain gage to level out, and obtaining a reading for the mean voltage. The static deflections were applied using a depth micrometer. Three positions were selected along the length of the spring and at each position, the successive deflections were repeated. The sampling rate was set at 20 Hz and the sample time was 20 seconds. The successive deflections were applied to a suitable maximum, and then incrementally released.

As well, a tare value with zero deflection was taken at the beginning and end of each different deflection position. This zero tare mean value was subtracted from the other mean values. The three positions selected were located between the free end of the spring and the end of the strain gage. The static deflection calibrations were attempted at the very tip of the spring, but the depth micrometer kept sliding off the end of the spring thus not allowing for an accurate reading.

The end goal of the calibration was to be able to obtain, for a given mean voltage reading, a value for the tip deflection angle of the spring. This angle could then be added to the set yaw angle to obtain the actual yaw angle.

4.2.3.2 Section Model Runs

Each of the five model sections were tested under smooth flow conditions. The yaw angle from the base plate was adjusted from -10° to 100° in 10° increments. The wind tunnel speeds were varied according to the reading on the DTA 4000 from 1 m/s to 5 m/s in 1 m/s increments. The models were triggered into free vibration by inserting a thin metal rod through a hole located in the base plate. The data was recorded at 80 Hz for a total of 50 seconds for each run. For each test section, yaw angle, and wind speed, three runs were performed. The general procedure followed for the tests was as follows:

1. Test section installed on leaf spring and base plate set to -10° yaw angle.
2. Wind tunnel adjusted to give a reading of ≈ 1 m/s on the DTA 4000.
3. Model set into free vibration and data recording commenced for 50 seconds at 80 Hz. Three runs were taken.
4. Base plate is turned manually to the next yaw angle.
5. Steps 1-4 are repeated until yaw angle reaches 100°.
6. Wind tunnel is turned off and a damping run is taken three times with no wind. These runs are used to calculate the structural damping.
7. Yaw angle reset to -10° and wind tunnel adjusted to next wind speed.

8. Steps 3-7 are repeated until the wind speed reaches 5 m/s.
9. Model section removed and next section installed on leaf spring. Steps 2-8 are repeated.

4.2.3.3 Calculating the Damping Ratios

Calculating the damping ratios involved the application of the logarithmic decrement method. The raw data files from the tests consisting of the volt counts were used. The same Fortran77 program as was used to obtain the model natural frequencies was used to extract the peak values from the raw data. Then, by hand, the two peaks corresponding to an approximate half-amplitude decay were extracted and the damping value could be calculated using the logarithmic decrement equation:

$$\delta = \frac{1}{2\pi n} \log\left(\frac{A_0}{A_n}\right) \tag{4.2}$$

here A_0 represents the first peak selected, A_n represents the peak corresponding to the half amplitude decay, and n is the number of peaks in between. Equation 4.2 gives the damping as a fraction of critical.

For each section, the structural damping was first calculated for each run. These calculations involved using the runs where the wind speed was zero. The average of all the appropriate runs was used as the overall structural damping ratio of the section. The structural damping ratios for each section were calculated using various numbers of decay cycles (n) to ensure that the structural damping ratios were not amplitude dependent. This was necessary because during the test runs, the initial amplitude was not always the same (initial amplitude was always triggered manually). For all five sections, varying the number of peaks (n) had little or no effect on the overall structural damping ratio. Total damping values were calculated for the runs where the wind speed was not zero. The aerodynamic damping was then the total damping minus the structural damping.

4.3 Results

4.3.1 Structural Damping Ratios

The following are the structural damping ratios obtained for the test sections. Because of the number of runs taken, each sectional damping ratio was observed in relation to the others and any values that did not appear within a reasonably range were ignored as outliers.

Section #	Structural Damping (% of Critical)
1	0.8190
2	0.7936
3	0.7654
4	0.7881
5	0.7737

Table 4.2 Structural Damping Ratios

4.3.2 True Wind Speed

In order to more accurately obtain relationships between the damping values and wind speeds, it was necessary to use the true wind speed values when studying the results. For each run, the true wind speed can be calculated from equation 4.1. Three runs were taken for each section, wind speed, and yaw angle configuration. A good approximation would be to average the wind speed over the three runs and use this as the true wind speed value. Figures 4.3 (1-5) present the true wind speed values for each test section and yaw angle.

4.3.3 True Yaw Angle

The free vibrations of the test sections always occurred about a mean position. For the case of no wind, this mean position corresponds to the case of no static deflection. As the wind speed was increased, and as the sections became more bluff, this static deflection was seen to

increase. A static deflection greater than zero results in a different wind yaw angle incident on the section. Because of this, it was necessary to calculate this mean deflection so that the true yaw angles could be investigated. In order to find the true yaw angle, the mean voltage deflection for the strain gage was found for each separate run. Using the calibration results from the strain gage (Section 4.2.3.1), this mean voltage reading could be extrapolated to the tip of the leaf spring to obtain the angular displacement of the tip. The model sections themselves were sufficiently rigid so as to move in a rectilinear fashion following the spring tip. This way, the tip angular displacement of the spring would give the overall increased yaw angle on the model. The true yaw angles are presented in Figures 4.4 (1-5). Looking at the results, we notice that even in the extreme cases, the increase in yaw angle was within a few degrees of the assumed yaw angle. For this reason, subsequent analysis results using the assumed yaw angles is used for simplicity and will not introduce significant error.

4.3.4 Aerodynamic Damping Ratios

The aerodynamic damping ratios for each section were obtained by subtracting the appropriate structural damping ratio. Plots of aerodynamic damping versus uncorrected yaw angle are presented in figures 4.5 (1-30). Plots of aerodynamic damping versus wind speed are presented in Figures 4.6 (1-17). Also, as part of the study, it was found useful to examine the effects of the sectional width to depth ratio (W/D) on aerodynamic damping values. Graphs of aerodynamic damping versus W/D are shown in Figures 4.7 (1-17).

4.3.5 Self-Excited Oscillations

At the outset of the testing, it was desired only to investigate the effects of yaw angle on the aerodynamic damping ratios of various cross sections. Through the wind tunnel testing, it was also noticed that some sections exhibited what appeared to be self-excited oscillations in the smooth flow. These oscillations were triggered after the initial induced vibration was damped out and in some cases the oscillations were quite noticeable. To investigate these self-excited vibrations, root-mean-squares (RMS) of the fluctuations were calculated from the

test data. For each run, the last 1000 data points (corresponding to the last 12.5 seconds of the test run) were used to calculate the RMS values. The selection of these data points was arbitrary but in all cases, by looking at plots of the damping traces, it is quite evident that the initial vibration had been damped out by this point. For each section, the average RMS for the case of no wind was subtracted from each of the runs corresponding to non zero wind speed to correct for any background vibrations which may have been present from the initial free vibration. The corrected RMS value is calculated as

$$\sigma_c = \sqrt{\sigma_{actual}^2 - \sigma_0^2} \tag{4.3}$$

were σ_c is the corrected RMS value, σ_{actual} is the actual RMS values calculated using the test data, and σ_0 is the RMS value corresponding to the average of all the free vibration test runs for the section under consideration. In some cases, σ_0 was greater than σ_{actual}, and for these cases it was assumed that no self excited oscillations existed so σ_c was taken as zero. Figures 4.8 (1-5) show the self excited oscillation RMS values versus yaw angle for each section. Each graph contains the results for all the wind speeds tested. Alternatively, Figures 4.8 (6-10) present similar data but for individual wind speeds containing all five sections on each graph. All the RMS values presented in these figures are in terms of volt counts.

Chapter 5

Application of Damping Results

5.1 Comment on the Applicability of Model Sections

In order to be able to draw conclusions from the test data in terms of actual prototype bridge performance, it is necessary to compare some of the common dimensionless parameters which are used to predict prototype calculations based on model sized tests. If tests are performed under conditions, which when scaled to actual size, represent scenarios that are not of good simulation, then some interpretation is required in order to apply test data.

In the case of bridge vibration, a commonly adopted dimensionless parameter is the reduced velocity. The reduced velocity is defined as $U/n_r B$. Here n_r is the natural frequency of vibration in the r^{th} mode (in our case the first mode only is treated), B is a linear dimension of the structure and is taken as the width, and U is the mean wind velocity on the section.

Following is a comparison of typical reduced velocities for actual bridge models during construction phases compared against the five sections used in the present tests:

Bridge / Section	First Lateral Frequency (Hz)	Width (m)	Wind Speed Range (m/s)	Reduced Frequency Range
Normandie	0.111	22.3	10 - 55	4.04 - 22.2
Kao Ping Hsi	0.153	34.5	5 - 100	0.95 - 18.9
Tatara	0.0663	25.3	5 - 60	2.98 - 35.8
Meiko-Chuo	0.128	37.7	10 - 80	2.1 - 16.6
Section 1	3.125	0.0127	1 - 5	25.2 - 126
Section 2	2.174	0.0254	1 - 5	18.1 - 90.5
Section 3	1.852	0.0381	1 - 5	14.2 - 70.9
Section 4	2.222	0.0127	1 - 5	35.4 - 177.2
Section 5	1.852	0.0127	1 - 5	42.5 - 212.6

Table 5.1 Comparison of Reduced Velocities

In the above table, the *Wind Speed Range* for the first four bridge models is reported as the full scale equivalent. As well, the values reported for the four bridges (Normandie, Kao Ping Hsi, Tatara, and Meiko-Chuo) were taken from Kimura et al. (1998).

In looking at the table, we see that in terms of a prototype response, the majority of our test section results represent extreme wind conditions which would likely have a lower probability of occurrence during construction phases than over the completed life of the structure. However, increasing span lengths lead to a reduction in natural frequency values thus leading to higher reduced velocities for the same shape cross section and incident wind velocity. Therefore comparable prototype reduced velocities are not unforeseeable. From the figure, it appears that Section 3 in our tests more closely represents a true bridge section. Regardless of this fact, however, the tests do provide some interesting discussion.

Another set of dimensionless parameters, those dealing with geometric dimension ratios, are also of relevance. For lift deflections, it is now quite common to modify the lift coefficient slope according to the aspect ratio. The aspect ratio is defined as the ratio of the bridge length divided by the width. For our test sections, however, all the model lengths were the same and because some of the sections shared a common width, the aspect ratio would not appear to be an applicable parameter. Instead, another dimensionless parameter was used; the width to depth (W/D) ratio. All five model cross sections were unique so there were five different W/D ratios. In examining the effects of this parameter, some interesting observations were made.

5.2 Damping versus Cosine of Angle

The aerodynamic damping for any section and wind speed will change with the incident yaw angle. The assumption of cosine proportionality has been experimentally verified for flat plates in vertical vibration (Kimura [1991]). For horizontal vibration of bluff cross sections, however, this assumption has only been extended in the absence of experimental test data (Huang [1995]). The results from the present experiment do shed some light as to the validity

of this cosine assumption. Figures 4.5 (1-25) present the aerodynamic damping versus yaw angle for each section and wind speed. As well, Figures 4.5 (26-30) present the same data but at each different wind speed with all five sections on each graph. With the exception of obvious outliers in the data, each section and wind speed was fitted with a cosine curve using a regression analysis (the cosine curve is shown as a solid line on each figure). The form of relation was taken to be $\xi_\beta = A\,\xi_{\beta=0}\cos\beta$. The constant A was found by trial and error through regression analysis. A value for A was assumed, then modified until the sum of the squares of the experimental and theoretical curves was a minimum. Under the theoretical quasi-steady method, A would take the value of unity. The $\xi_{\beta=0}$ value was taken as the average of the three experimental runs for the case of zero yaw angle. Comparing the experimental results with the regression line fits, an interesting observation can be made. As the wind speed increases, combined with a decrease in the W/D ratio of the section, the following trend becomes more and more evident:

1. At a yaw angle around 20°, the experimental aerodynamic damping begins to fall below the cosine regression curve.
2. At a yaw angle around 60°, the experimental aerodynamic damping appears to be greater than the cosine regression curve.

These observations are quite significant and the effects of changing the aerodynamic damping on the overall buffeting response will be examined in the parametric study in Section 6.2. For now, it is only important to point out the discrepancies observed between the experimental evidence and the cosine approximation. This observation is interesting because it may serve to explain the occurrence of higher lateral buffeting responses in the 30° yaw angle range which were observed in some wind tunnel studies of cable-stayed bridges during their construction phase (see Section 3). Keeping all other factors constant, a lower than expected damping ratio will result in a higher RMS response.

Another useful method of comparing all the results is to calculate the root-mean-square (RMS) of the experimental data from the regression analysis cosine fits. The results are shown in Figure 5.1 and are presented as RMS versus mean wind speed for each section. Section 3 shows the least scatter from the cosine fit, followed by Section 2. Section 1 is a slightly higher than sections two and three but considerably lower than Sections 4 and 5. Sections 4 and 5 show much more scatter about the regression line and this scatter appears to increase non linearly with an increasing mean wind speed.

Figures 5.2 (1-5) present the RMS values for each section as a function of the yaw angle. Also, Figures 5.2 (6-10) present a similar relationship but for individual wind speeds. Decreasing the W/D ratio has the effect of increasing the scatter of the data over the full range of yaw angles. Increasing the mean wind speed for a particular section also has the effect of increasing the scatter over the full range of yaw angles. For all the sections, the RMS values are relatively constant over the full range of yaw angles when the wind speed is low. As the wind speed increases, the scatter becomes more random over the yaw angles. For Sections 4 and 5, the scatter exhibits a peak at an angle of 60°. Section 5 also reveals a peak around 20°, whereas Section 4 shows higher RMS values near 0°, while showing lower values at 20°. Section 3 has RMS values which are fairly constant over all wind speeds, with the exception of 5 m/s, where a sharp peak occurs around 70°. Section 2 exhibits similar characteristics as Section 3, with the same sharp peak. This section also has somewhat of a peak in the 20° range, becoming increasingly noticeable with increasing wind speed. The RMS results are consistent with the observation of lower than theoretical damping at 20° and higher than theoretical damping at 60°.

5.3 Damping versus Wind Speed

Figures 4.6 (1-12) present the aerodynamic damping as a function of the wind speed for the full range of yaw angles tested. Each figure includes the results for each of the five sections tested. Alternatively, Figures 4.6 (13-17) show the same results but each section is plotted separately with the full range of yaw angles shown on each figure. All the experimental data

is fitted with a linear regression line which extends through the origin in each case. The extension through the origin was used because at zero wind speed, the aerodynamic damping is zero for any section at any yaw angle. The results for the case of 90° yaw angle are not fitted with a linear regression line. For this particular case, the aerodynamic damping values are all very close to zero as the theory would predict. No further comment is necessary for this case. The quasi-steady assumption would require the aerodynamic damping to be a linear function of the mean wind speed. For each section and yaw angle, this general trend is seen to quite well upheld. The experimental results fit with good accuracy about their linear regression lines and there is not a large difference in the amount of scatter between various sections and yaw angles. Figure 5.3 shows the RMS versus yaw angle for each section. All values are relatively constant with an average value of 0.93. Comparing this to the standard deviation values obtained in Section 5.2 above, however, we see that this average value is more than twice the highest value of all the data in Section 5.2. This indicates less certainty in the assumption of a linear relation between the aerodynamic damping and mean wind speed although an RMS value of 0.93 would still be considered to be quite low.

Figure 5.4 presents the slope of the linear fits against the yaw angle for each test section. Looking at this figure, a trend is seen to emerge: at each yaw angle, the lower the width to depth ratio of the section, the higher the slope of the damping versus wind speed linear regression line and so the sharper the change in damping with increased wind speed. The results shown in Figures 4.6 (13-17) indicate that for a given section, increasing the yaw angle tends to decrease the slope of the linear regression line. This is to be expected, and at 90°, the theoretical slope should be zero. Although this case is not fitted with a linear regression line, the surrounding yaw angles (80° and 100°) would appear to be close to the value as expected.

5.4 Damping versus Width/Depth Ratio

The Figures 4.7 (1-12) present the graphs of aerodynamic damping against sectional width to depth ratios for each yaw angle. Each figure contains the results for all five wind speeds tested. It was desired to investigate whether or not a general trend could be applied to the data. It was found that by applying a logarithmic type fit of the form $\xi_{aero} = A \ln(W/D) + B$, all the test data could be quite reasonably represented. The constants A and B were obtained through the linear regression, which was performed in this case through a trend line fitting analysis in an Excel spreadsheet. The discrepancy between the experimental values and the logarithmic fit equations is represented by calculating the corresponding RMS values for each wind speed. Figure 5.5 shows the RMS values versus the yaw angle. The RMS values are relatively constant over the entire data field with an average value of 0.94. This is comparable to the average RMS value obtained from the linear damping versus wind speed fits discussed in Section 5.3 and indicates that the logarithmic fit is a good choice. Of note, the RMS values for 1 m/s seem to drop off sharply when the yaw angle reaches 90°. An attempt was also made (although not reported here) to fit the data with an exponential type equation of the form $\xi_{aero} = A e^{-B(W/D)}$, however the RMS values for this regression were higher than those of the logarithmic fit. The exponential fit did not seem to accurately represent the data at lower width to depth ratios, where the aerodynamic damping values seem to increase sharply.

Looking at the constants A and B from the logarithmic regression fits, some comment can also be made. Figure 5.6 shows the constant A versus wind yaw angle for each wind speed. In general, as the wind speed increases, the values of A seem to decrease. Here, for all cases, A values are below zero. At the lowest two wind speeds, A is relatively constant until 50° when it shifts to approach zero as the yaw angle approaches 90°. Although the 90° case is not shown on the graph, the graph of aerodynamic damping versus width/depth for 90° (Figure 4.7 (11)) shows a scatter of values with very low aerodynamic damping, reflecting the quasi steady assumption. As the wind speed increases, a region between 30° and 60° emerges where A falls away from zero. This trend is most pronounced for the 5 m/s case whereas it is

only slightly noticeable for the 3 m/s case.

Figure 5.7 shows the constant B versus yaw angle. Values of B are always positive showing an increase with increasing wind speed. At the lowest three wind speed, B is approximately constant until 40°, upon which it begins to decrease towards zero. At 3 m/s, this decrease is sharper than the case for 1 m/s. For the 4 m/s and 5 m/s cases, the same general trend is apparent, except that at a yaw angle of about 40°, B shows a slight increase prior to starting is decline to zero. The graph of B versus yaw angle also represents aerodynamic damping versus yaw angle for Section 1 because the width to depth ratio for this section is unity.

5.5 Self-Excited Oscillations

It is difficult to draw any clear conclusions regarding the self-excited oscillations which were observed under various flow conditions. Because it was not known prior to the experiment nor expected for these oscillations to occur, we will not undertake a rigorous study, but instead bring them to attention to perhaps lead way for a later study.

The RMS values of these fluctuations were calculated as described in Section 4.3.5 above. Results were plotted for both individual sections (Figures 4.8 (1-5)) and individual wind speeds (Figures 4.8 (6-10)). Some very general conclusions can be drawn as to the likelihood of a certain section to be susceptible to these self-excited oscillations. For any given wind speed, the majority of significant oscillations appears to occur in the 0° - 30° yaw angle range. At higher yaw angles, the oscillations are not nearly as pronounced. This fact was also supported by observations made during the actual experiments, when in some cases, significant oscillations occurred in this 0° - 30° yaw angle range. The magnitude of the oscillations increases with a corresponding decrease in the W/D ratio of the section indicating that more streamlined type sections are less likely to be susceptible to vibrations of this sort. Increasing the mean wind speed had the overall effect of increasing the magnitude of the oscillations for all sections and yaw angles. The natural frequencies of these oscillations were observed to be the same as the first mode lateral frequencies of the models.

Bridge sections are usually designed to withstand flutter type oscillations relatively early in the design stage. Flutter oscillations are generally characterized by dominant cross-wind motion. The horizontal oscillations observed in this case have a similar dynamic to the vertical flutter case, however a lateral type flutter is not known to exist in bridges yet. A possibility for these instabilities may be due the evolution and frequency of the vortex pattern shed as the incident flow strikes the leading edge and passes both over and along the section. The unsupported end may cause a vortex pattern, which by its orientation, produces a lateral force. As an area of further study, it would be worth investigating the flow patterns which are formed for this particular case.

5.6. Summary of Results

The following conclusions and comments can be made following the experiments and data analysis:

1. The cosine approximation is generally valid for sections with higher W/D ratios. For these sections, the experimental scatter about the cosine regression line was minimal for all wind speeds. The cosine approximation provided an excellent fit for Section 3. For sections with lower W/D ratios, the experimental data showed an increasing amount of scatter with increasing wind speed and decreasing W/D ratios--characterized by the peaks at 20° and 60° discussed in Section 5.2. For these sections, the cosine approximation may not be the best fit for the data.

2. The assumption of aerodynamic damping increasing linearly with an increase in mean wind speed was experimentally verified for each individual section and yaw angle. This is an interesting observation in particular for sections with lower W/D ratios because for these sections, damping versus yaw angle indicated some definite deviation from the cosine fit, yet the relation between wind speed and damping remained as assumed through the quasi-steady analysis. For individual sections, plotting the slopes of the linear fits against yaw angle revealed a decreasing trend with increasing yaw angle. This trend appears to be

approximately linear for sections with higher W/D ratios, but for lower W/D sections, this trend becomes increasingly more non linear.

3. From all the observations, the W/D ratio of the sections was the common link for all the data trends. Damping plotted against yaw angle showed increasing scatter with decreasing W/D ratio. Damping plotted against wind speed showed an increasing slope with a decrease in W/D. Perhaps the most interesting observation occurred for the damping versus W/D plots, which showed a definite logarithmic trend. Although not attempted in this study, it would be interesting to examine whether the constants A and B from the logarithmic regression could be expressed as functions of wind speed and yaw angle.

4. The occurrence of the self excited oscillations was indeed interesting. The presence of these oscillations at lower yaw angles may be responsible for reducing the ability of the structure to withstand buffeting loads and may serve to partly explain the higher buffeting response observed at non-zero yaw angles in some of the experimental studies mentioned in Section 3. An attempt to better explain these self excited oscillations is an interesting area of future study.

Chapter 6

Parametric Study

6.1 Theoretical Versus Experimental Aerodynamic Damping

Before applying the test results in calculating hypothetical buffeting responses, it was necessary to compare the experimental damping results against the theoretically derived values. In order to derive the theoretical damping expression, an appropriate model was required to describe the actual test setup.

The aerodynamic damping equations from 2.32 and 2.65 are derived for multiple degree of freedom systems. The model used in this experiment can be modeled as a single degree of freedom torsional spring. Figure 6.1 presents the model and other relevant information needed in the derivation.

The equation of motion for the torsional displacement Θ is

$$J\ddot{\Theta} + C_{\phi}\dot{\Theta} + K_{\phi}\Theta = M_t \tag{6.1}$$

where $J = mL^3 / 3$ is the polar mass moment of inertia; $C_{\phi} = 2\omega_o J\xi$ is the torsional damping coefficient; $K_{\phi} = \omega_o^2 J$ is the torsional spring stiffness; and $M_t = \int_0^L y\,dF$ is the externally applied torque moment. In the above definitions, m is the mass per unit length of the model section, L is the length, and ω_o is the natural frequency of the system.

The external force dF acting on a strip of width dy and height D will be due to the relative wind velocity on that strip:

$$dF = \frac{1}{2}\rho U_r^2 D C_D[y, \beta+\gamma(t)]dy \tag{6.2}$$

where $U_r = U'+u(t,y)+\dot{x} = U'+u(t,y)+y\dot{\Theta}$ and $C_D[y, \beta+\gamma(t)]$ is the drag force coefficient accounting for both the spanwise change of the drag force at yaw angle β and incremental yaw angle change $\gamma(t) = \tan^{-1}\left(v(t)/(U'+u(t))\right) \approx v(t)/U'$ (Kimura [1998]).

By ignoring smaller terms in U_r^2 and linearizing $C_D[y, \beta+\gamma(t)]$ as

$C_D(y, \beta)+\left(dC_D(y, \beta)/d\beta\right)\left(v(t,y)/U'\right)$, the strip force dF will reduce to

$$dF = \frac{1}{2}\rho D U'\left[U'+2u(t,y)+2y\dot{\Theta}\right]C_D(y, \beta)dy + \frac{1}{2}\rho D U' v(t,y)\frac{dC_D(y, \beta)}{d\beta} \tag{6.3}$$

The second part of 6.3 is the same as was derived by Kimura (1998). From here, we can employ the concept of self-excited forces:

The aerodynamic damping term can be derived by considering only the self-excited term in the torque moment. The self-excited force term arises from the structural motion under the action of the wind and includes only the velocity term $\dot{\Theta}$. Considering only the self-excited term $\rho D U' y C_D(y, \beta)dy\dot{\Theta}$, the self-excited torque moment becomes:

$$M_t = \rho D U'\left(\int_0^L y^2 C_D(y, \beta)dy\right)\dot{\Theta} \tag{6.4}$$

Substituting 6.4 into 6.1, and collecting terms gives:

$$J\ddot{\Theta} + \left[2\omega_o J\xi - \rho D U'\int_0^L y^2 C_D(y, \beta)dy\right]\dot{\Theta} + K_\phi\Theta = 0 \tag{6.5}$$

The aerodynamic damping is defined as the condition when the term inside the brackets equals zero:

$$\xi_{aero} = \frac{\rho D U'}{2\omega_o J}\int_0^L y^2 C_D(y, \beta)dy \tag{6.6}$$

Notice the consistency between the above form and 2.65. Also, if the original strip assumption is employed, $C_D(y, \beta)$ becomes constant along y and simply equal to C_D. The above form will then reduce to 2.33.

To retain a similar form to Kimura (1998), 6.6 can be reduced to (although not equivalent to)

$$\xi_{aero} = \frac{\rho D U' \cos\beta}{2\omega_o J} \int_0^L y^2 C_D(y, \beta=0)\, dy \tag{6.7}$$

where the perpendicular component $U' \cos\beta$ is used as the effective wind velocity and the normal force distribution is taken as the value for $\beta=0$. Making this simplification essentially eliminates any contribution from the lateral component $v(t)$.

To obtain the drag force distribution, experimental results were used from Kimura et al.'s (1998) experiments and adjusted to fit our model sections. Adjusting the drag force distribution simply involves multiplying the $C_D(0)$ and $C_D(L)$ values obtained from Section A2 (of Kimura et al.'s experiments) with the ratio of the steady state drag force of our model section over Section A2. The steady-state drag force values for the test sections used in the current experiment were found from ESDU (1986), which are reported for a cantilever type bluff body. Although for the current model sections the presence of the finite length torsional spring likely has the effect of reducing the actual drag force near the support and so reduces the overall drag coefficient, the effect is presumed minimal so that the ESDU (1986) steady-state drag force can be employed. For Section A2, steady-state drag coefficients are obtained from the test data at 0° yaw angle. Following are the values used for the calculation:

Section	C_D	C_D (0, β=0)	C_D (L, β=0)
A2	1.1	1.05	0.96
1	1.9	1.99	1.81
2	1.4	1.46	1.34
3	1.15	1.2	1.1
4	1.6	1.67	1.53
5	1.34	1.4	1.28

Table 6.1 Steady-State Drag Coefficients

Using 6.7, theoretical damping values can be compared with the values obtained from the cosine regression fits. Figures 6.2 (1-5) compare the values for each section at each wind speed. For each section and wind speed, the true wind speed from Figures 4.3 (1-5) was used

to calculate the theoretical aerodynamic damping. The true wind speed used was taken as the average for all the yaw angle for each section and wind speed.

Looking at the results, it is observed that all theoretical damping values are greater than the experimental values. This is contrary to that observed by Huang (1995) who reported lower theoretical values. The table below shows the ratio of theoretical to experimental values for each section and wind speed. For each section and wind speed, the ratio in the table represents the average of all the yaw angles.

Section #	1 m/s	2 m/s	3 m/s	4 m/s	5 m/s	Average
1	1.97	1.99	2.1	2.03	2.06	2.03
2	1.75	1.87	1.75	1.75	1.82	1.81
3	1.99	1.83	1.73	1.81	1.8	1.83
4	1.46	1.58	1.6	1.59	1.66	1.58
5	1.15	1.2	1.26	1.32	1.44	1.27

Table 6.2 Ratio of Theoretical to Experimental Aerodynamic Damping Values

6.2 Lateral Buffeting Calculations Using Experimental Data

As a final investigation, it was desired to examine the effects various different aerodynamic damping ratios had on the overall RMS response of our model sections. From buffeting theory, reducing the overall damping of a system will increase the overall response. The magnitude of this response increase for different overall damping values needs to be investigated to determine if the differences between the experimental, cosine regression, and theoretical values has an appreciable effect on the RMS response. If, say, doubling the total damping, only decreases the peak response by 1%, then it is quite reasonable to assume that the theoretical model can be used without introducing much error. If the increase is the in the order of 10% or higher (for example), then the theoretical model may not be relied upon to give an accurate picture of the response and further study is required.

The first step in setting up the calculations was the selection of an appropriate theoretical model. The model selected was similar to Kimura et al.'s (1998) model, except that the exponential forms for the along-wind and lateral coherence were used. A description of the theoretical model can be found in Appendix C and will not be discussed here.

The incident wind parameters were selected for the models in an attempt to represent a realistic wind model. For this, three different wind cases were selected using different length scales. For each wind case, a value for L_u^x and I_u was set and the remaining values calculated using the appropriate relationships (see Appendix C). Following is a table describing the wind characteristics for the wind cases:

Wind Case	L_u^x (m)	L_u^y (m)	L_v^x (m)	L_v^y (m)	I_u (%)	I_v (%)
WC1	0.01	0.0021	0.00012	1.42E-005	10	8.03
WC2	0.02	0.0045	0.00030	4.22E-005	10	8.03
WC3	0.03	0.0070	0.00052	7.98E-005	10	8.03

Table 6.3 Incident Wind Properties for Theoretical Buffeting Calculations

The results from the calculations are presented in Appendix D. Each page presents one section subjected to a particular wind case for all five wind speeds.

The objective of this study was to investigate the effects of changing the aerodynamic damping and how the RMS responses may be subsequently affected. Looking at the results in general, the following comments are summarized:

1. Comparing the RMS values obtained using the experimental damping tests results (or cosine regression equations) with the RMS values obtained using the theoretical damping expressions, it is observed that the noted differences in damping do generally result in significant changes in the RMS values. This trend is consistent for the full range of results. A sample selection of the results comparing RMS responses using the experimental damping results (in this case using the three run average values) with responses using the theoretical damping values are shown in the following table:

Section	Wind Case	Wind Speed (m/s)	Yaw Angle	% difference in damping	% difference in RMS
1	1	1	0	46	29
1	2	3	40	53	66
2	1	2	20	44	30
2	3	4	60	51	31
3	2	1	30	41	9
3	3	5	50	46	31
4	1	2	10	38	40
4	2	3	50	28	26
5	2	4	0	31	43
5	3	5	30	43	75

Table 6.4 Selected Theoretical Buffeting Response Calculations for all Test Sections

Although the above table is only a sample, it demonstrates the importance of an accurate theoretical expression for the aerodynamic damping term as the percent differences reported in the last column are significant.

2. In Section 5.2, it was reported that as the wind speed increased, combined with a decrease in the sectional width to depth ratio, the experimentally obtained aerodynamic damping values fell below the cosine regression curve in the 20° yaw angle range and rose above the regression curve in the 60° yaw angle range. For Sections 4 and 5, the results from the parametric study for wind speeds of 4 and 5 m/s are examined below. The table below compares the differences in calculated RMS values at the critical yaw angles where the experimental results are furthest away from the cosine regression curve:

Section	Wind Case	Wind Speed (m/s)	Yaw Angle	% difference in damping	% difference in RMS
4	1	4	10	17	19
4	1	5	70	48	23
4	2	4	70	43	20
4	2	5	10	15	20

Section	Wind Case	Wind Speed (m/s)	Yaw Angle	% difference in damping	% difference in RMS
4	3	4	10	17	14
4	3	5	60	50	26
5	1	4	20	22	27
5	1	5	60	89	44
5	2	4	60	103	45
5	2	5	20	34	45
5	3	4	20	22	19
5	3	5	70	100	41

Table 6.5 Theoretical Buffeting Response Calculations for Critical Yaw Angle Cases

The percent differences for the RMS values using the experimentally obtained damping versus the damping obtained from cosine regression again illustrate the impact and importance of accurately describing the aerodynamic damping term. The cosine approximation is used based on the existing theoretical framework for aerodynamic damping with varying yaw angle yet when RMS values are compared against the experimentally obtained damping, a noticeable difference is seen. This may be a cause for concern because calculations using existing theory may predict responses significantly different to those actually observed. This final point stresses the need for further investigation of the aerodynamic damping parameter and the development of a more accurate theoretical framework.

Chapter 7
Concluding Remarks

7.1 Suggested Further Study

The model test and subsequent analysis results have provided some interesting areas of study and discussion. Much like any experimental study, however, there are still areas which require further examination in order to more completely understand the processes involved. As a result, the author would like to suggest the following areas which may make interesting further study:

1. To more closely relate the test data in terms of actual bridge response, the same tests as were carried out in this research could be undertaken using sections and test setups which more closely represent true bridge sections. This would lead to a more practical application of the experimental results. Extending this concept, the model sections could be designed to incorporate the stay cables of the bridge.
2. The lateral fluctuating velocity component v is also an area which requires further study. Expressions for S_u and S_w are quite common and readily obtainable from field data, but accurate expressions for S_v are not as common. As well, expressions for the lateral coherence R_w are usually taken to be the same as R_{uu}, and further study is required to determine more accurate models of this parameter as well.
3. The changing spanwise drag force coefficient is also another interesting area. The linearly varying model utilized in this study is a more refined approach than the strip theory, but still should be investigated further for its applicability for different cross-sectional shapes. As well, because spanwise drag force measurements are obtained from sections which are not moving, it would be worthy to investigate how the spanwise drag force distribution changes with time on a laterally oscillating body.

4. An investigation into the observed self-excited oscillations to further clarify the conditions of their occurrence also serves as an interesting subject. This might be accomplished by utilizing flow visualization techniques whereby the actual flow pattern around the oscillating body may be observed and studied.

7.2 Conclusion

At the outset of the experimental testing, it was desired to examine how a changing yaw angle affected the lateral aerodynamic damping for various bluff sections in different wind conditions. Results from the experimental testing and data analysis concluded that the validity of the cosine approximation is affected by the sectional width to depth ratio as well as the mean wind speed. The lateral flutter-type instabilities observed were interesting and require further consideration. The parametric study showed that small changes in the aerodynamic damping can indeed have a noticeable effect on the RMS response. Overall results suggest that a more rigorous study is required for the lateral aerodynamic damping case.

References

1. Winter, H., "Flow Phenomena on Plates and Airfoils of Short Span", National Advisory Committee for Aeronautics, Technical Memorandum No. 798, July 1936.

2. Liepmann, H.W., "On the Application of Statistical Concepts to the Buffeting Problem", Journal of Aeronautical Sciences, Vol. 19, No. 12, pp. 793-800, December 1952.

3. Milne-Thomson, L.M., Theoretical Aerodynamics, 2nd ed., MacMillan and Company Ltd., London, 1952.

4. Bisplinhoff, R.L., Ashley, H., and Halfman, R.L., Aeroelasticity, Addison-Wesley, Cambridge, Massachusetts, 1955.

5. Eringen, A.C., "Response of Beams and Plates to Random Loads", Journal of Applied Mechanics, Vol. 20, pp. 46-52, March 1957.

6. Davenport, A.G., "The Spectrum of Horizontal Gustiness Near the Ground in High Winds", Quarterly Journal of the Royal Meteorological Society, Vol. 87, pp. 194-211, April 1961a.

7. Davenport, A.G., "The Application of Statistical Concepts to the Wind Loading of Structures", Proc. ICE, Vol. 19, pp. 449-472, August 1961b.

8. Davenport, A.G., "The Response of Slender, Line-Like Structures to a Gusty Wind", Proc. ICE, Vol. 23, pp. 389-408, 1962a.

9. Davenport, A.G., "Buffeting of a Suspension Bridge by Storm Winds", Journal of the Structural Division, Proc. ASCE, Vol. 88, No. ST3, pp. 233-268, June 1962b.

10. Sabzevari, A. and Scanlan, R.H., "Aerodynamic Instability of Suspension Bridges", Journal of the Engineering Mechanics Division, Proc. ASCE, Vol. 94, No. EM2, pp. 489-519, April 1968.

11. Davenport, A.G., Isyumov, N., Fader, D.J., and Bowen, P., "An Aeroelastic Study of the Northumberland Straits Bridge - Cantilevered Concrete Design", BLWT-3-69, University of Western Ontario, May 1969.

12. Roberts, J.B. And Surry, D., "Coherence of Grid-Generated Turbulence", Journal of the Engineering Mechanics Division, Proc. ASCE, Vol. 99, No. EM6, pp. 1227-1245, December 1973.

13. ESDU, "Characteristics of Atmospheric Turbulence Near the Ground. Part III: Variations in Space and Time for Strong Winds (Neutral Atmosphere)", Engineering Sciences Data, Item No. 75001, Engineering Sciences Data Unit, London, 1975.

14. Irwin, H.P.A.H., "Wind Tunnel and Analytical Investigations of the Response of Lions' Gate Bridge to a Turbulent Wind", National Research Council, NAE-LTR-LA-210, June 1977.

15. McCormick, B.W., Aerodynamics, Aeronautics, and Flight Mechanics, John Wiley & Sons, New York, p. 281, 1979.

16. Panofsky, H.A., and Dutton, J.A., Atmospheric Turbulence: Models and Methods for Engineering Applications, John Wiley & Sons, New York, 1984.

17. ESDU, "Mean Fluid Forces and Moments on Rectangular Prisms: Surface-Mounted Structures in Turbulent Shear Flow", Engineering Sciences Data, Item No. 80003, Amendment A, Engineering Sciences Data Unit, London, 1986.

18.Xie, J., Tanaka, H., Wardlaw, R.L., and Savage, M.G., "Buffeting Analysis of Long Span Bridges Concerning the Wind Directional Effects", Proc. Canada-Japan Workshop on Bridge Aerodynamics, National Research Council Canada, National Aeronautics Establishment, Ottawa, pp. 203-215, September 1989.

19.Kimura, K., "Flat Plate Buffeting in Yawed Wind with Possible Applications to Bridges", Ph.D. Thesis, University of Ottawa, September 1991.

20.Xie, J., Tanaka, H., Wardlaw, R.L., and Savage, M.G., "Buffeting Analysis of Long Span Bridges to Turbulent Wind with Yaw Angle", Journal of Wind Engineering and Industrial Aerodynamics, Vol. 37, No. 1, pp. 65-77, February 1991.

21.Larose, G.L. and Livesey, F.M., "Wind-Tunnel Study of the Pont de Normandie During Construction", Danish Maritime Institute, DMI 92159.03, June 1993.

22.Scanlan, R.H., "Bridge Buffeting by Skew Winds in Erection Stages", Journal of Engineering Mechanics, Proc. ASCE, Vol. 119, No. 2, pp. 251-269, February 1993.

23.Huang, Z.Y., "Buffeting Analysis of Cable-Stayed Bridges During their Erection", M.A.Sc. Thesis, University of Ottawa, 1995.

24.Larsen, S.V. and Livesey, F.M., "Wind-Tunnel Investigations of the Kao Ping Hsi Bridge During Erection", Danish Maritime Institute, DMI 96186, 1997.

25.Kimura, K., Ohara, T., Huang, Z.Y., and Tanaka, H., "Lateral Sway Buffeting of Bridge Decks due to Yawed Wind", Proc. 10th International Conference on Wind Engineering, Copenhagen, Vol. 2, pp. 919-926, June 1999.

Figures

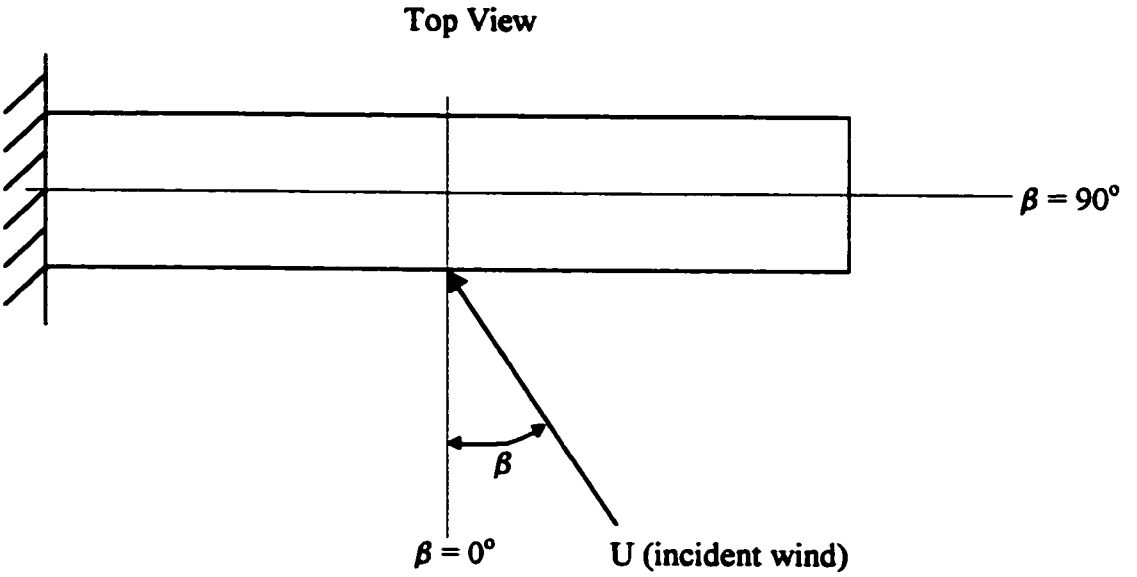

Figure 1.1 – Definition of Yaw Angle

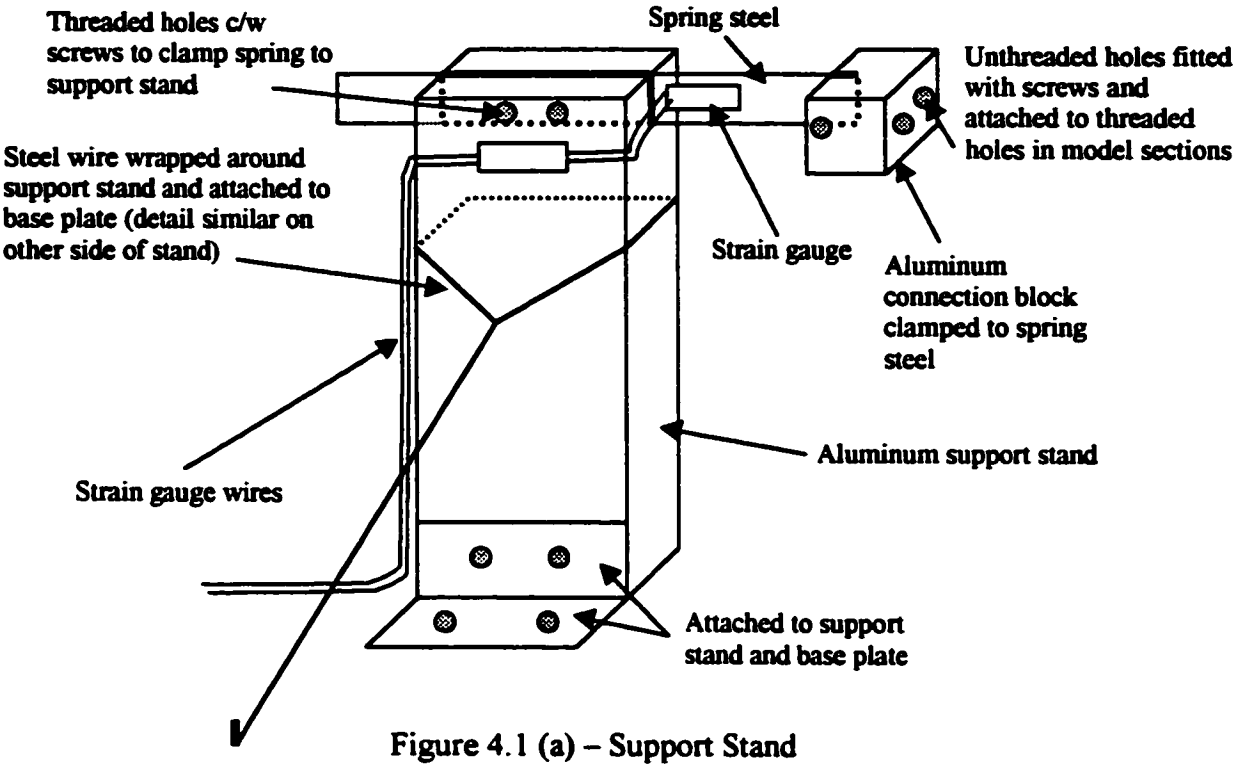

Figure 4.1 (a) – Support Stand

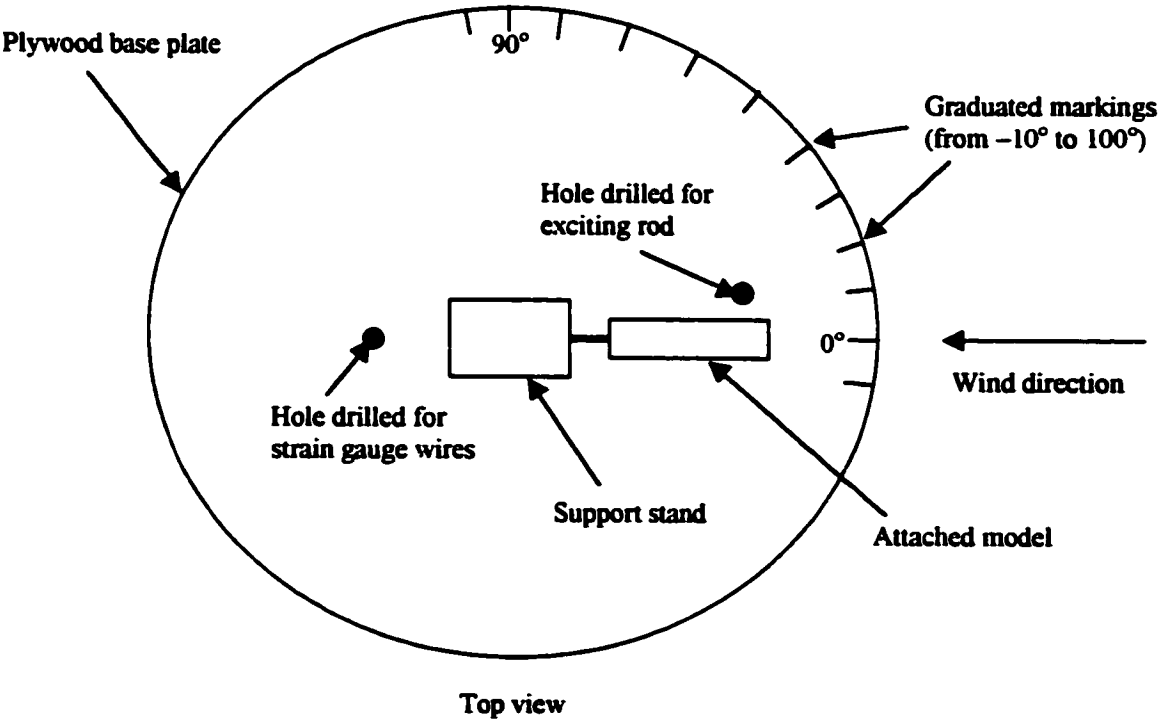

Figure 4.1 (b) – Base Plate

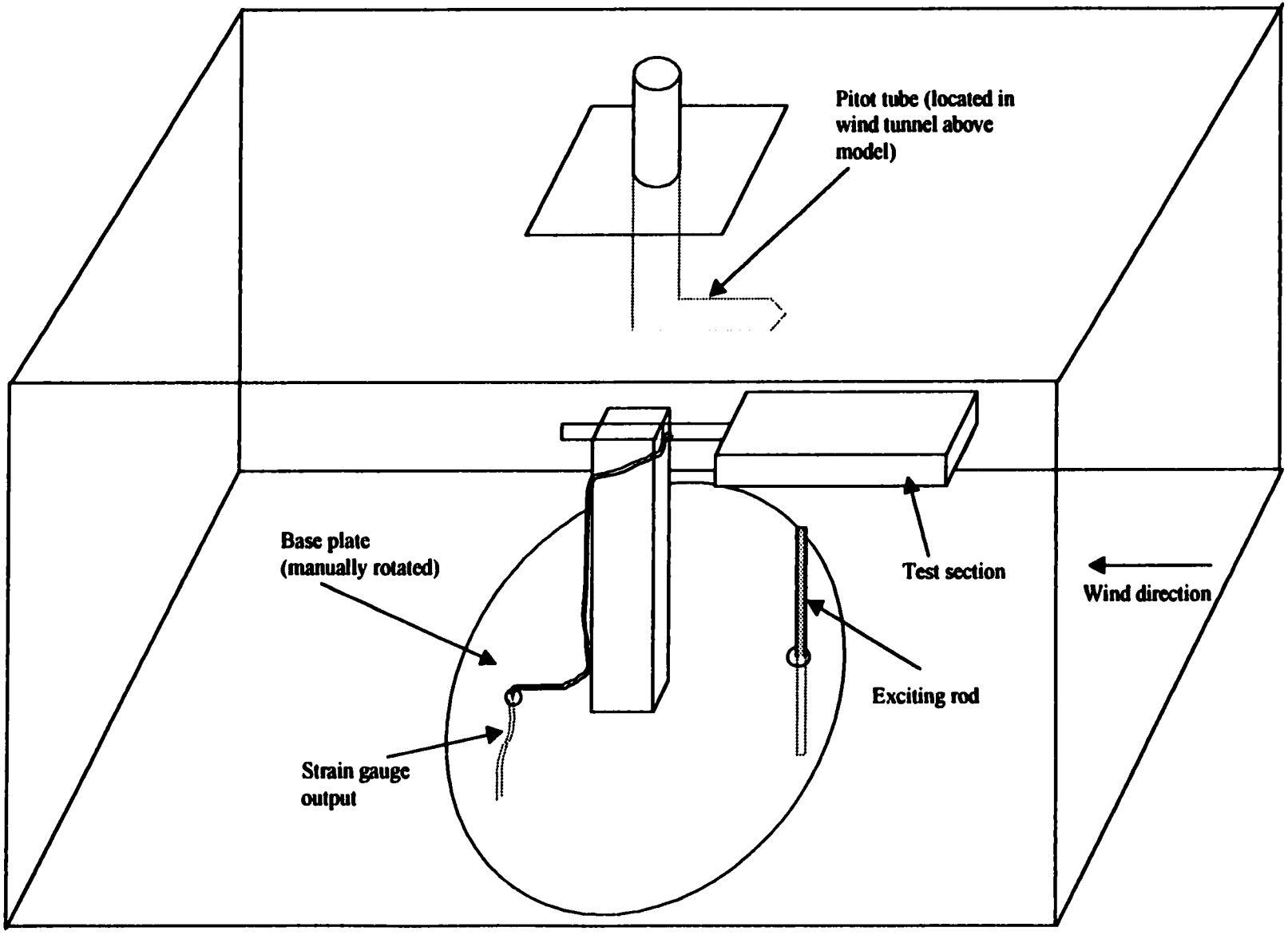

Figure 4.1 (c) – Wind Tunnel Setup

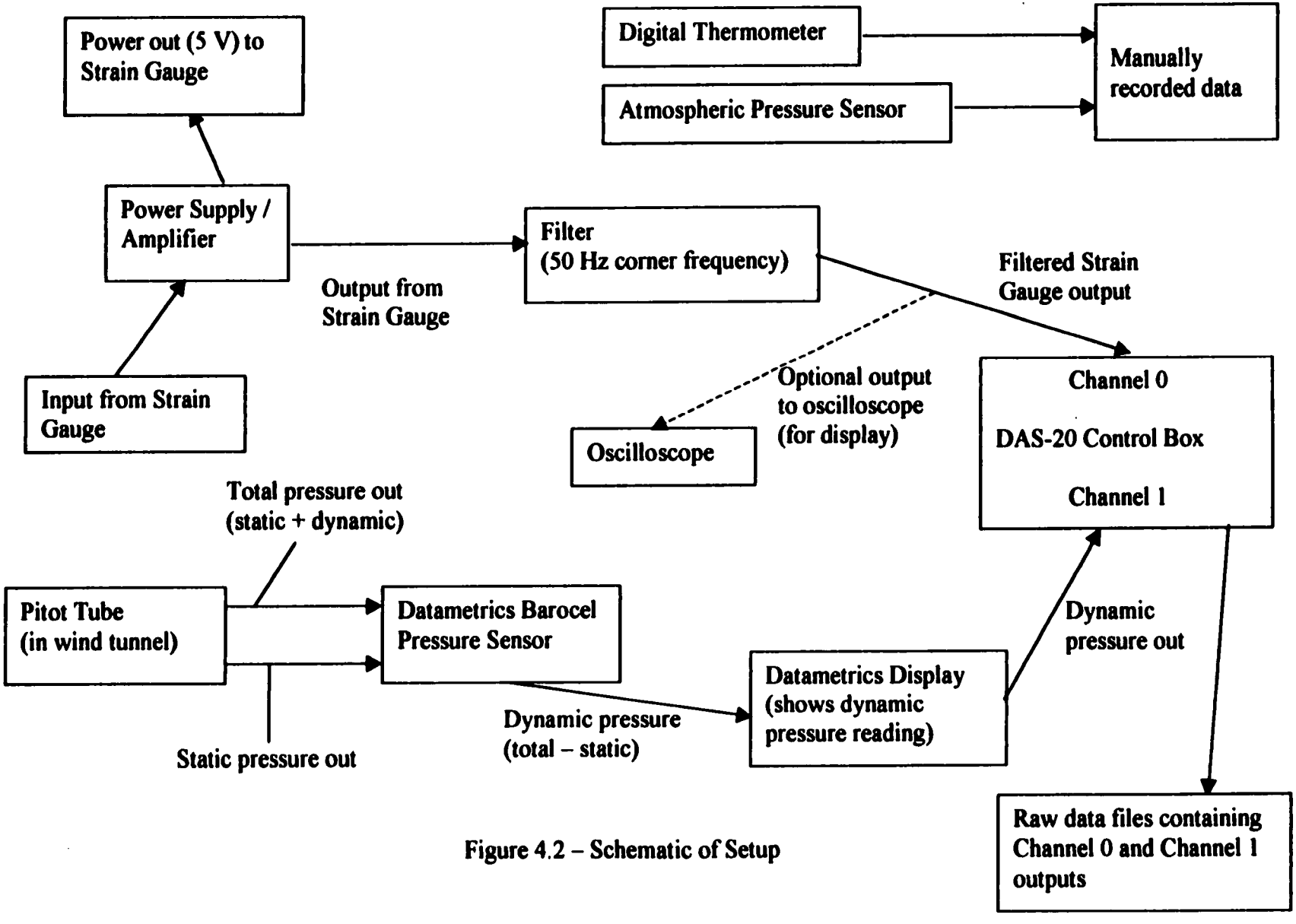

Figure 4.2 – Schematic of Setup

Figure 4.3.1
Section 1: True Wind Speed

Yaw Angle	True Wind Speed				
	1 m/s	2 m/s	3 m/s	4 m/s	5 m/s
-10	1.240	2.079	3.188	4.049	4.943
0	1.237	2.077	3.188	4.049	4.944
10	1.234	2.078	3.205	4.048	4.945
20	1.235	2.076	3.239	4.048	4.946
30	1.233	2.075	3.239	4.047	4.945
40	1.230	2.073	3.239	4.047	4.948
50	1.226	2.072	3.238	4.047	4.947
60	1.226	2.073	3.239	4.047	4.949
70	1.226	2.072	3.239	4.045	4.949
80	1.225	2.072	3.238	4.044	4.948
90	1.224	2.069	3.238	4.045	4.950
100	1.222	2.069	3.237	4.044	4.949
Overall	1.230	2.074	3.227	4.047	4.947

Figure 4.3.2
Section 2: True Wind Speed

Yaw Angle	True Wind Speed				
	1 m/s	2 m/s	3 m/s	4 m/s	5 m/s
-10	1.223	1.992	2.951	3.954	4.936
0	1.222	1.99	2.95	3.954	4.938
10	1.22	1.99	2.951	3.952	4.939
20	1.22	1.988	2.951	3.952	4.938
30	1.217	1.988	2.95	3.952	4.941
40	1.215	1.986	2.952	3.951	4.940
50	1.212	1.985	2.951	3.951	4.943
60	1.209	1.985	2.95	3.95	4.944
70	1.205	1.986	2.951	3.95	4.945
80	1.201	1.984	2.95	3.949	4.945
90	1.198	1.983	2.948	3.948	4.946
100	1.195	1.984	2.948	3.947	4.945
Overall	1.212	1.987	2.950	3.951	4.942

Figure 4.3.3
Section 3: True Wind Speed

Yaw Angle	True Wind Speed				
	1 m/s	2 m/s	3 m/s	4 m/s	5 m/s
-10	1.196	2.065	2.885	4.012	4.895
0	1.195	2.065	2.941	4.011	4.897
10	1.196	2.066	2.984	4.011	4.897
20	1.197	2.066	3.01	4.01	4.897
30	1.198	2.064	3.01	4.009	4.898
40	1.198	2.064	3.01	4.009	4.899
50	1.196	2.064	3.008	4.009	4.9
60	1.196	2.063	3.008	4.009	4.901
70	1.194	2.063	3.007	4.009	4.901
80	1.193	2.062	3.006	4.007	4.901
90	1.191	2.062	3.004	4.007	4.902
100	1.187	2.06	3.003	4.006	4.901
Overall	1.195	2.064	2.990	4.009	4.899

Figure 4.3.4
Section 4: True Wind Speed

Yaw Angle	True Wind Speed				
	1 m/s	2 m/s	3 m/s	4 m/s	5 m/s
-10	1.189	2.07	2.988	3.942	4.947
0	1.188	2.07	2.988	3.941	4.941
10	1.192	2.07	2.987	3.94	4.939
20	1.192	2.069	2.985	3.939	4.939
30	1.191	2.069	2.984	3.937	4.939
40	1.192	2.068	2.984	3.936	4.939
50	1.191	2.068	2.984	3.936	4.94
60	1.19	2.068	2.985	3.938	4.945
70	1.191	2.069	2.989	3.941	4.95
80	1.19	2.07	2.989	3.943	4.953
90	1.188	2.066	2.983	3.935	4.945
100	1.191	2.065	2.981	3.934	4.943
Overall	1.190	2.068	2.986	3.939	4.943

Figure 4.3.5
Section 5: True Wind Speed

Yaw Angle	True Wind Speed				
	1 m/s	2 m/s	3 m/s	4 m/s	5 m/s
-10	1.193	2.072	2.993	4.073	4.937
0	1.198	2.072	2.995	4.074	4.938
10	1.205	2.075	2.996	4.075	4.937
20	1.211	2.075	2.994	4.073	4.935
30	1.216	2.077	2.994	4.07	4.933
40	1.222	2.079	2.995	4.07	4.934
50	1.226	2.082	2.998	4.071	4.937
60	1.229	2.082	3.001	4.073	4.94
70	1.233	2.087	3.007	4.08	4.948
80	1.237	2.09	3.008	4.079	4.947
90	1.238	2.089	3.005	4.075	4.943
100	1.238	2.089	3.003	4.072	4.938
Overall	1.220	2.081	2.999	4.074	4.939

Figure 4.3.1
Section 1: True Yaw Angle

Yaw Angle	True Yaw Angle				
	1 m/s	2 m/s	3 m/s	4 m/s	5 m/s
-10	-10.30	-10.36	-10.34	-10.29	-10.39
0	-0.31	-0.36	-0.33	-0.37	-0.35
10	9.68	9.65	9.72	9.76	9.68
20	19.66	19.66	19.73	19.80	19.75
30	29.65	29.67	29.76	29.86	29.85
40	39.68	39.69	39.87	39.94	39.96
50	49.67	49.70	49.72	50.03	50.07
60	59.67	59.69	59.78	60.08	60.16
70	69.66	69.70	69.78	70.11	70.21
80	79.67	79.71	79.79	80.11	80.24
90	89.67	89.70	89.74	90.08	90.18
100	99.66	99.68	99.71	100.08	100.15

Figure 4.3.2
Section 2: True Yaw Angle

Yaw Angle	True Yaw Angle				
	1 m/s	2 m/s	3 m/s	4 m/s	5 m/s
-10	-10.50	-10.48	-10.44	-10.27	-10.34
0	-0.60	-0.43	-0.46	-0.25	-0.30
10	9.45	9.63	9.55	9.78	9.73
20	19.45	19.64	19.51	19.81	19.80
30	29.68	29.56	29.43	29.86	29.88
40	39.66	39.60	39.45	39.91	39.95
50	49.74	49.63	49.49	49.96	50.03
60	59.74	59.66	59.49	60.03	60.09
70	69.74	69.67	69.52	70.06	70.15
80	79.74	79.67	79.53	80.07	80.17
90	89.73	89.73	89.52	90.06	90.13
100	99.67	99.79	99.50	100.04	100.10

Figure 4.3.3
Section 3: True Yaw Angle

Yaw Angle	True Yaw Angle				
	1 m/s	2 m/s	3 m/s	4 m/s	5 m/s
-10	-10.17	-10.21	-10.23	-10.19	-10.37
0	-0.16	-0.21	-0.22	-0.17	-0.34
10	9.83	9.81	9.79	9.85	9.69
20	19.83	19.81	19.86	19.89	19.75
30	29.83	29.84	29.88	29.93	29.82
40	39.84	39.86	39.91	39.97	39.87
50	49.84	49.87	49.94	50.01	49.92
60	59.84	59.89	59.96	60.04	59.97
70	69.84	69.85	69.97	70.06	70.00
80	79.84	79.85	79.98	80.07	80.02
90	89.84	89.89	89.98	90.06	90.00
100	99.83	99.88	99.97	100.05	99.98

Figure 4.3.4
Section 4: True Yaw Angle

Yaw Angle	True Yaw Angle				
	1 m/s	2 m/s	3 m/s	4 m/s	5 m/s
-10	-10.32	-10.36	-10.33	-10.36	-10.40
0	-0.31	-0.34	-0.30	-0.30	-0.31
10	9.68	9.67	9.73	9.75	9.79
20	19.69	19.70	19.81	20.05	19.98
30	29.70	29.74	29.91	30.03	30.25
40	39.71	39.78	40.00	40.19	40.52
50	49.73	49.82	50.10	50.36	50.77
60	59.73	59.84	60.15	60.46	60.92
70	69.73	69.86	70.17	70.49	70.96
80	79.72	79.82	80.08	80.37	80.75
90	89.71	89.80	90.07	90.35	90.72
100	99.71	99.77	100.00	100.25	100.57

Figure 4.3.5
Section 5: True Yaw Angle

Yaw Angle	True Yaw Angle				
	1 m/s	2 m/s	3 m/s	4 m/s	5 m/s
-10	-10.27	-10.27	-10.33	-10.41	-10.48
0	-0.26	-0.24	-0.27	-0.29	-0.32
10	9.76	9.79	9.79	9.83	9.86
20	19.78	19.86	19.93	20.09	20.24
30	29.81	29.94	30.10	30.41	30.73
40	39.83	40.01	40.25	40.72	41.19
50	49.86	50.07	50.38	50.95	51.53
60	59.87	60.09	60.43	61.04	61.64
70	69.85	70.05	70.34	70.88	71.37
80	79.85	80.01	80.26	80.70	81.14
90	89.84	89.98	90.20	90.60	91.00
100	99.83	99.96	100.16	100.54	100.91

Figure 4.5.1
Aero Damping vs. Angle
Section 1 - 5 m/s

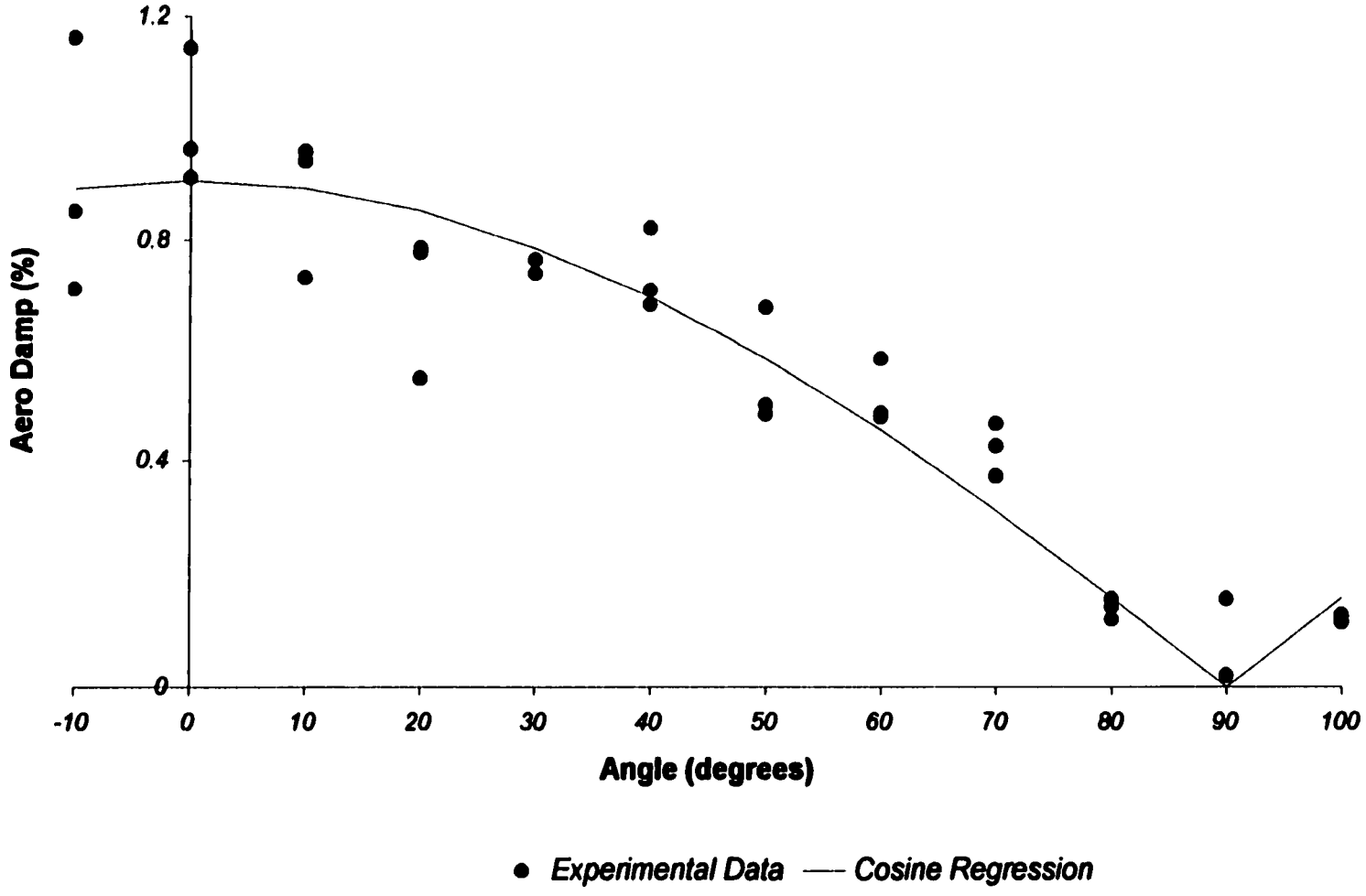

Figure 4.5.2
Aero Damping vs. Angle
Section 1 - 4 m/s

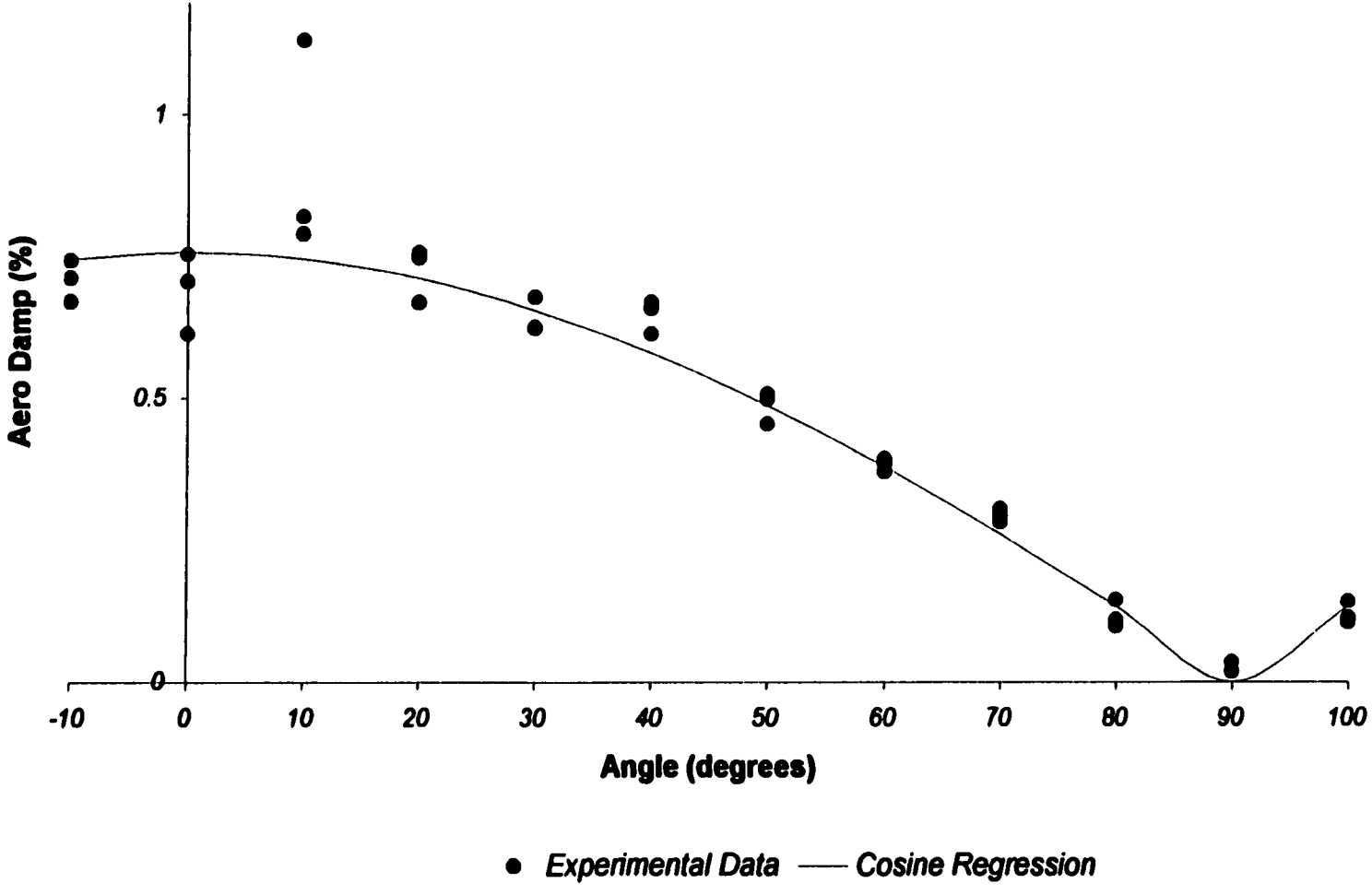

Figure 4.5.3
Aero Damping vs. Angle
Section 1 - 3 m/s

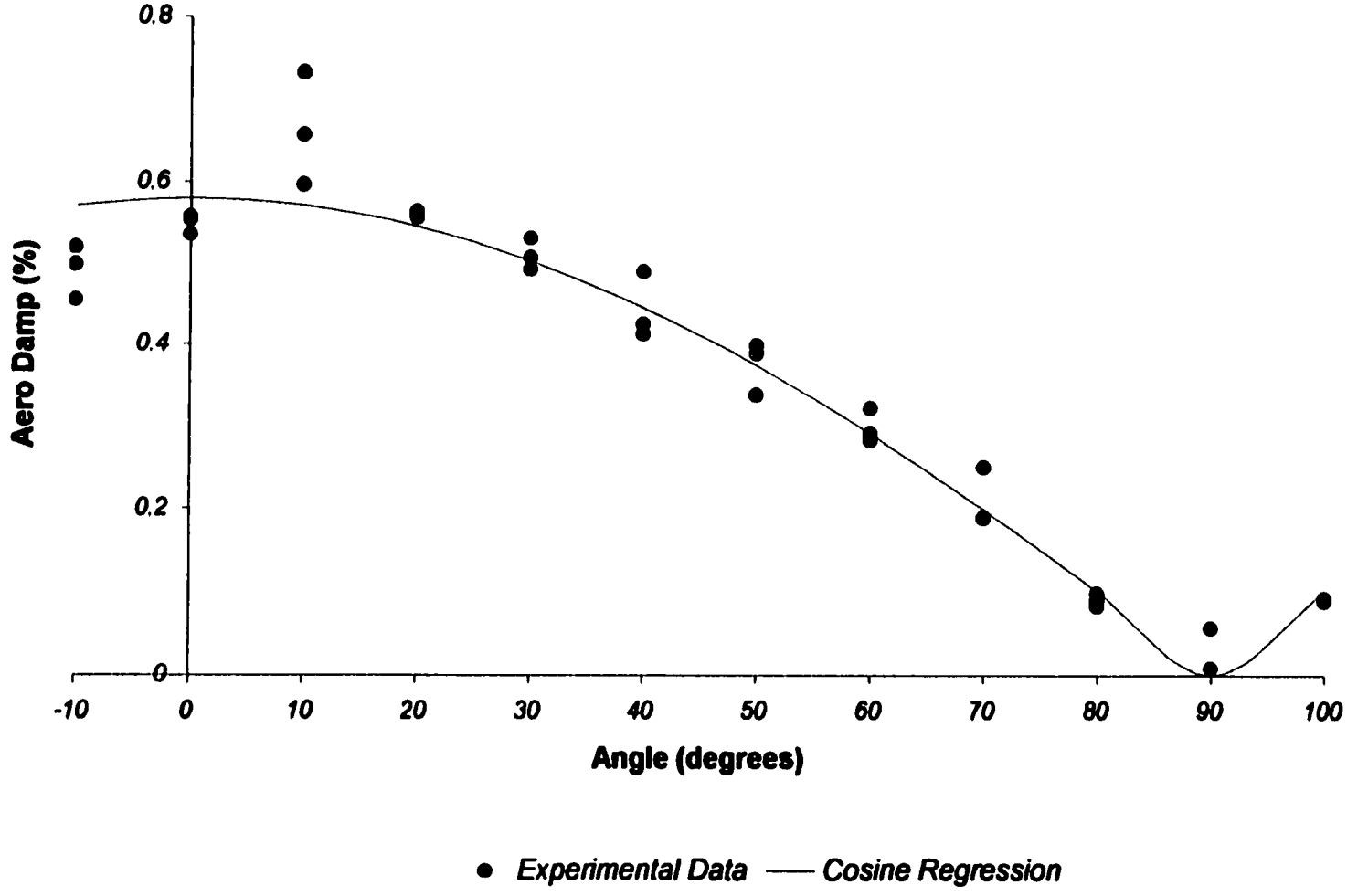

Figure 4.5.4
Aero Damping vs. Angle
Section 1 - 2 m/s

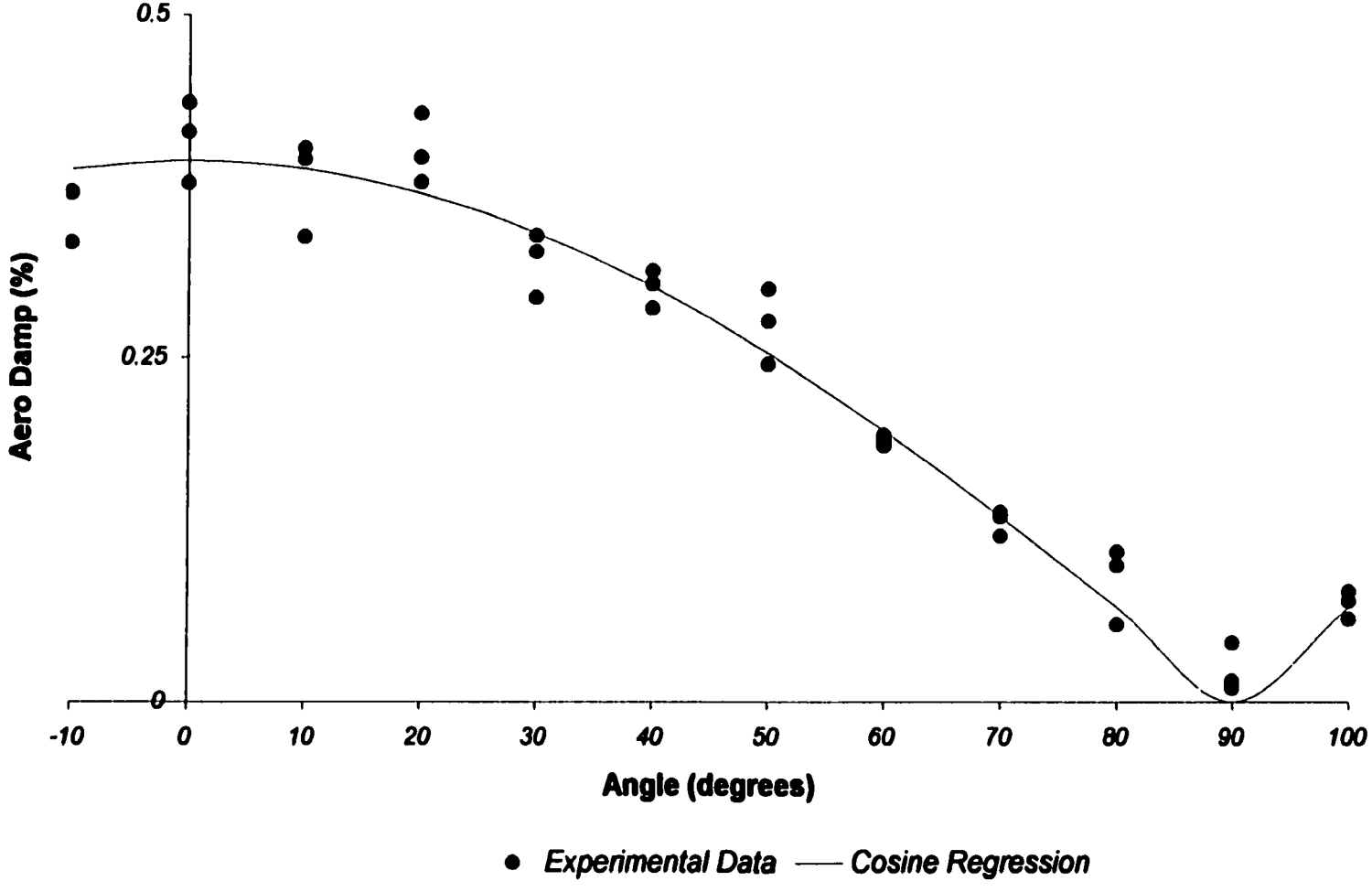

Figure 4.5.5
Aero Damping vs. Angle
Section 1 - 1 m/s

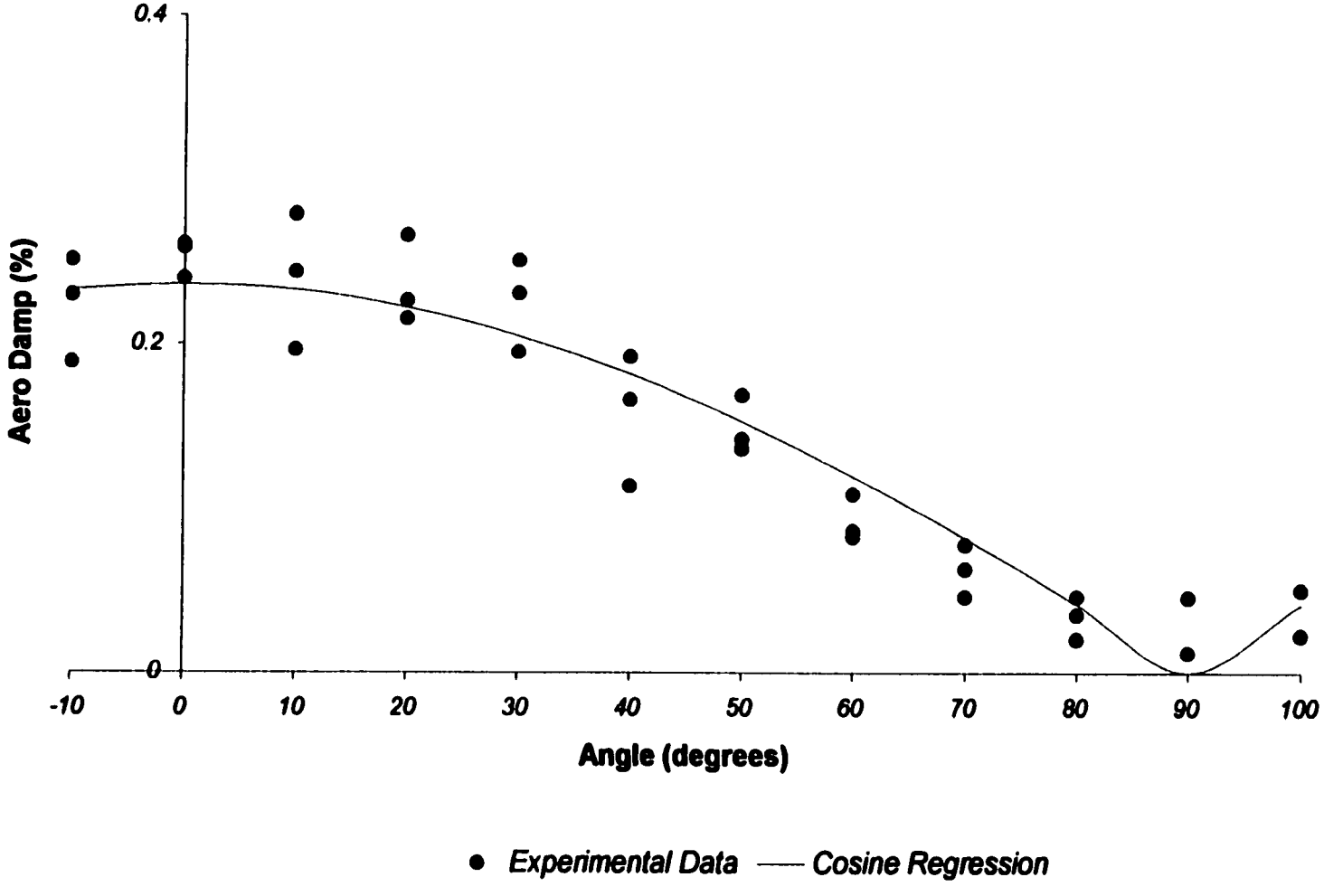

Figure 4.5.6
Aero Damping vs. Angle
Section 2 - 5 m/s

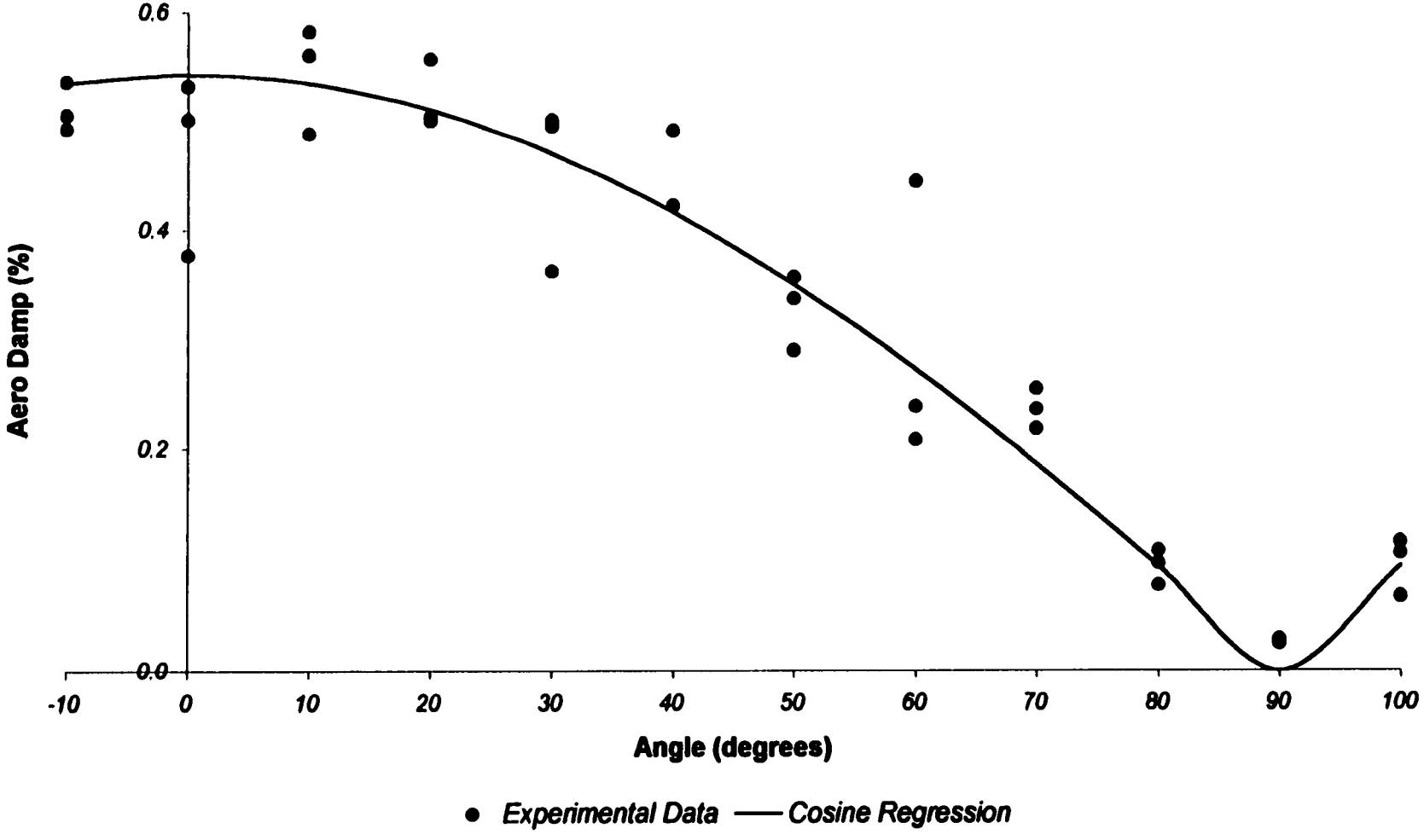

Figure 4.5.7
Aero Damping vs. Angle
Section 2 - 4 m/s

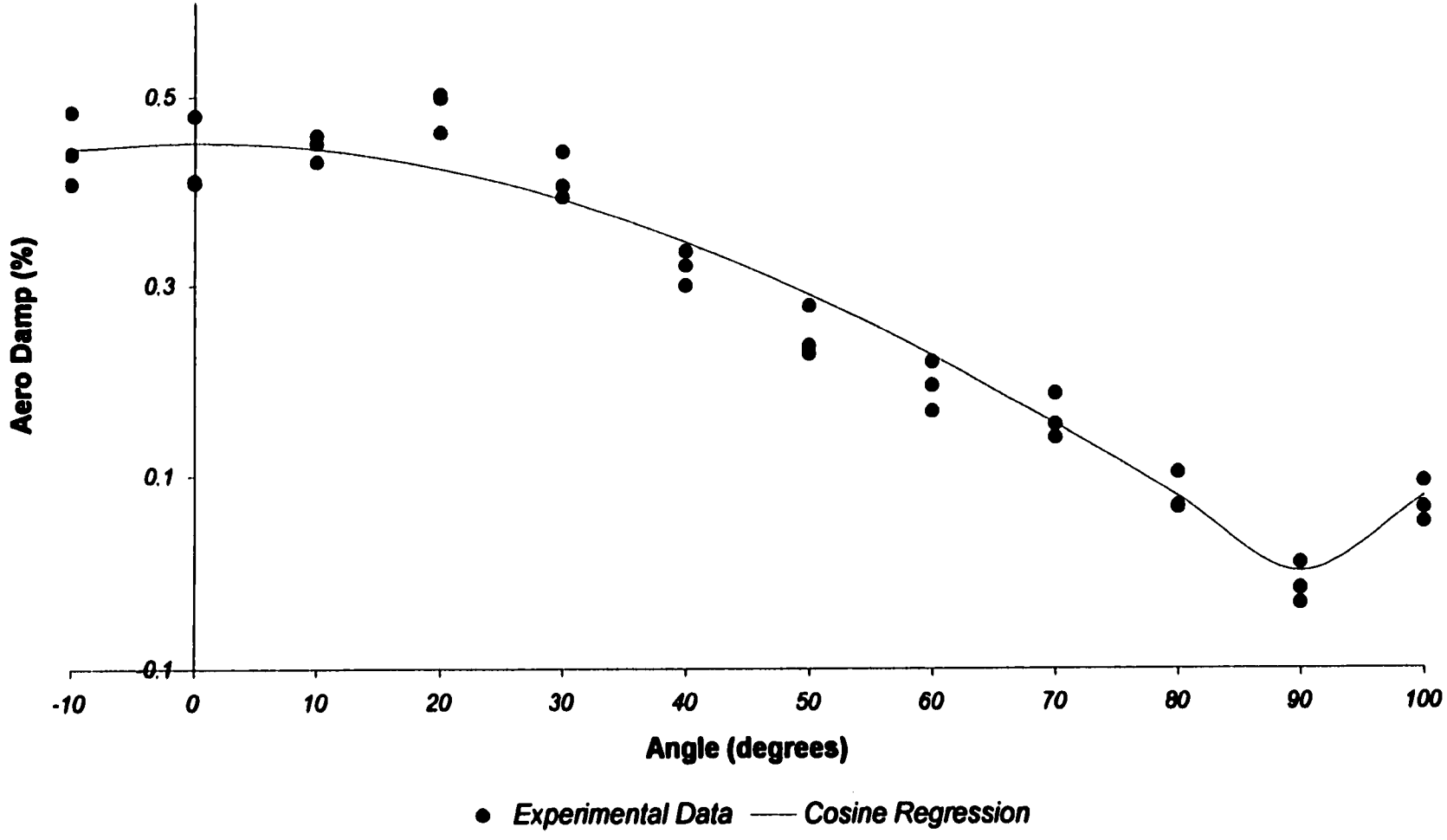

Figure 4.5.8
Aero Damping vs. Angle
Section 2 - 3 m/s

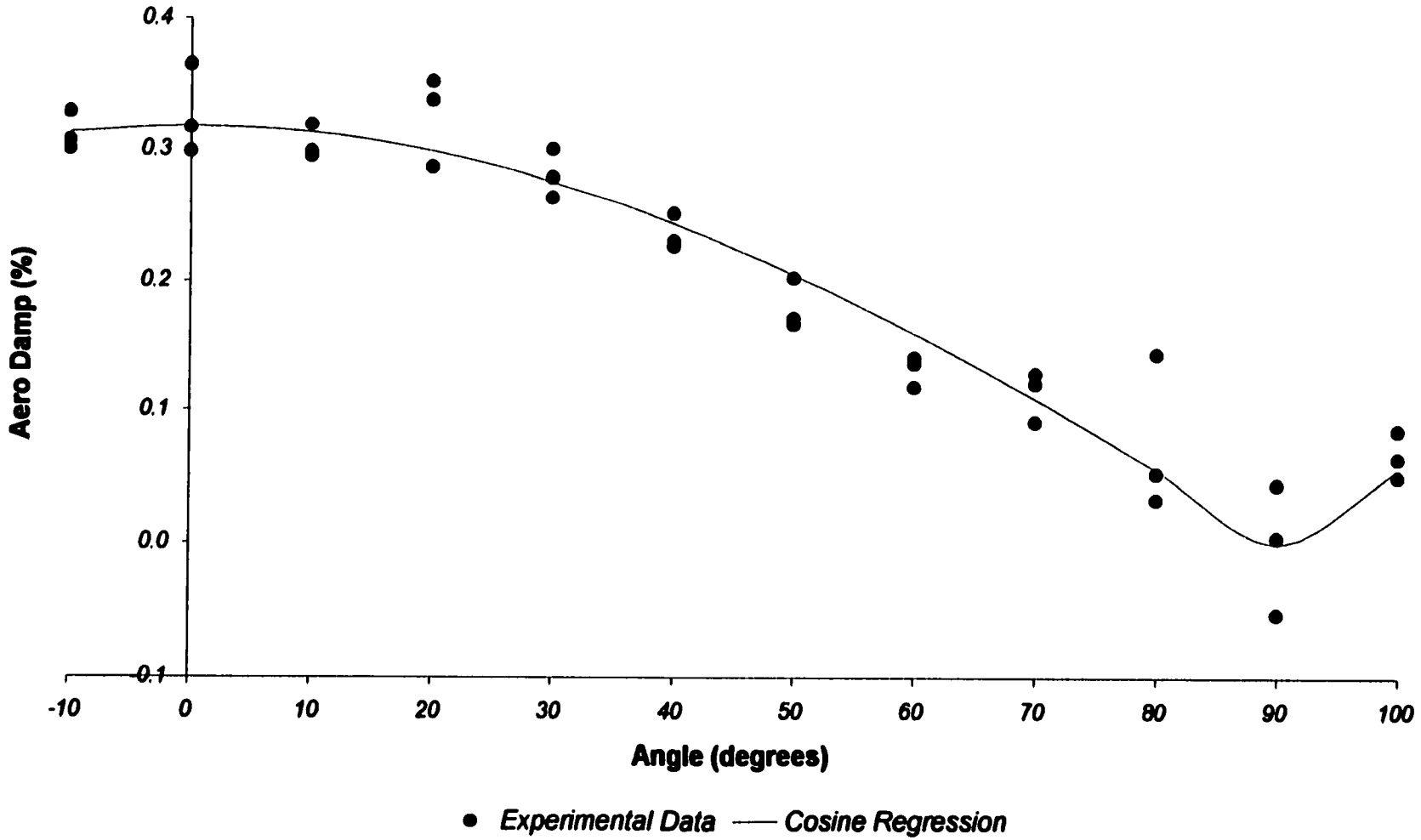

Figure 4.5.9
Aero Damping vs. Angle
Section 2 - 2 m/s

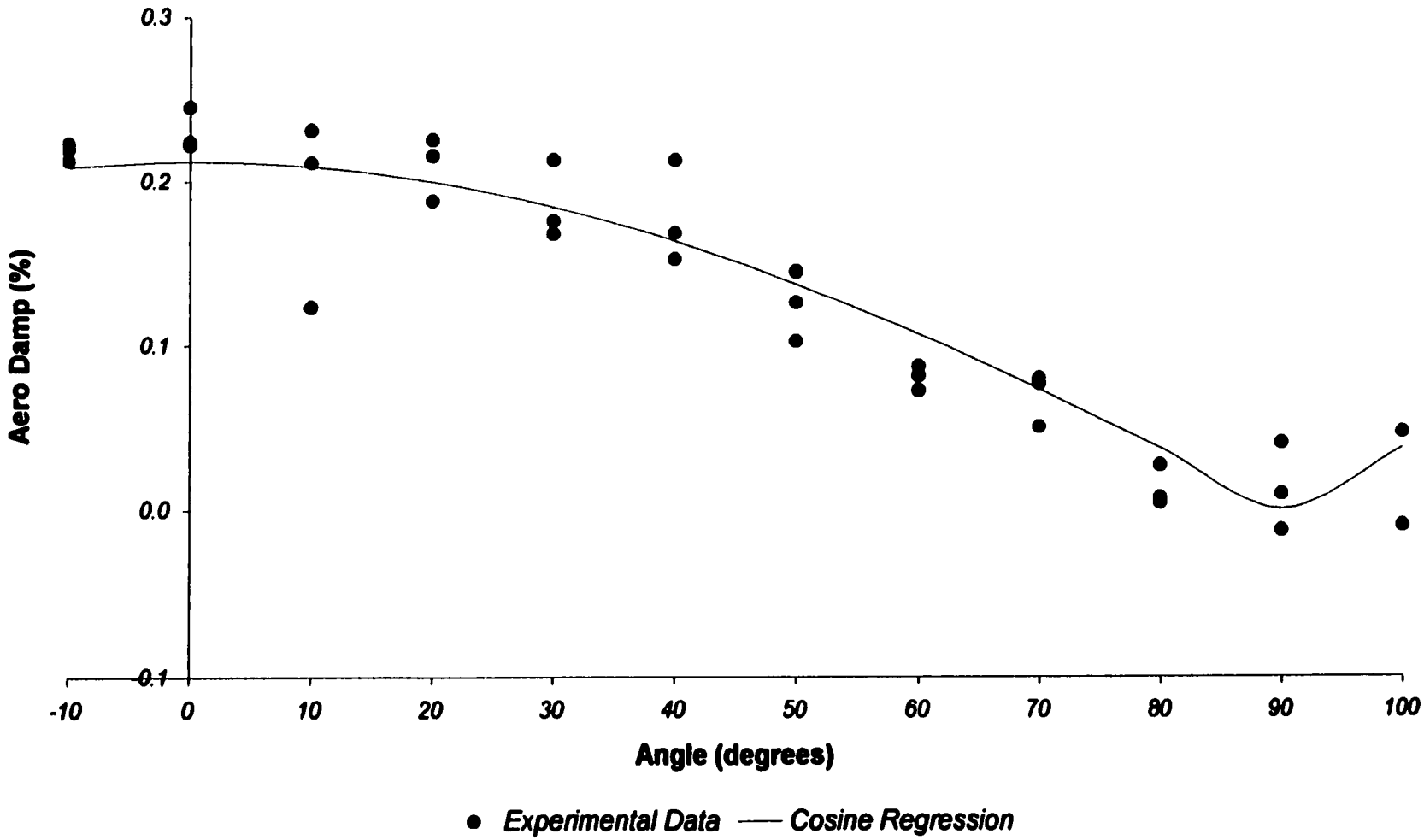

Figure 4.5.10
Aero Damping vs. Angle
Section 2 - 1 m/s

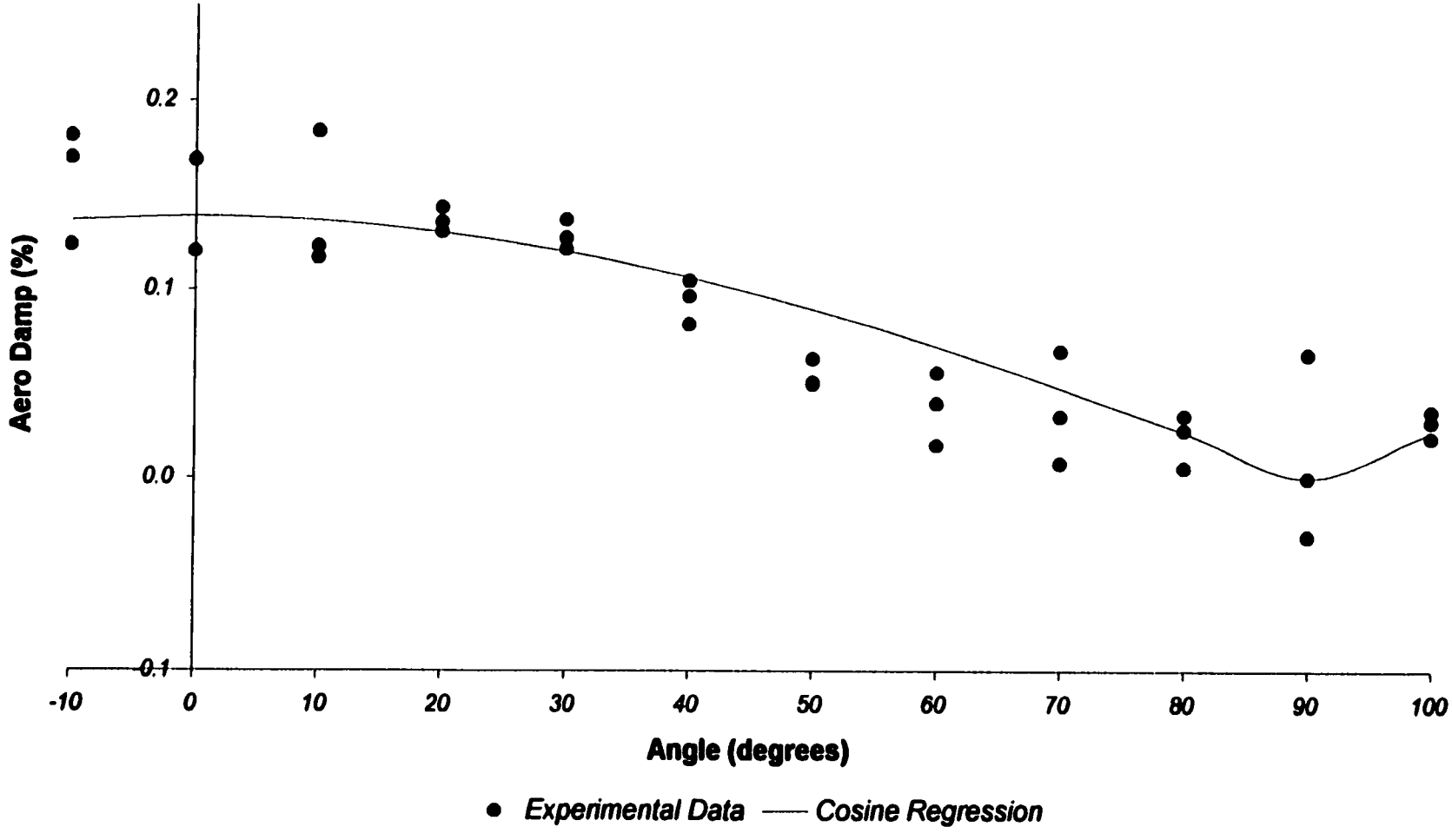

Figure 4.5.11
Aero Damping vs. Angle
Section 3 - 5 m/s

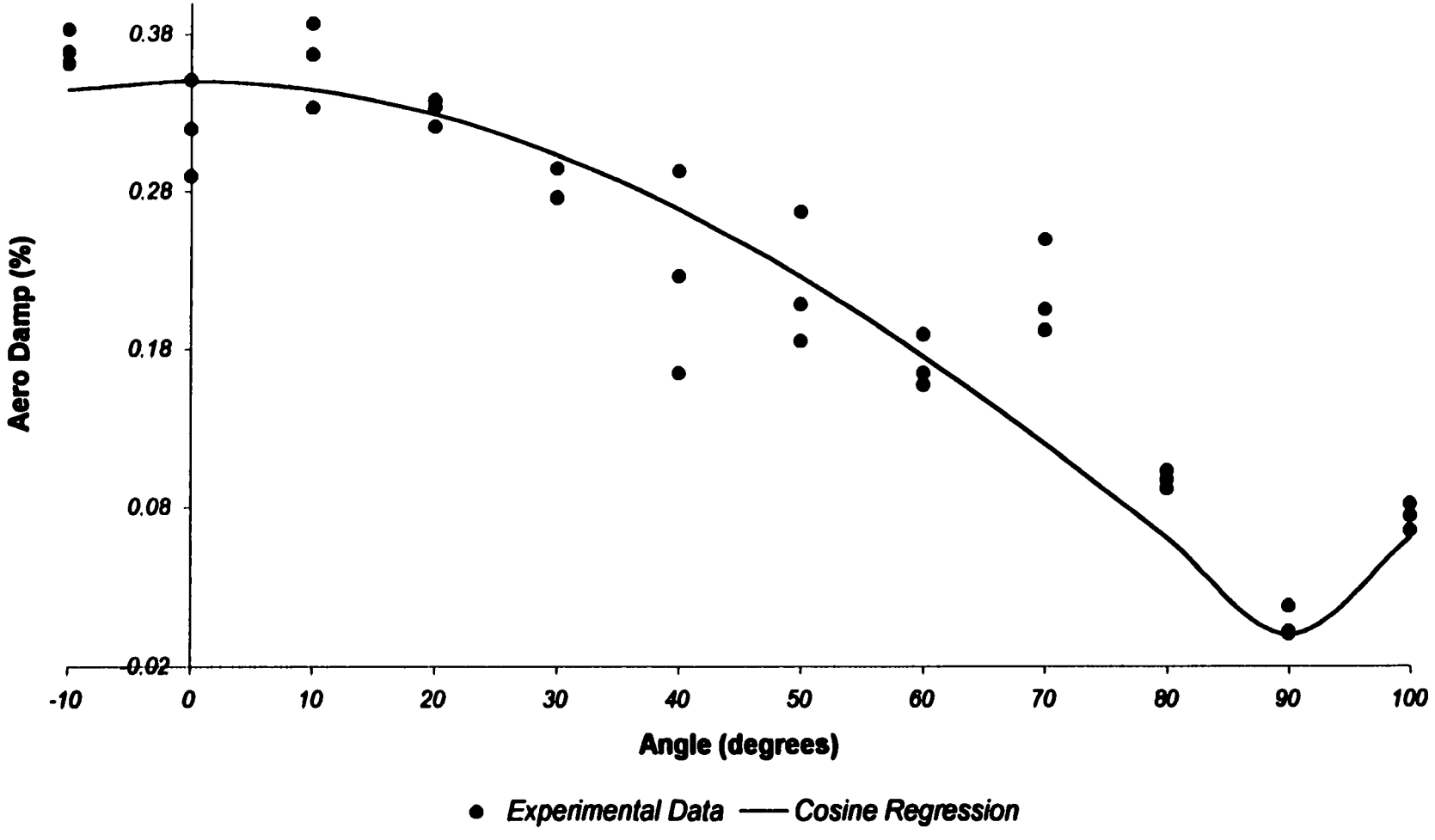

Figure 4.5.12
Aero Damping vs. Angle
Section 3 - 4 m/s

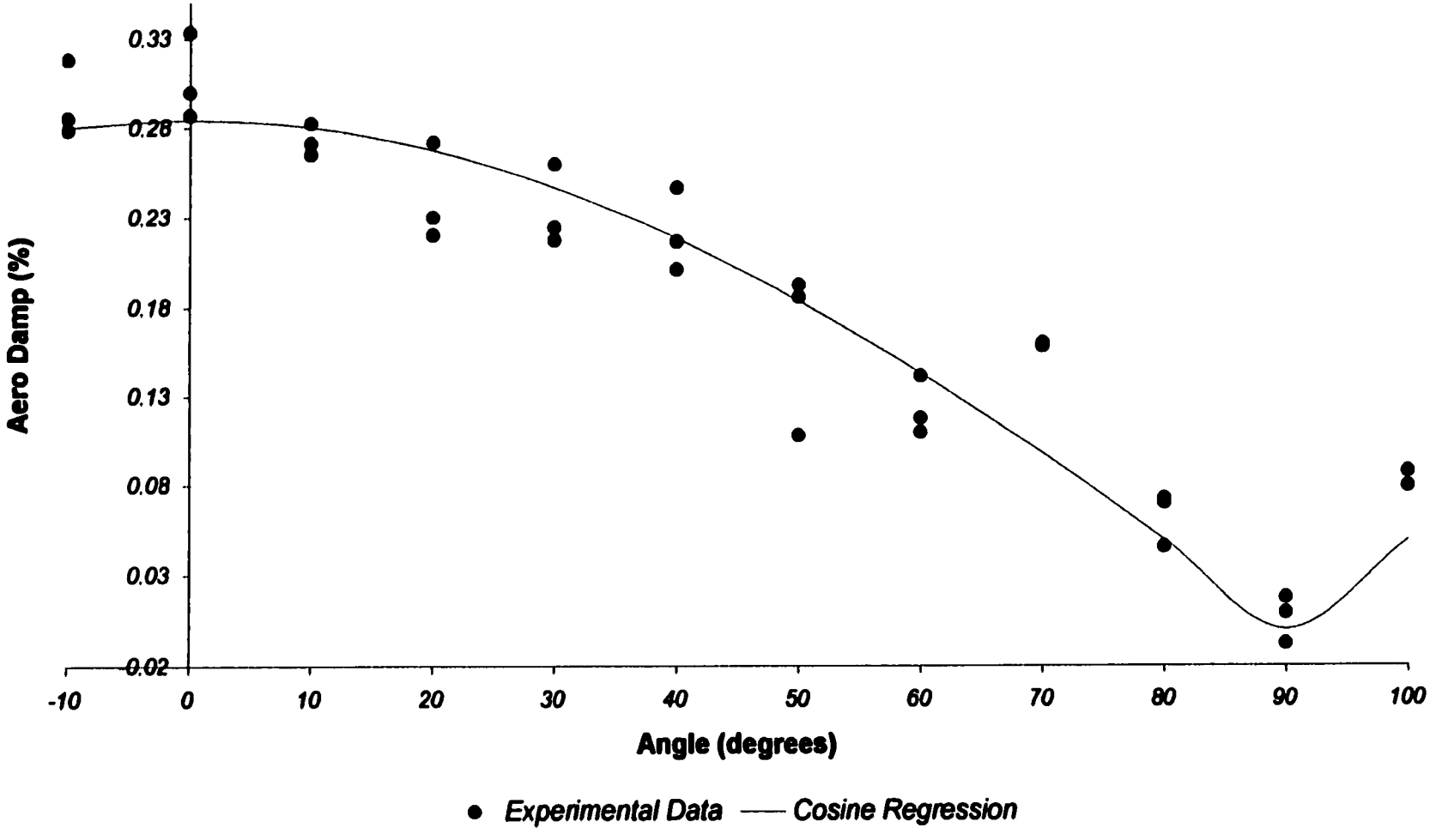

Figure 4.5.13
Aero Damping vs. Angle
Section 3 - 3 m/s

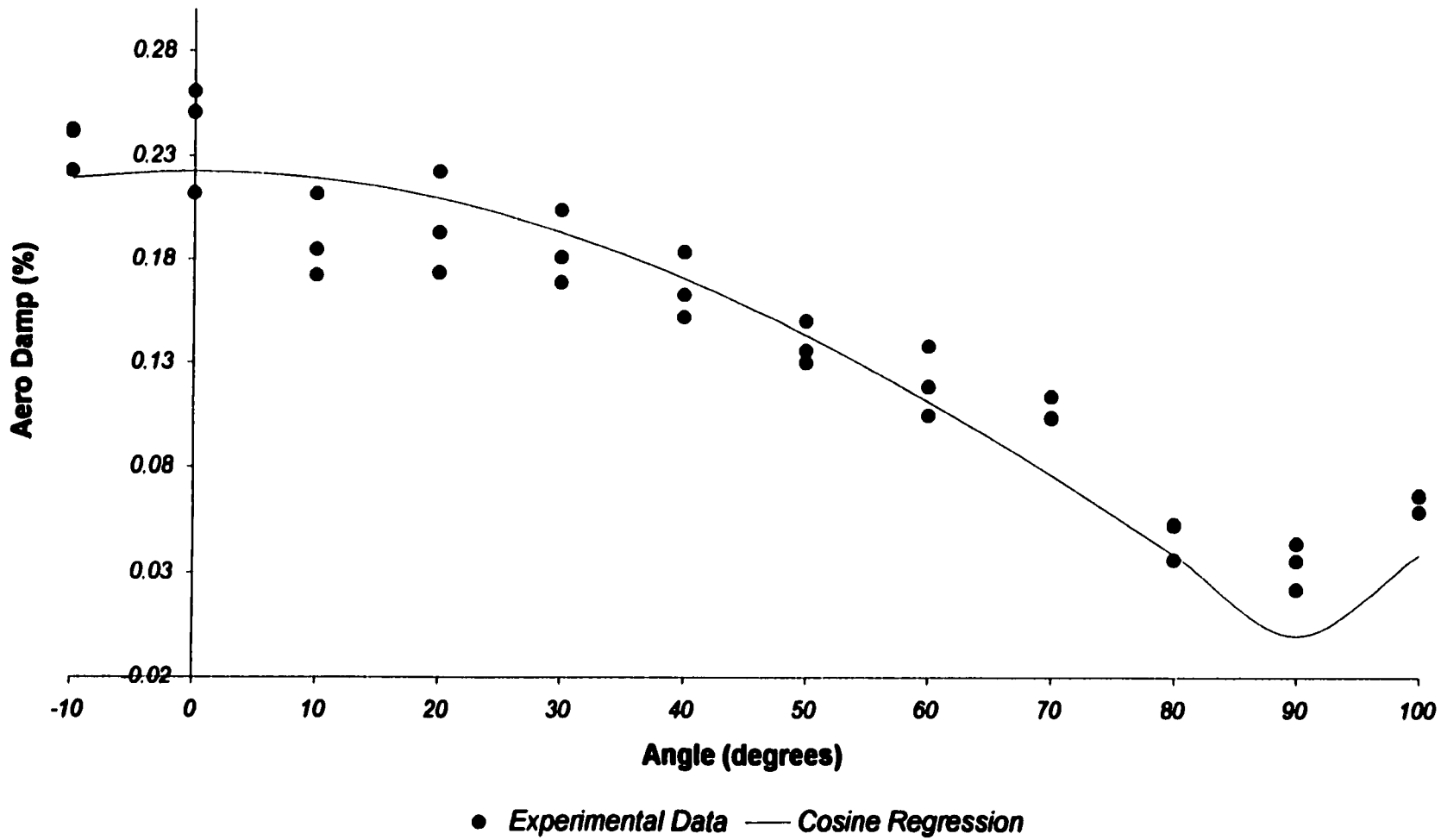

Figure 4.5.14
Aero Damping vs. Angle
Section 3 - 2 m/s

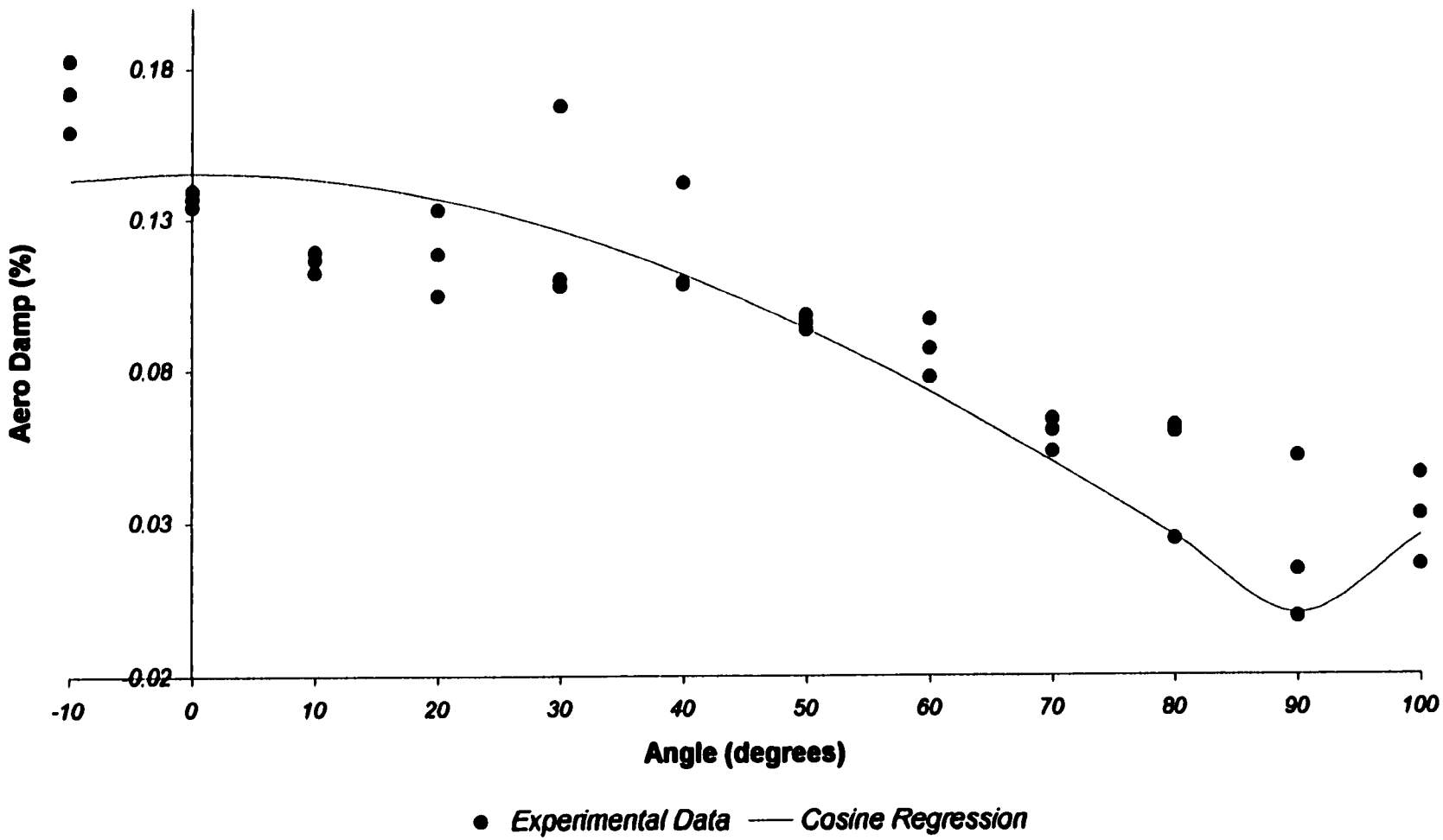

Figure 4.5.15
Aero Damping vs. Angle
Section 3 - 1 m/s

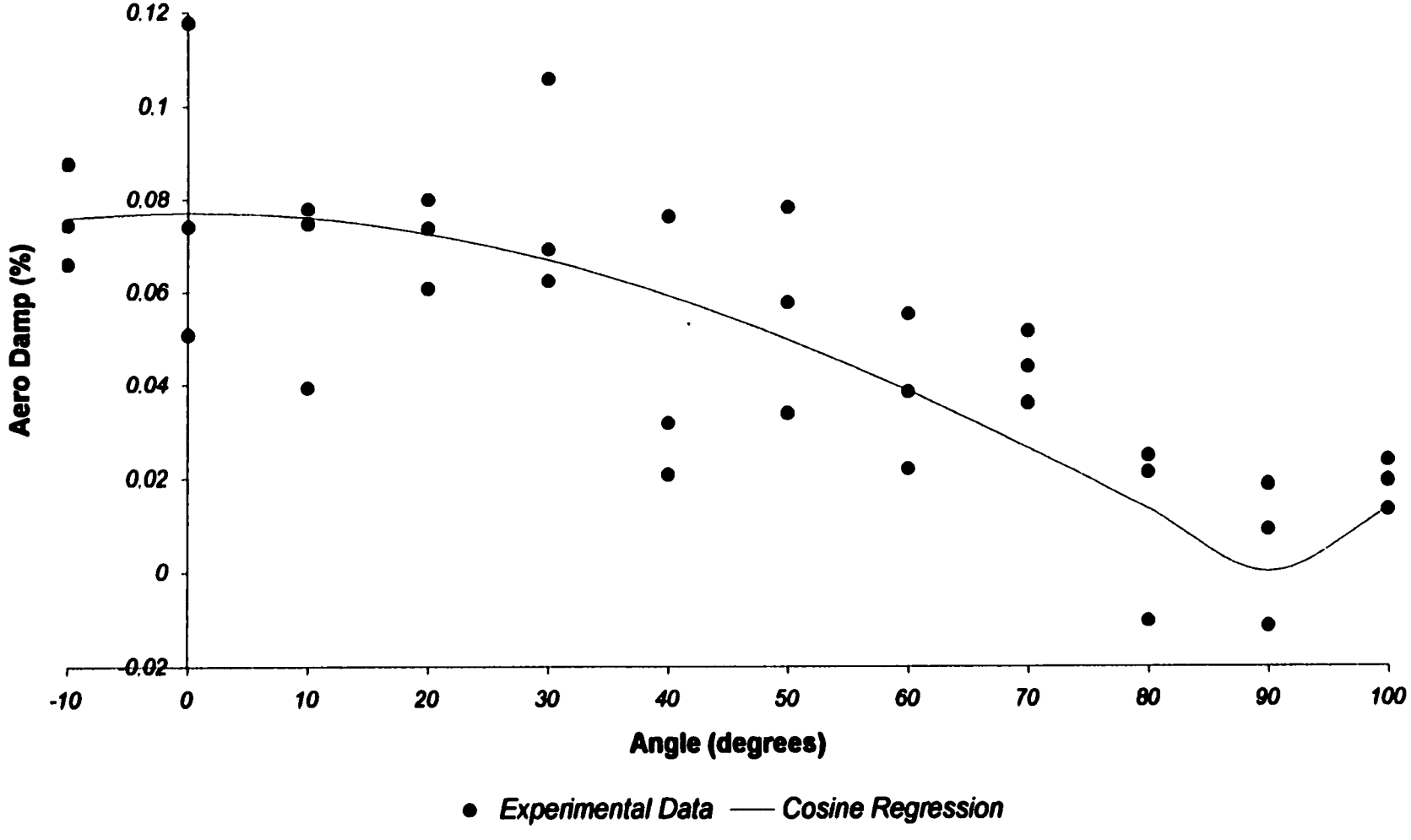

Figure 4.5.16
Aero Damping vs. Angle
Section 4 - 5 m/s

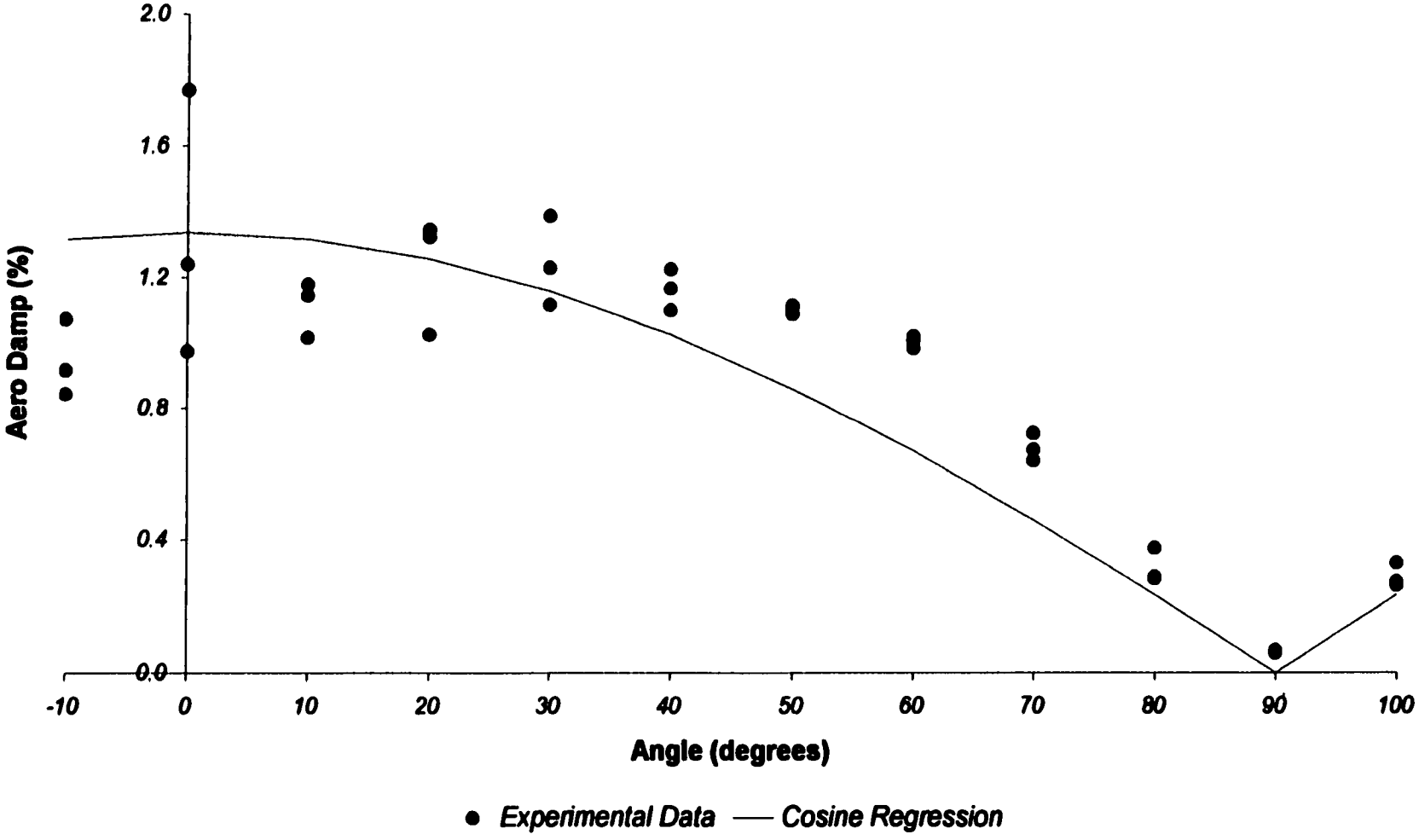

Figure 4.5.17
Aero Damping vs. Angle
Section 4 - 4 m/s

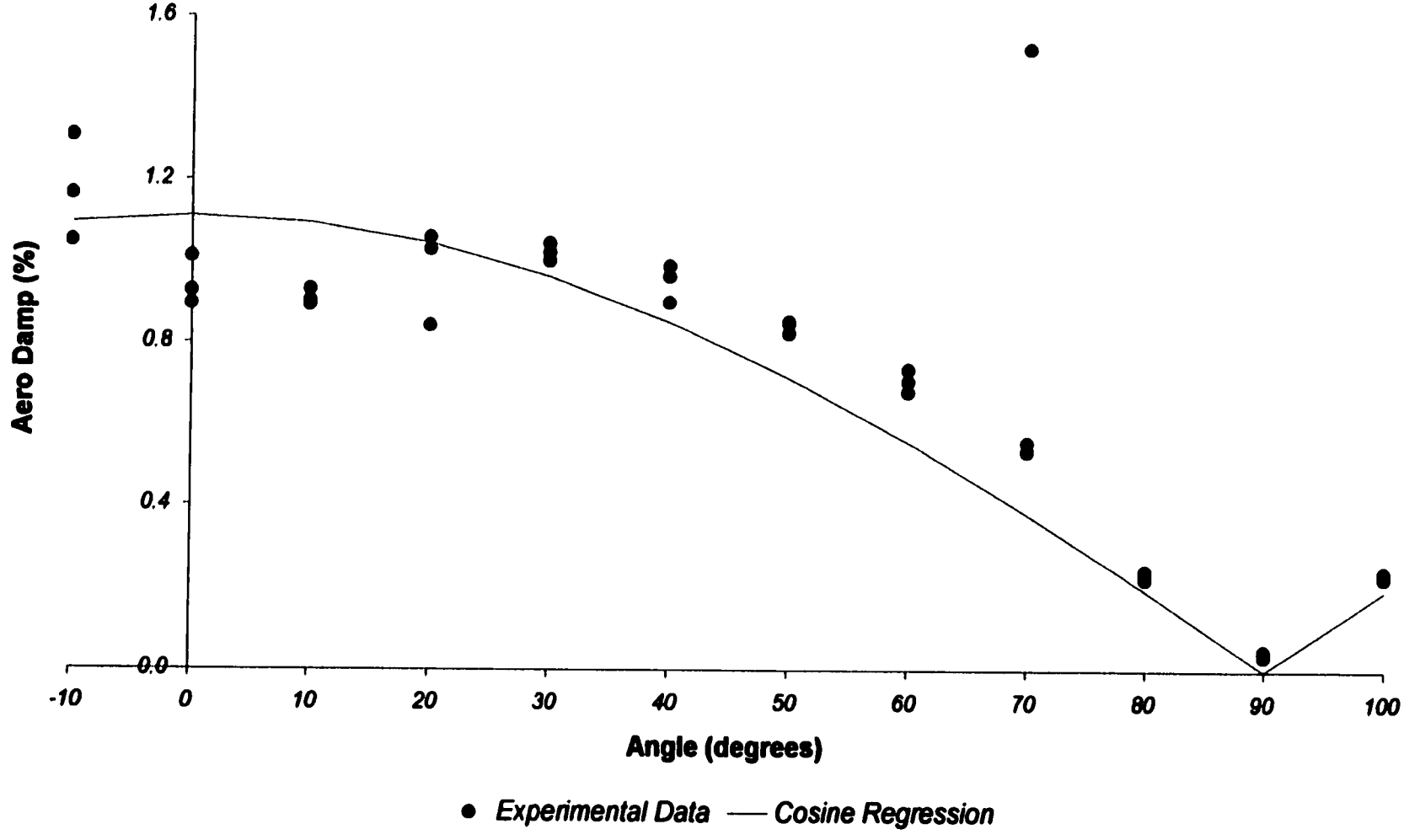

Figure 4.5.18
Aero Damping vs. Angle
Section 4 - 3 m/s

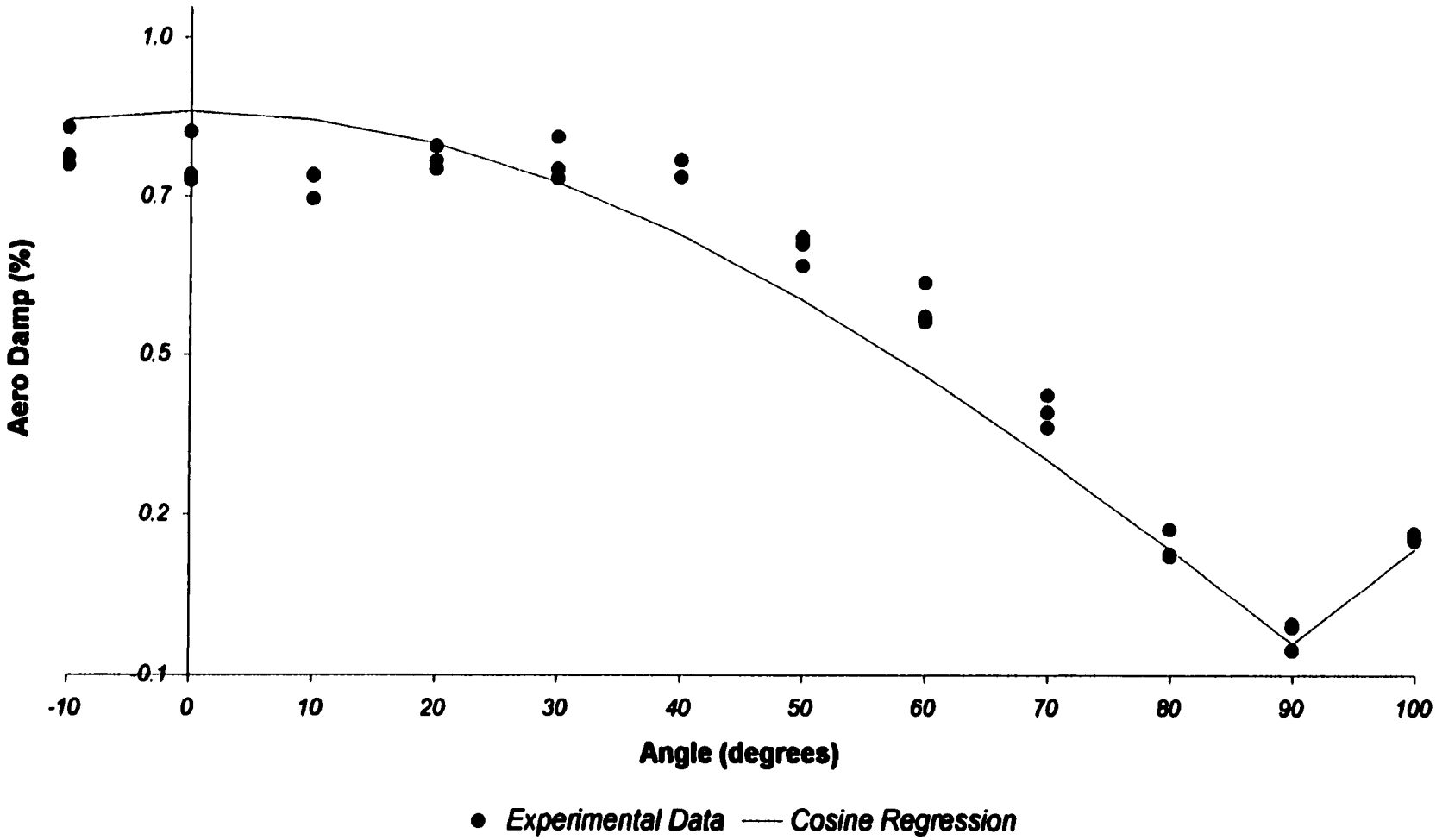

Figure 4.5.19
Aero Damping vs. Angle
Section 4 - 2 m/s

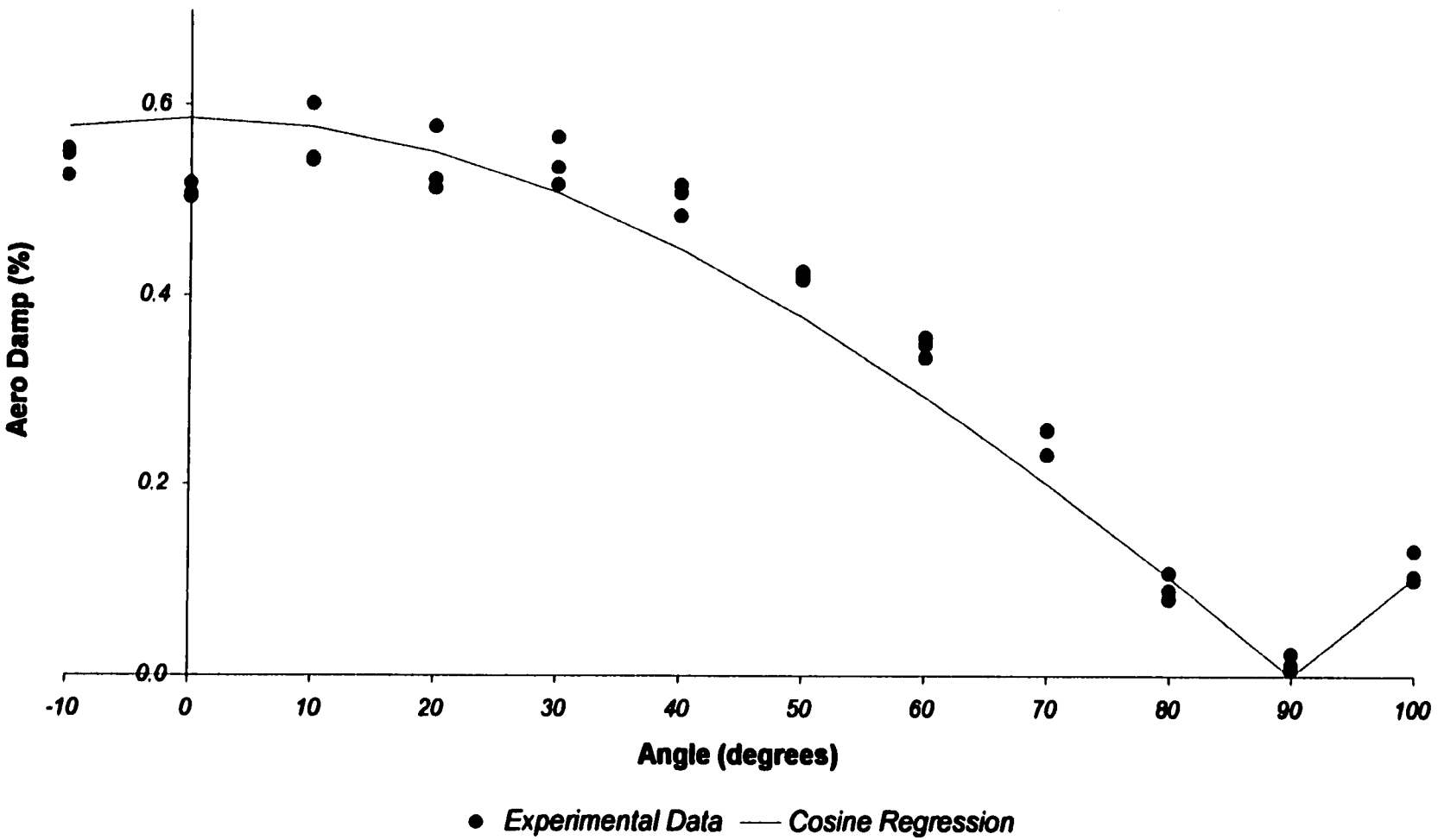

Figure 4.5.20
Aero Damping vs. Angle
Section 4 - 1 m/s

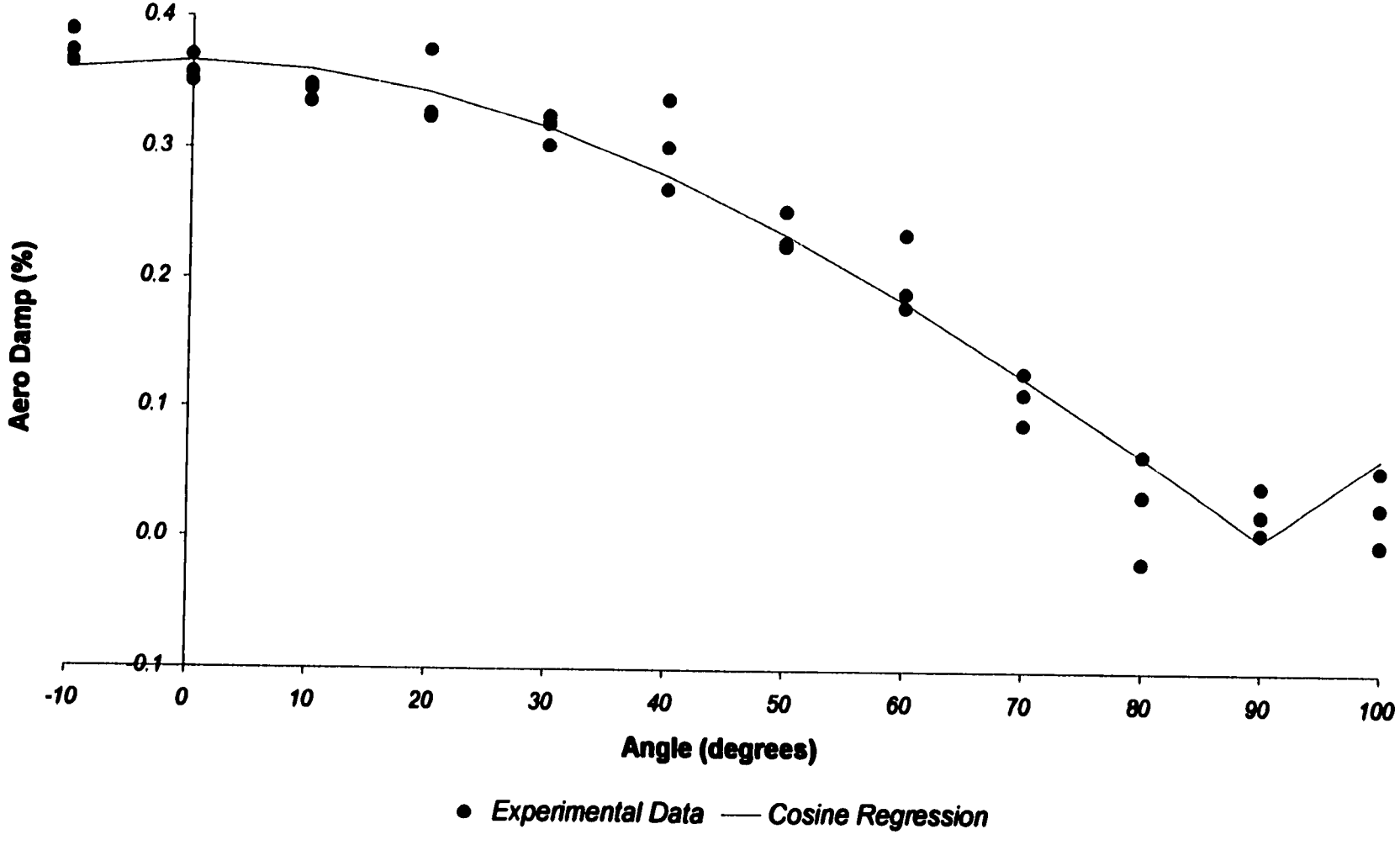

Figure 4.5.21
Aero Damping vs. Angle
Section 5 - 5 m/s

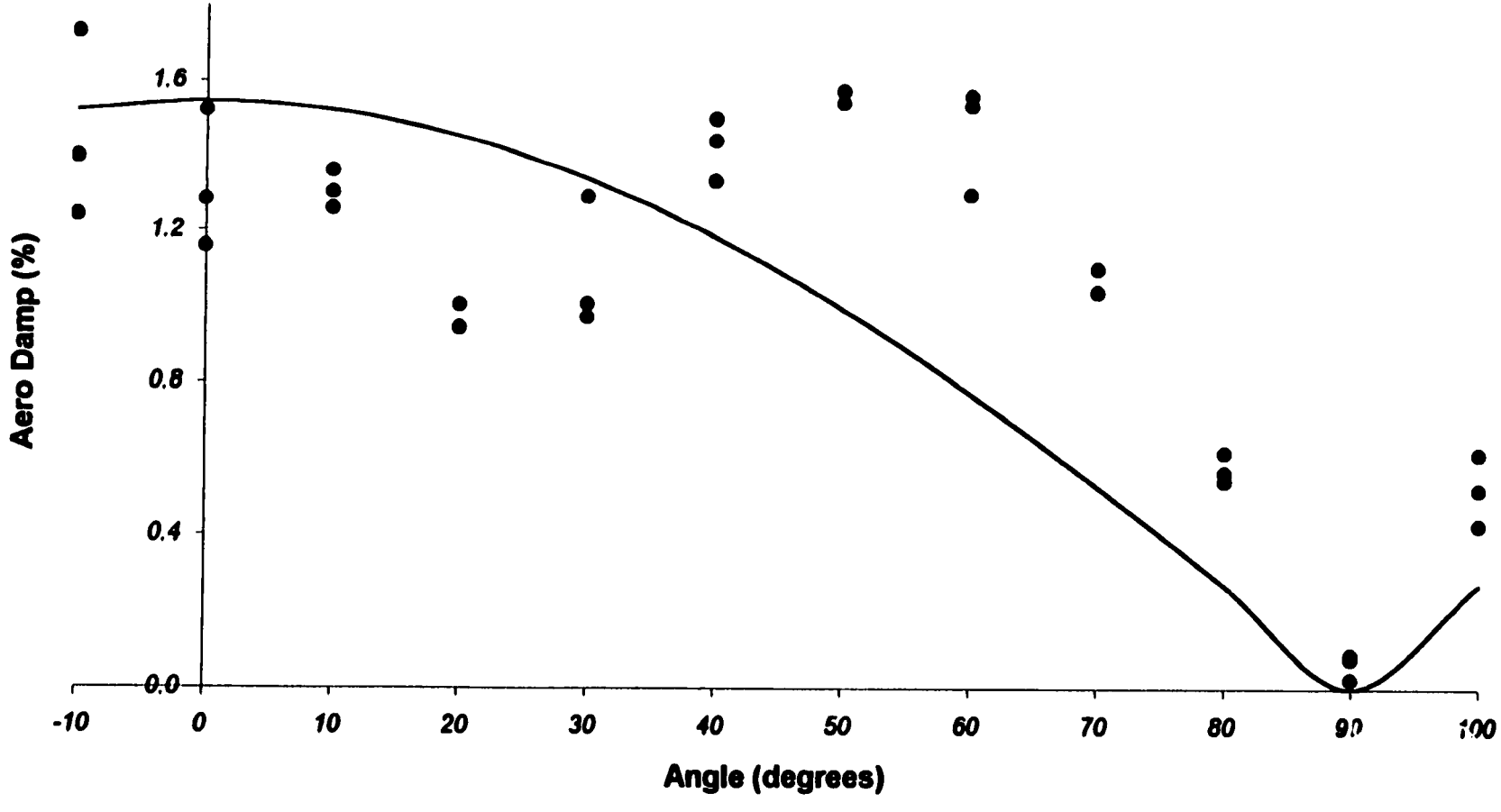

Figure 4.5.22
Aero Damping vs. Angle
Section 5 - 4 m/s

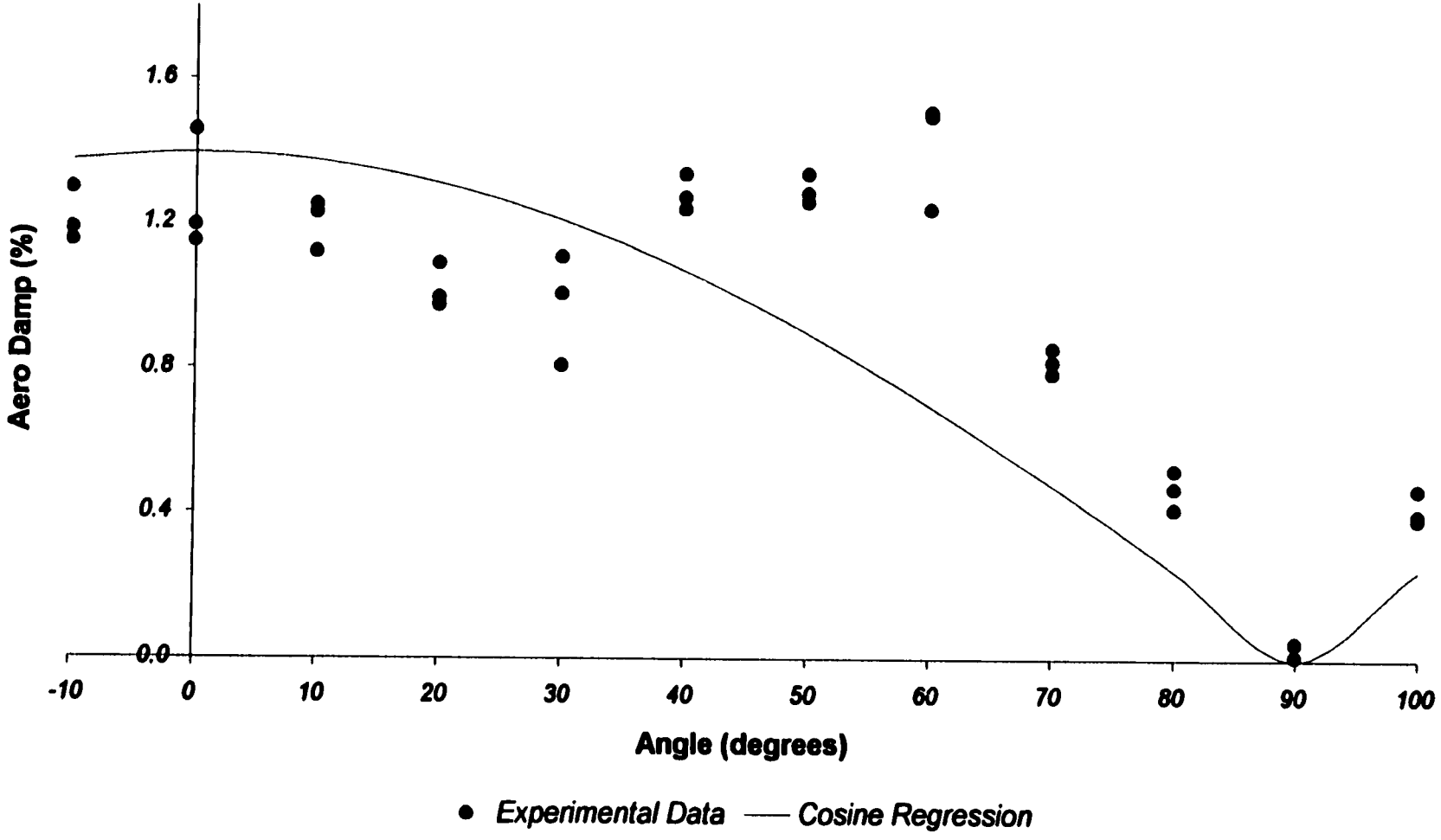

Figure 4.5.23
Aero Damping vs. Angle
Section 5 - 3 m/s

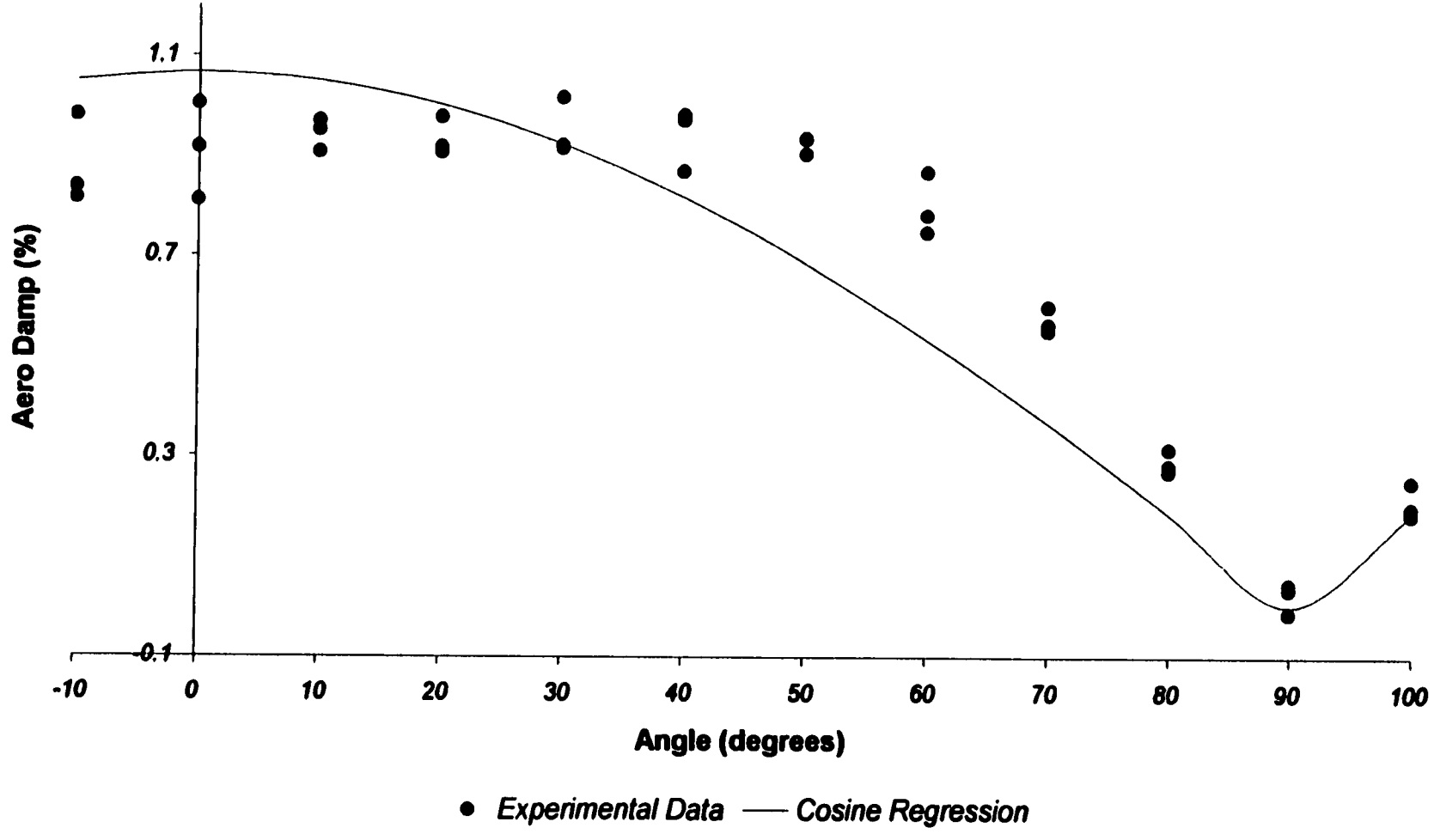

Figure 4.5.24
Aero Damping vs. Angle
Section 5 - 2 m/s

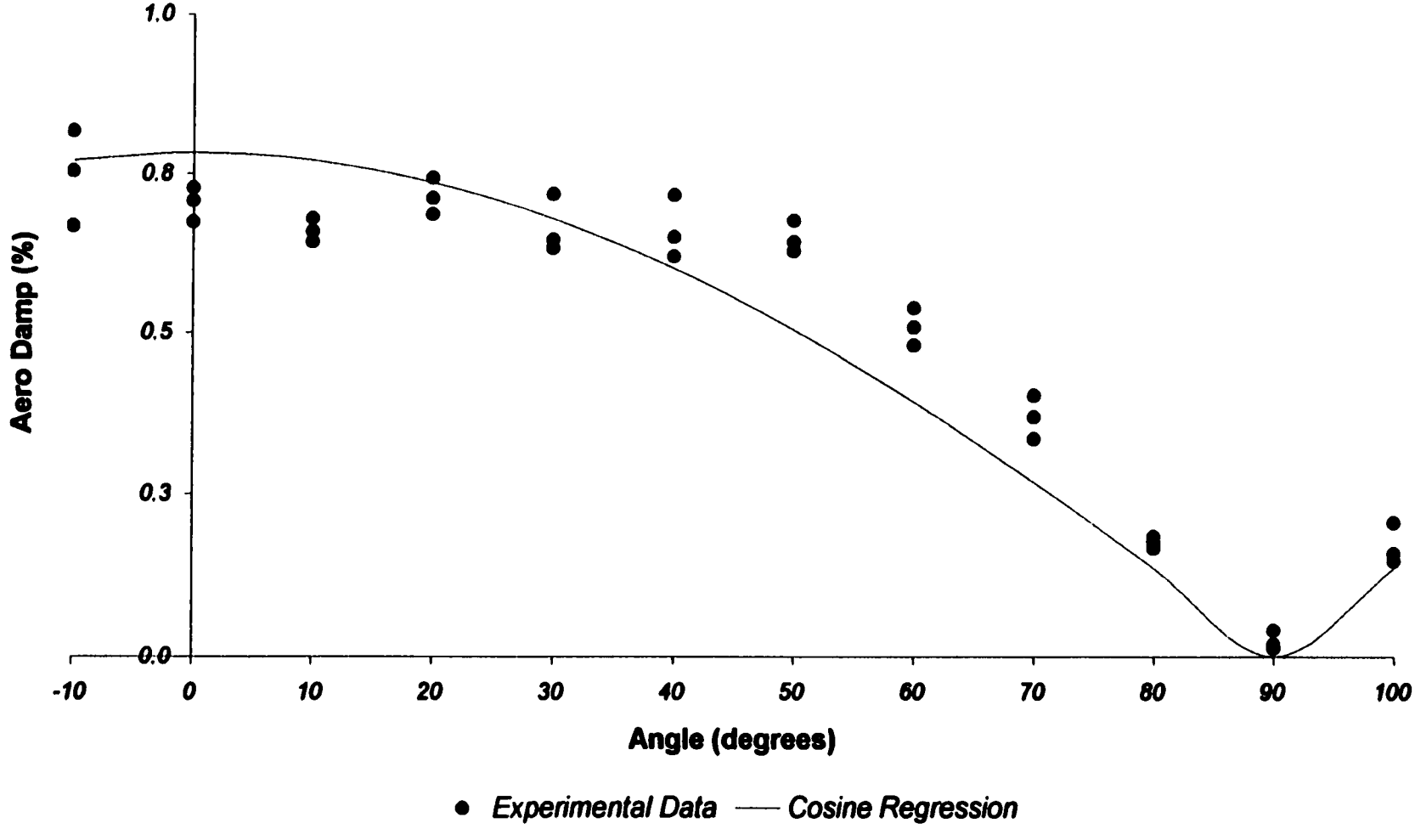

Figure 4.5.25
Aero Damping vs. Angle
Section 5 - 1 m/s

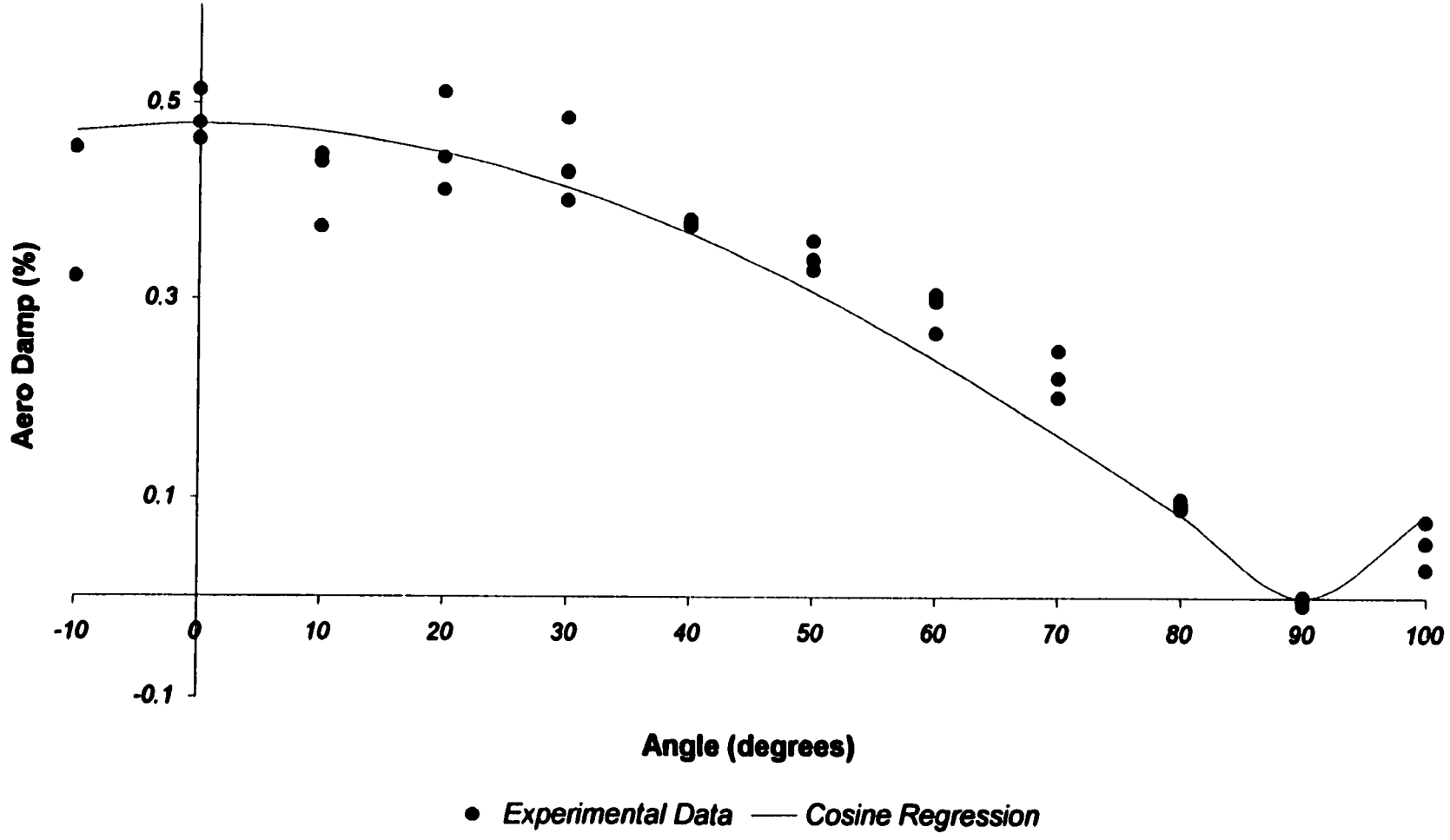

Figure 4.5.26
Aero Damping vs. Angle
1 m/s

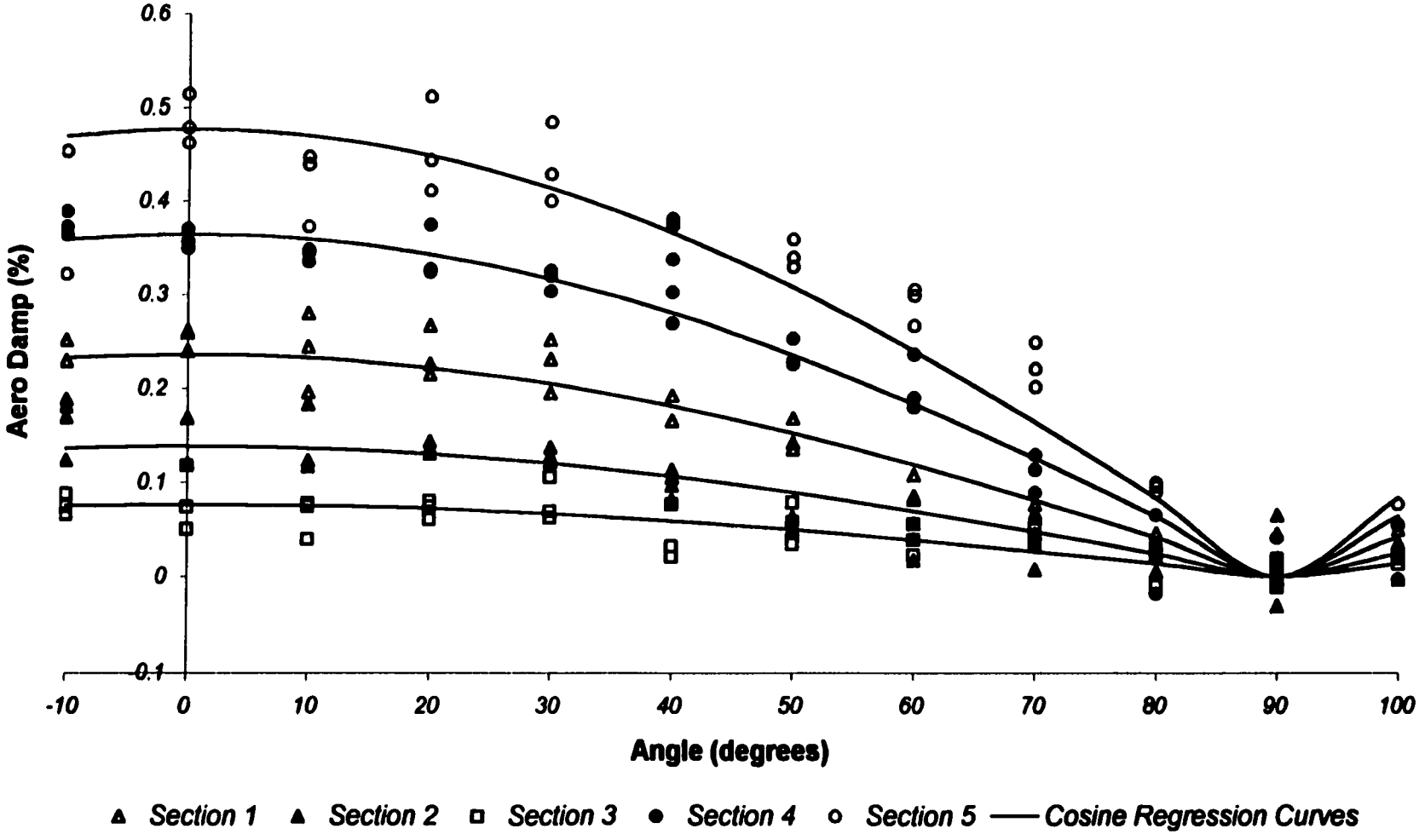

Figure 4.5.27
Aero Damping vs. Angle
2 m/s

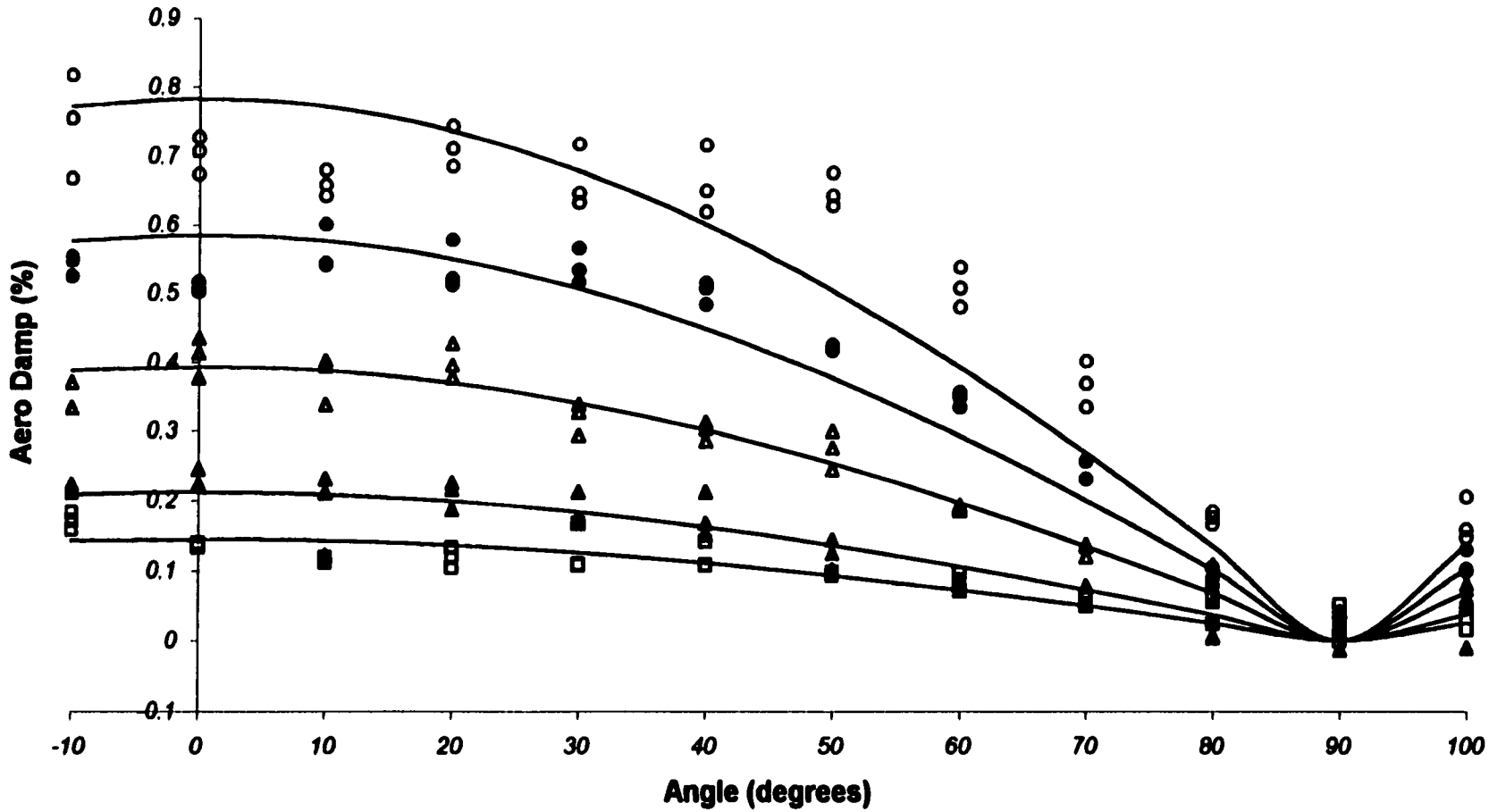

Figure 4.5.28
Aero Damping vs. Angle
3 m/s

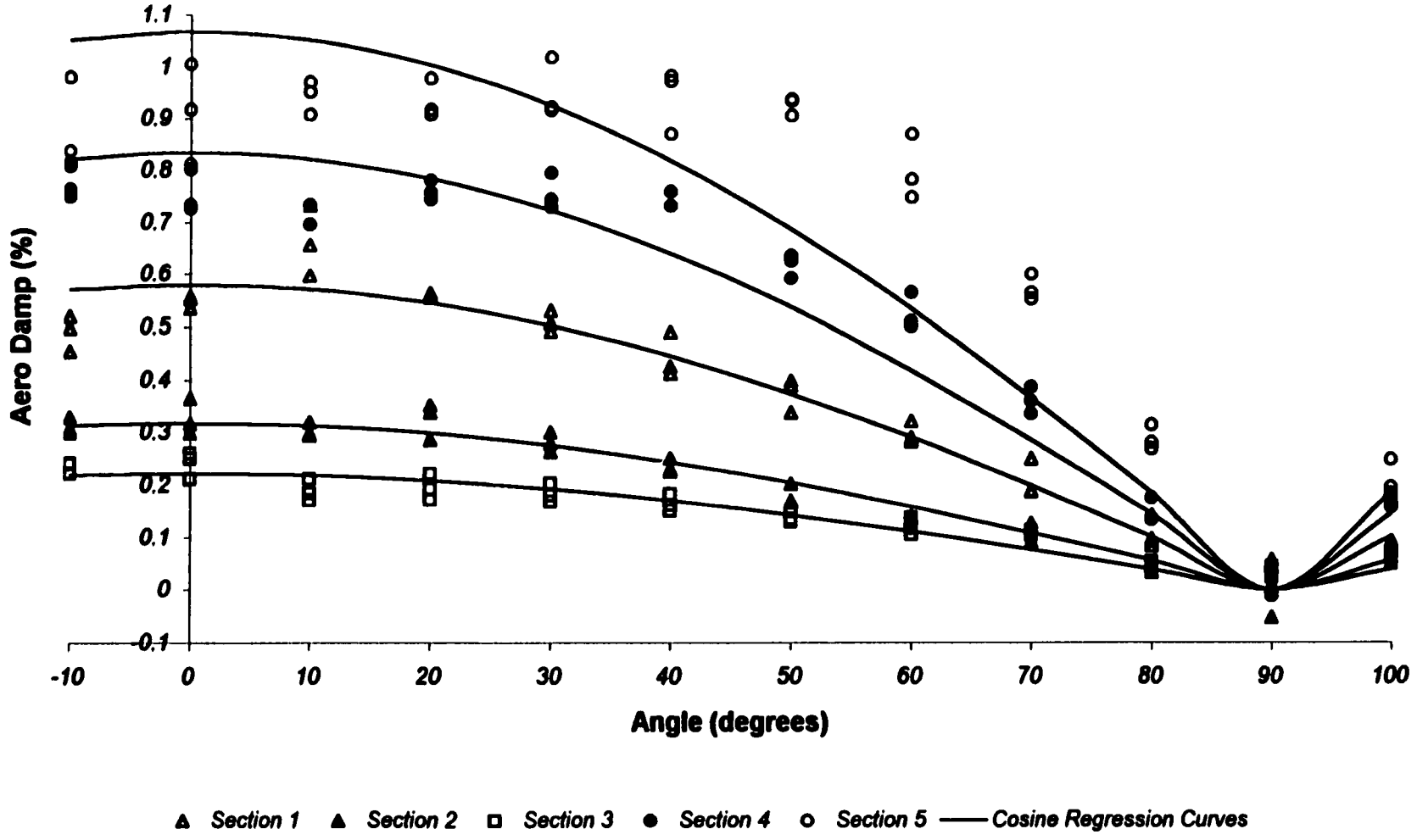

Figure 4.5.29
Aero Damping vs. Angle
4 m/s

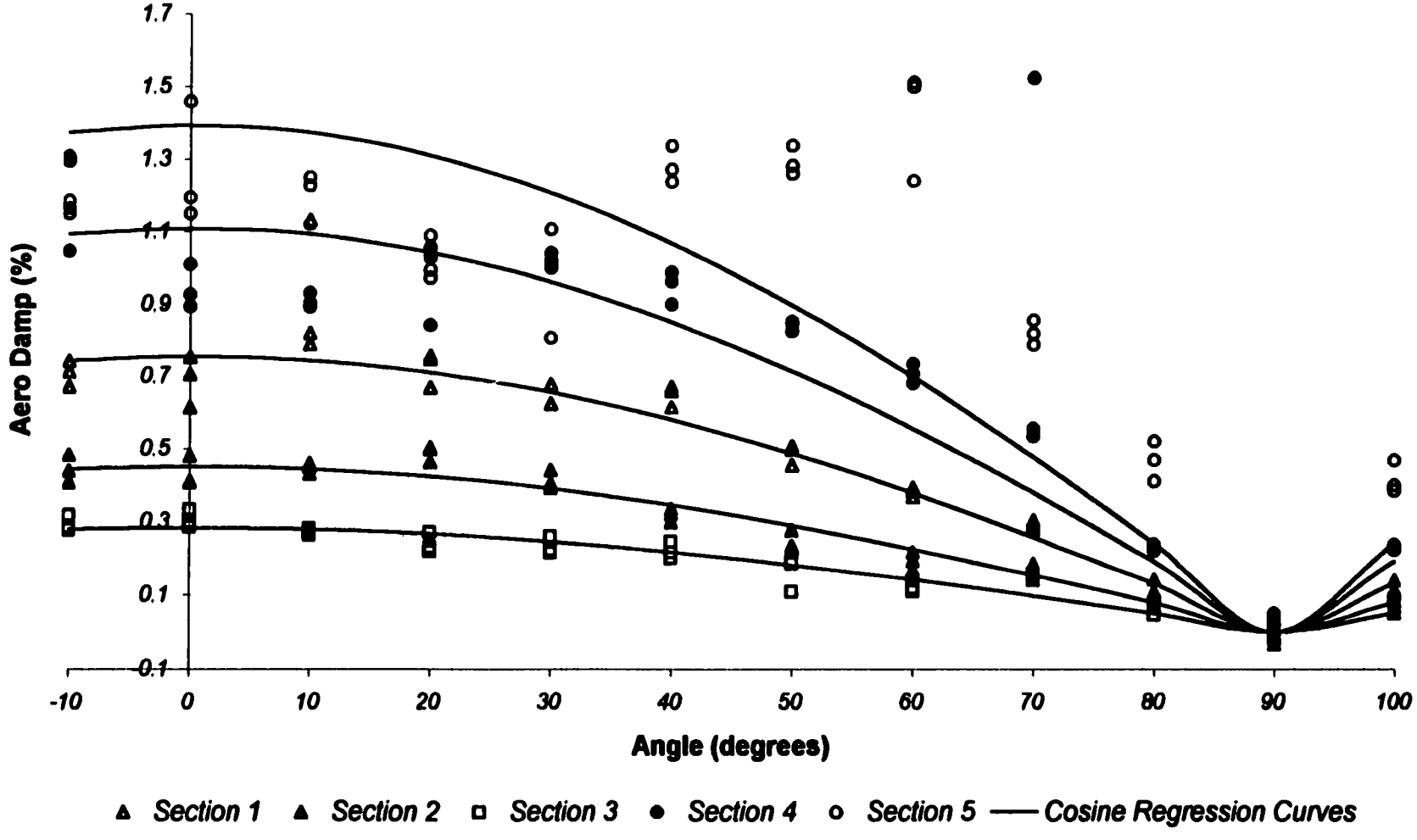

Figure 4.5.30
Aero Damping vs. Angle
5 m/s

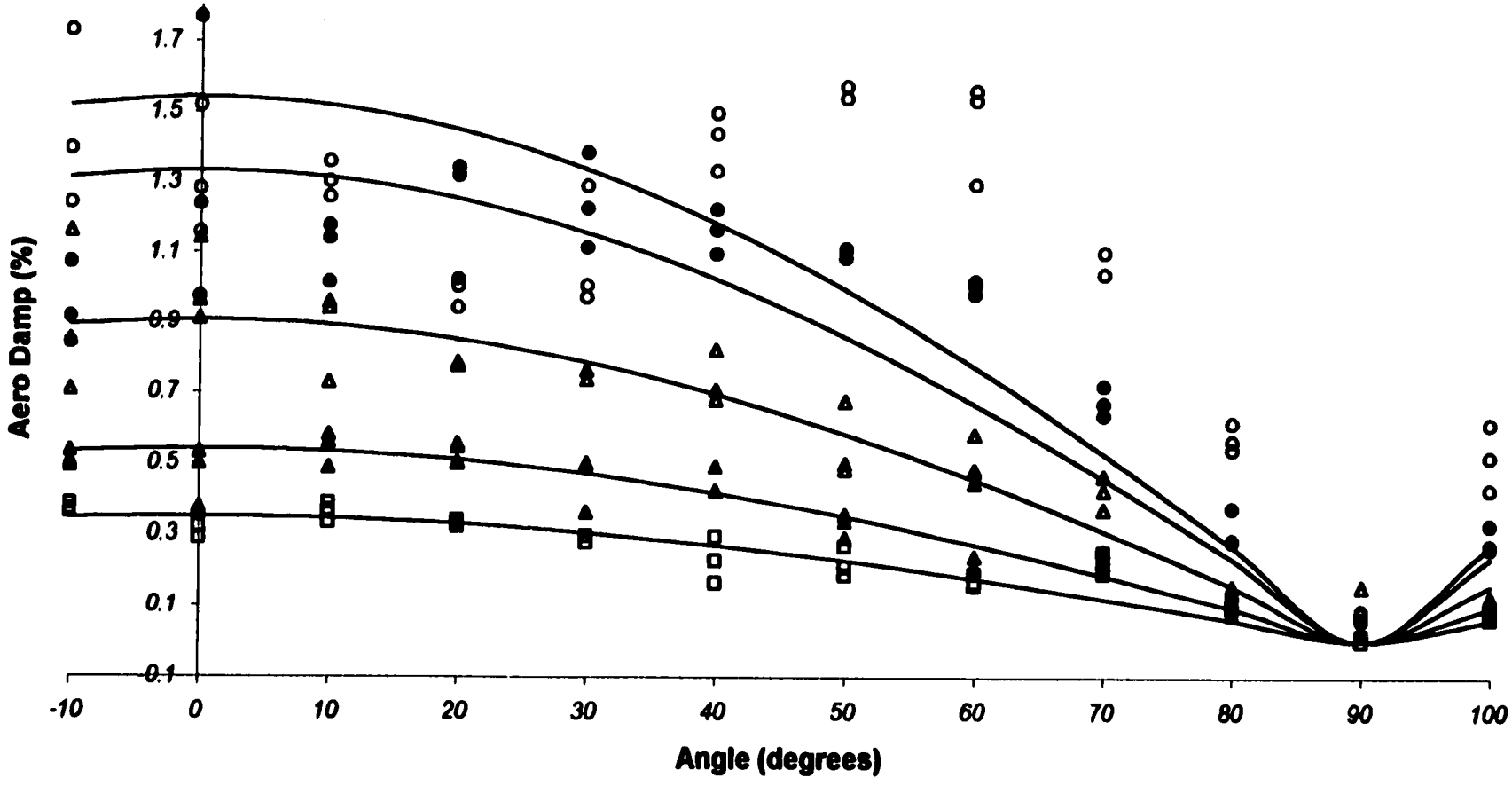

Figure 4.6.1
Aero Damping vs. Wind Speed
-10 degree yaw angle

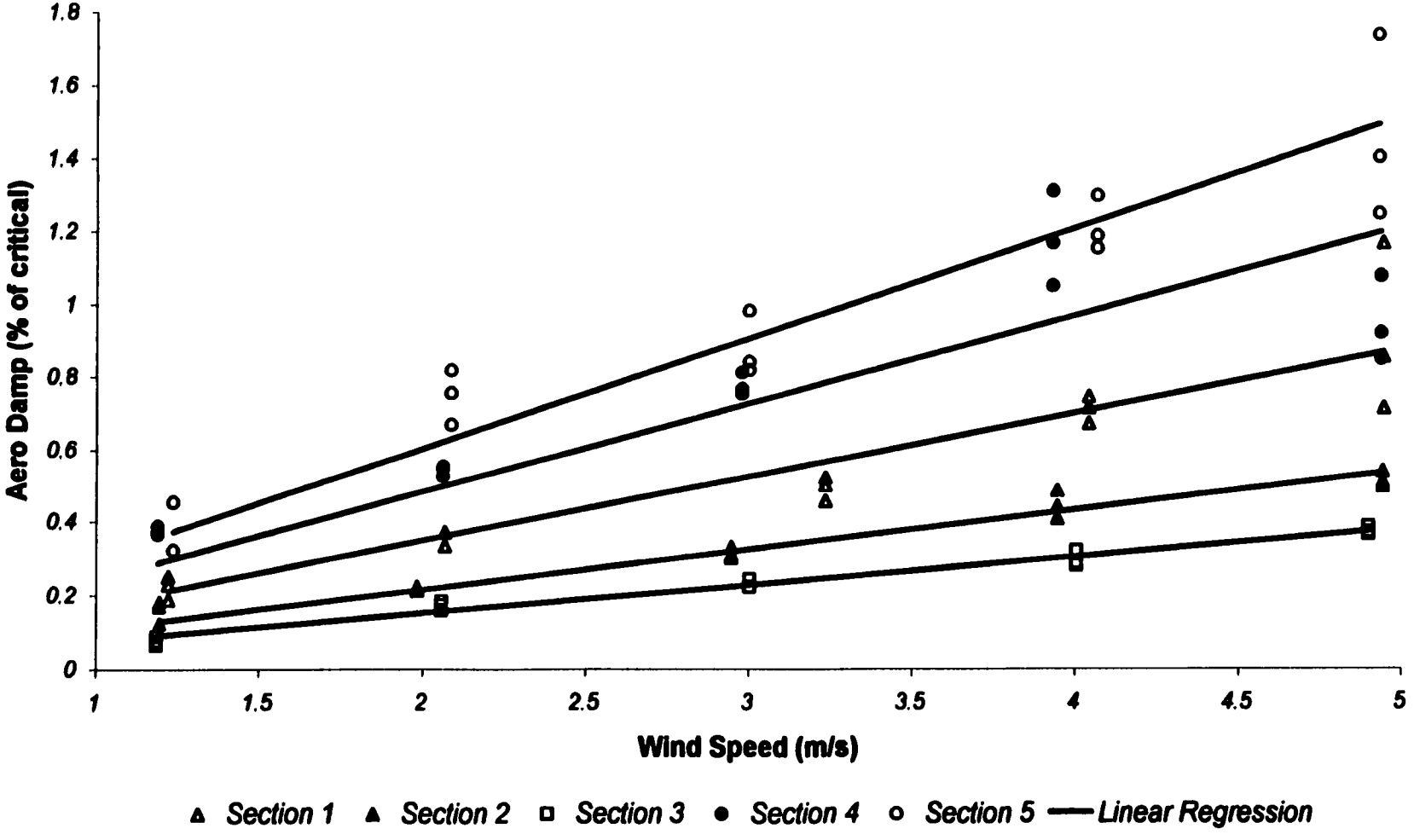

Figure 4.6.2
Aero Damping vs. Wind Speed
0 degree yaw angle

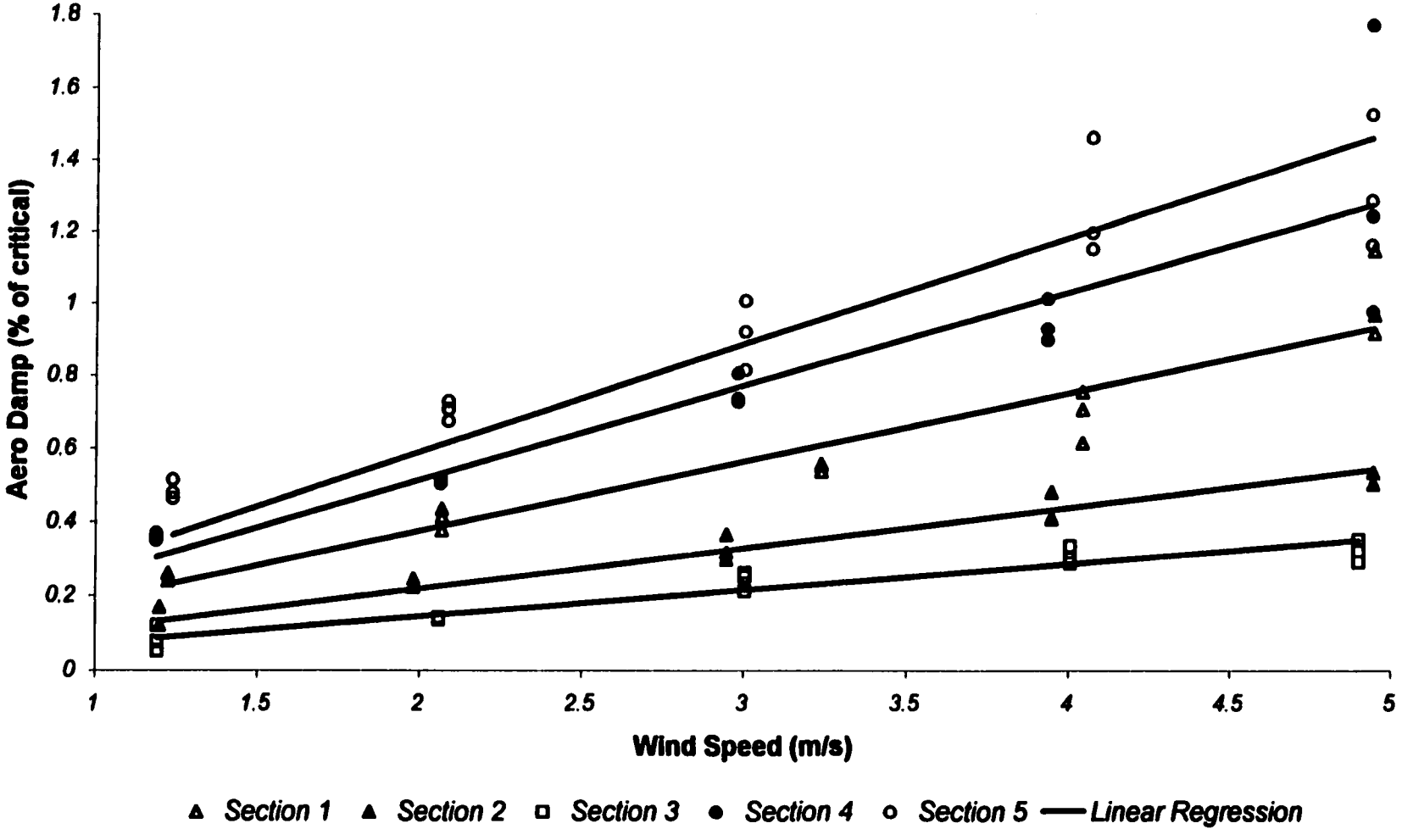

Figure 4.6.3
Aero Damping vs. Wind Speed
10 degree yaw angle

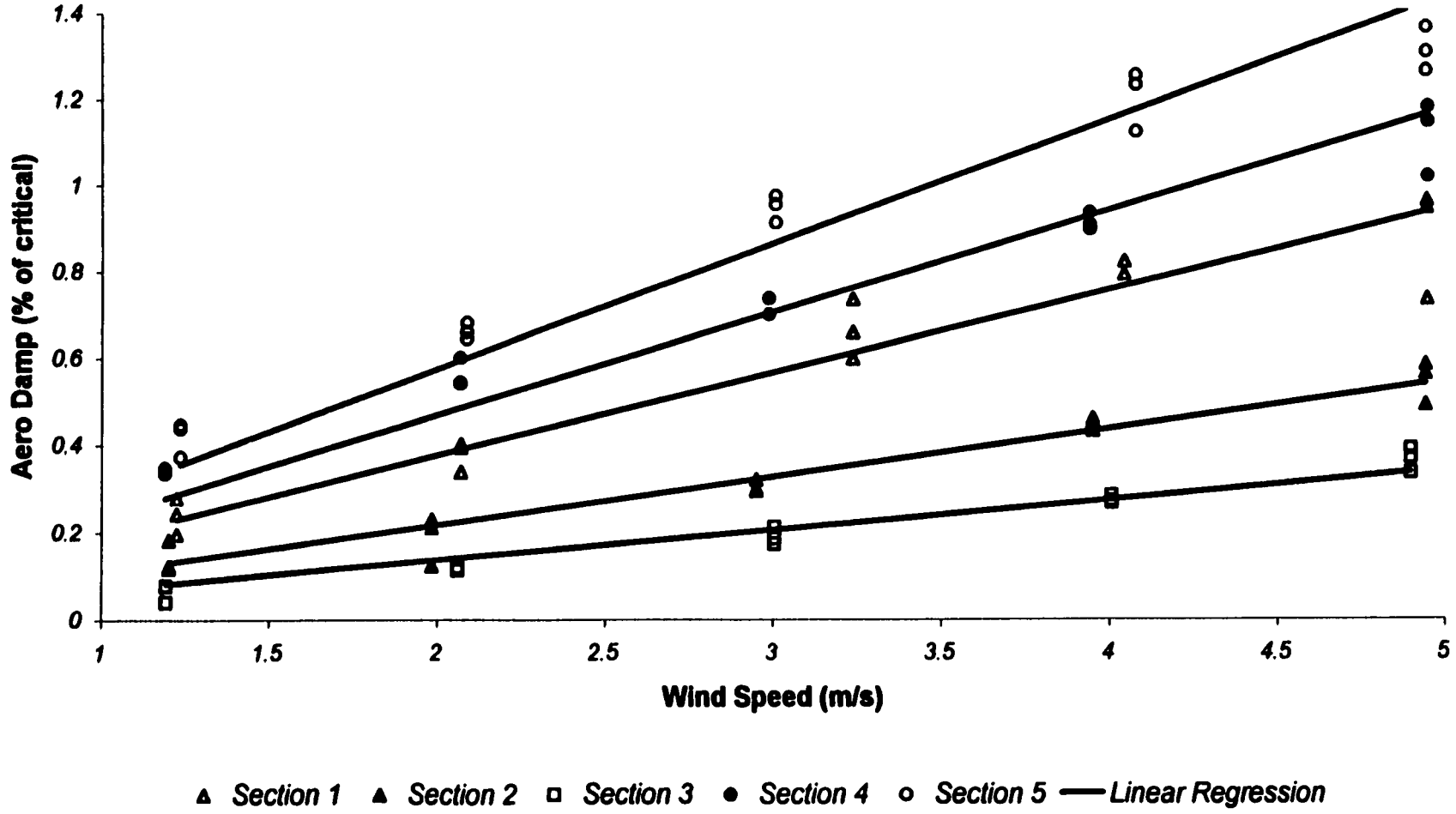

Figure 4.6.4
Aero Damping vs. Wind Speed
20 degree yaw angle

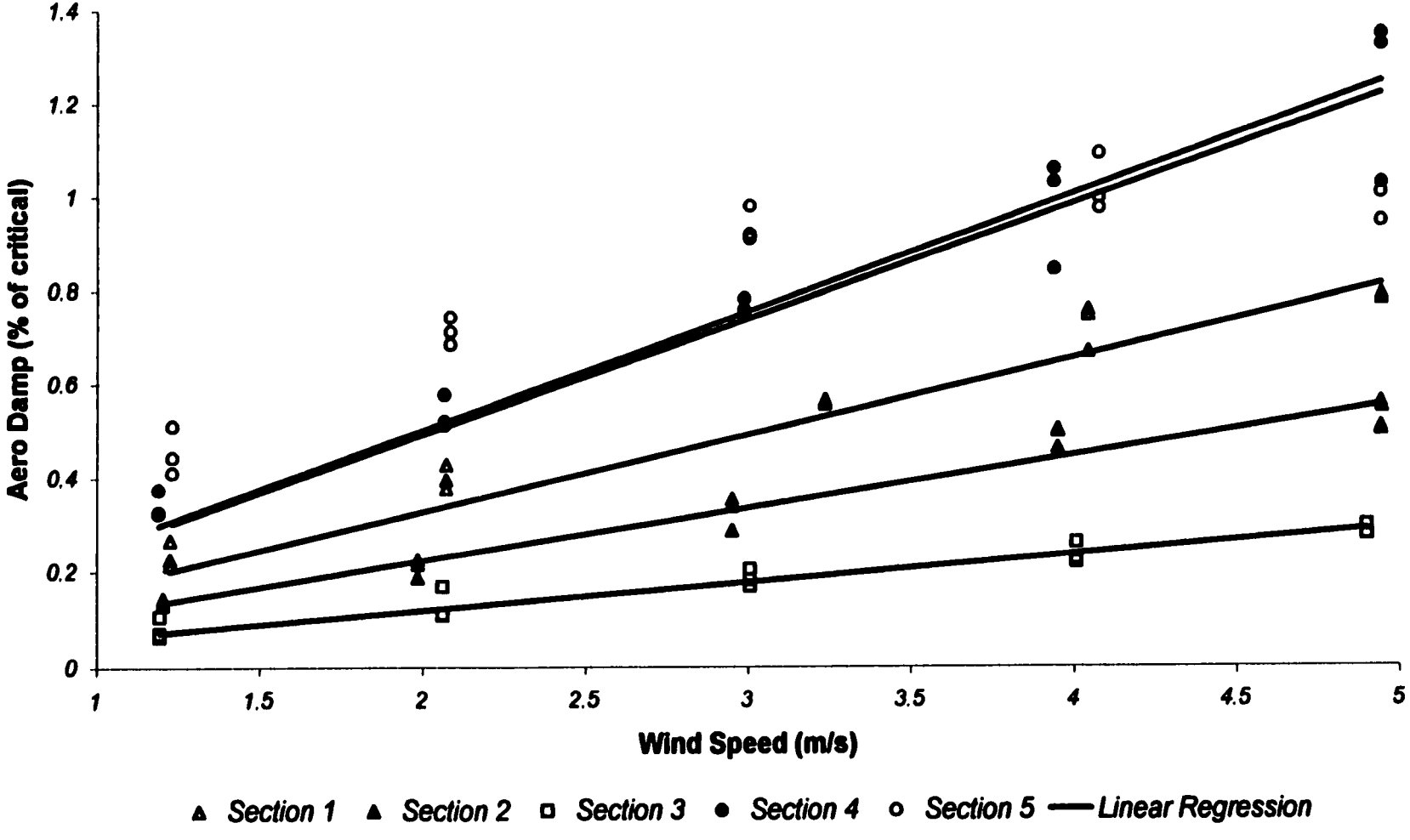

Figure 4.6.5
Aero Damping vs. Wind Speed
30 degree yaw angle

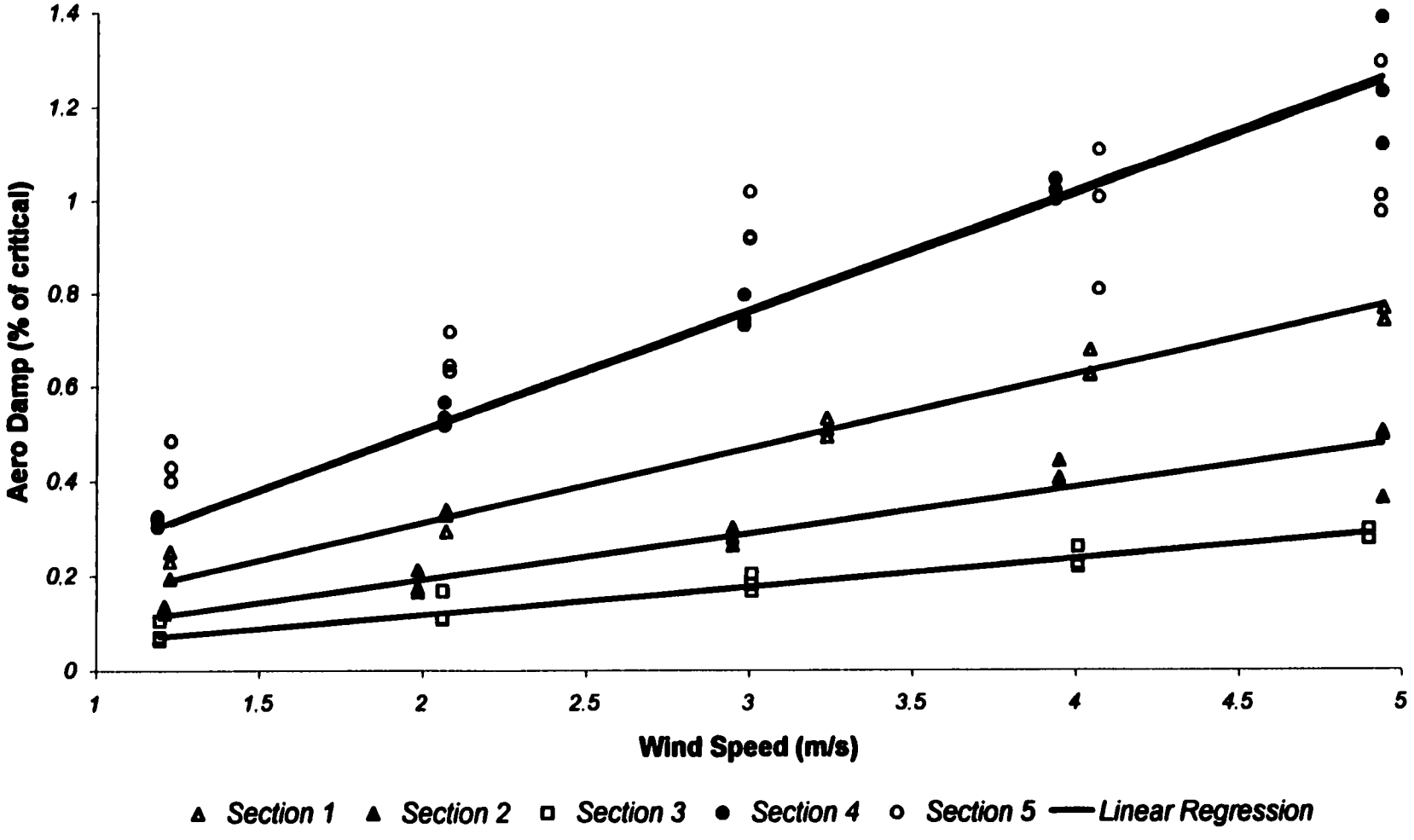

Figure 4.6.6
Aero Damping vs. Wind Speed
40 degree yaw angle

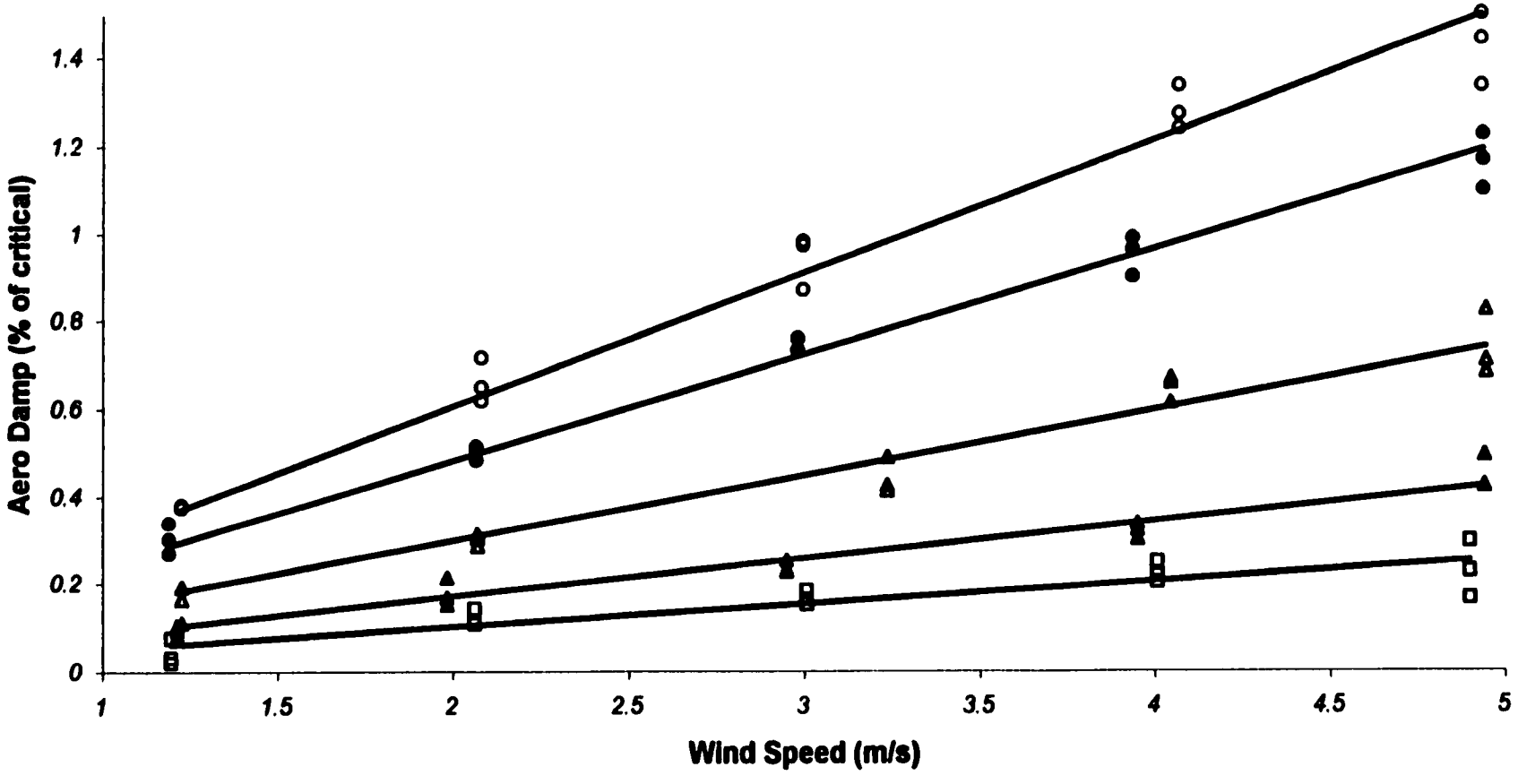

Figure 4.6.7
Aero Damping vs. Wind Speed
50 degree yaw angle

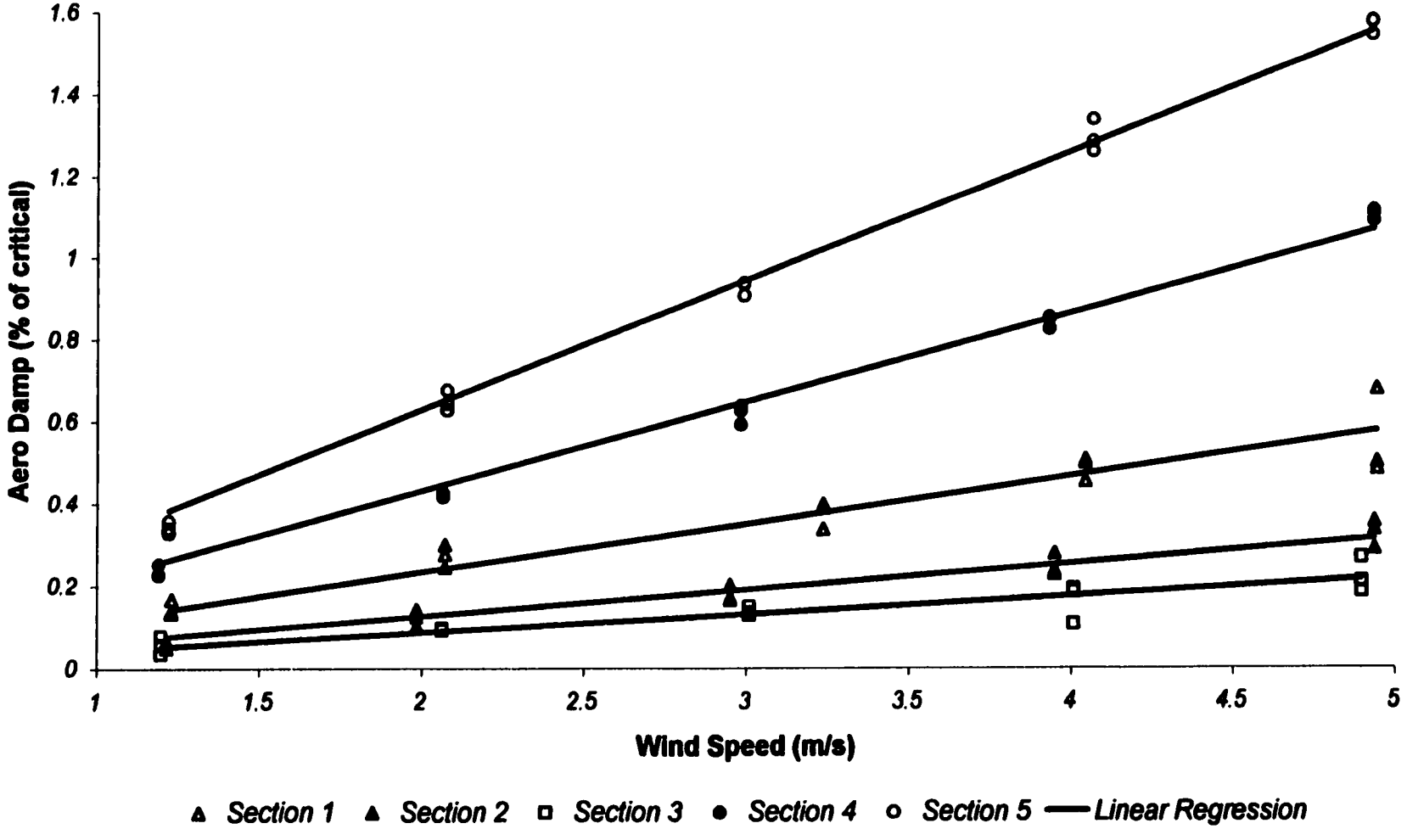

Figure 4.6.8
Aero Damping vs. Wind Speed
60 degree yaw angle

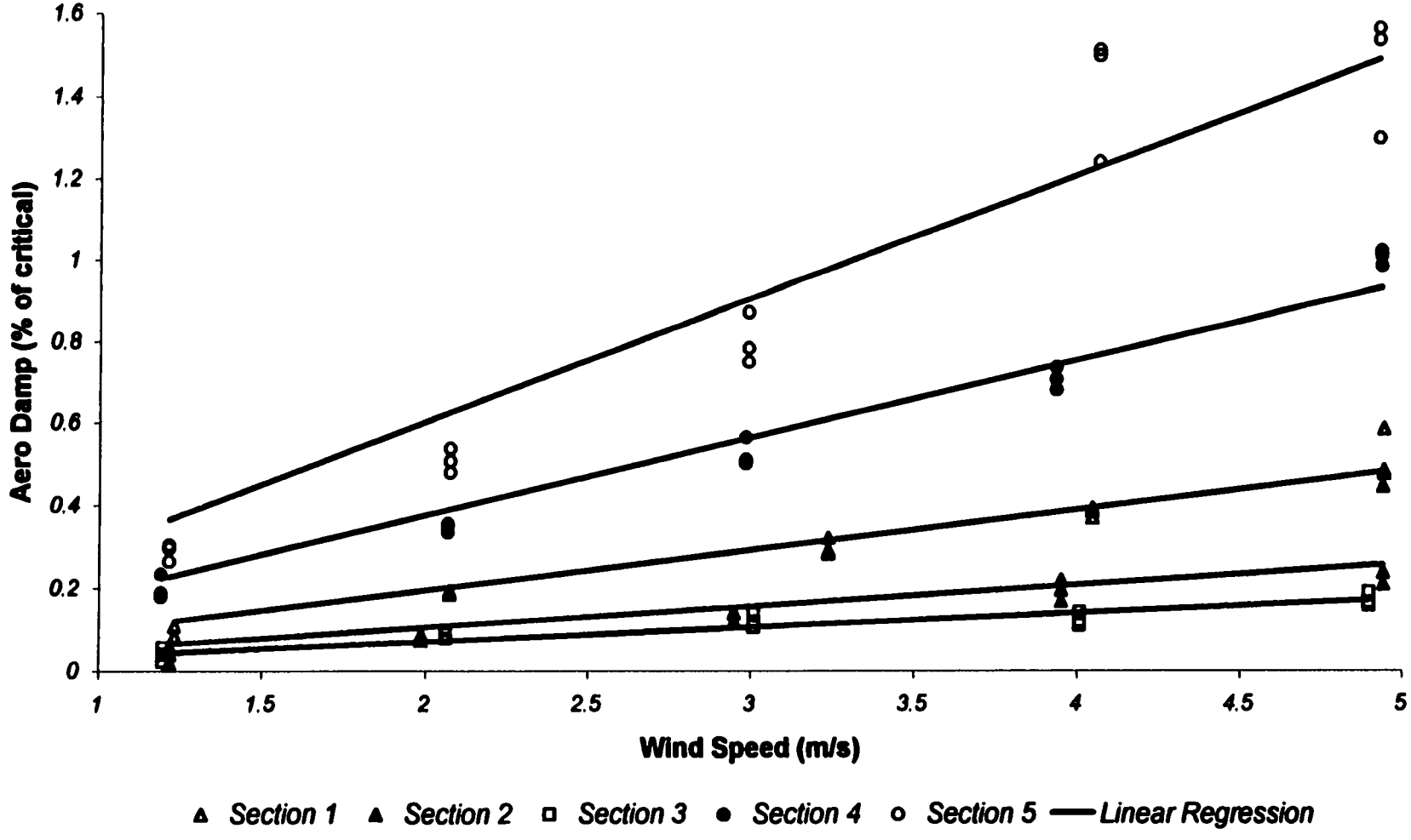

Figure 4.6.9
Aero Damping vs. Wind Speed
70 degree yaw angle

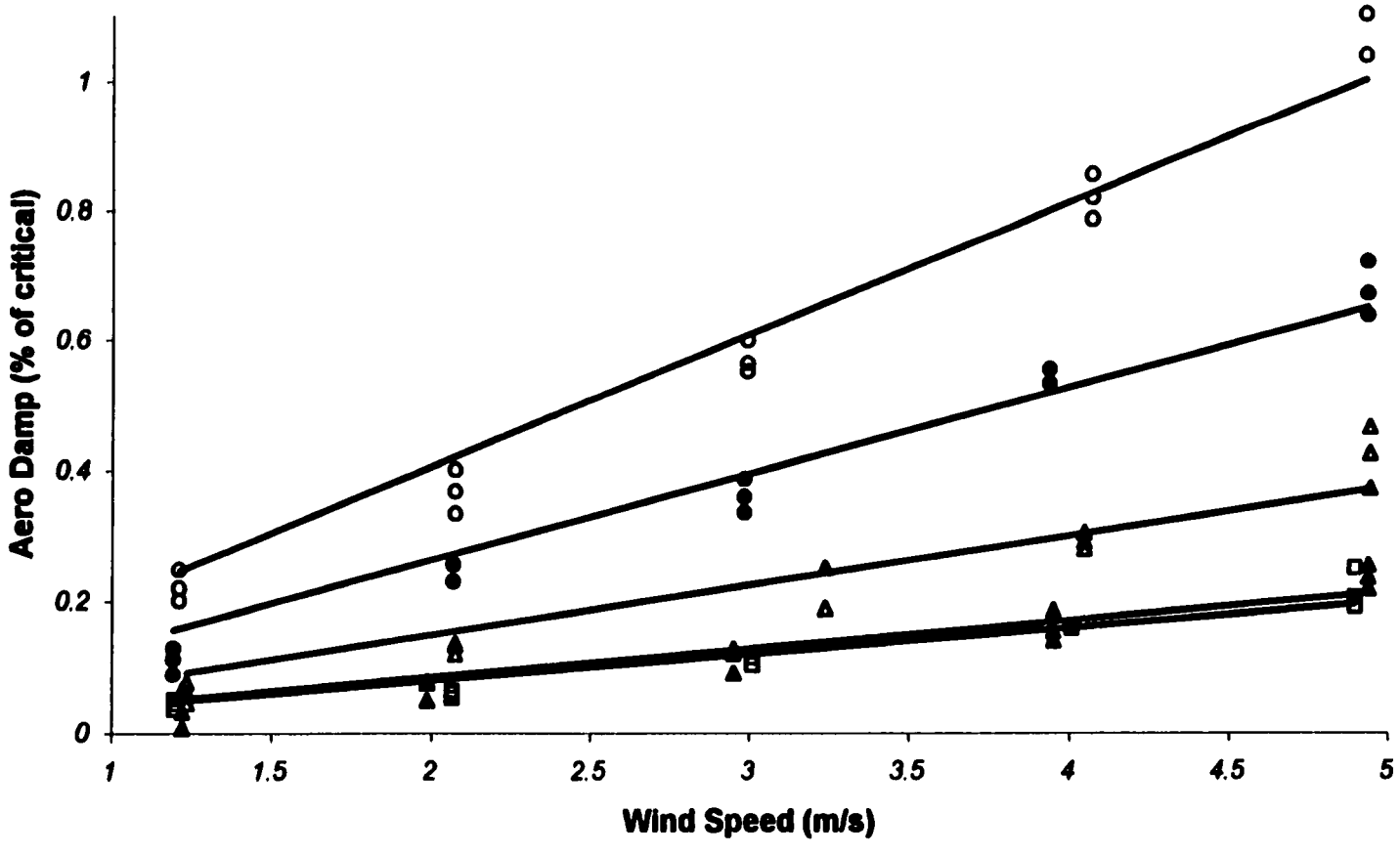

Figure 4.6.10
Aero Damping vs. Wind Speed
80 degree yaw angle

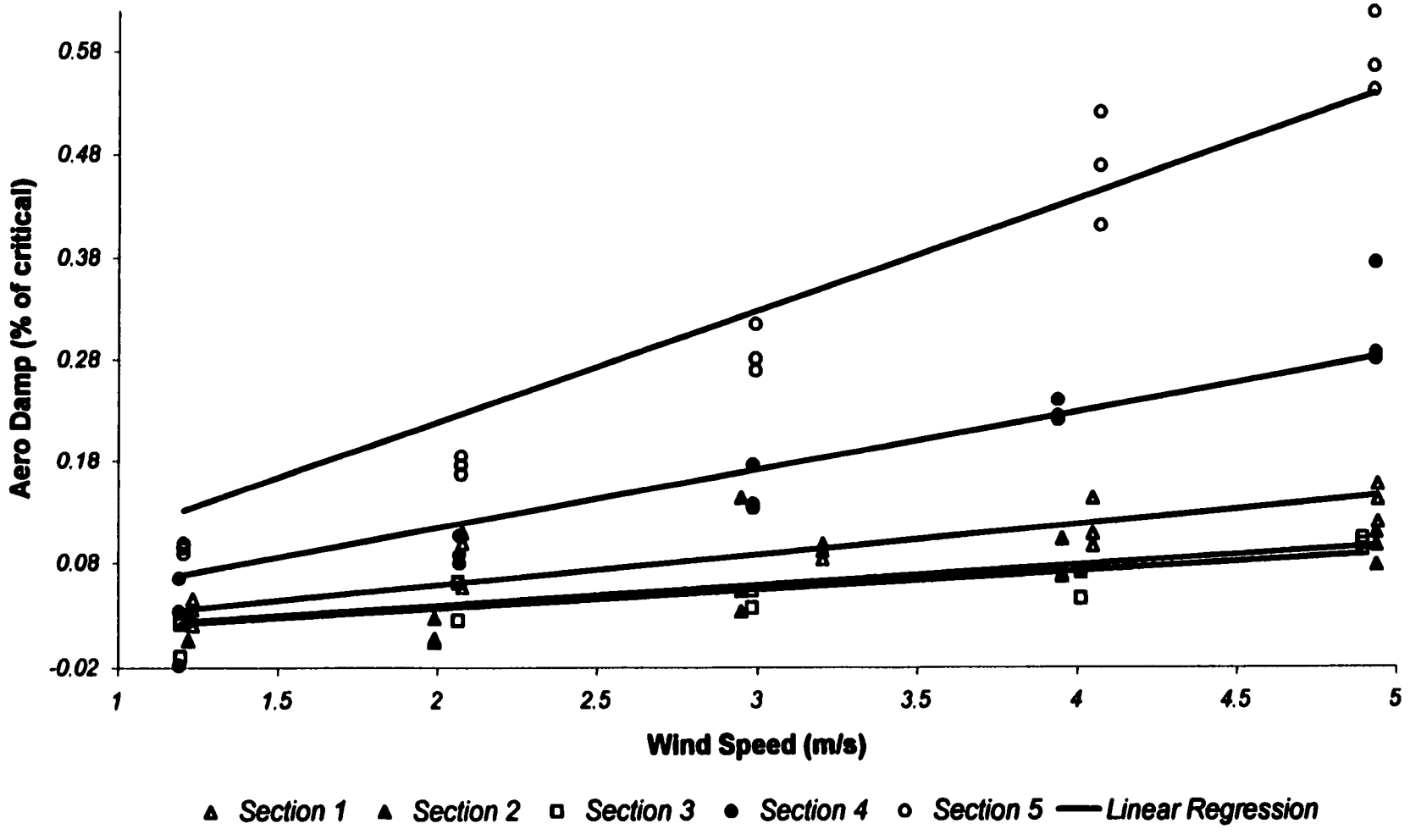

Figure 4.6.11
Aero Damping vs. Wind Speed
90 degree yaw angle

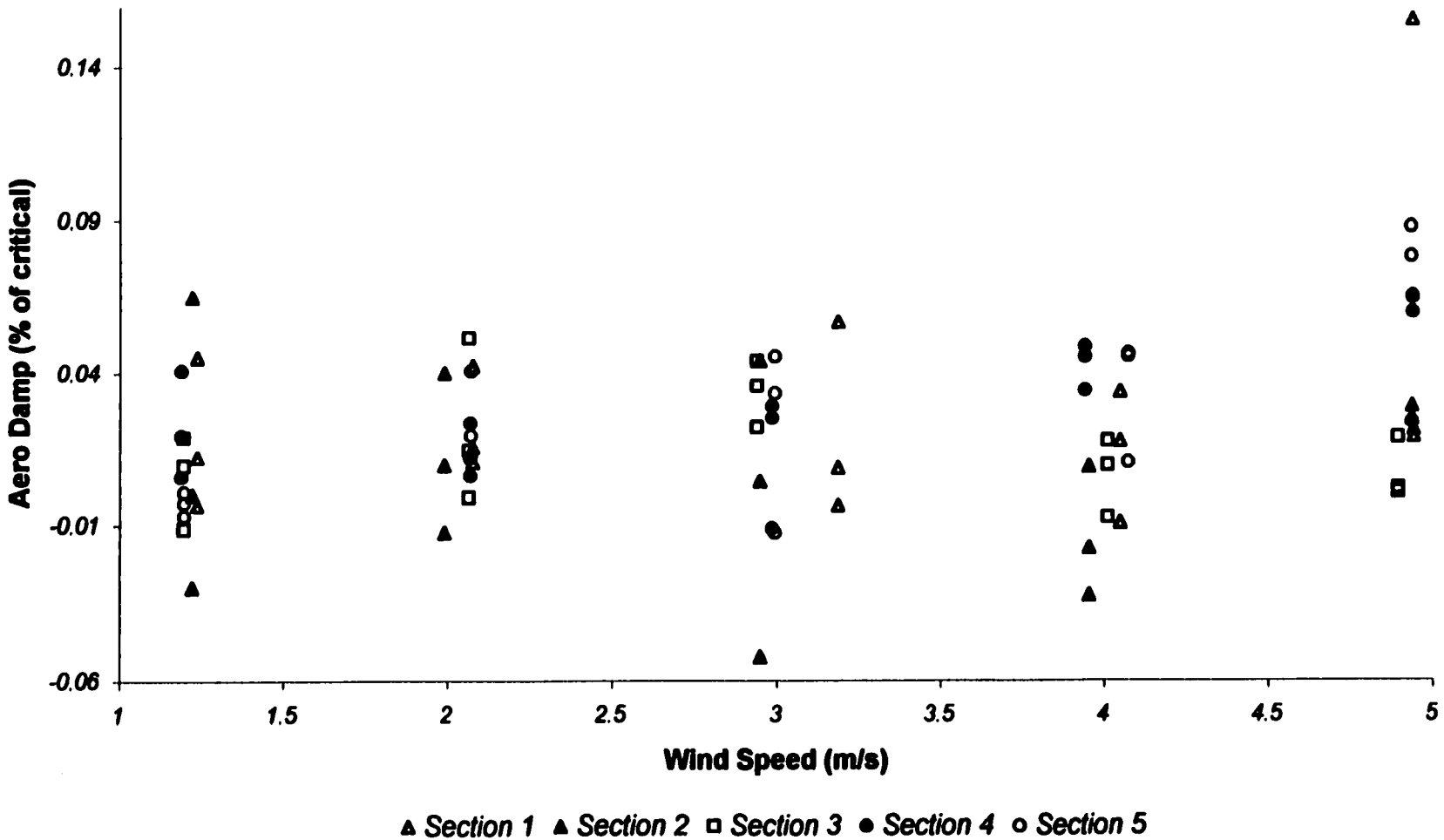

Figure 4.6.12
Aero Damping vs. Wind Speed
100 degree yaw angle

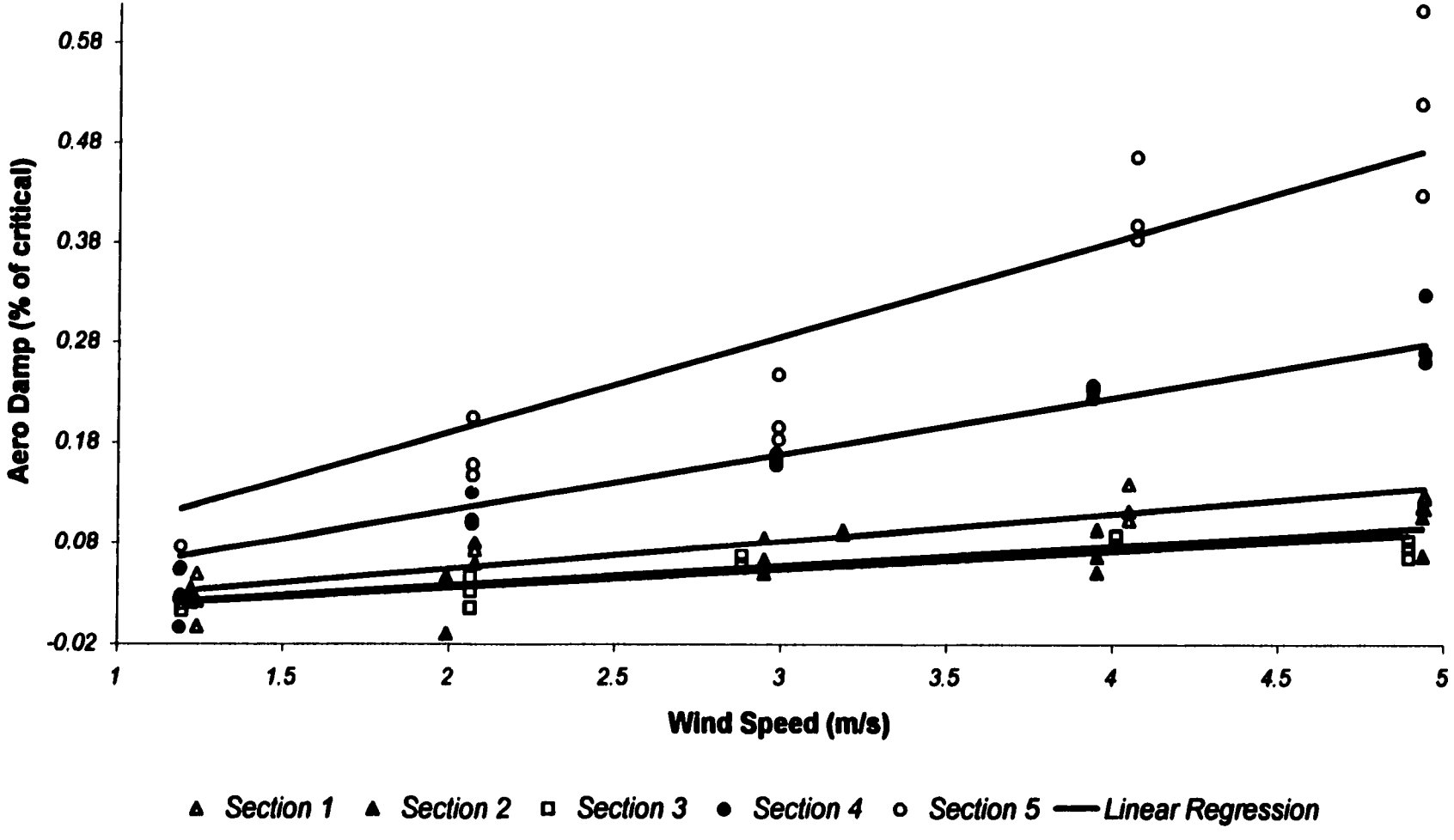

Figure 4.6.13
Aero Damping vs. Wind Speed
Section 1

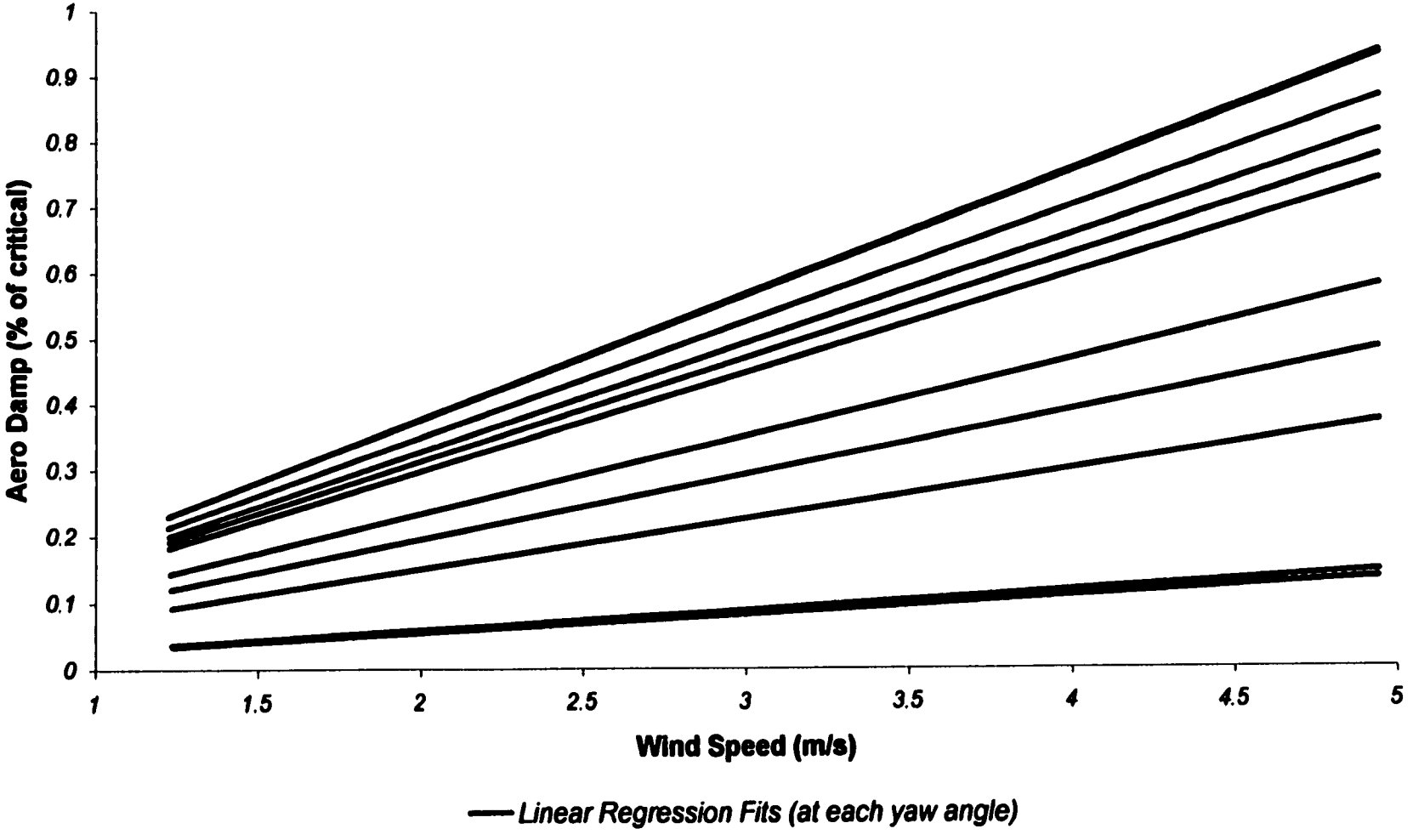

Figure 4.6.14
Aero Damping vs. Wind Speed
Section 2

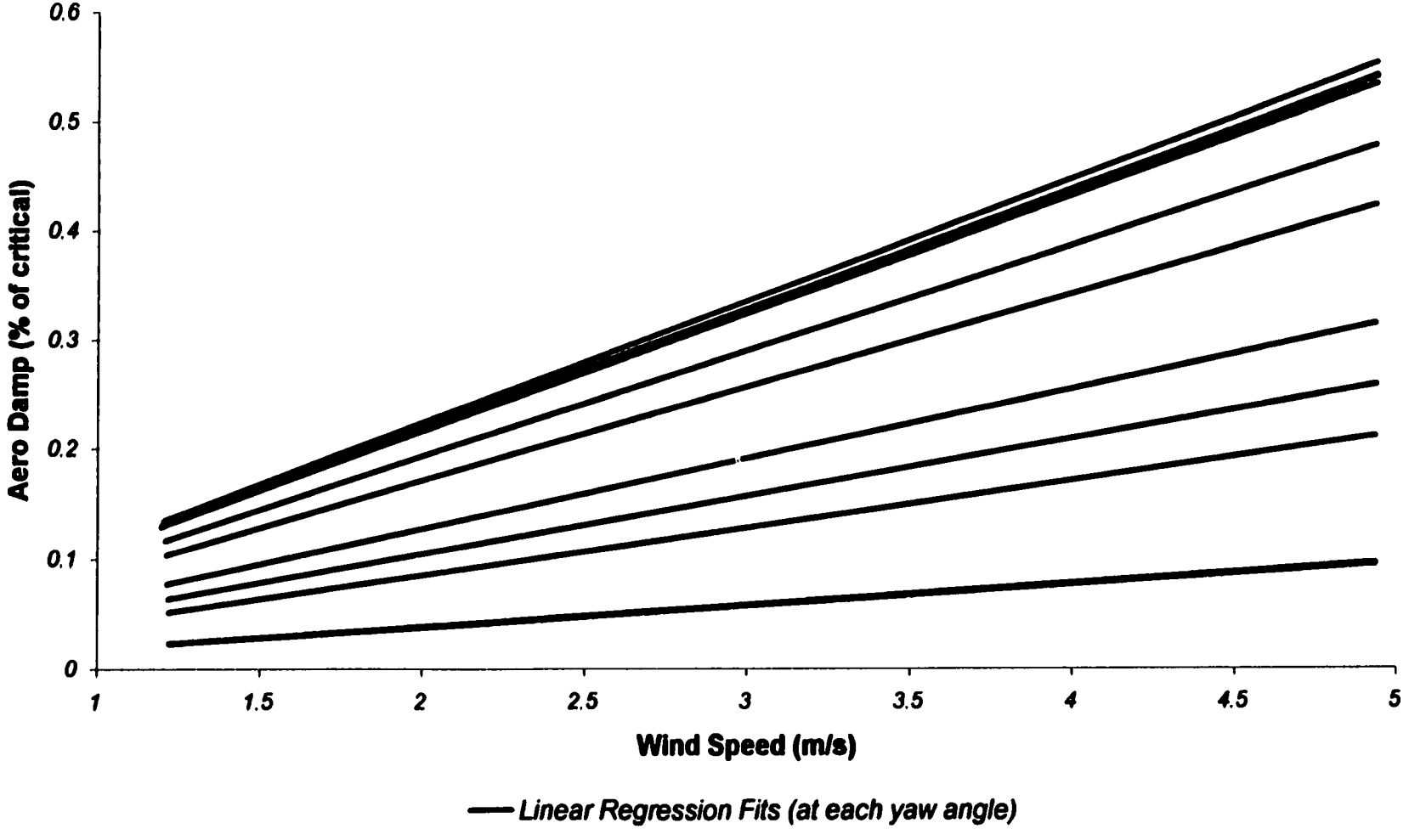

Figure 4.6.15
Aero Damping vs. Wind Speed
Section 3

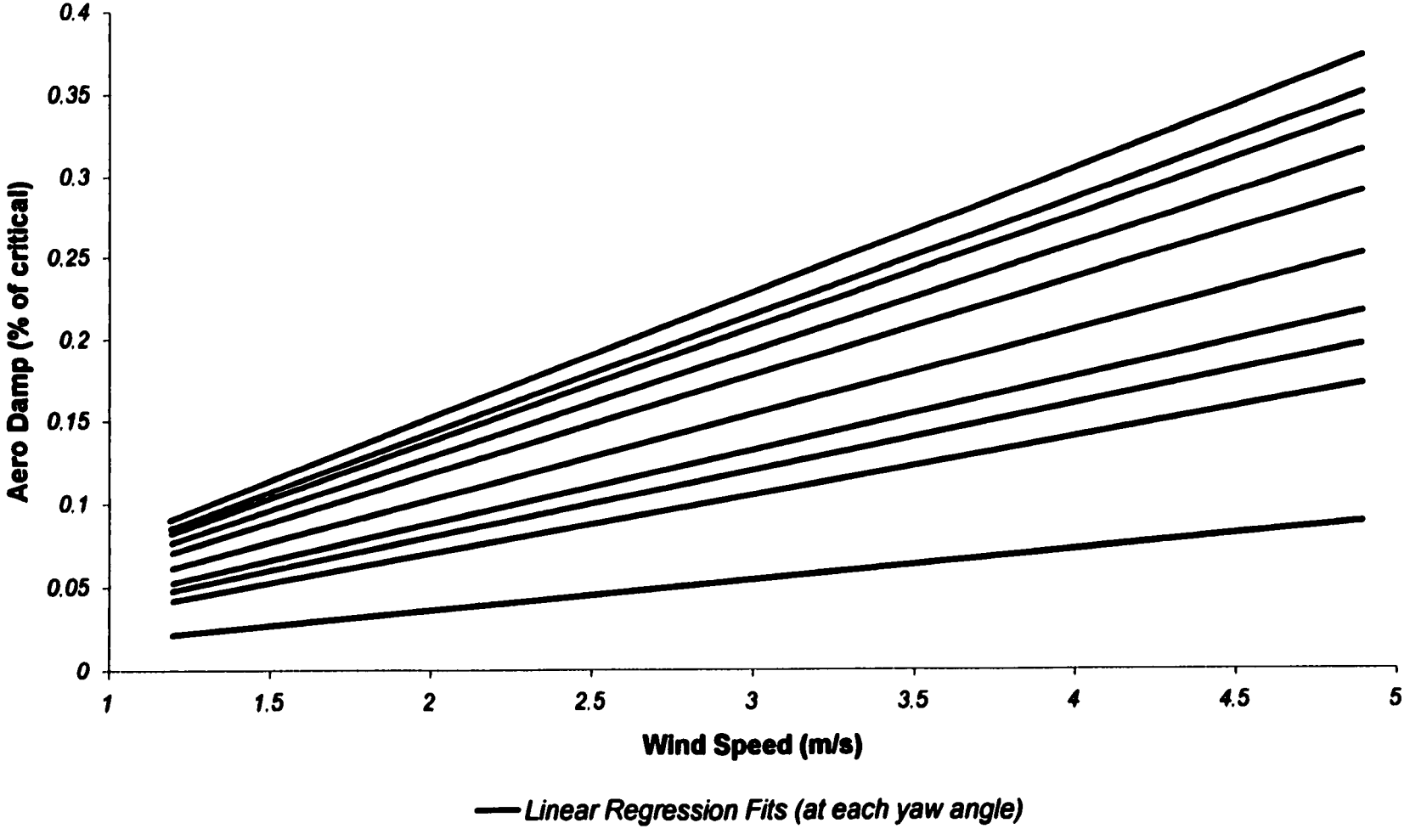

Figure 4.6.16
Aero Damping vs. Wind Speed
Section 4

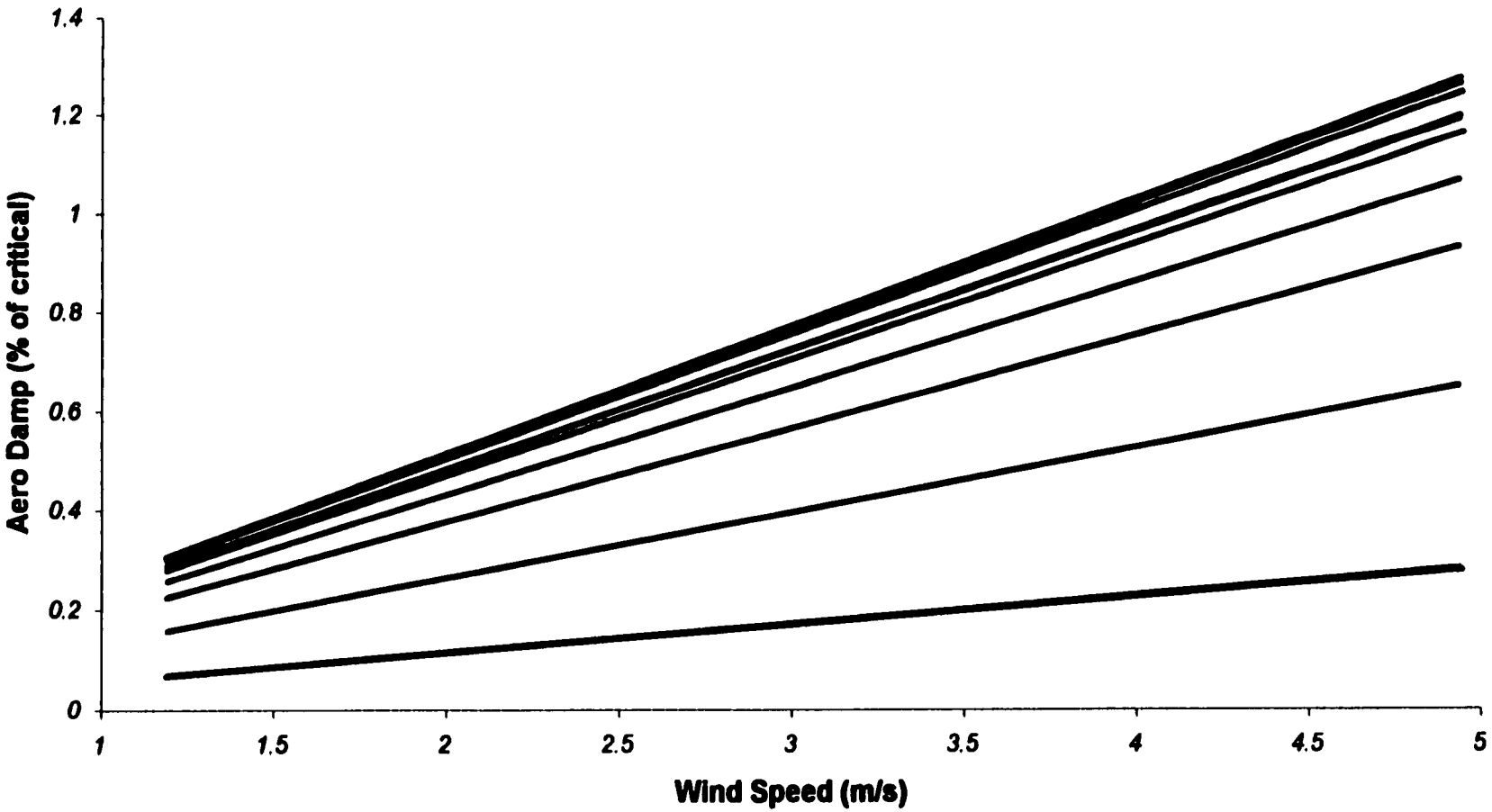

Figure 4.6.17
Aero Damping vs. Wind Speed
Section 5

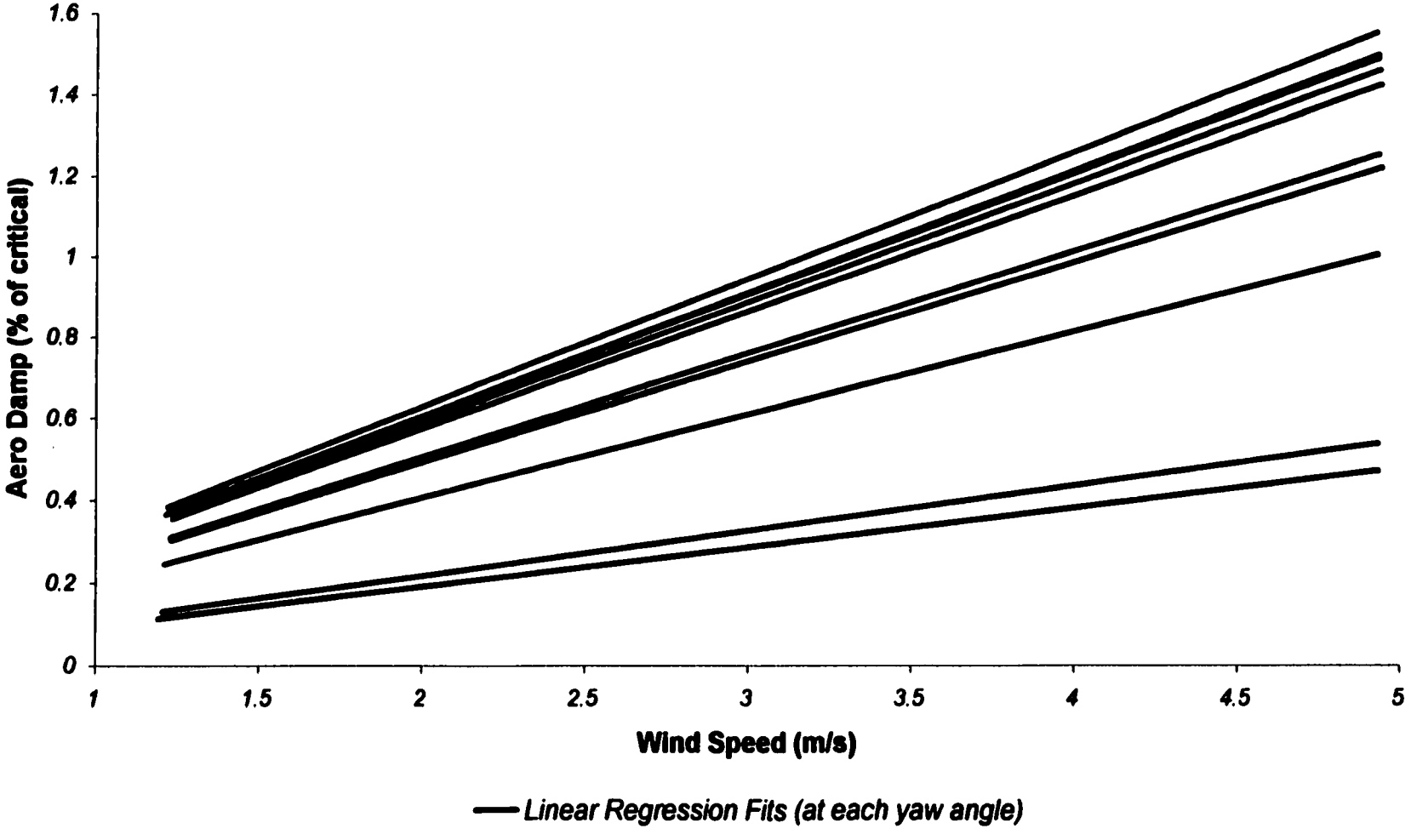

Figure 4.7.1
Aero Damping vs. Width/Depth Ratio
-10 degrees

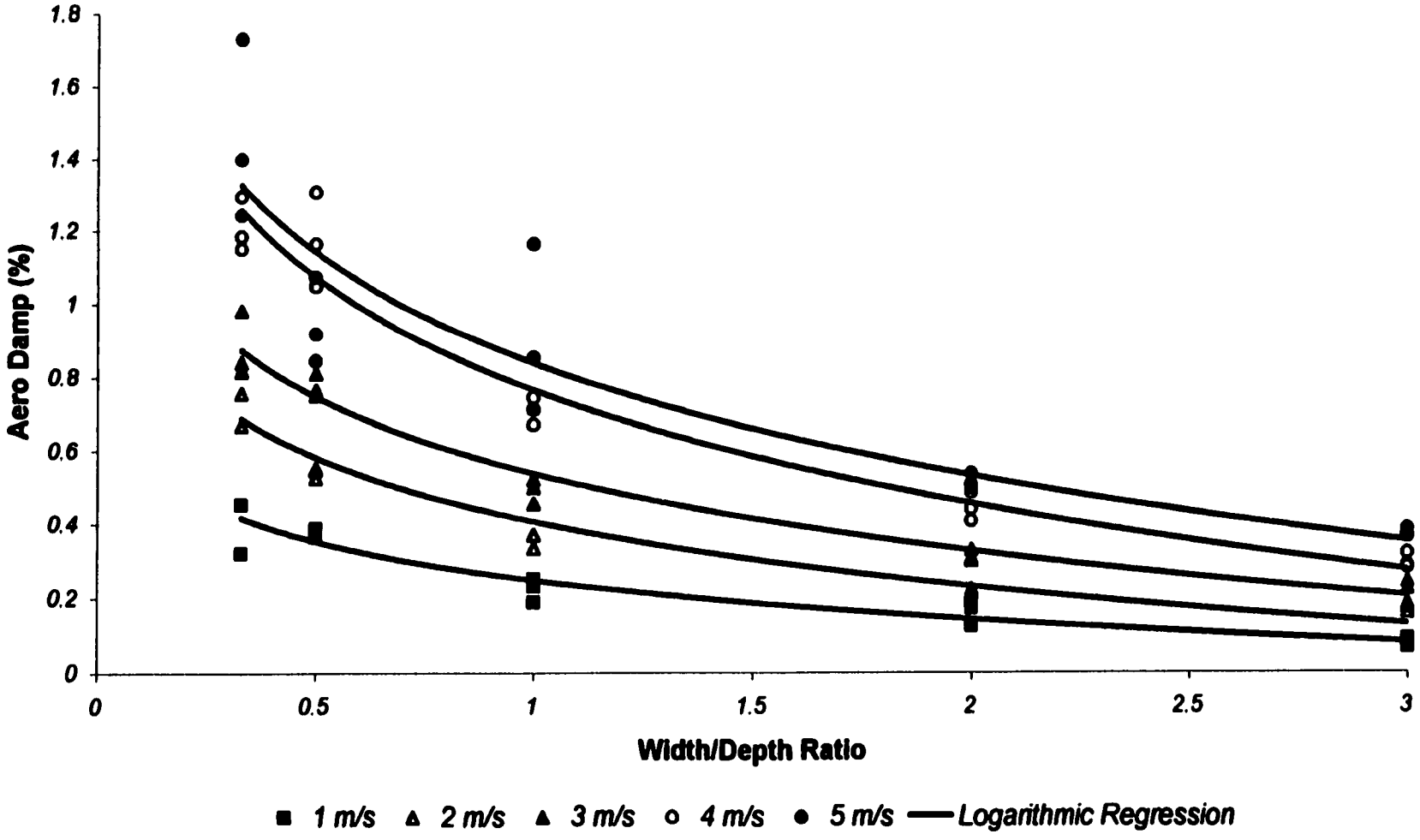

Figure 4.7.2
Aero Damping vs. Width/Depth Ratio
0 degrees

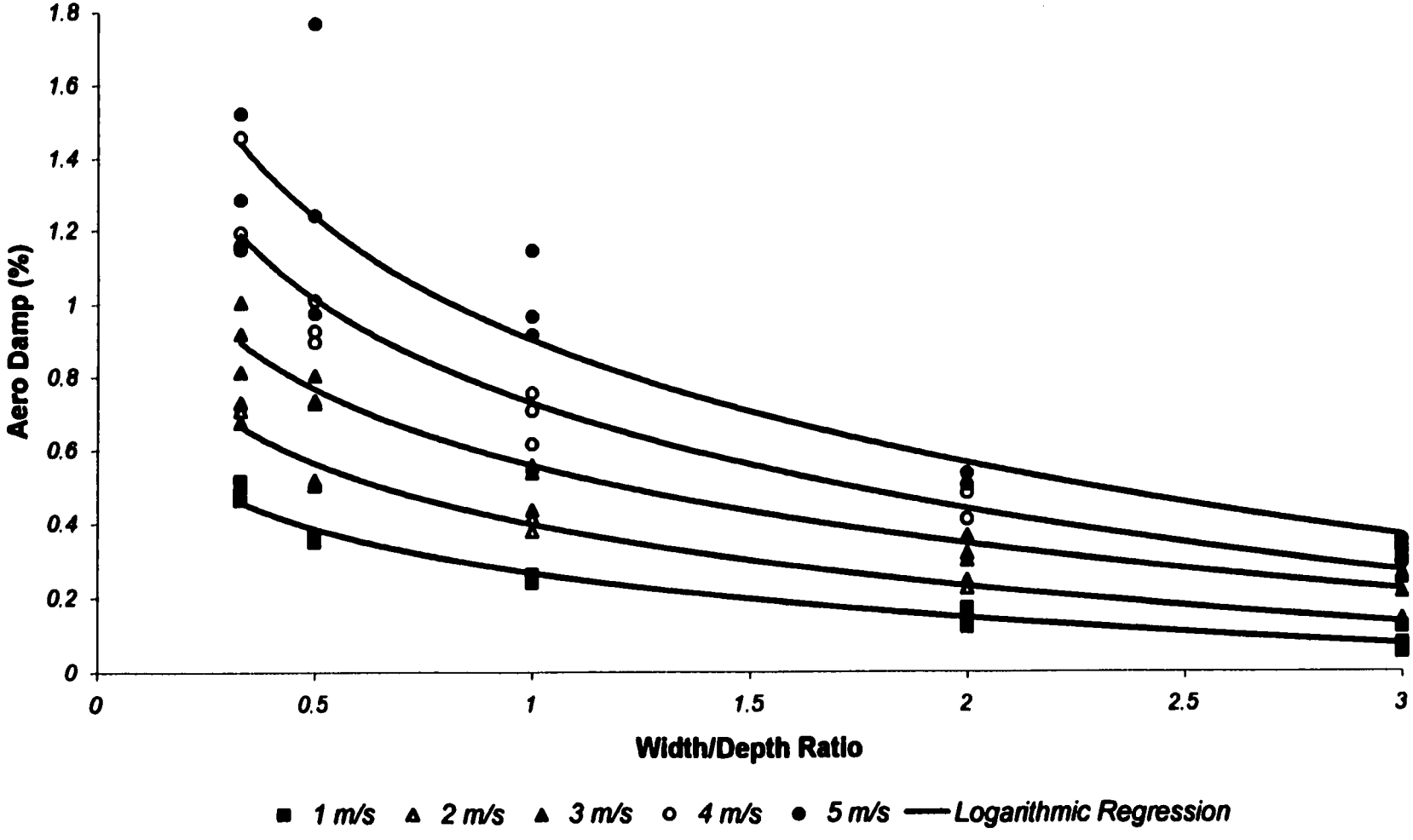

Figure 4.7.3
Aero Damping vs. Width/Depth Ratio
10 degrees

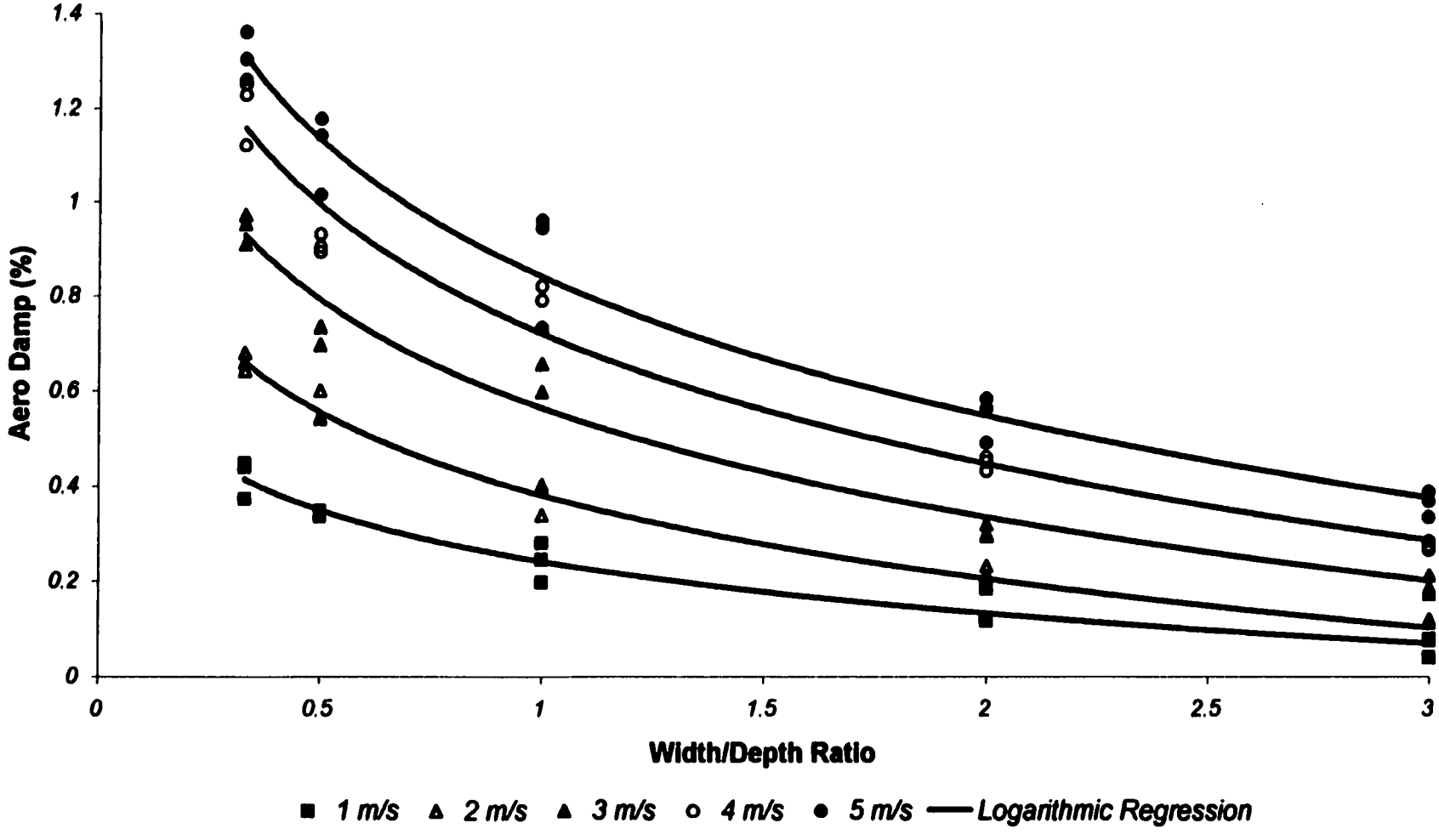

Figure 4.7.4
Aero Damping vs. Width/Depth Ratio
20 degrees

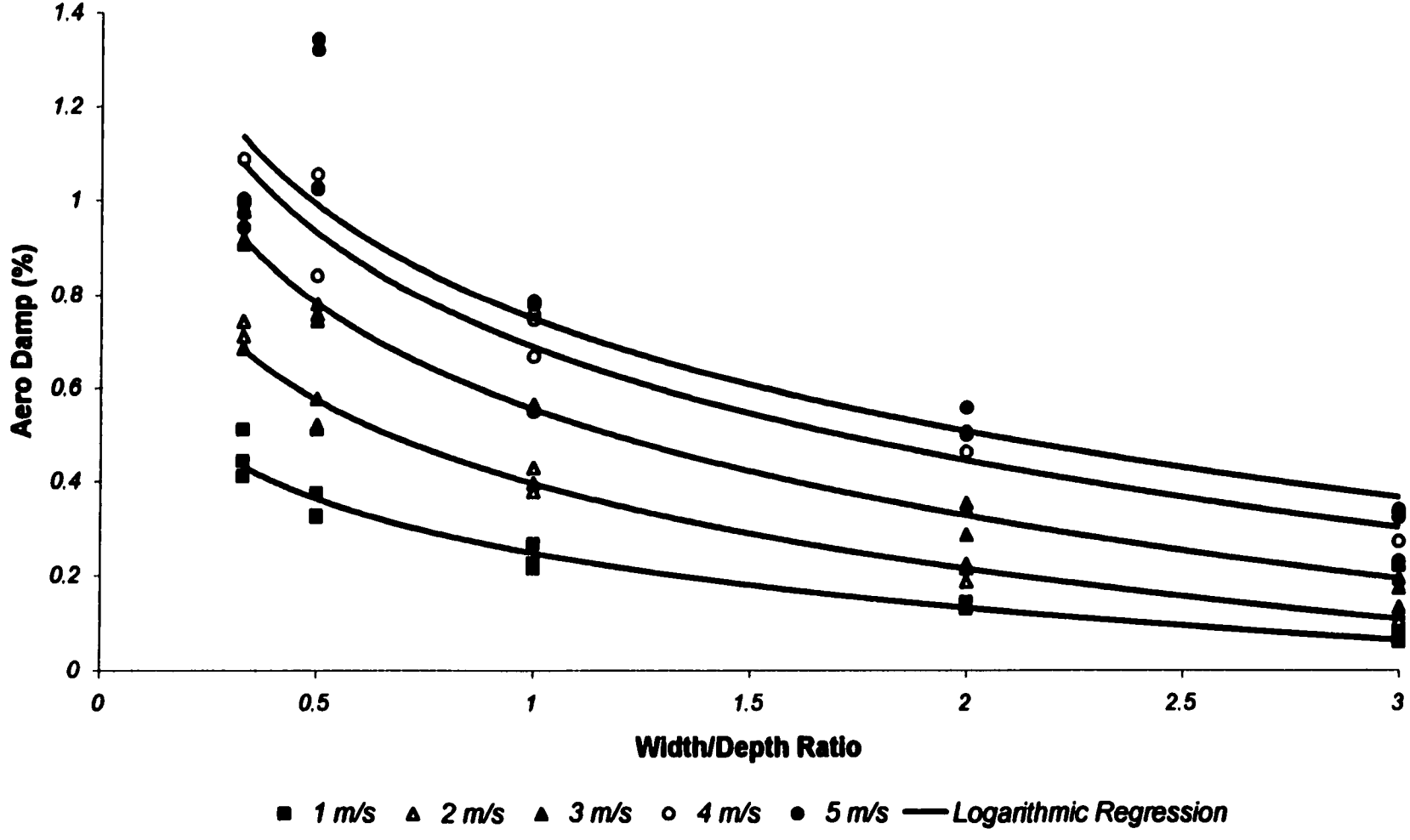

Figure 4.7.5
Aero Damping vs. Width/Depth Ratio
30 degrees

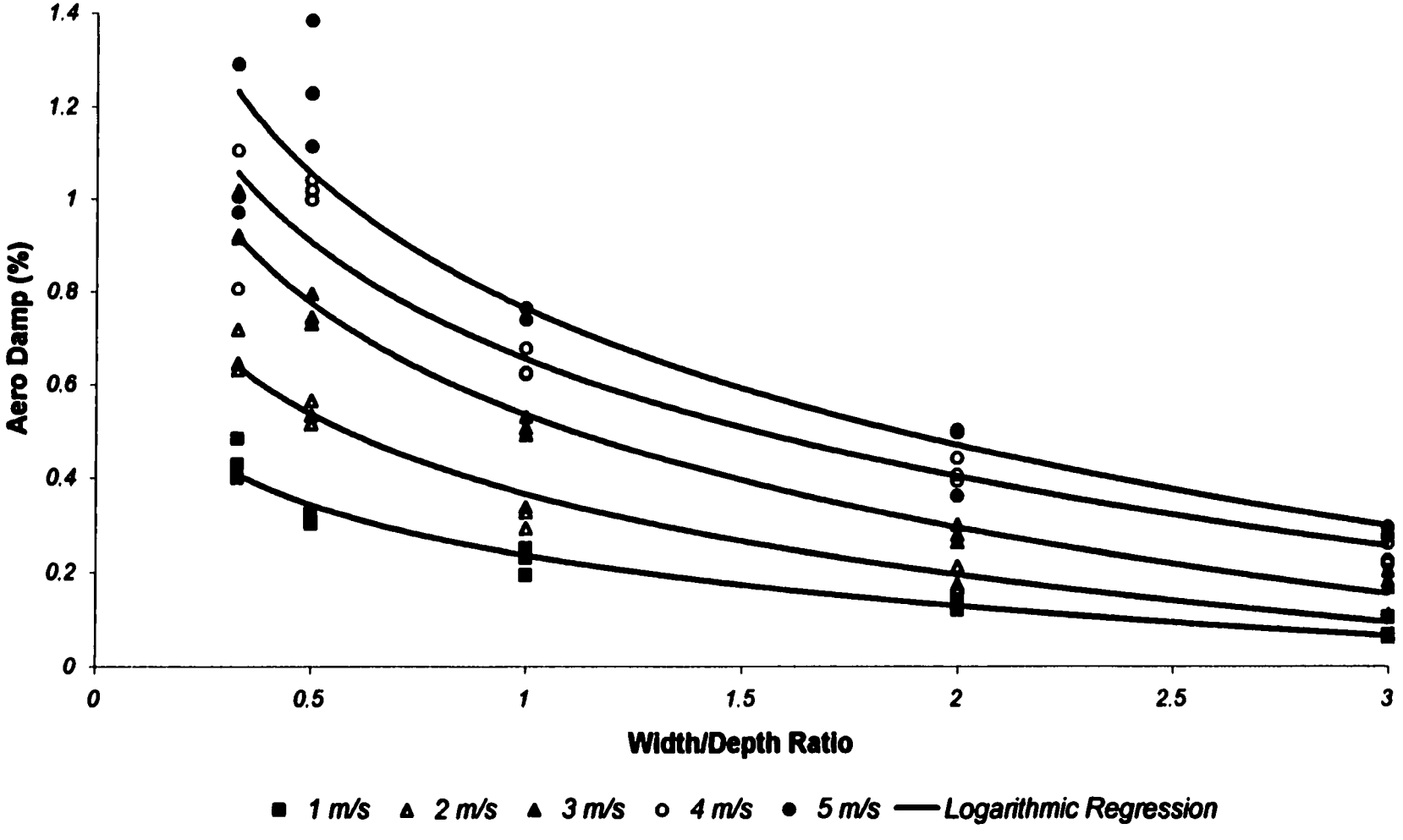

Figure 4.7.6
Aero Damping vs. Width/Depth Ratio
40 degrees

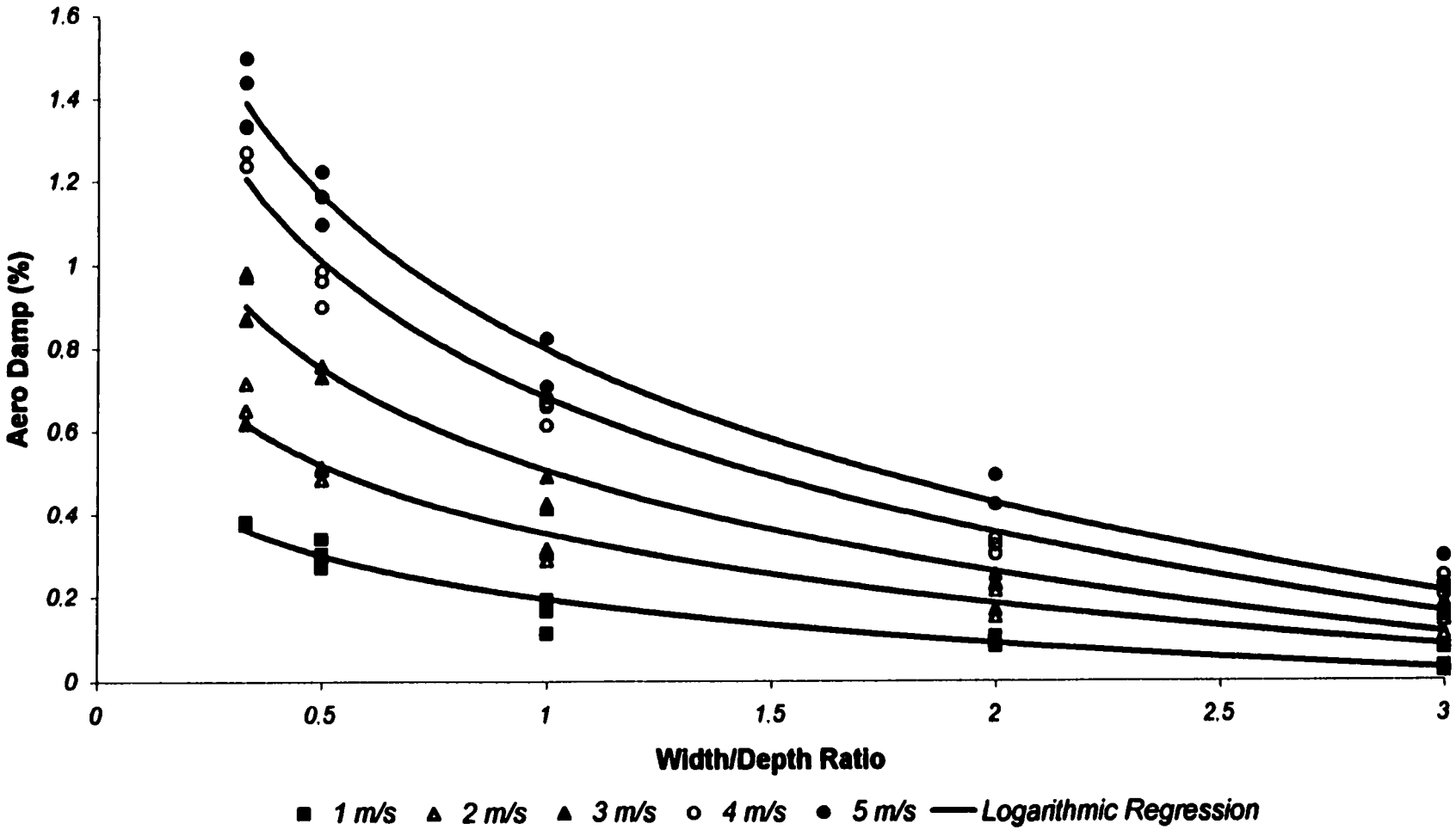

Figure 4.7.7
Aero Damping vs. Width/Depth Ratio
50 degrees

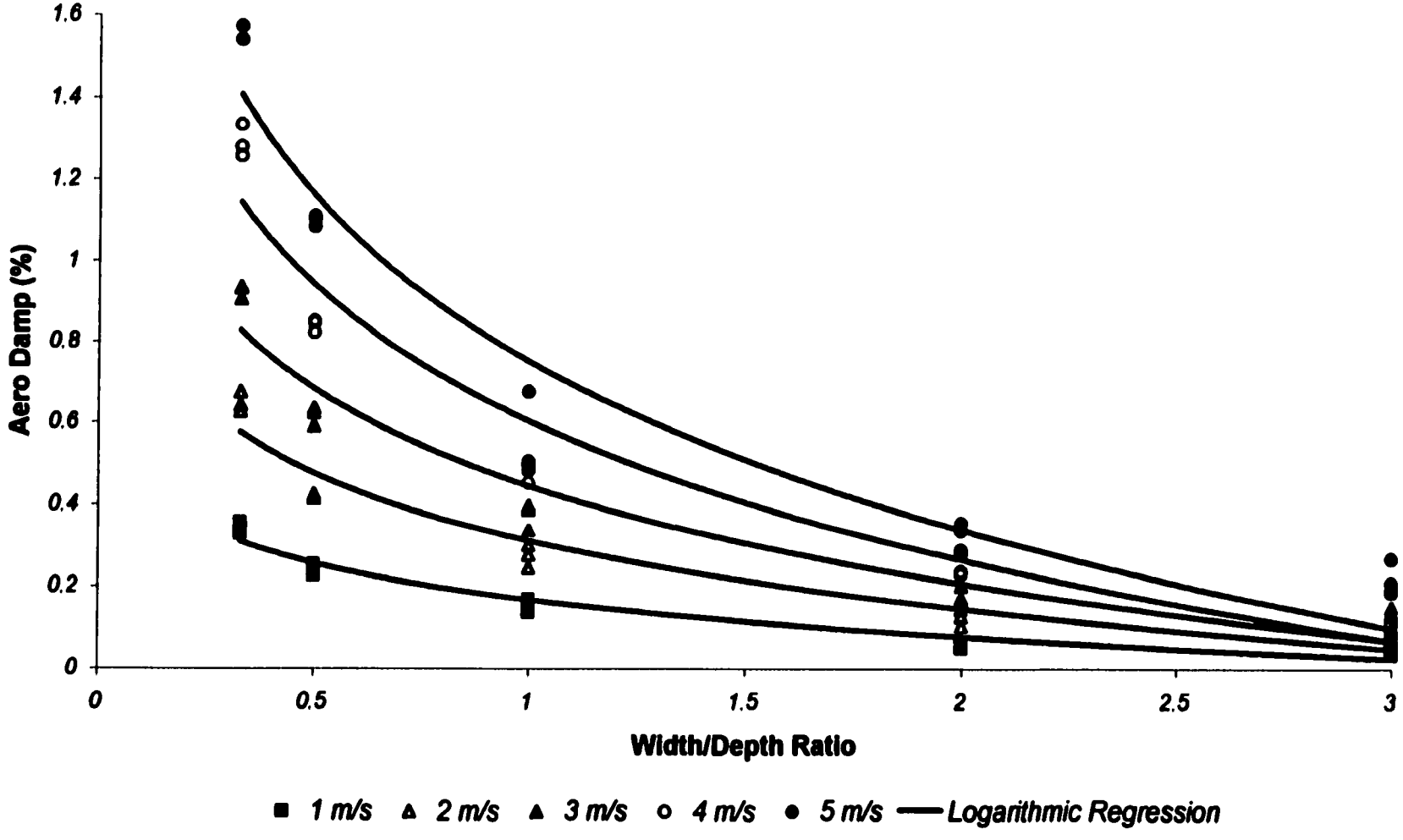

Figure 4.7.8
Aero Damping vs. Width/Depth Ratio
60 degrees

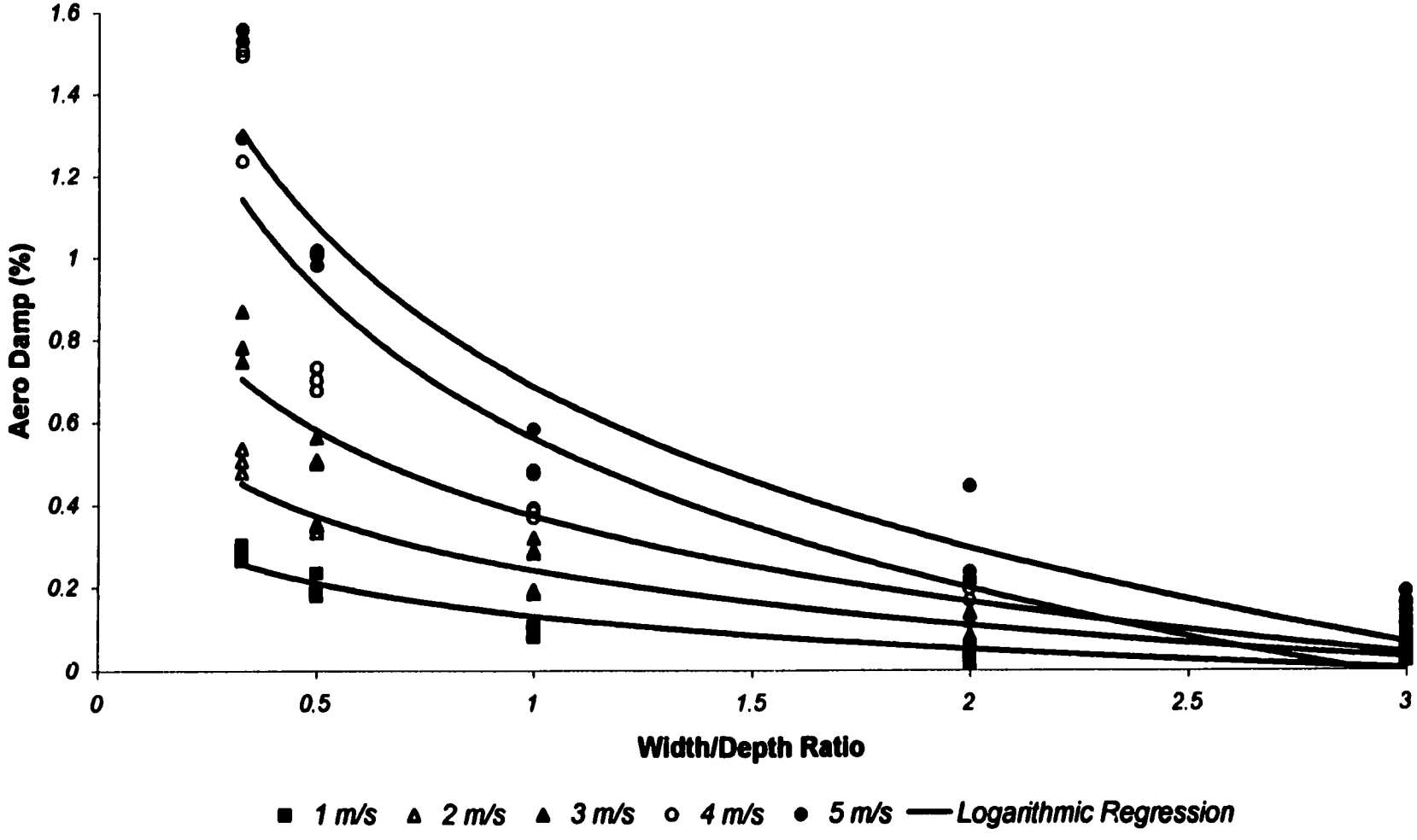

Figure 4.7.9
Aero Damping vs. Width/Depth Ratio
70 degrees

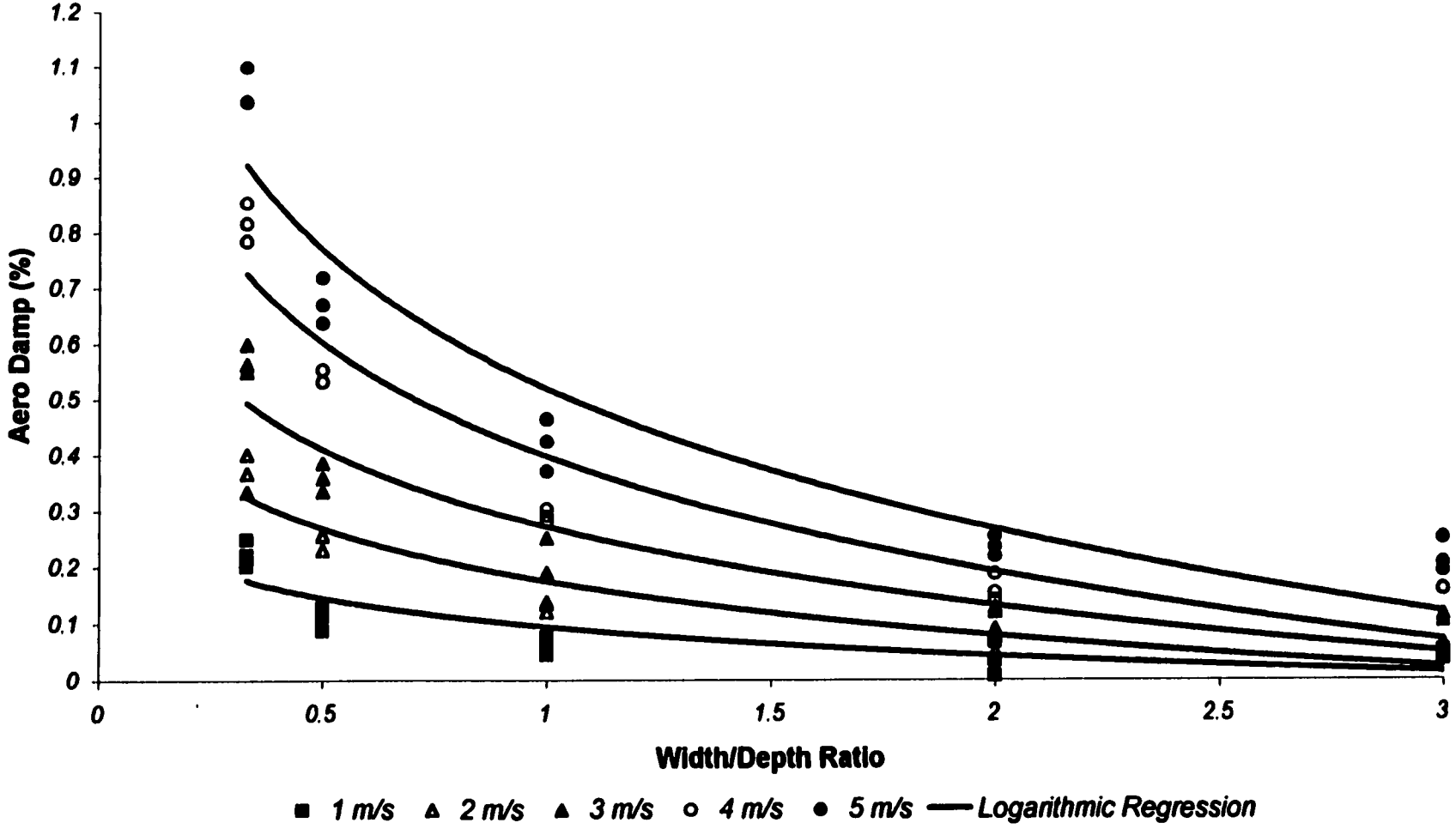

Figure 4.7.10
Aero Damping vs. Width/Depth Ratio
80 degrees

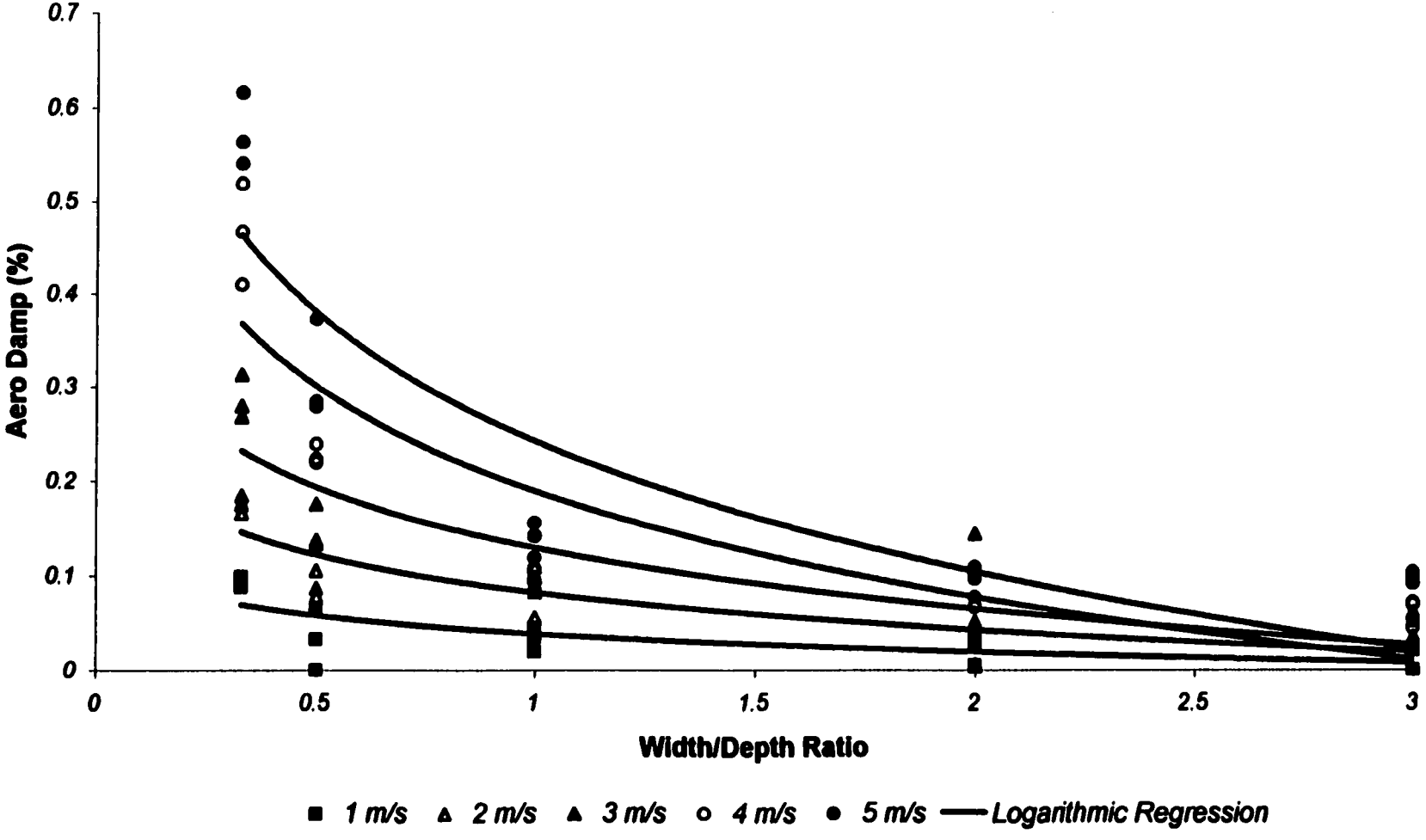

Figure 4.7.11
Aero Damping vs. Width/Depth Ratio
90 degrees

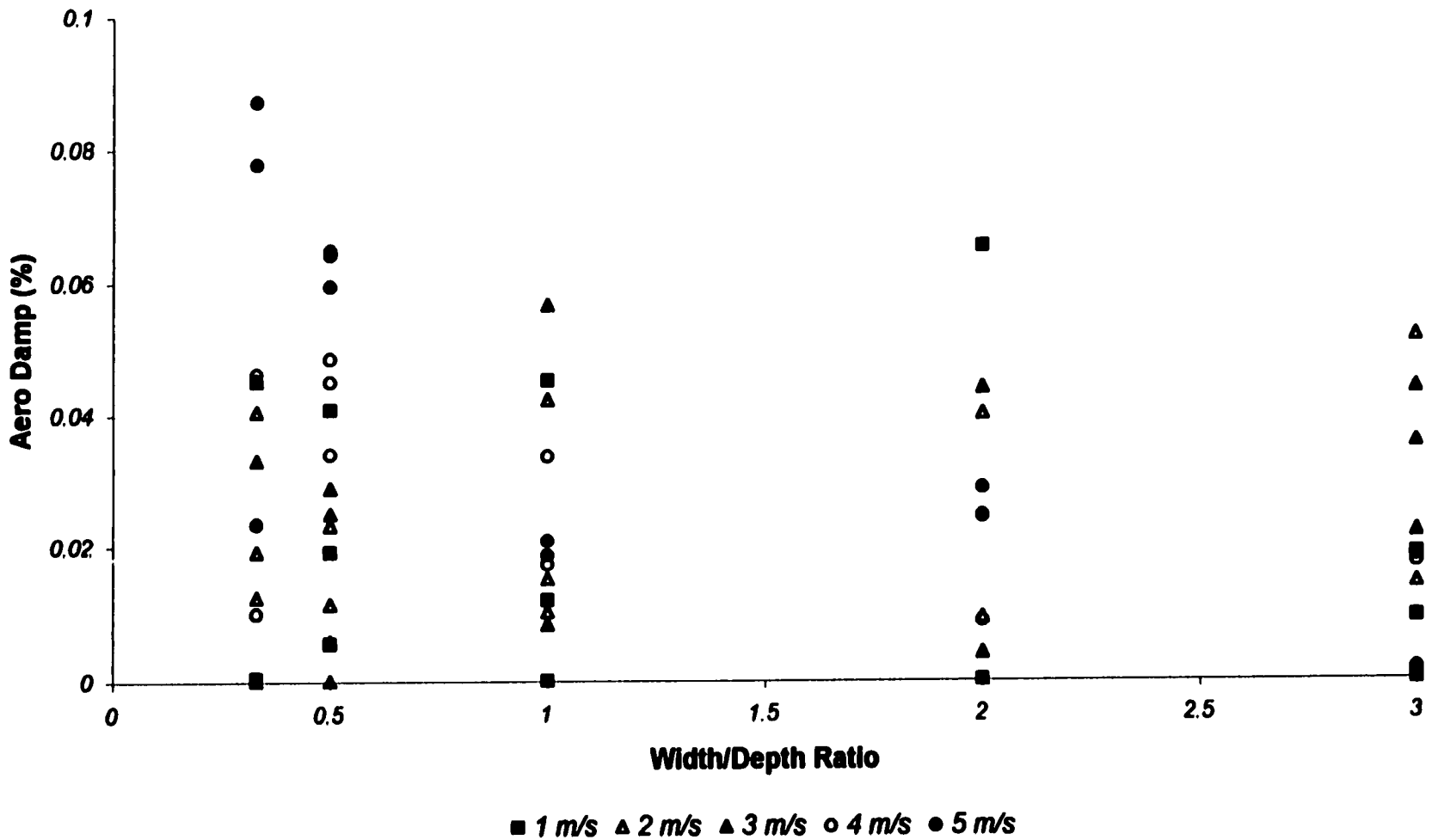

Figure 4.7.12
Aero Damping vs. Width/Depth Ratio
100 degrees

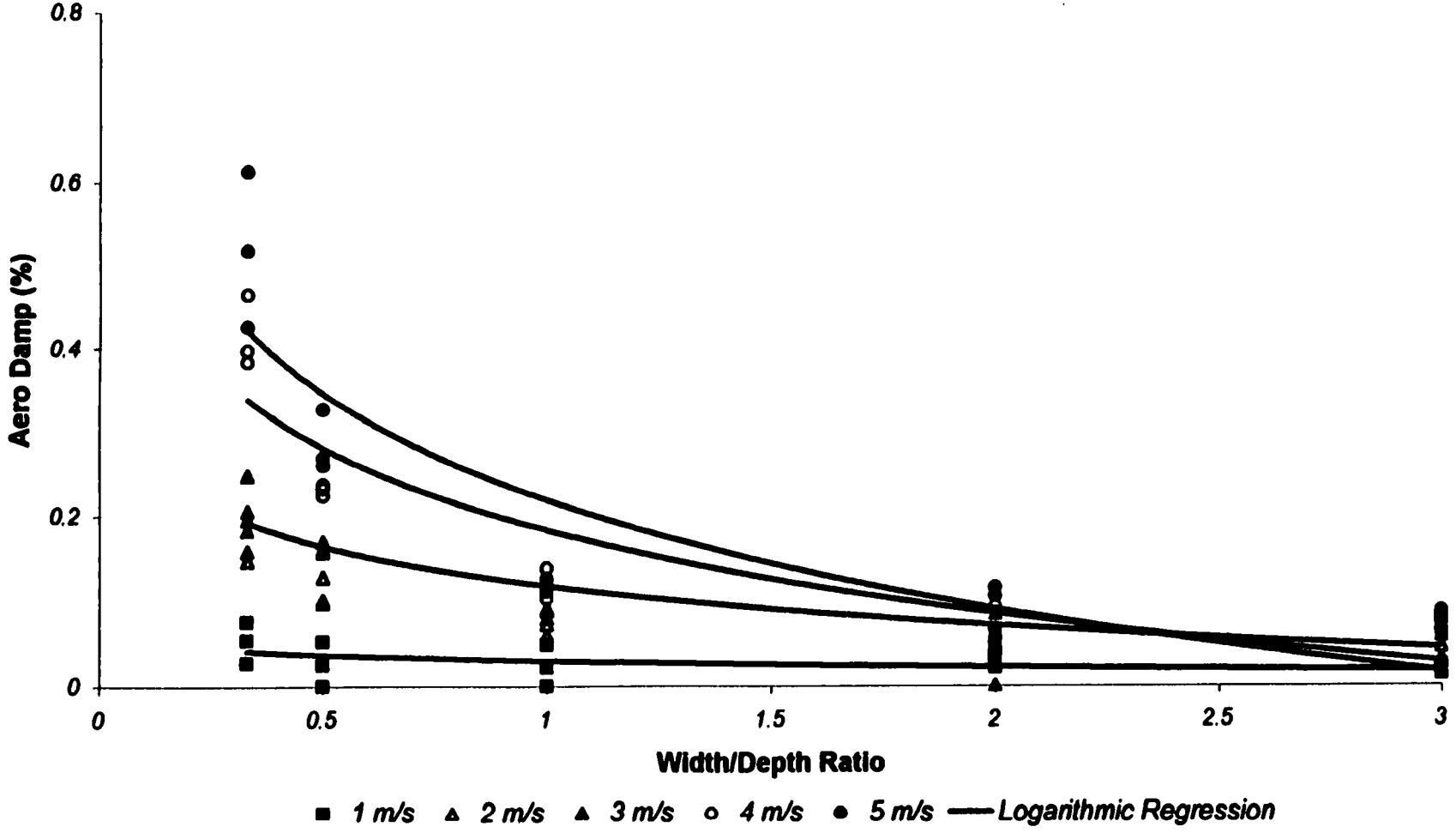

Figure 4.7.13
Aero Damping vs. Width/Depth
1 m/s

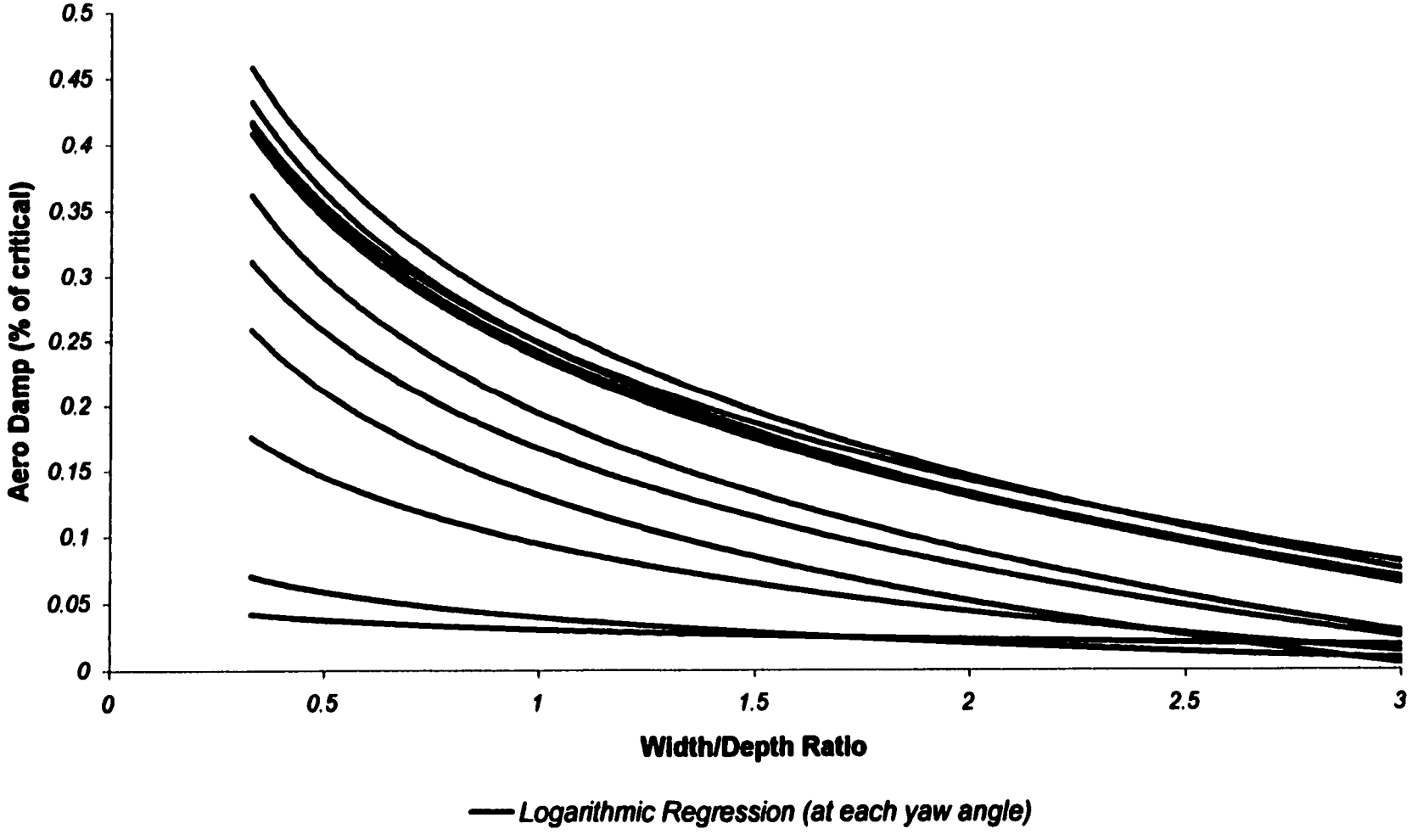

Figure 4.7.14
Aero Damping vs. Width/Depth
2 m/s

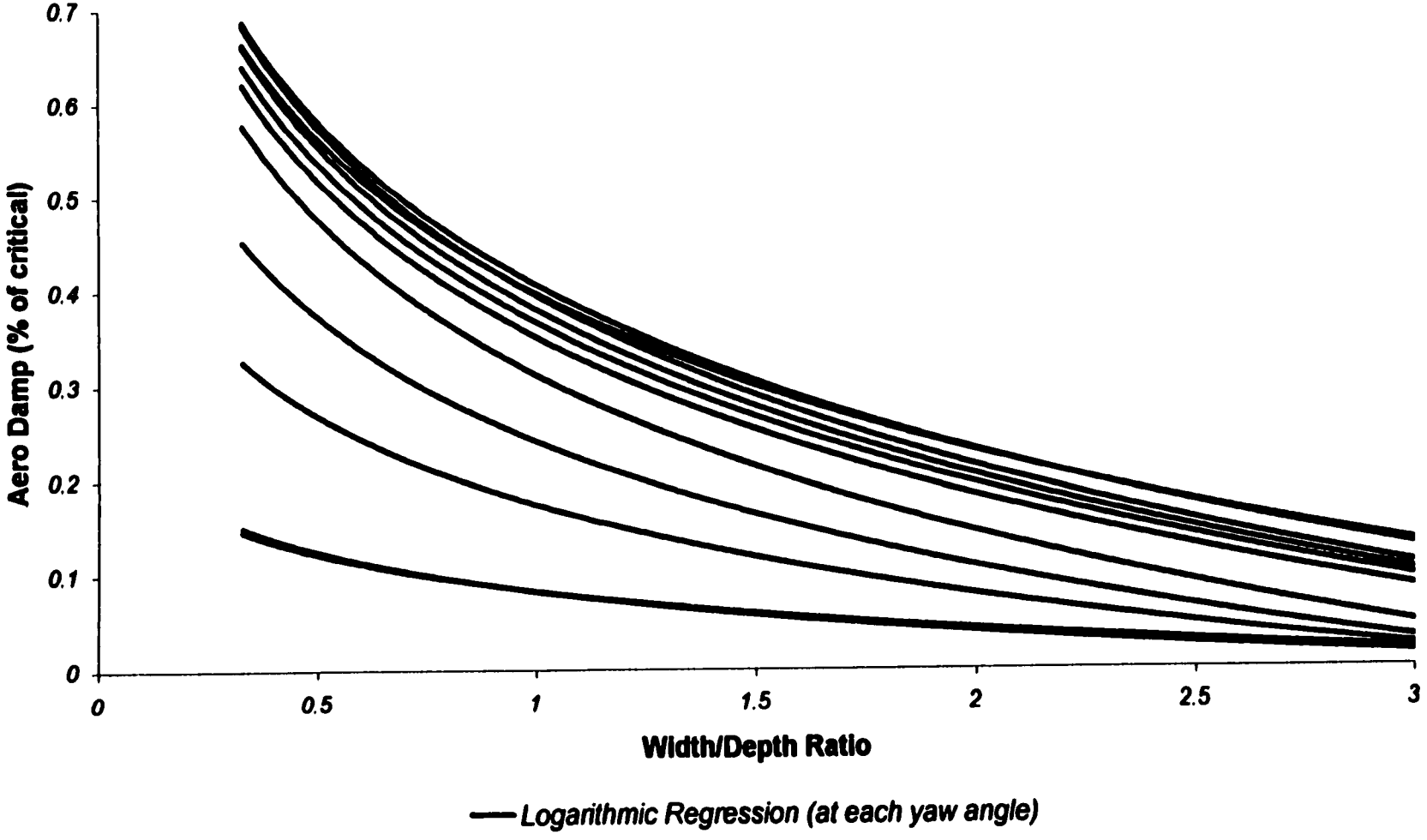

Figure 4.7.15
Aero Damping vs. Width/Depth
3 m/s

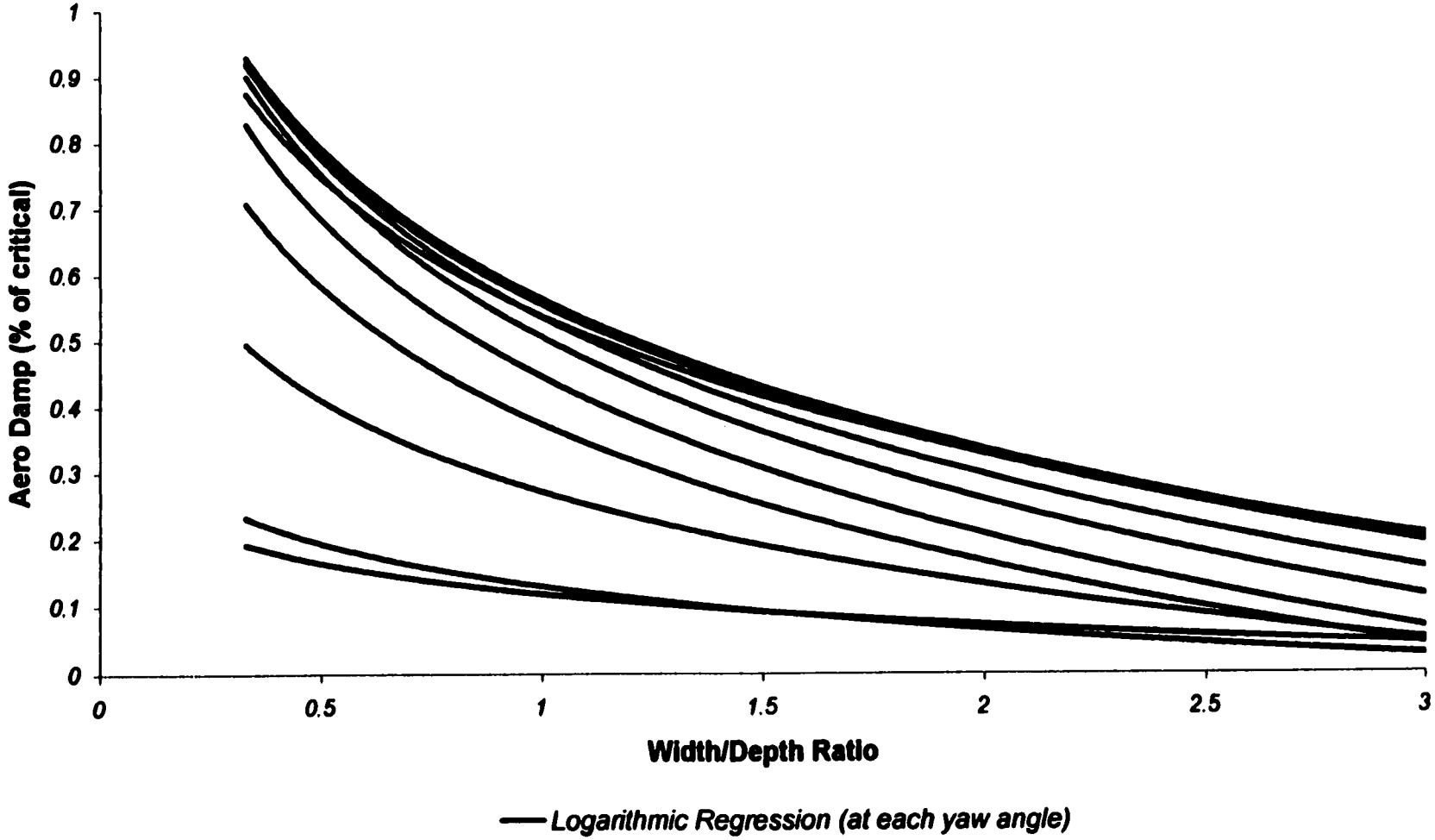

Figure 4.7.16
Aero Damping vs. Width/Depth
4 m/s

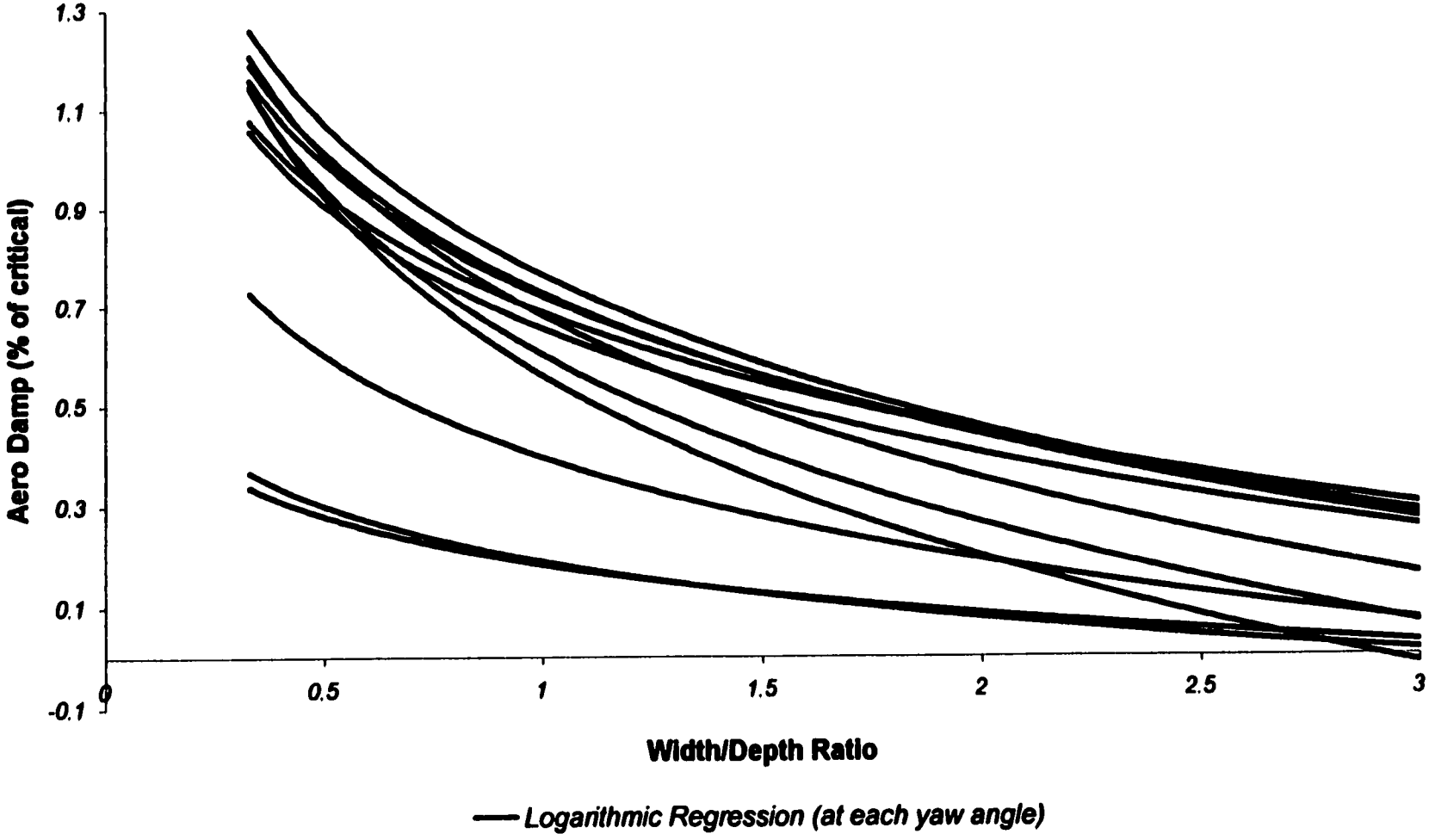

Figure 4.7.17
Aero Damping vs. Width/Depth
5 m/s

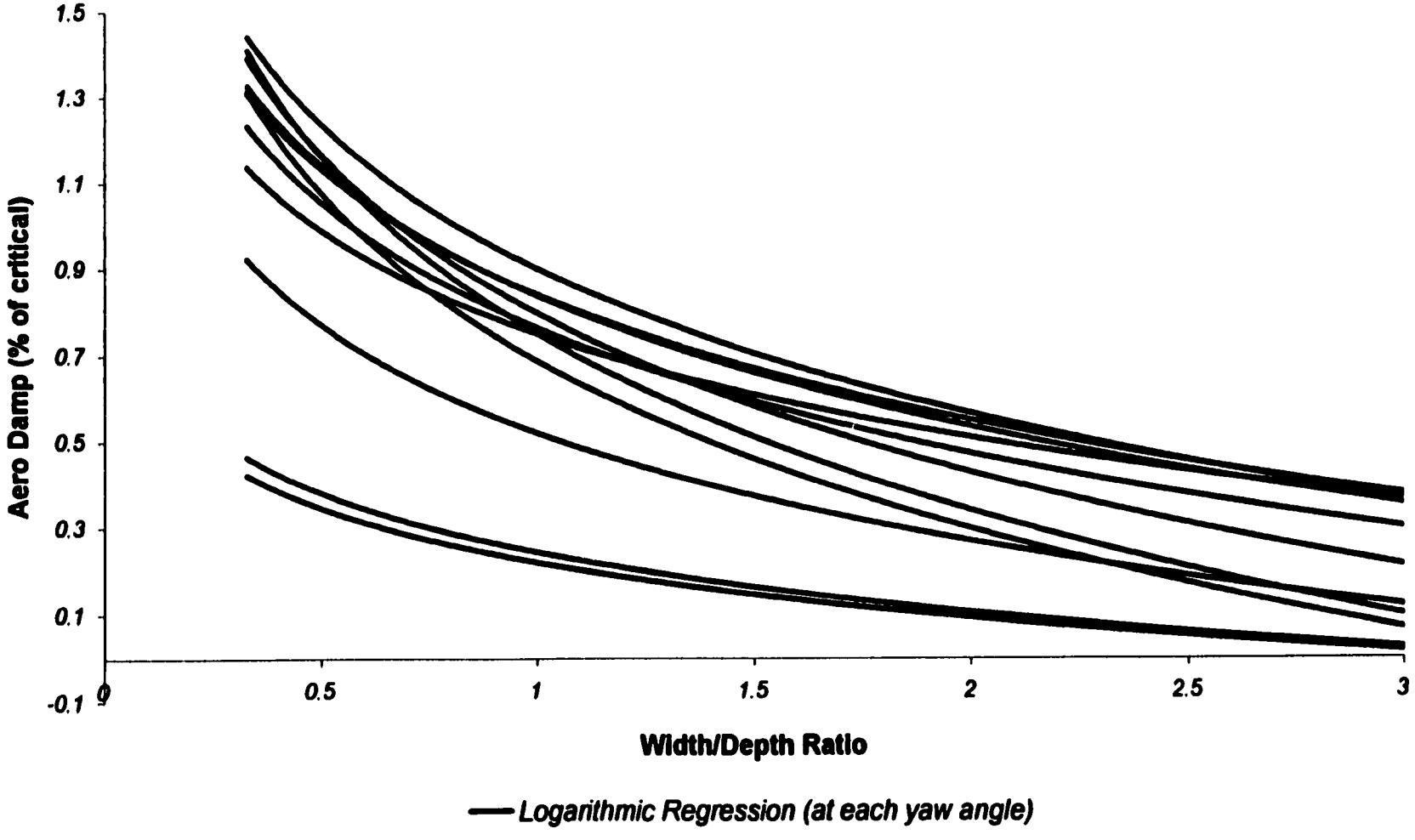

Figure 4.8.1
Self Excited RMS vs. Yaw Angle
Section 1

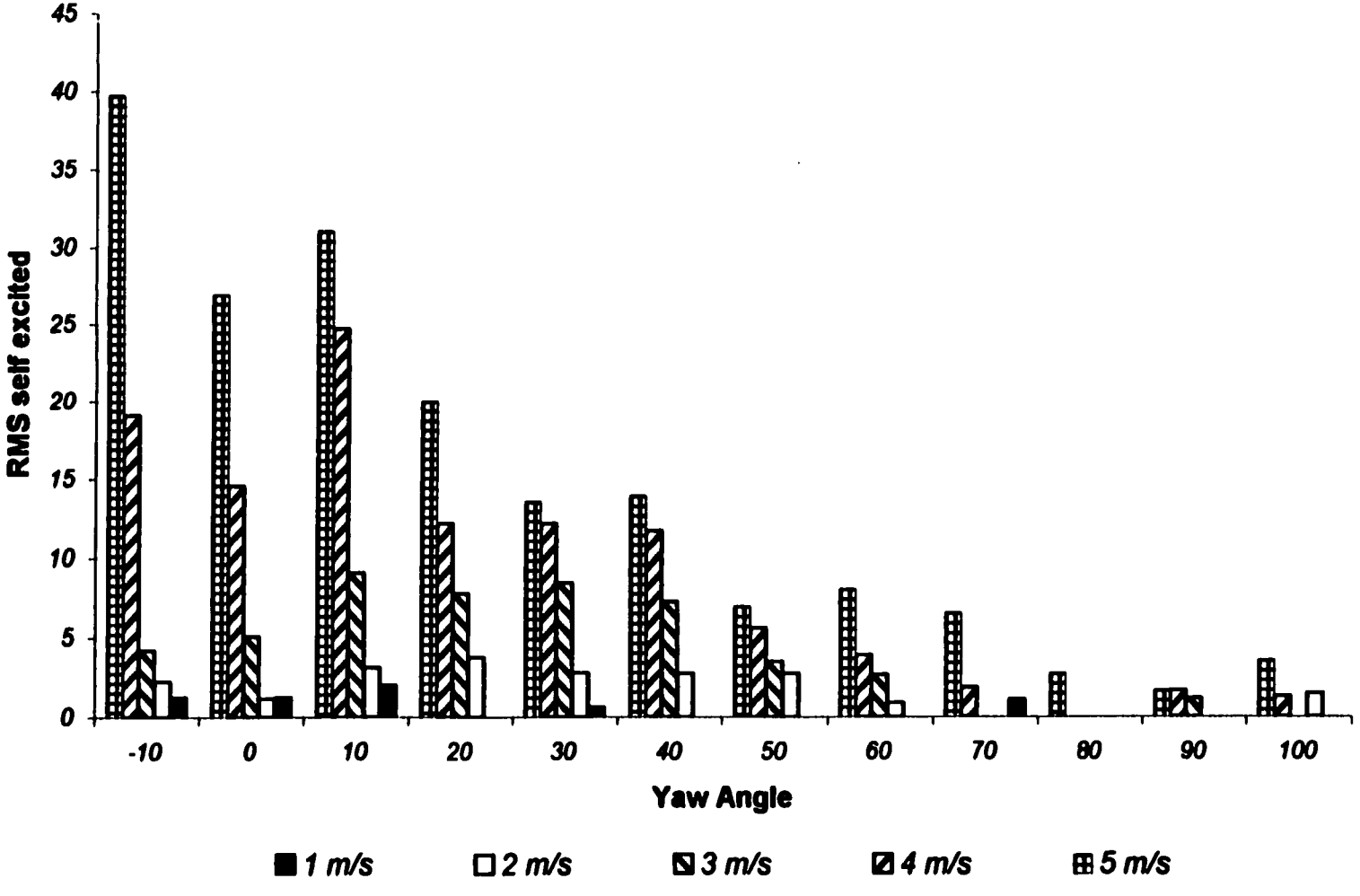

Figure 4.8.2
Self Excited RMS vs. Yaw Angle
Section 2

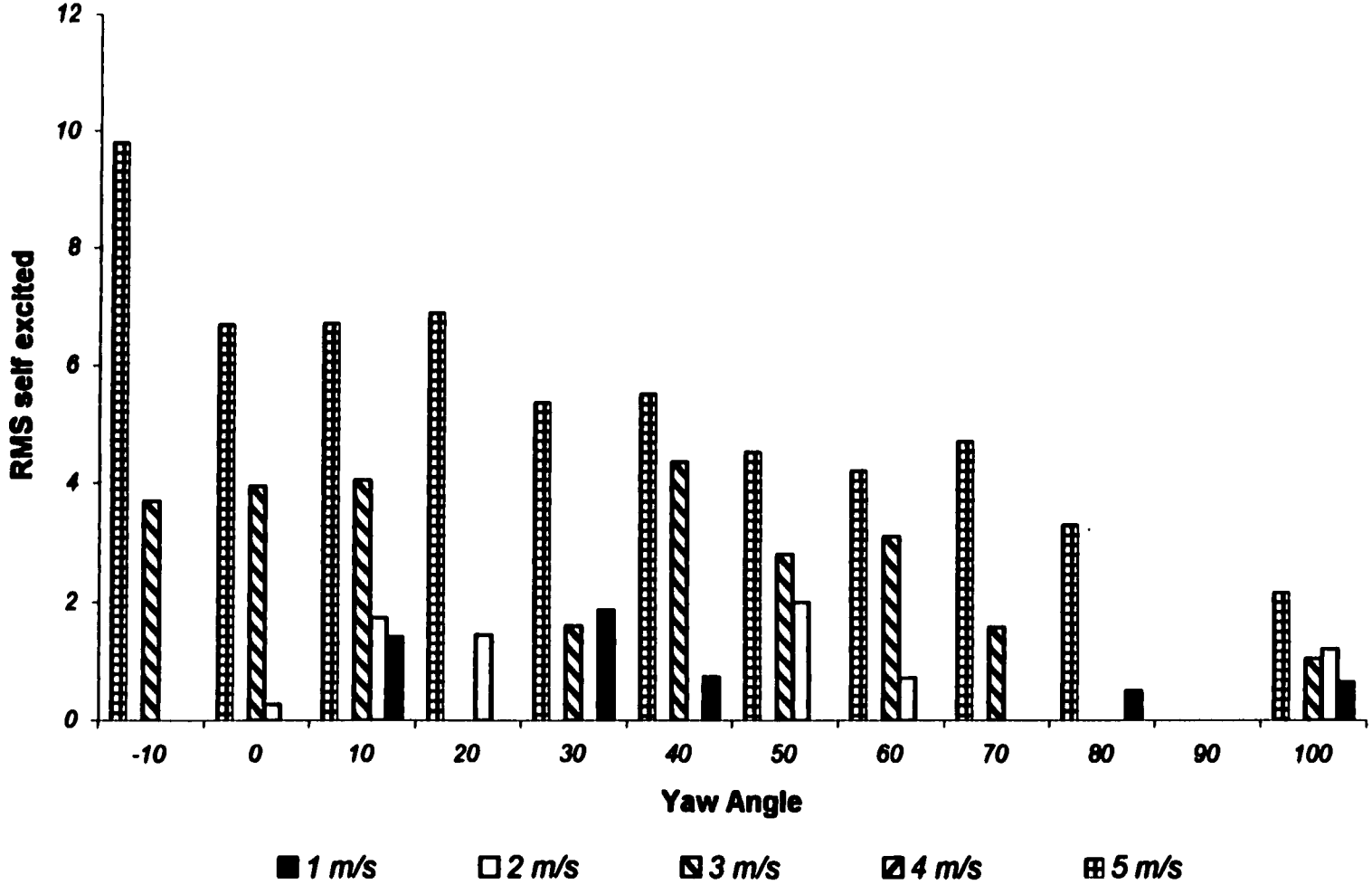

Figure 4.8.3
Self Excited RMS vs. Yaw Angle
Section 3

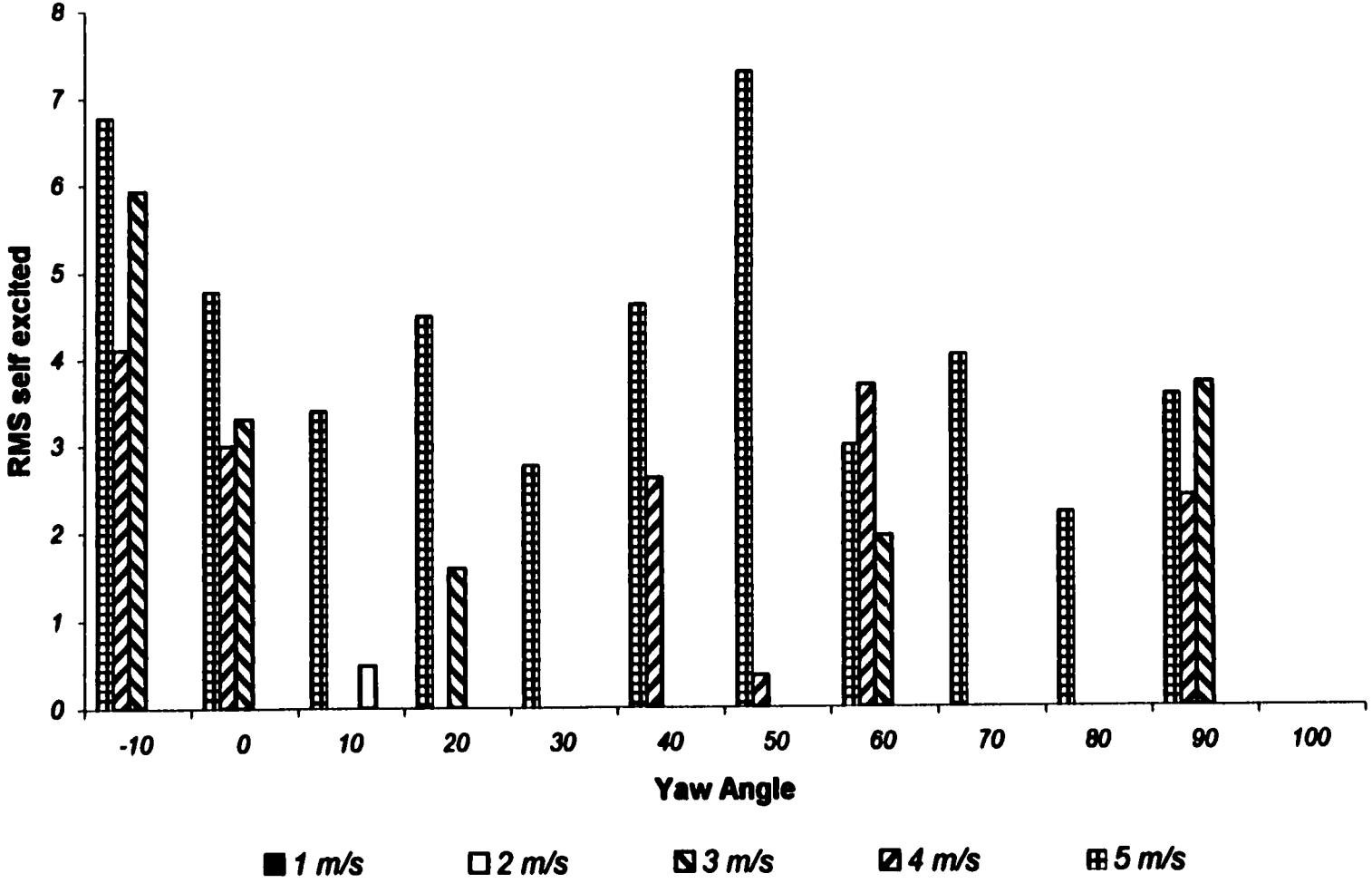

Figure 4.8.4
Self Excited RMS vs. Yaw Angle
Section 4

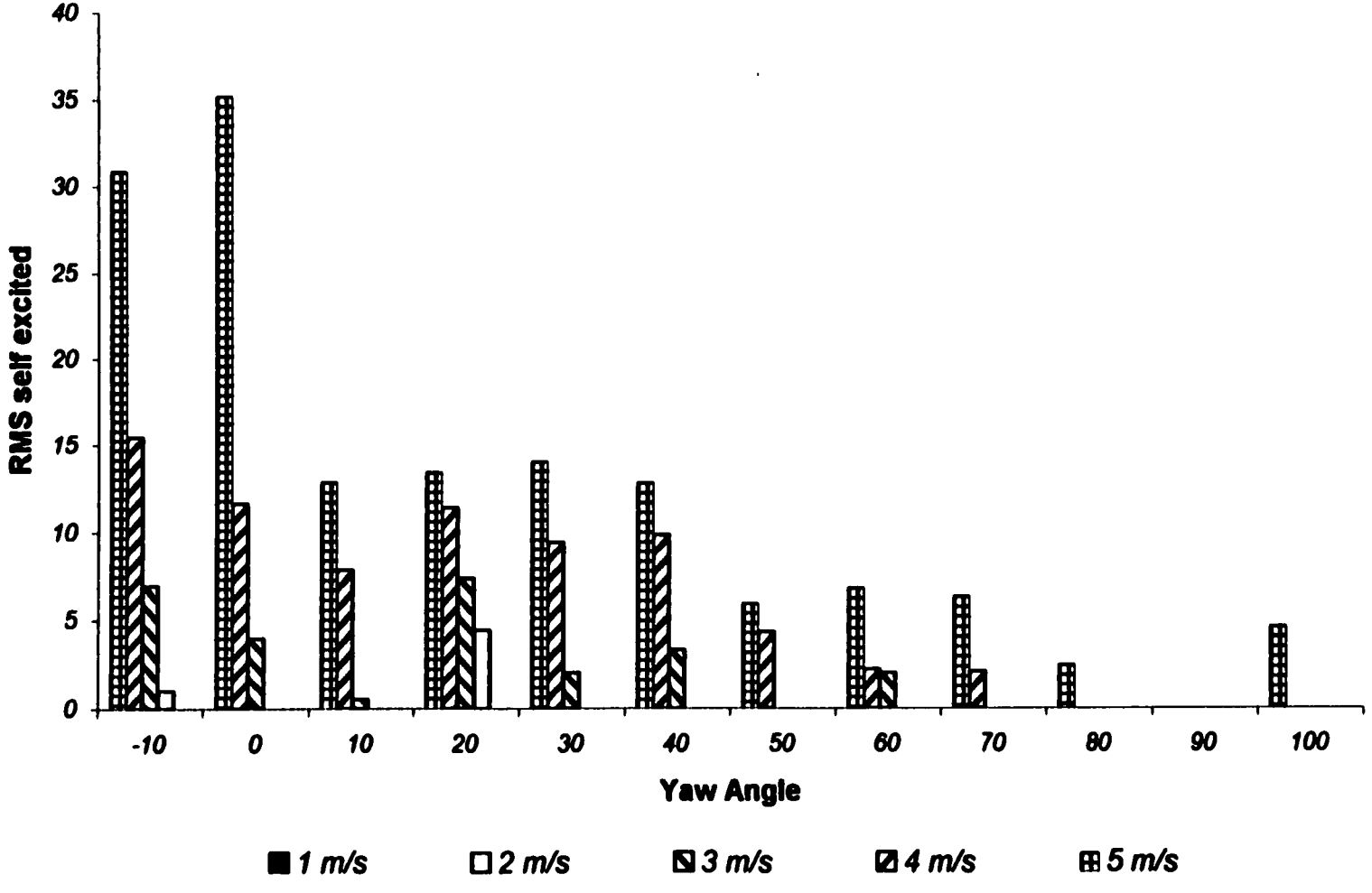

Figure 4.8.5
Self Excited RMS vs. Yaw Angle
Section 5

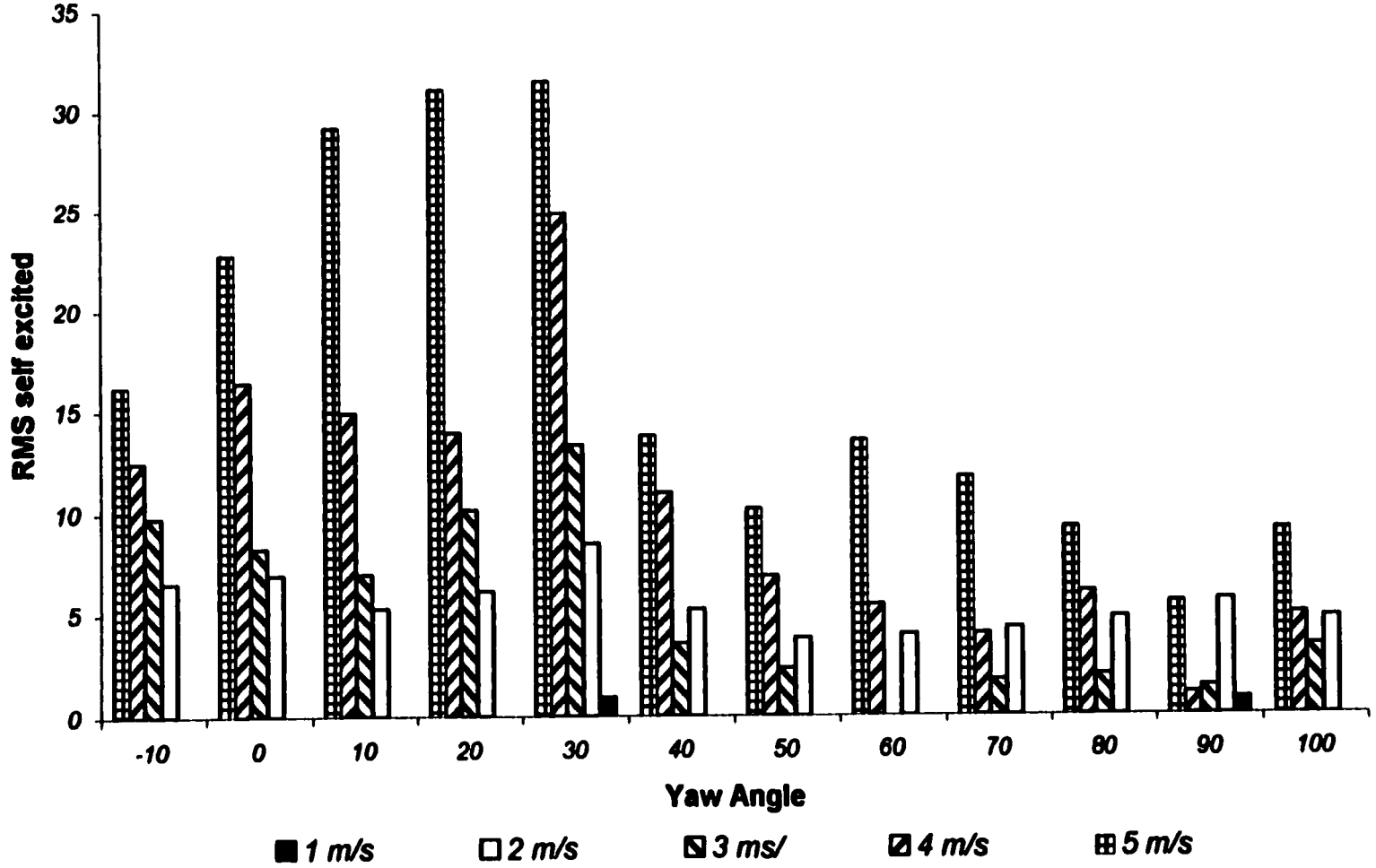

Figure 4.8.6
Self Excited RMS vs. Yaw Angle
1 m/s

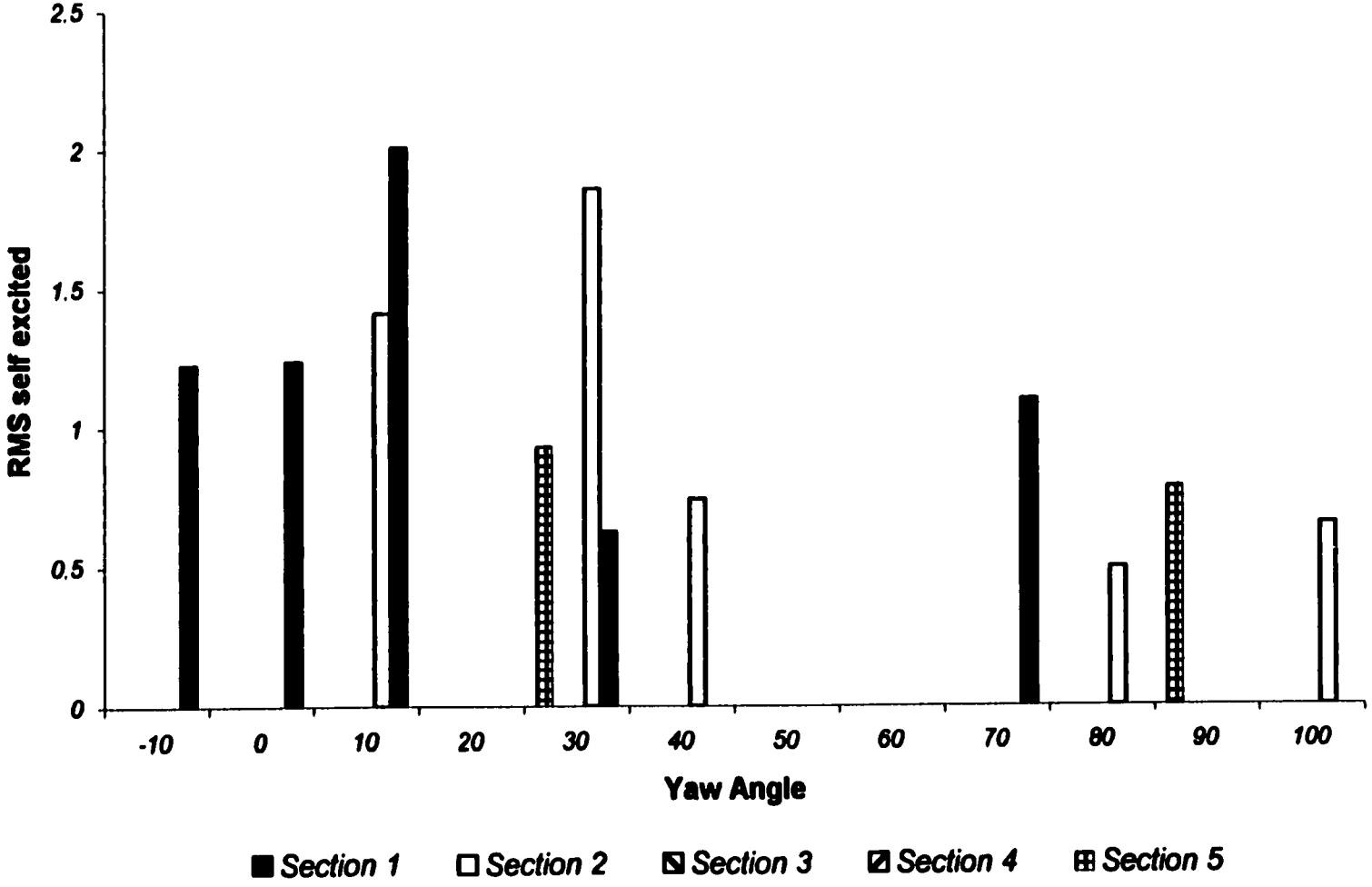

Figure 4.8.7
Self Excited RMS vs. Yaw Angle
2 m/s

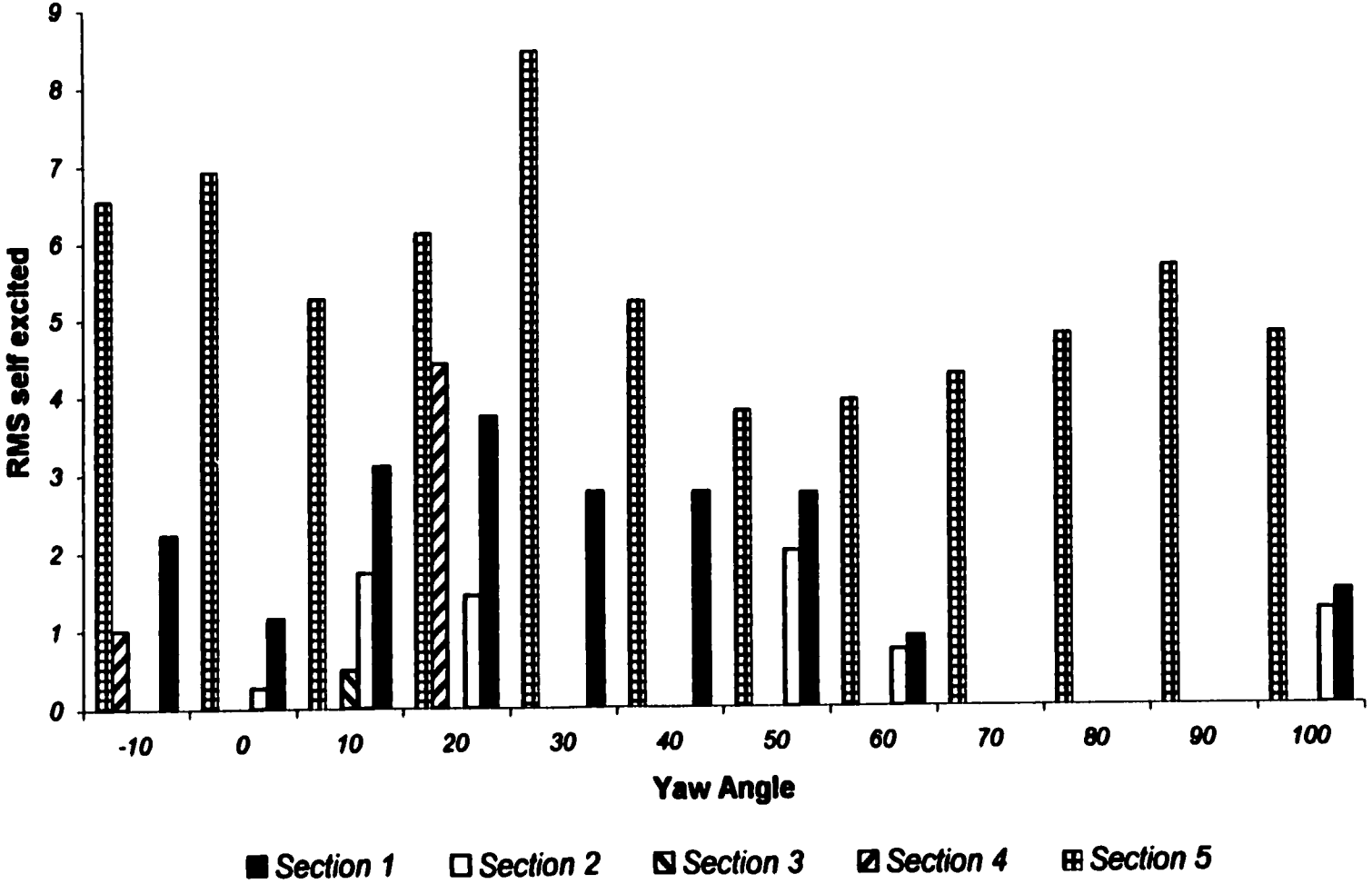

Figure 4.8.8
Self Excited RMS vs. Yaw Angle
3 m/s

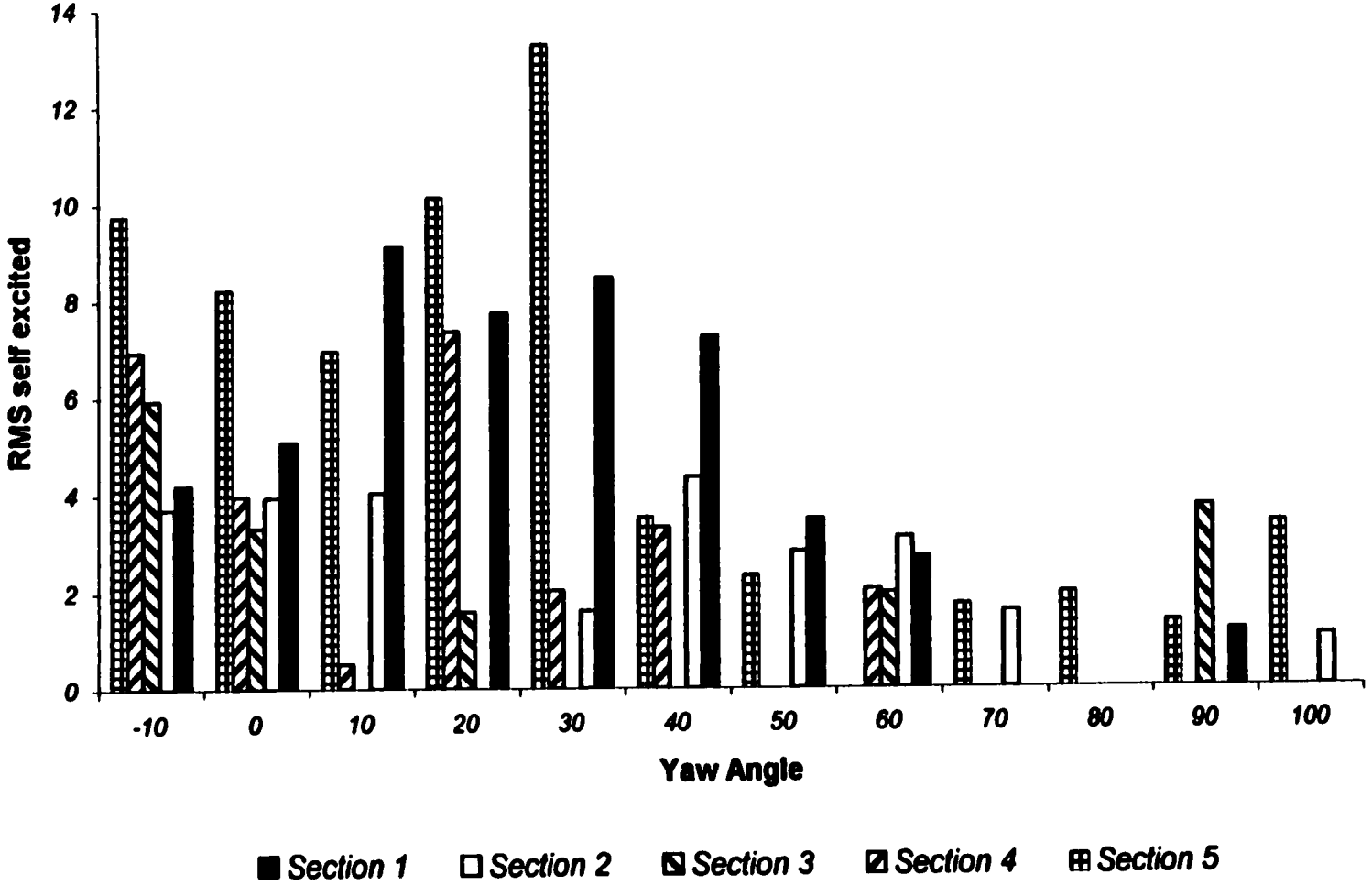

Figure 4.8.9
Self Excited RMS vs. Yaw Angle
4 m/s

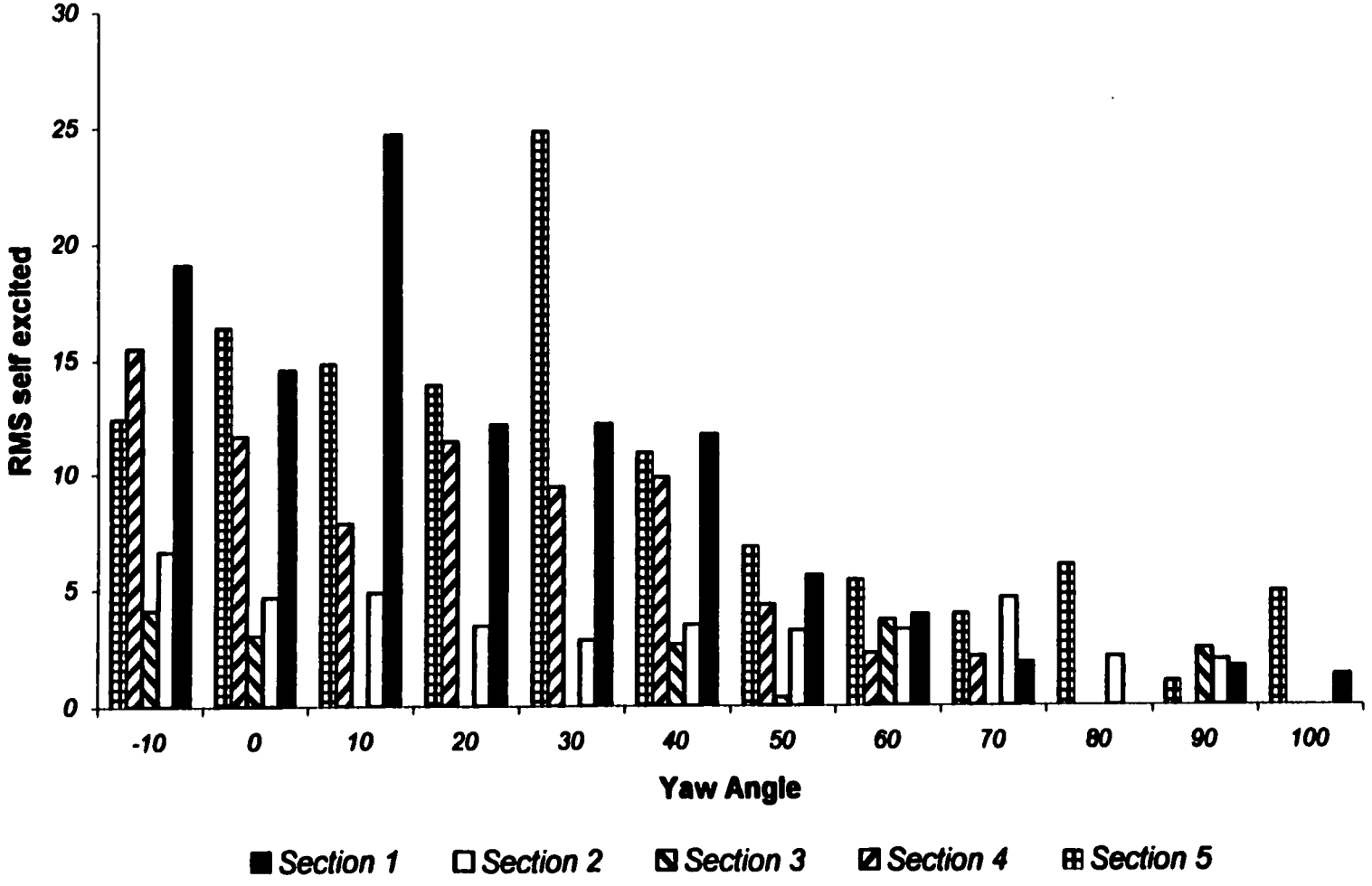

Figure 4.8.10
Self Excited RMS vs. Yaw Angle
5 m/s

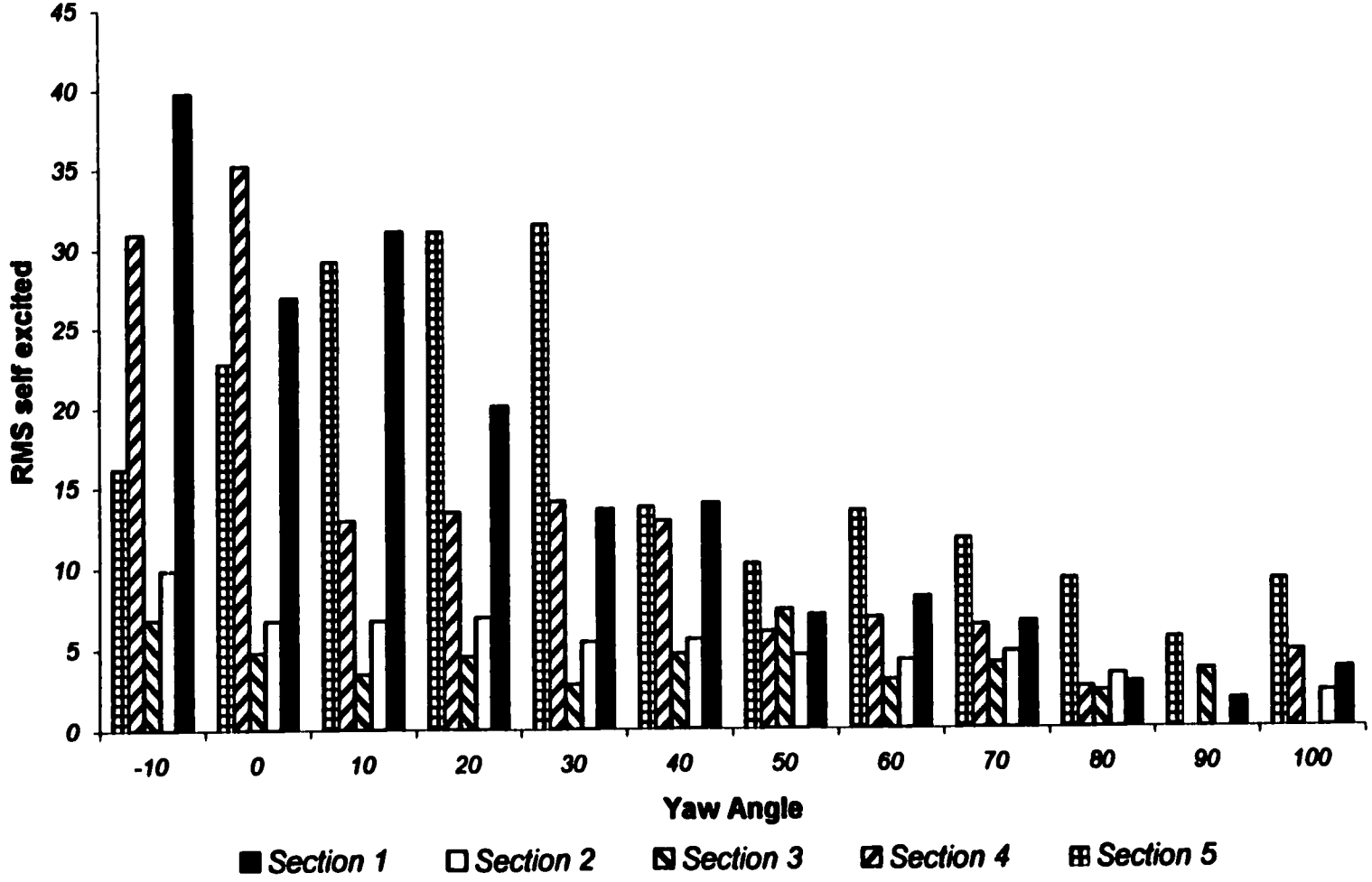

Figure 5.1
RMS vs. Mean Wind Speed

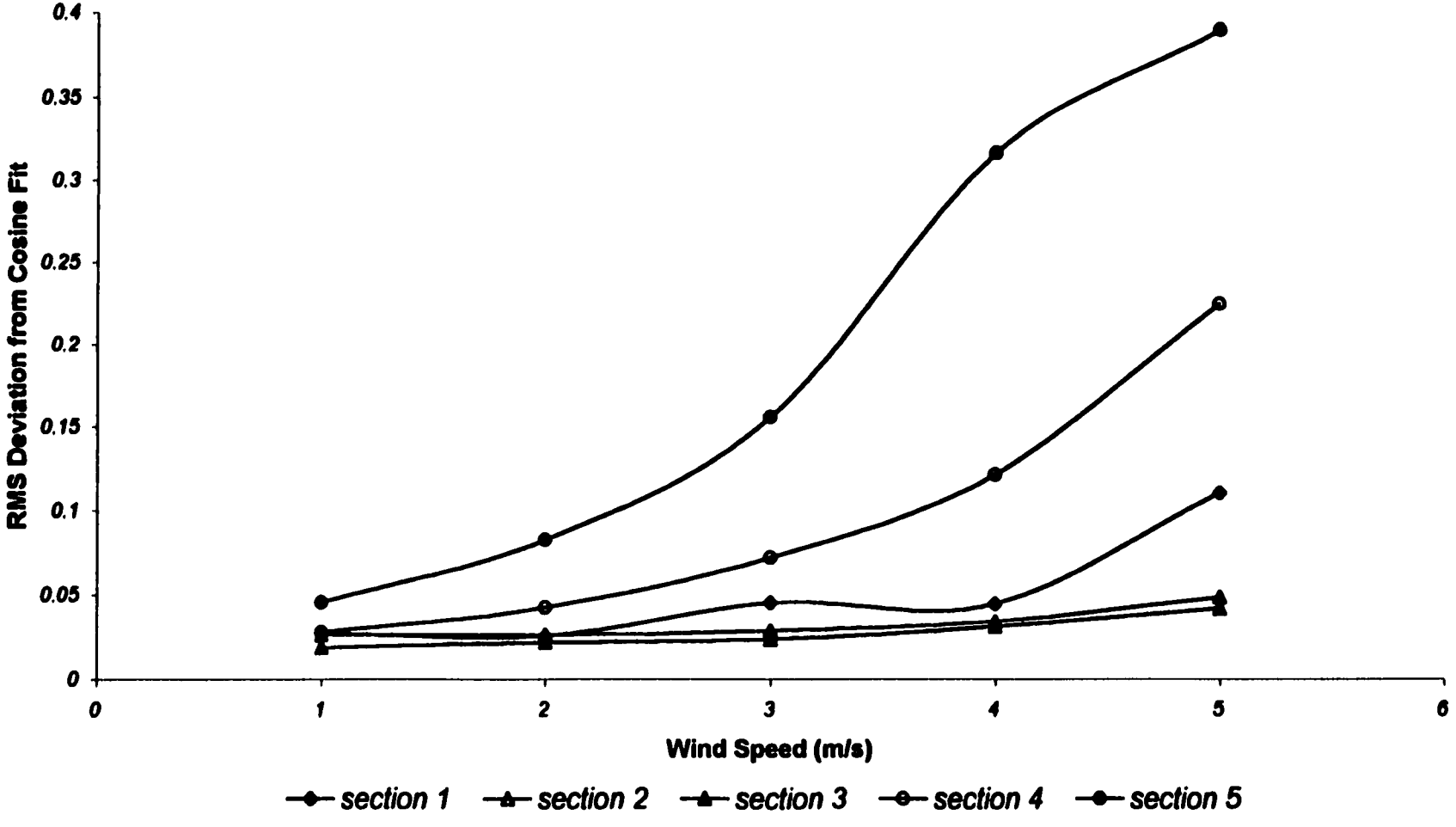

Figure 5.2.1
RMS vs. Yaw Angles
Section 1

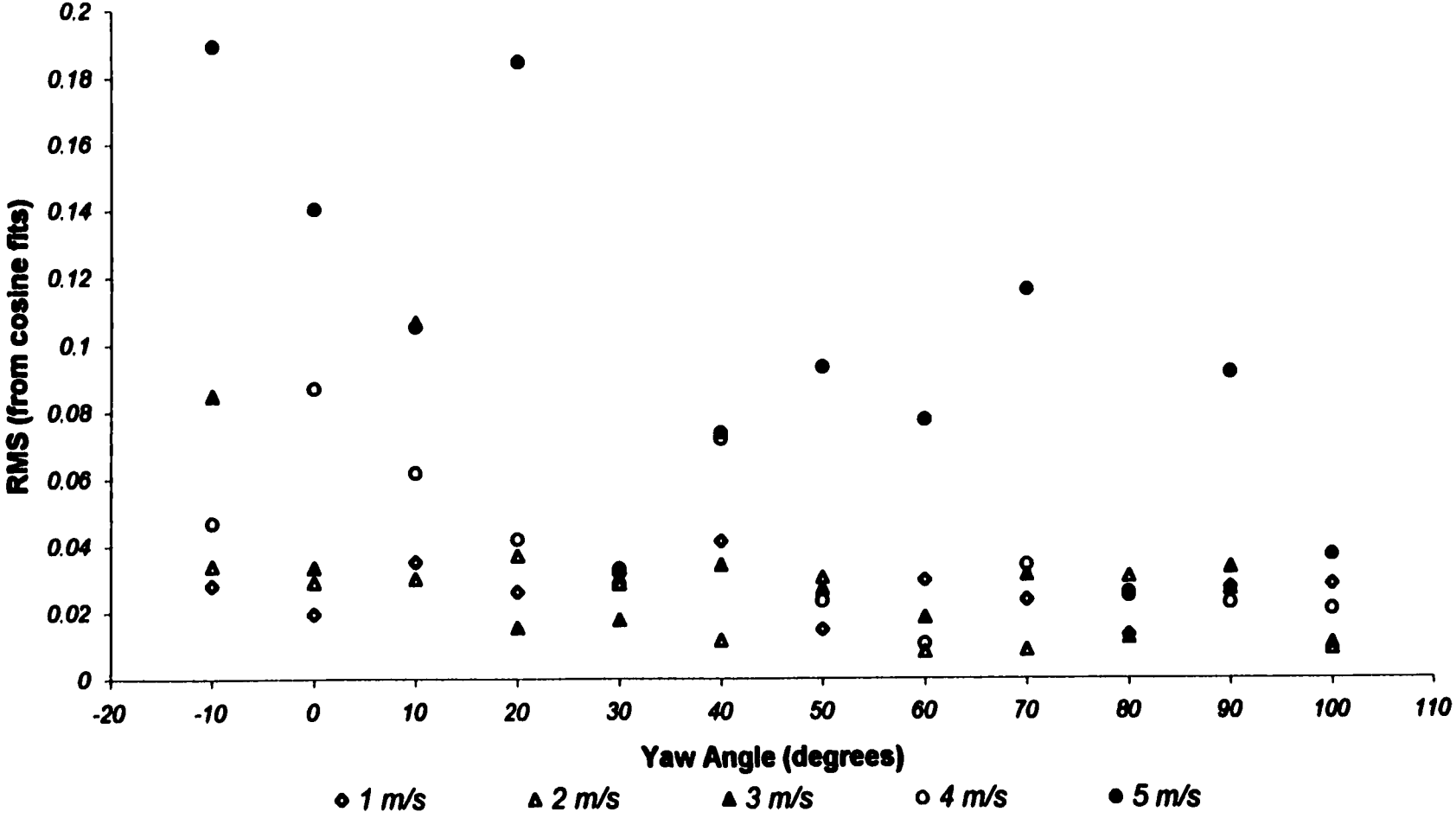

Figure 5.2.2
RMS vs. Yaw Angles
Section 2

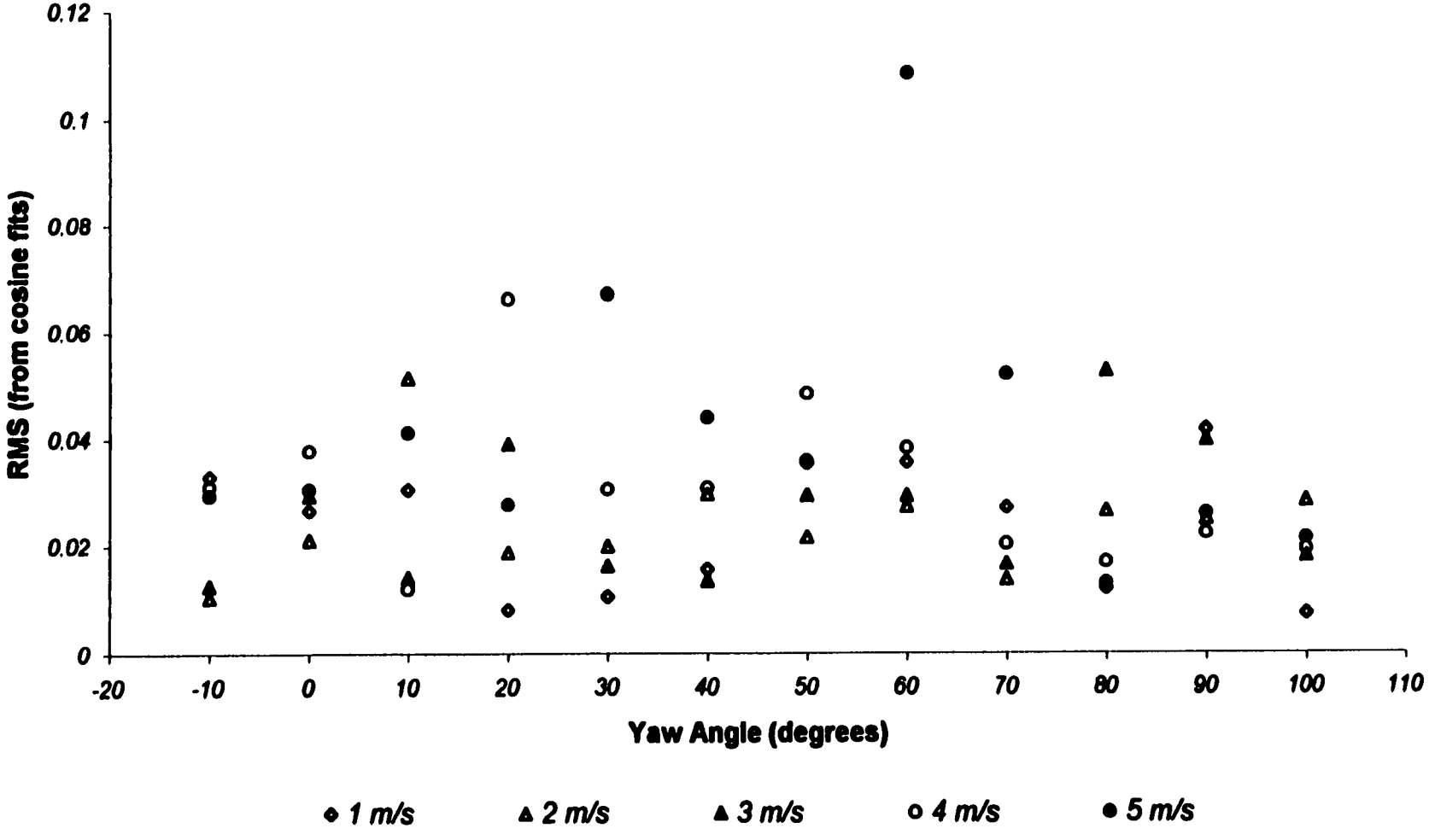

Figure 5.2.3
RMS vs. Yaw Angles
Section 3

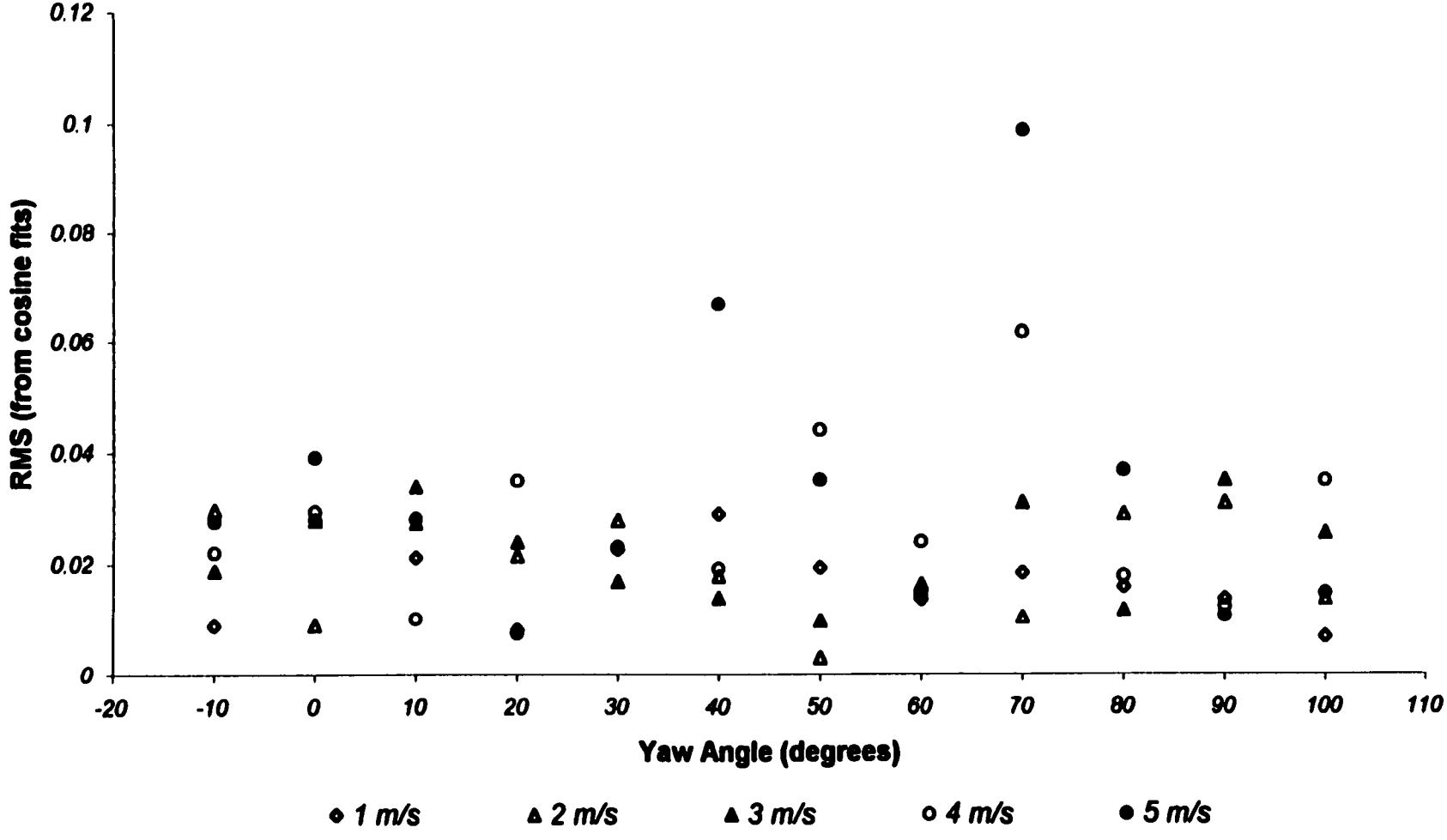

Figure 5.2.4
RMS vs. Yaw Angles
Section 4

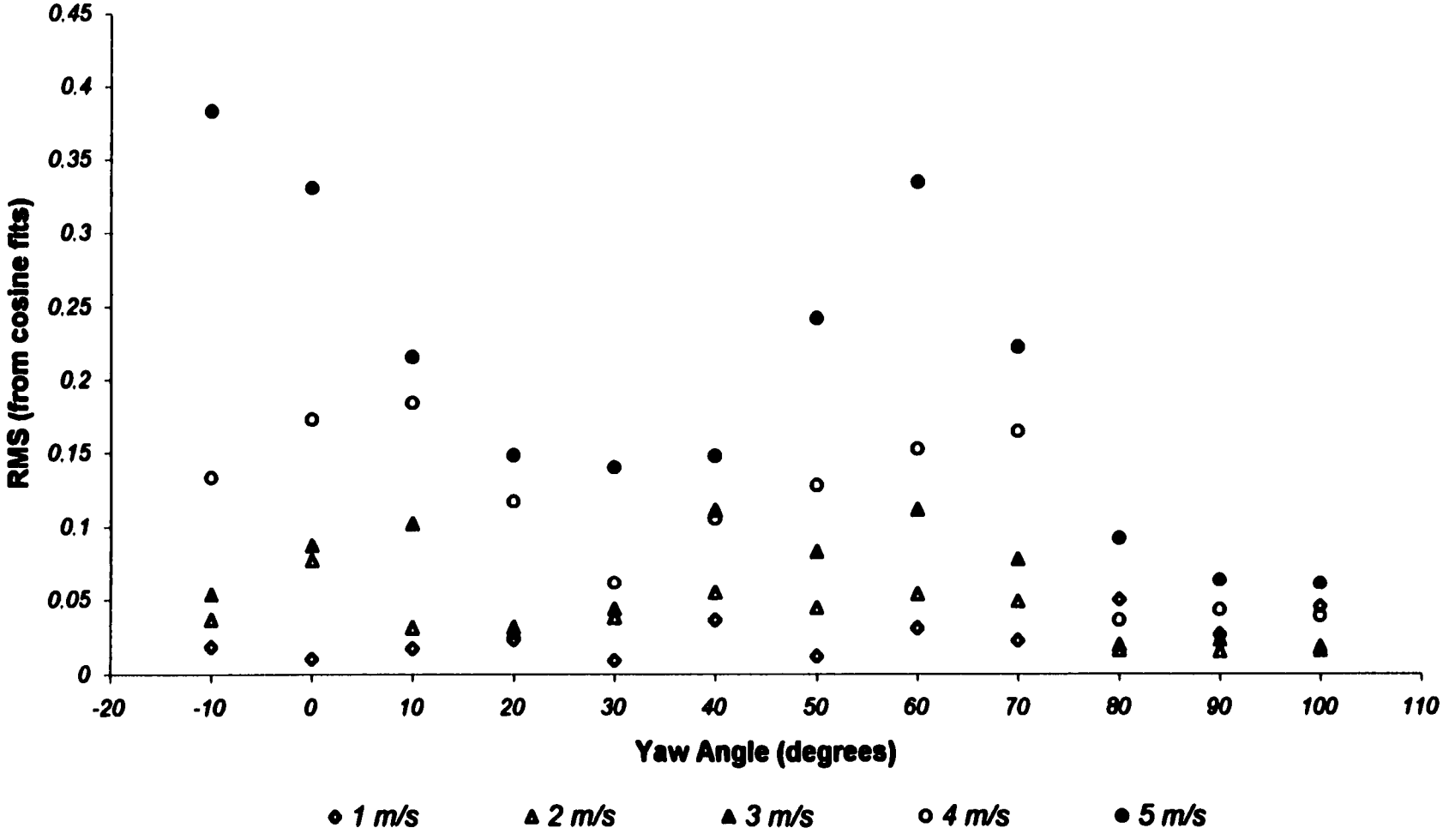

Figure 5.2.5
RMS vs. Yaw Angles
Section 5

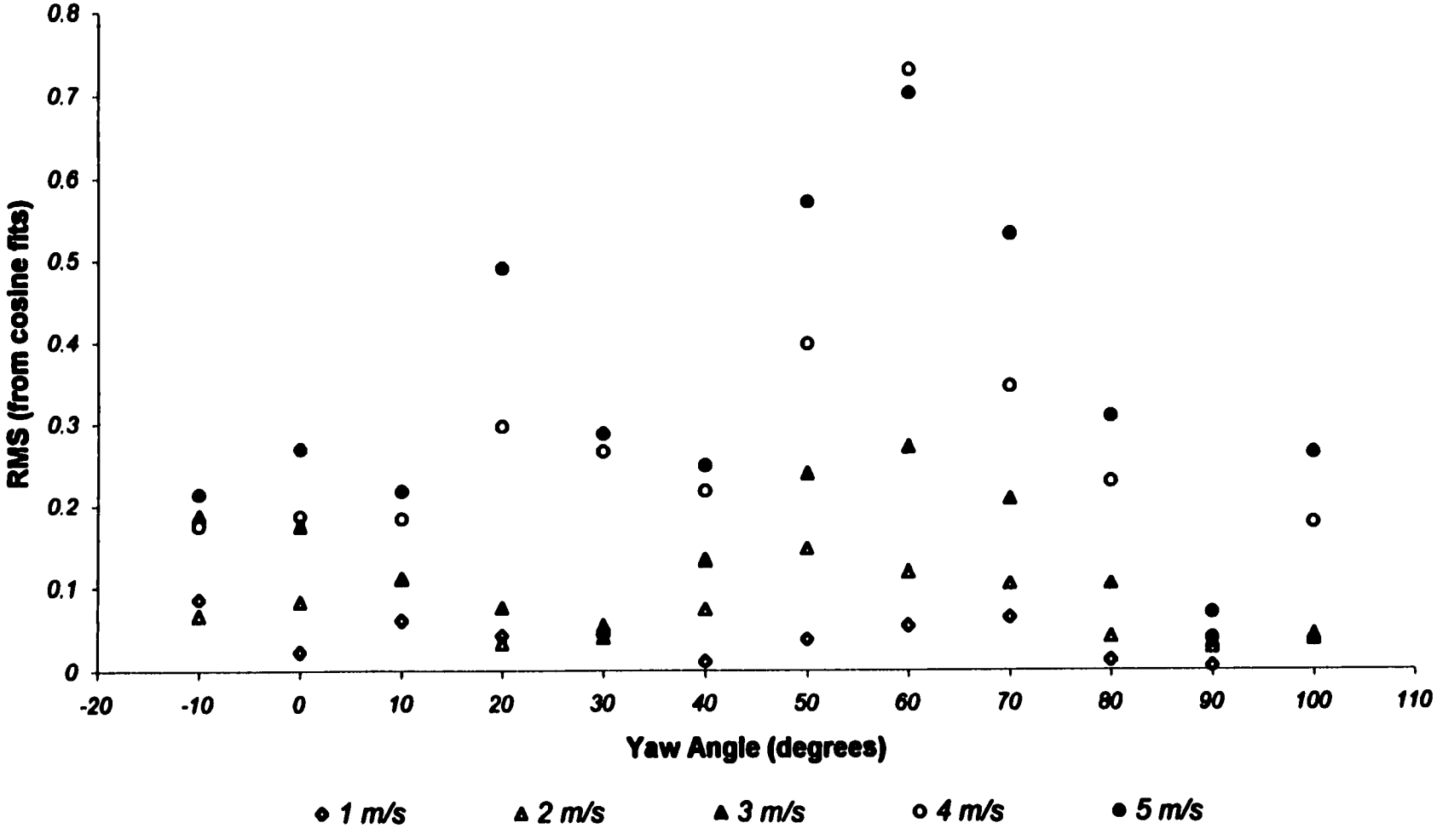

Figure 5.2.6
RMS vs. Yaw Angles
1 m/s

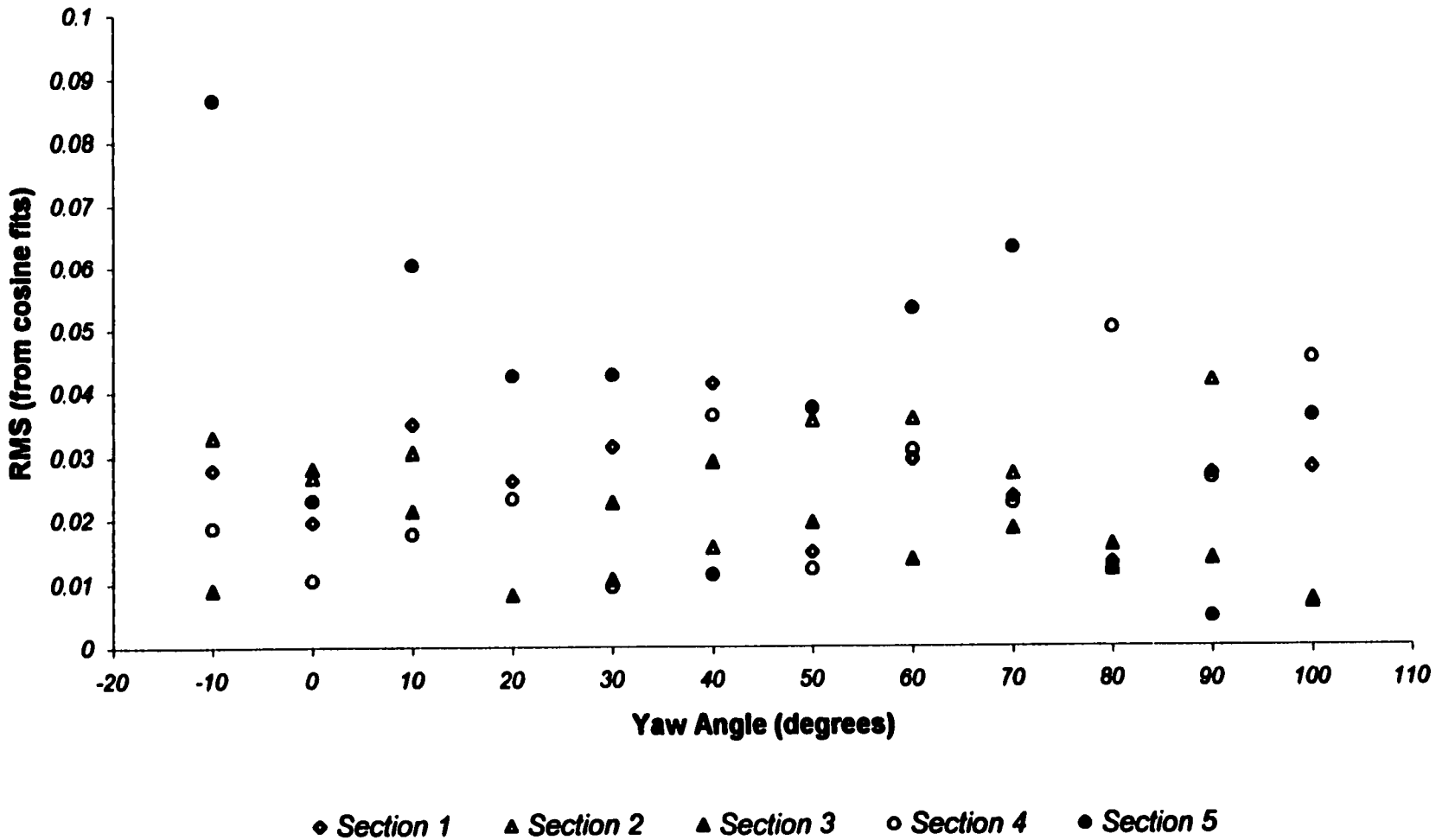

Figure 5.2.7
RMS vs. Yaw Angles
2 m/s

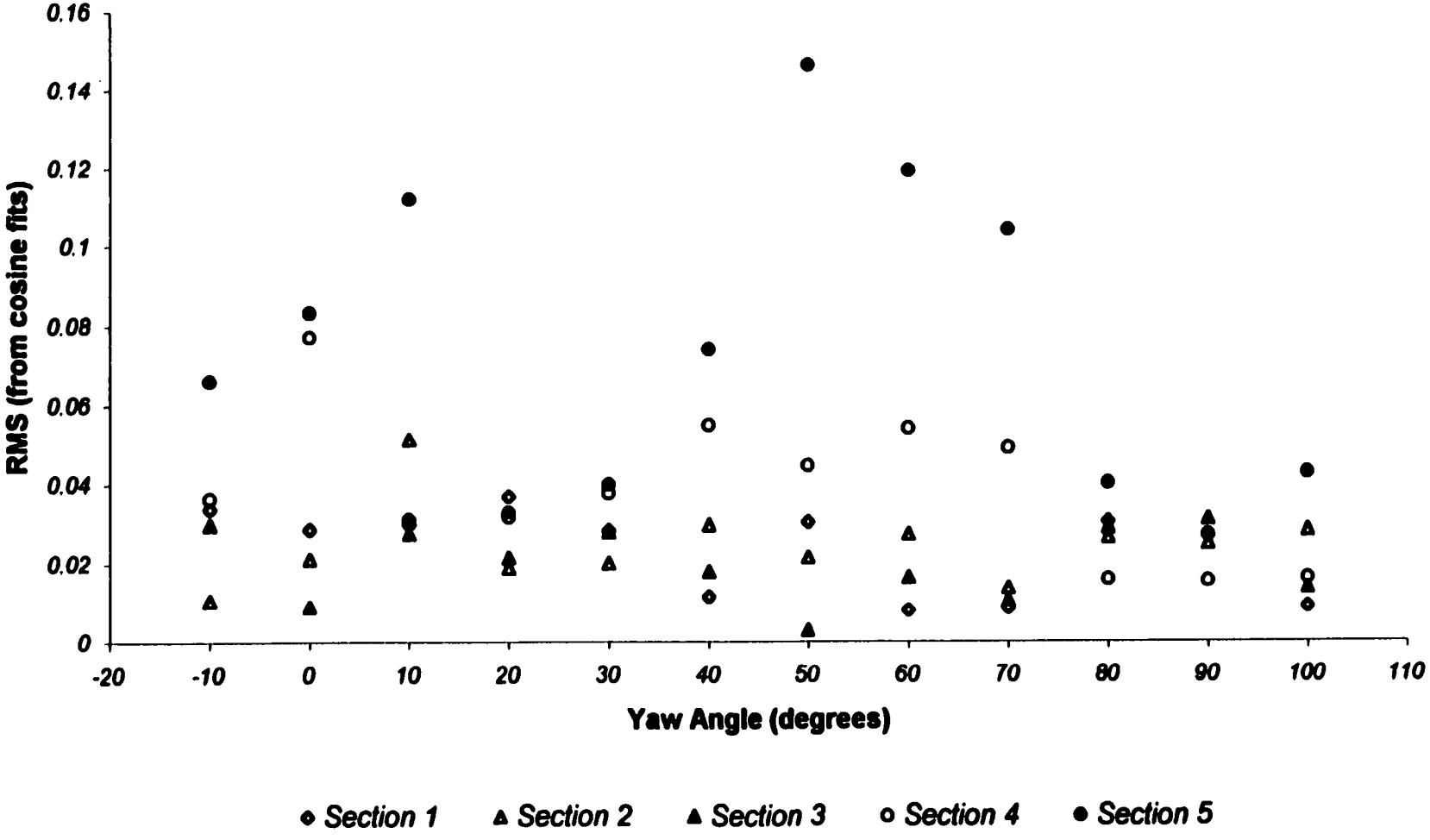

Figure 5.2.8
RMS vs. Yaw Angles
3 m/s

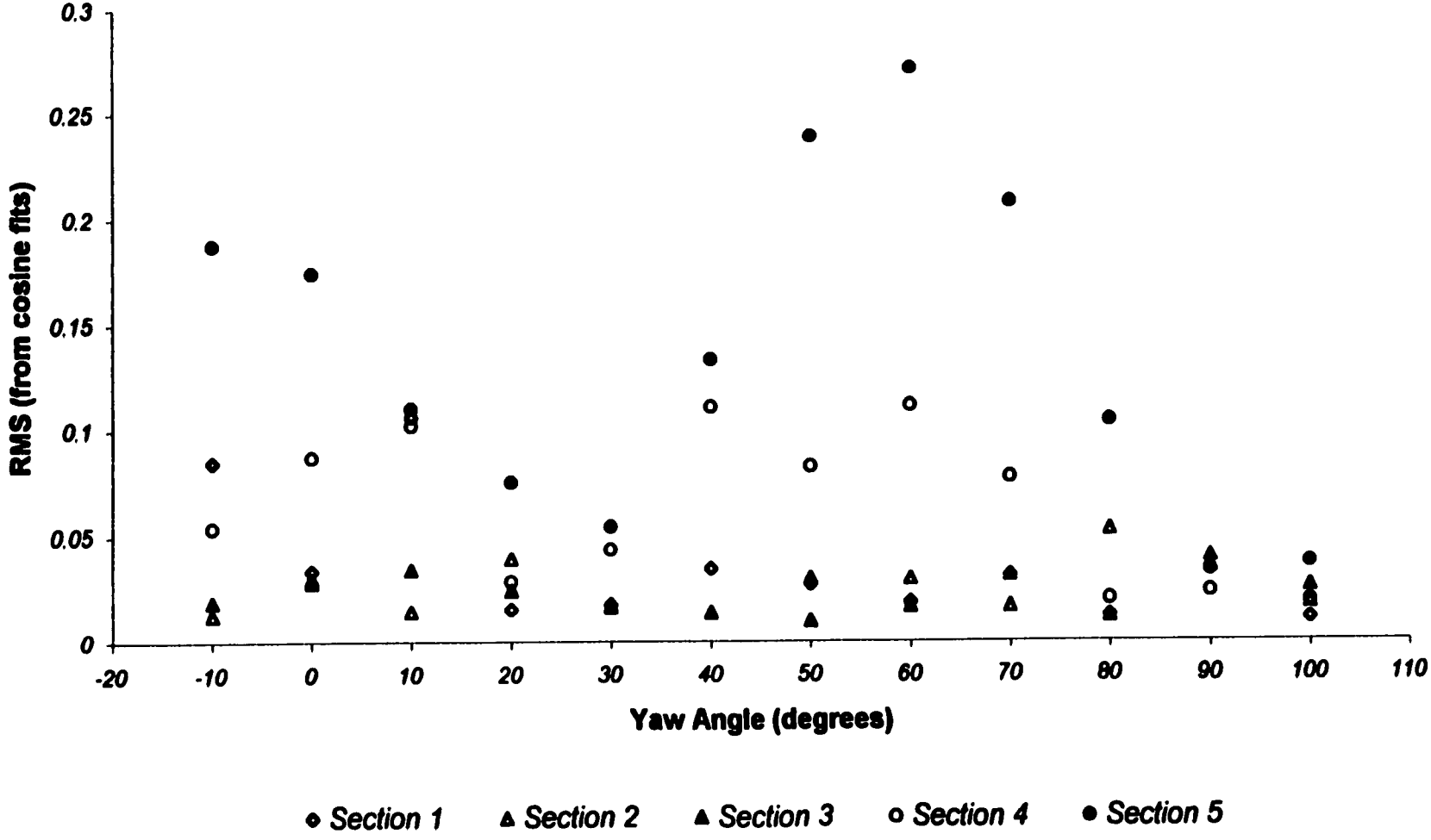

Figure 5.2.9
RMS vs. Yaw Angles
4 m/s

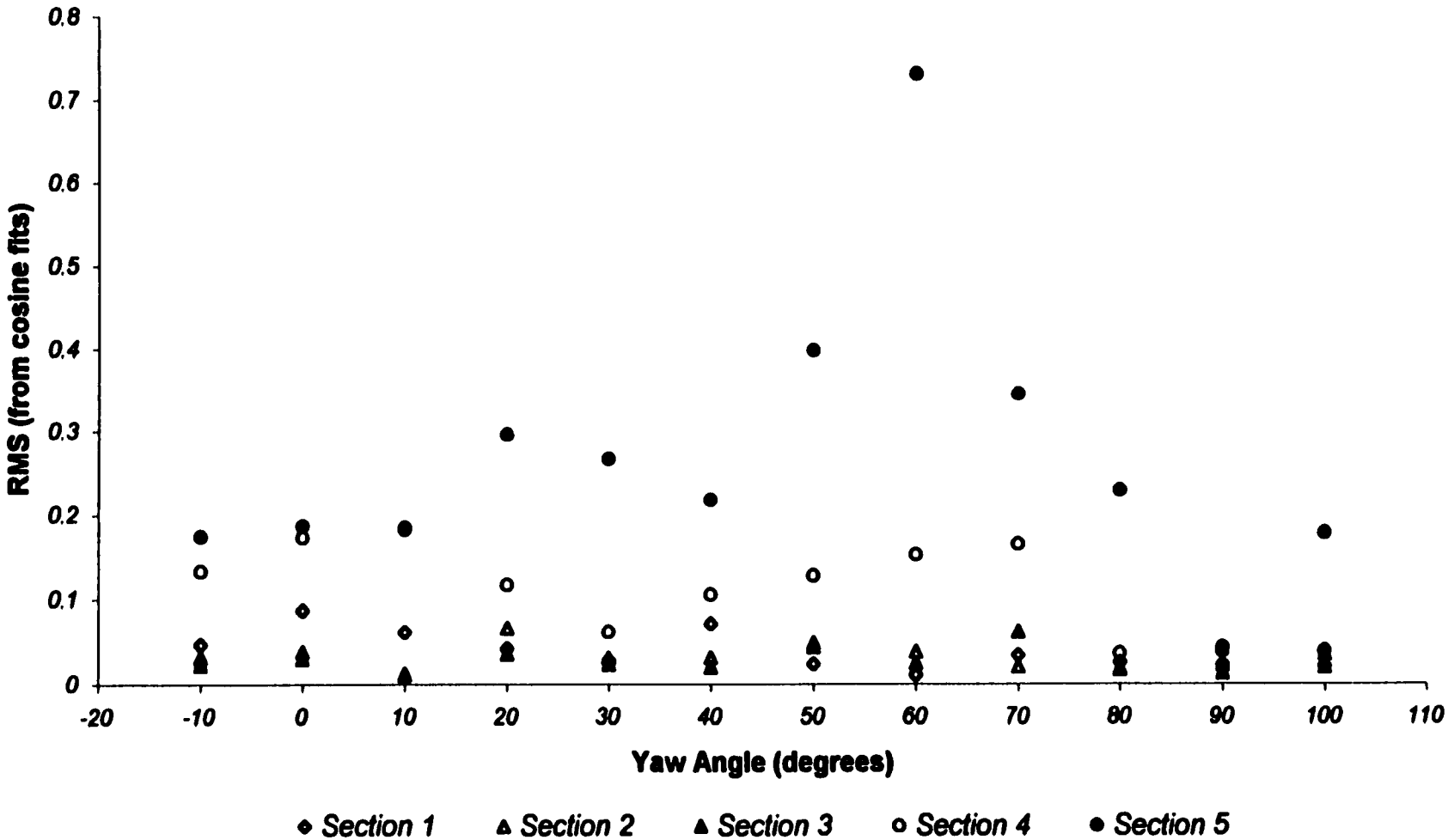

Figure 5.2.10
RMS vs. Yaw Angles
5 m/s

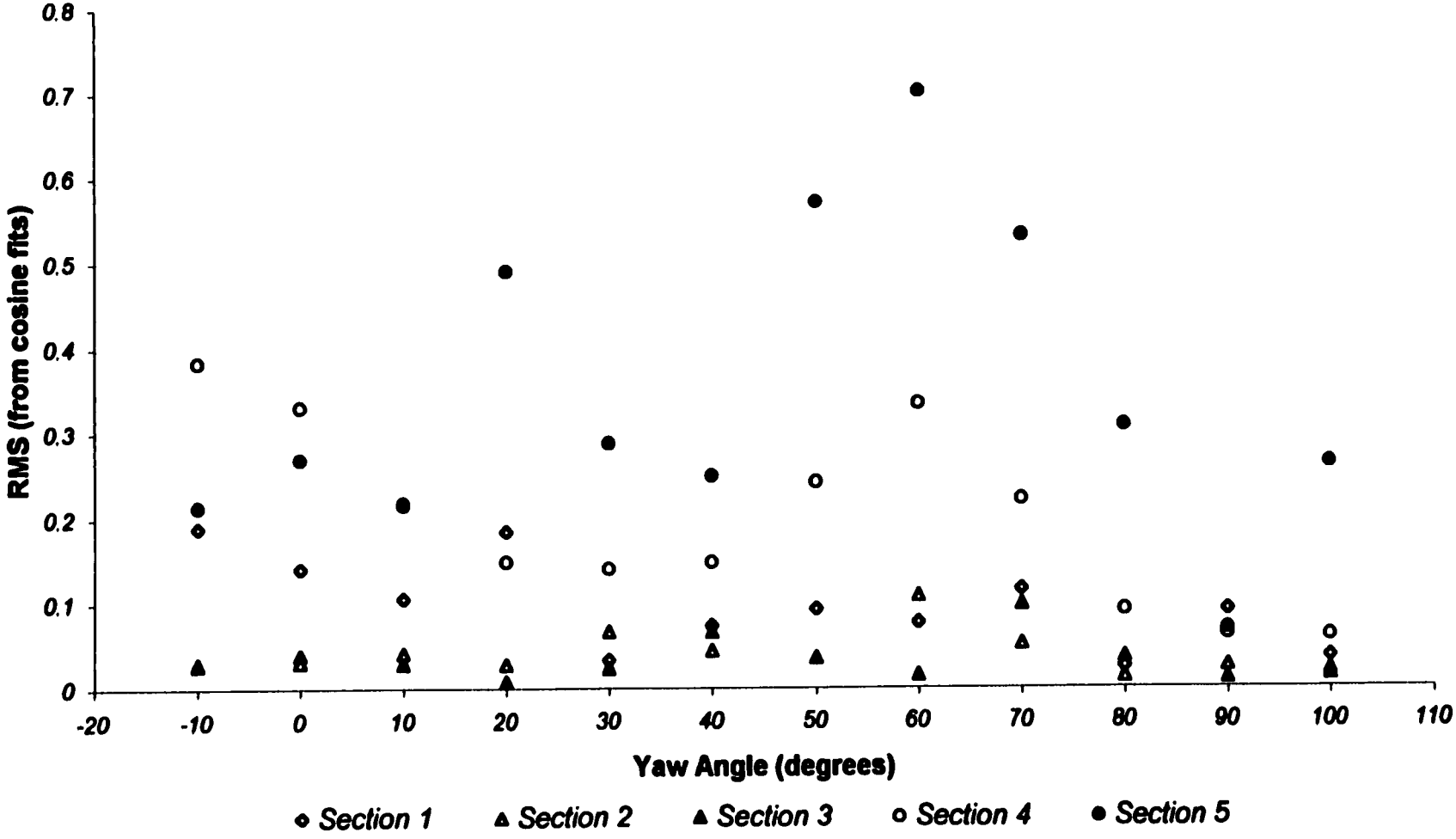

Figure 5.3
RMS vs. Yaw Angle

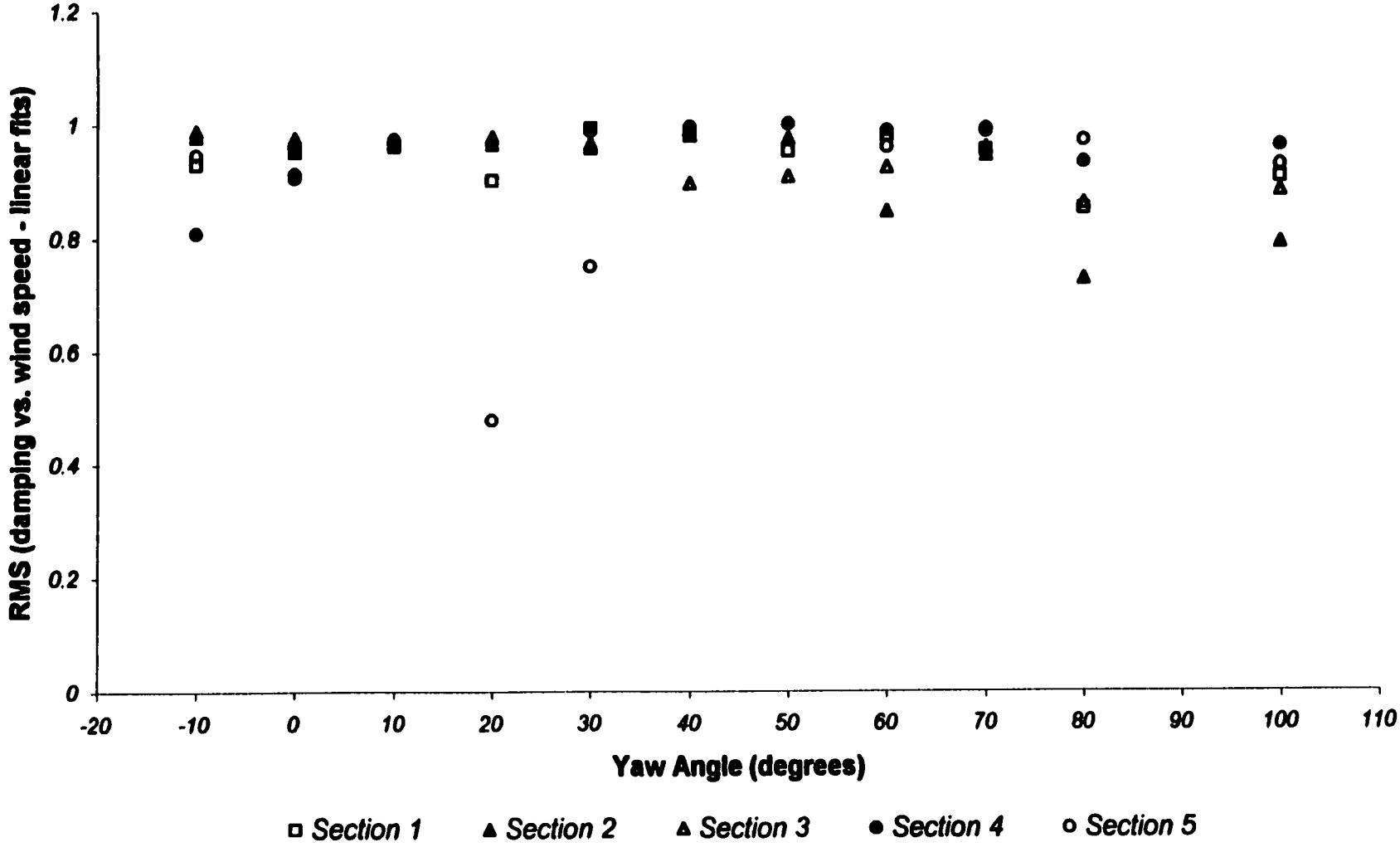

Figure 5.4
Slope vs. Yaw Angle

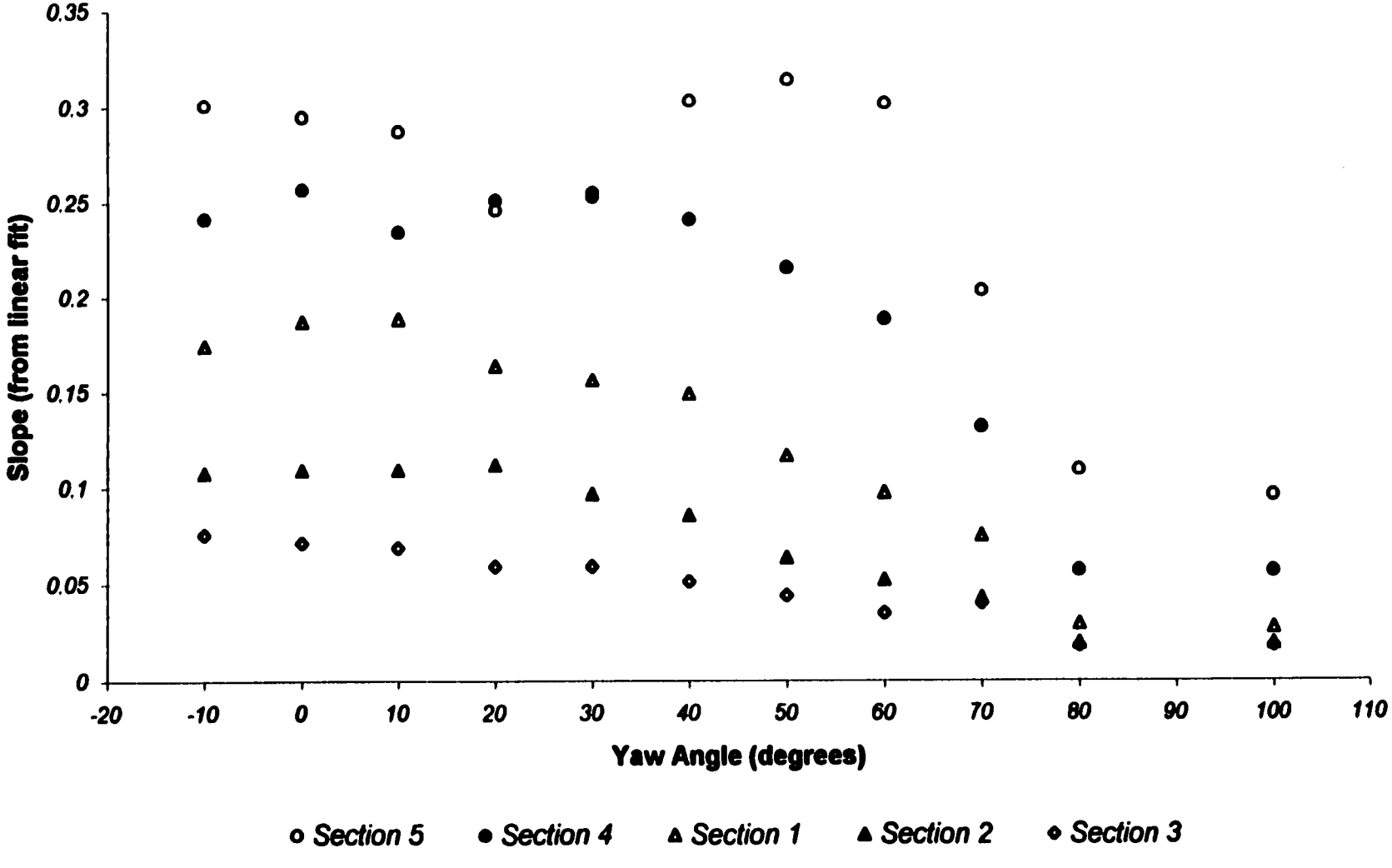

Figure 5.5
RMS vs. Yaw Angle

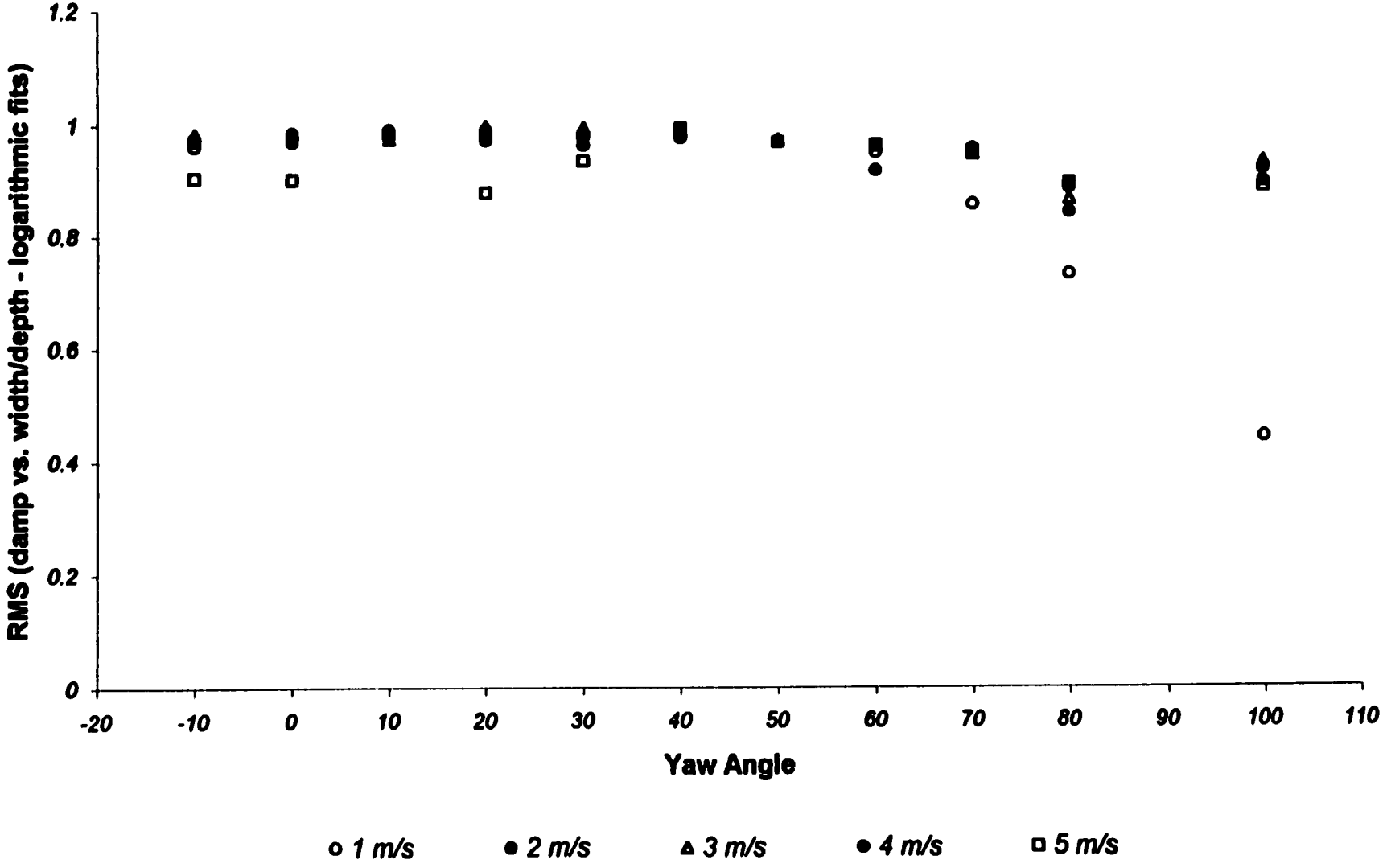

Figure 5.6
A vs. Yaw Angle

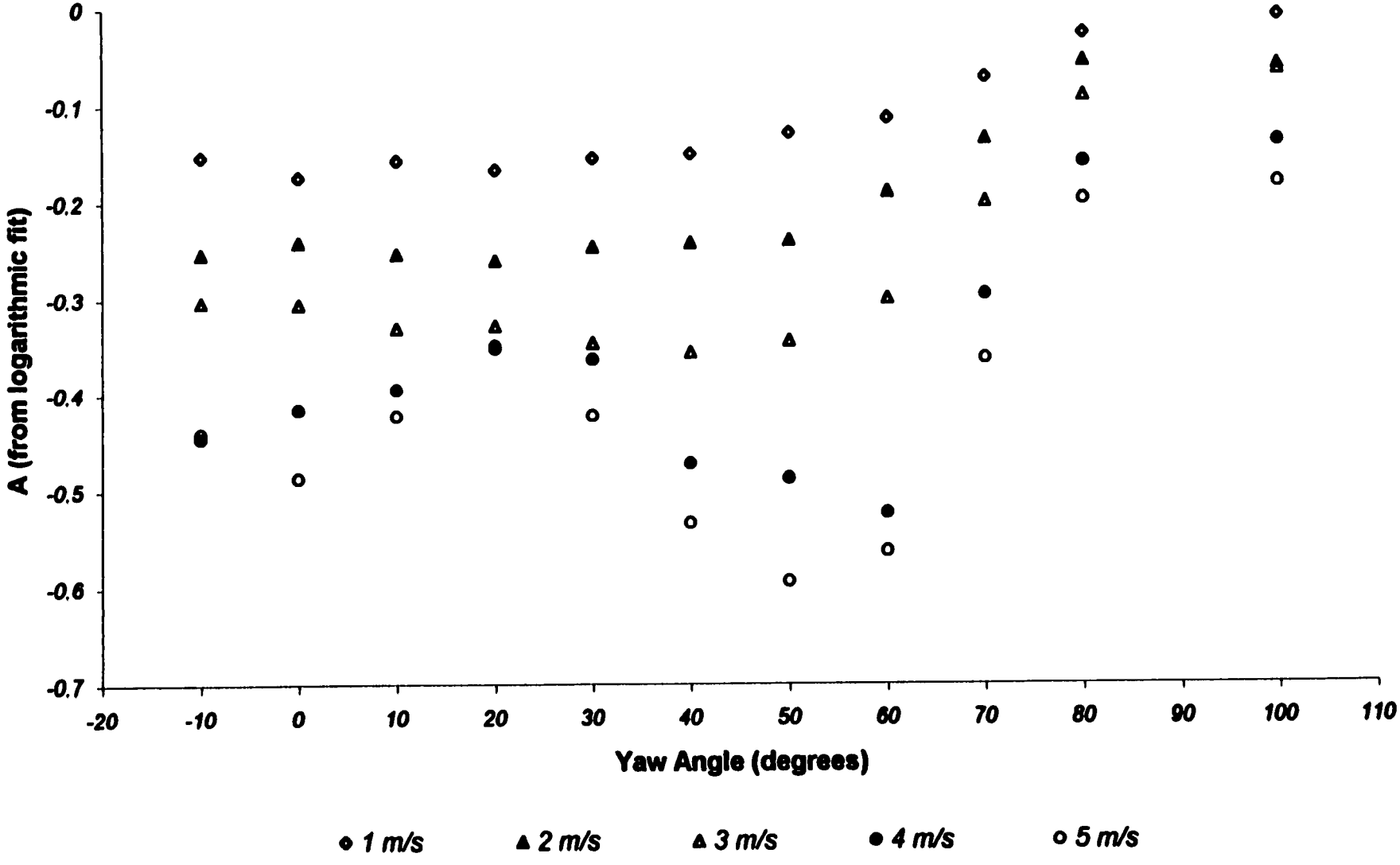

Figure 5.7
B vs. Yaw Angle

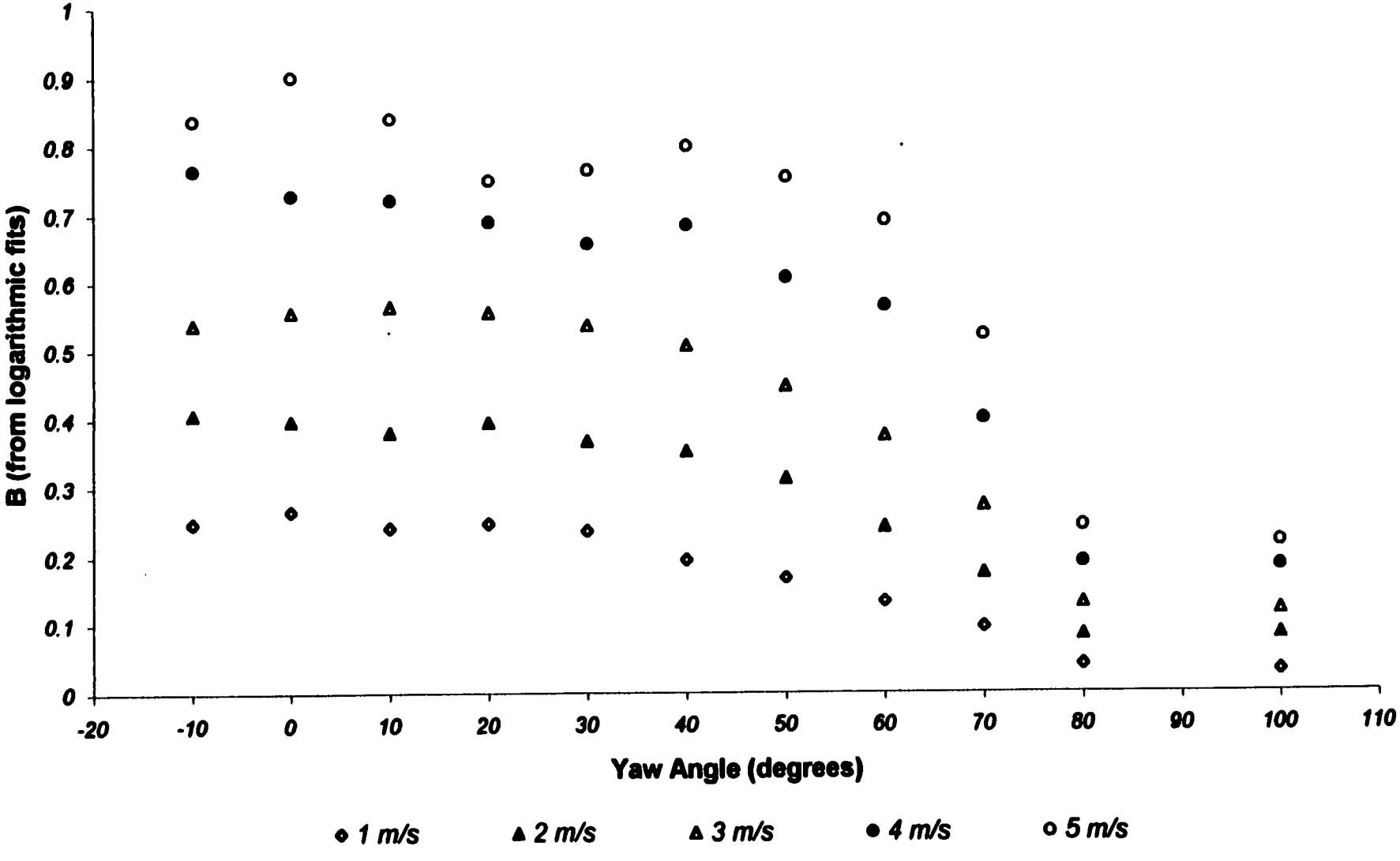

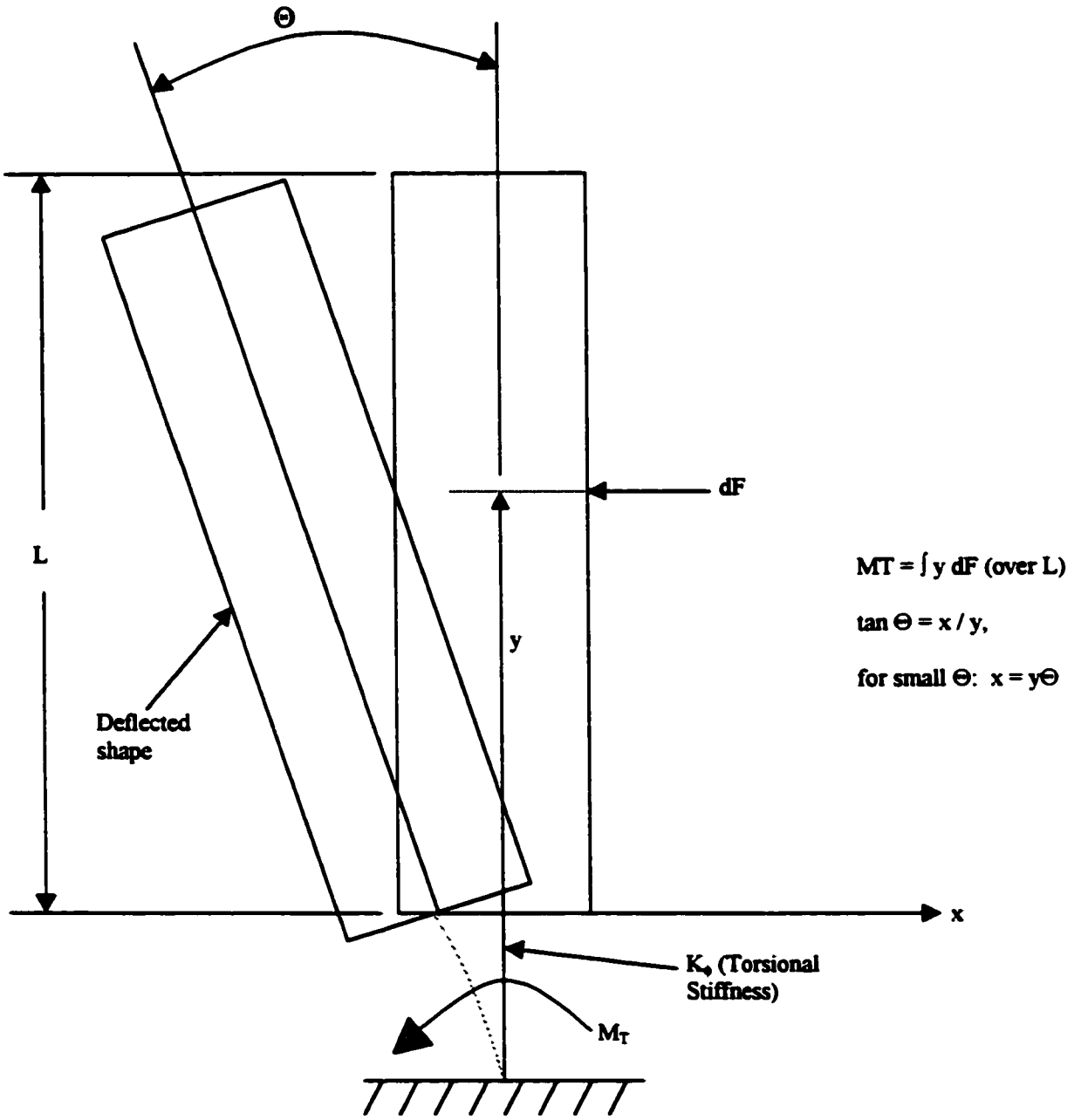

Figure 6.1 – Model for Theoretical Derivation of Aerodynamic Damping

Figure 6.2.1
Aerodynamic Damping vs. Yaw Angle
Section 1

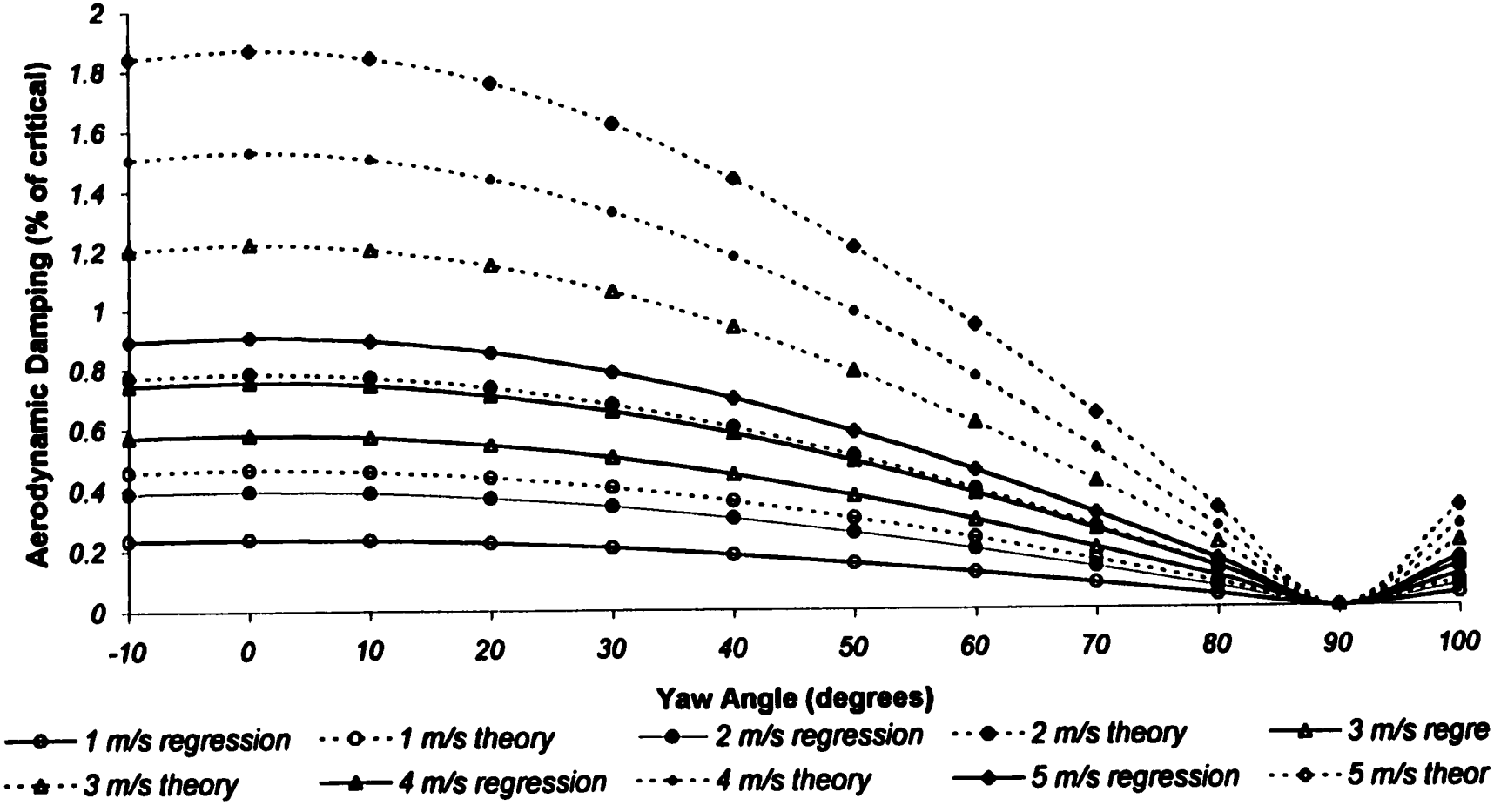

Figure 6.2.2
Aerodynamic Damping vs. Yaw Angle
Section 2

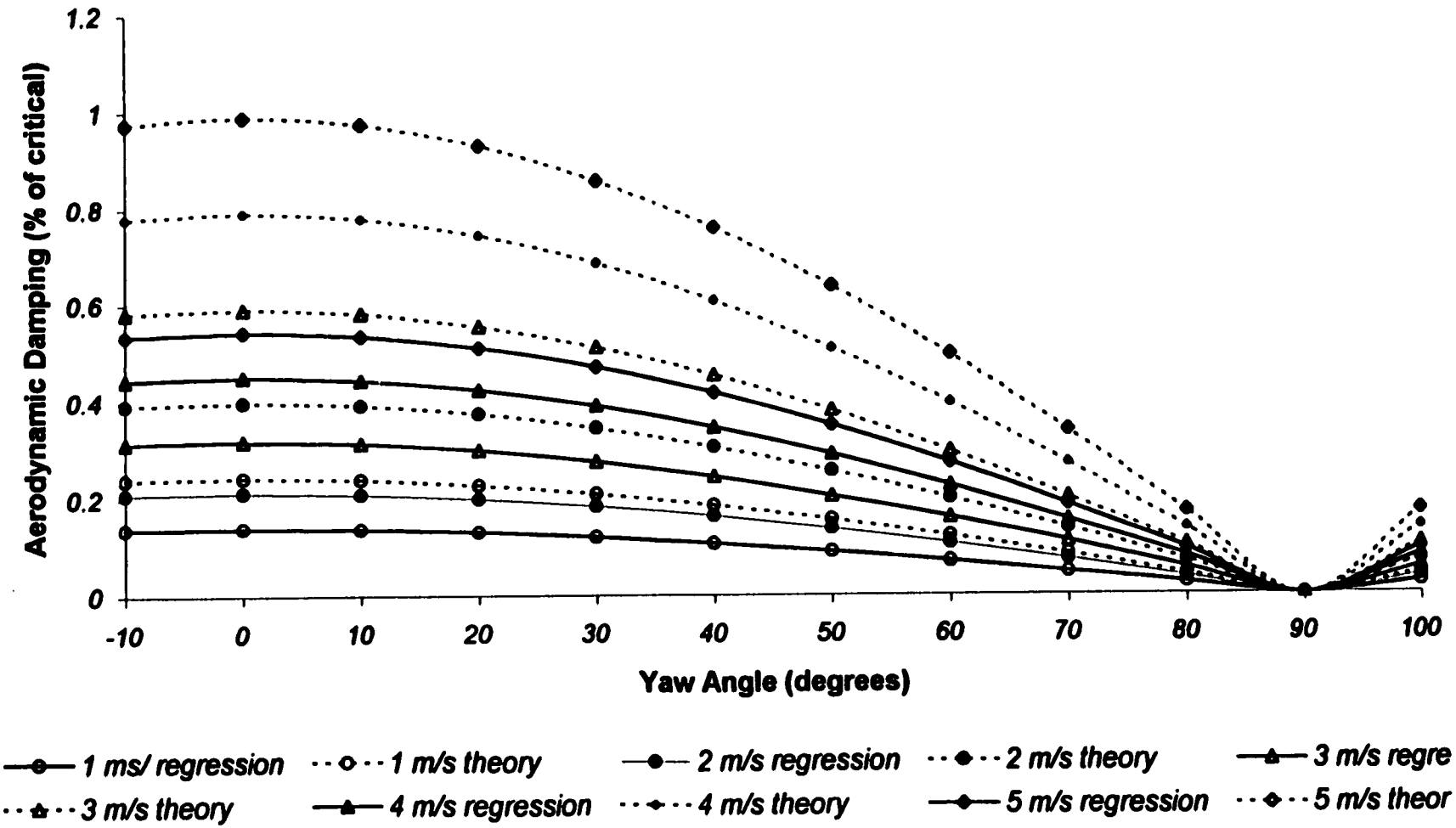

Figure 6.2.3
Aerodynamic Damping vs. Yaw Angle
Section 3

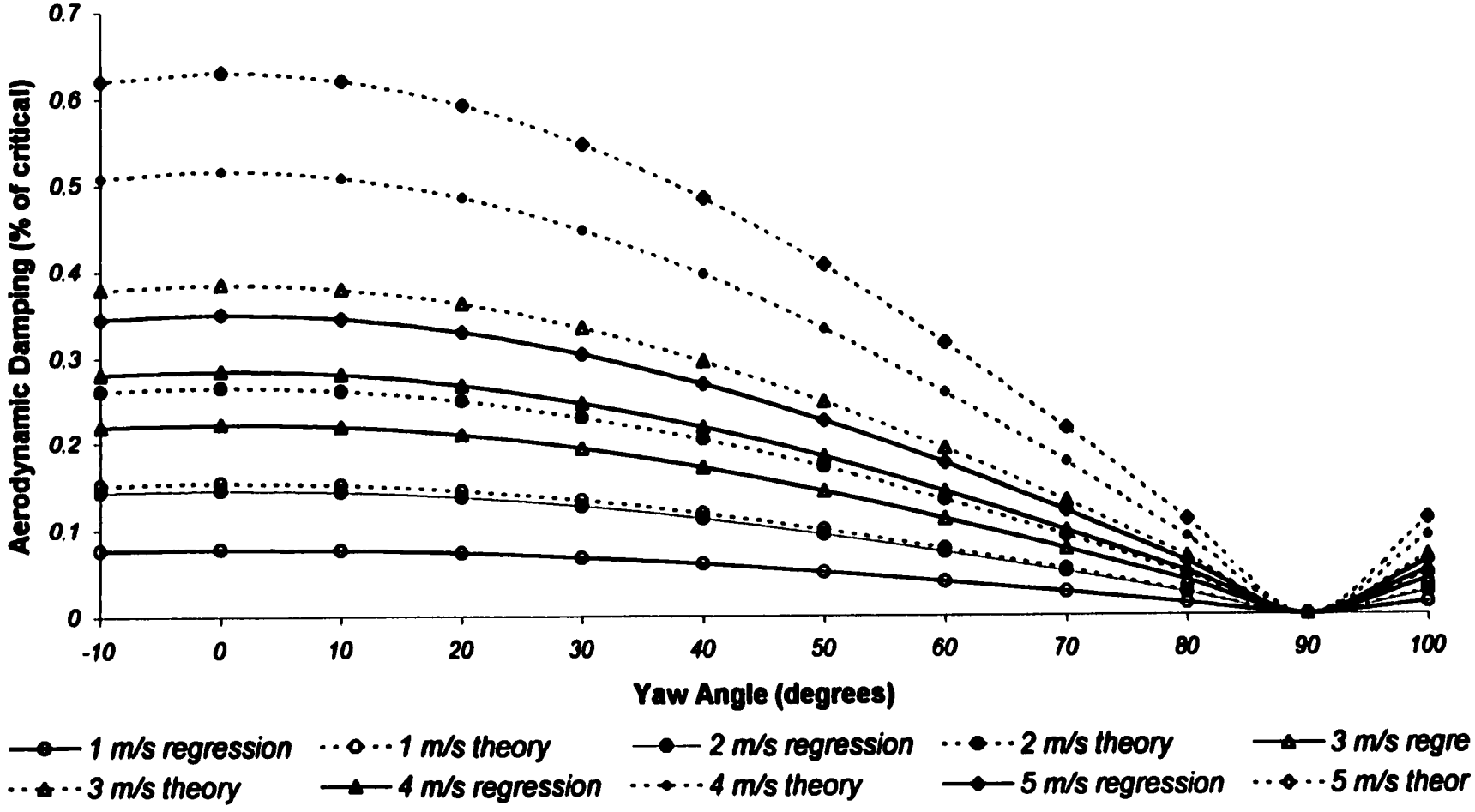

Figure 6.2.4
Aerodynamic Damping vs. Yaw Angle
Section 4

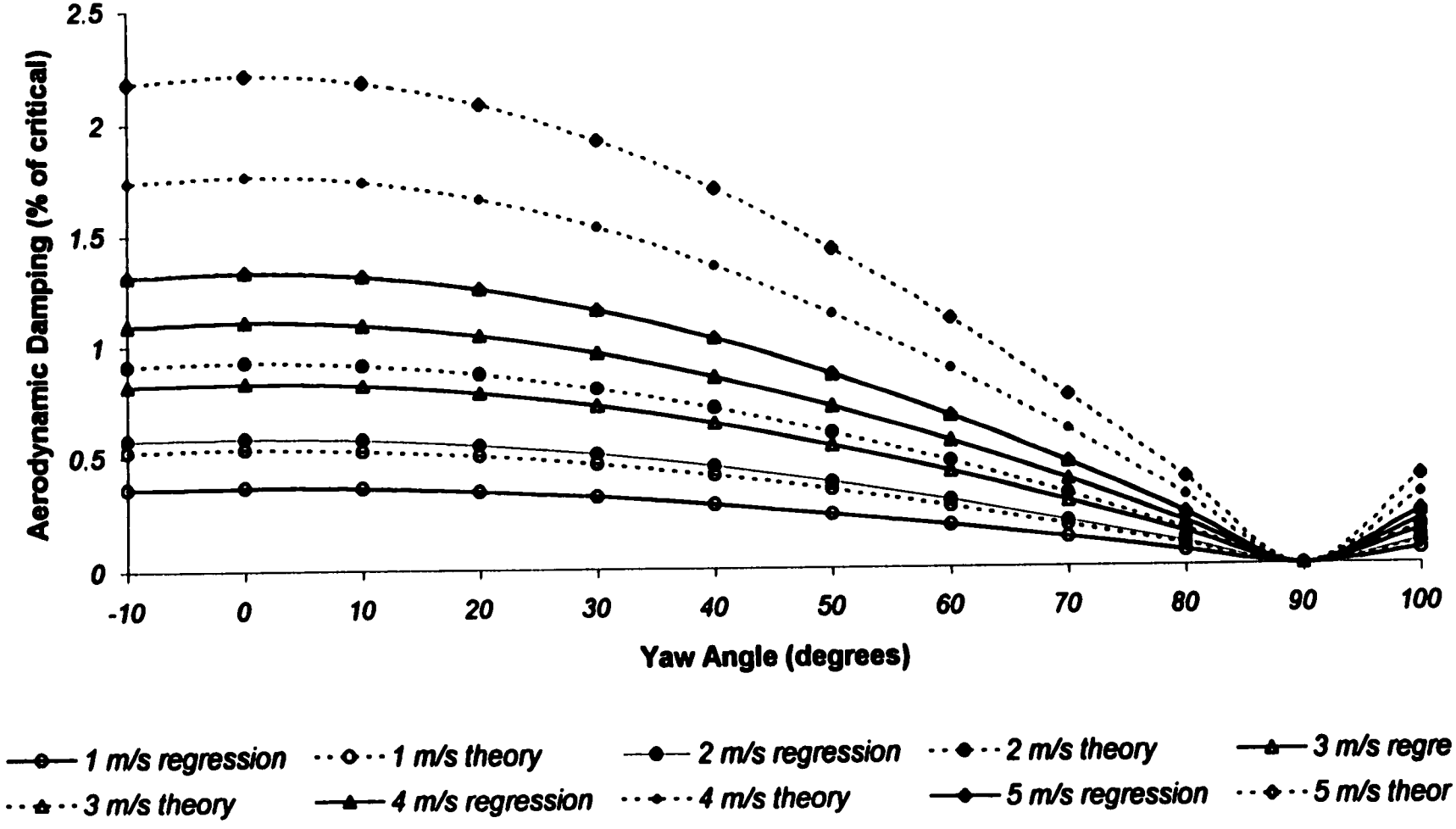

Figure 6.2.5
Aerodynamic Damping vs. Yaw Angle
Section 5

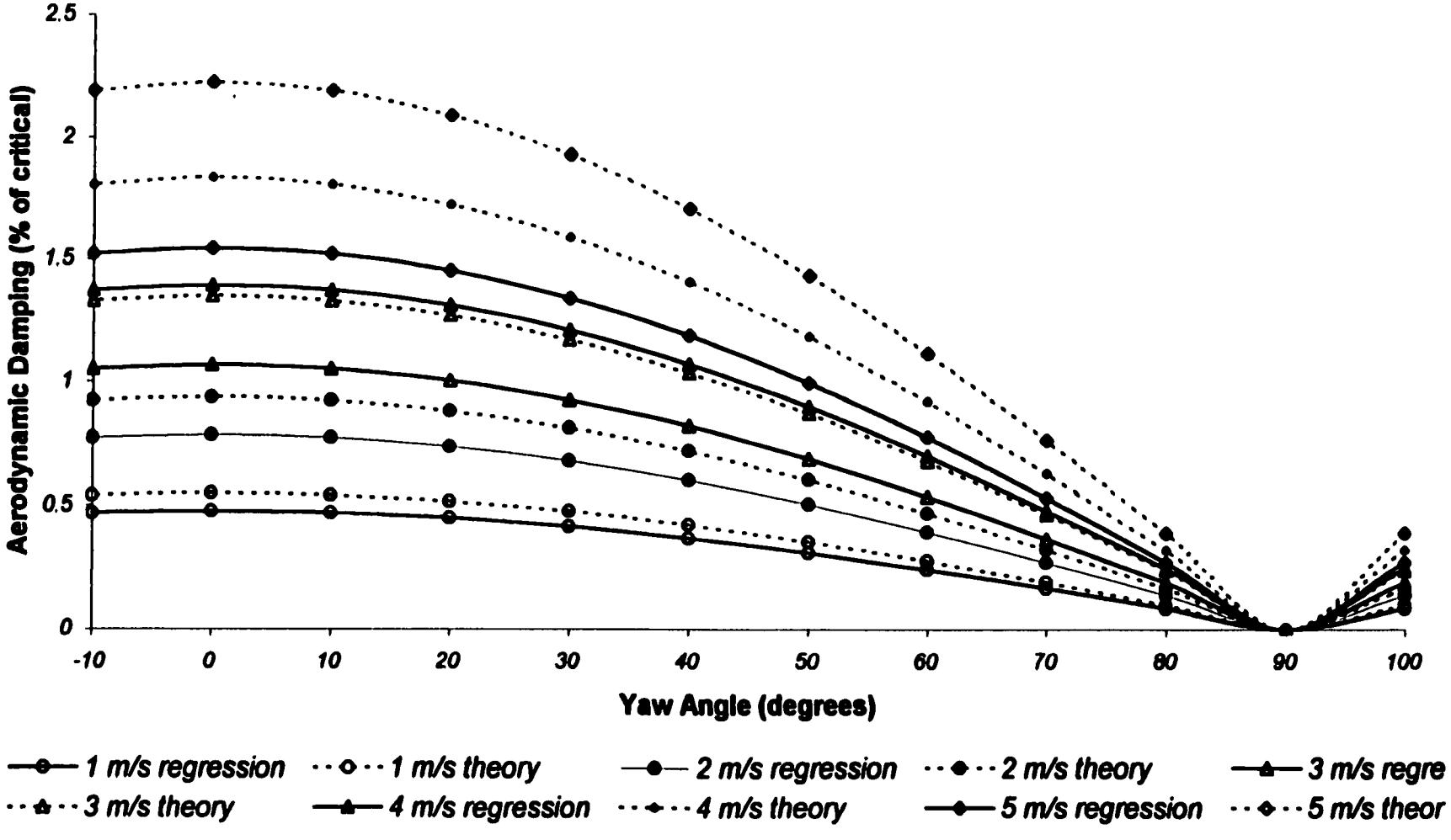

Appendix A
Fortran77 Routine

```
*    -program finds all peak values for the entire run
*    -and prints to the output file along with their
*    -relative positions within
     PROGRAM PEAKS

     REAL SVALUE,MEAN,VALUE,PREV,NEXT,TPREV,TNEXT,DATA(4001,10),
    + PEAK(1000,20)

     INTEGER SUM,M,J,N,A,B,NFILES,K,C

     CHARACTER INPUT*11,OUTPUT*11,OUT2*11

     PRINT *, 'Enter the name of the input data file in quotes'
     READ *, INPUT

     PRINT *, 'Enter the number of damping runs in the data file'
     READ *, NFILES

     OPEN (UNIT=2,FILE=INPUT,STATUS='OLD')
     DO 88 A=1,4001
      READ(2,*) (DATA(A,B),B=1,NFILES)
88   CONTINUE

     DO 89 B=1,1000
      DO 90 C=1,20
       PEAK(B,C)=0
90    CONTINUE
89   CONTINUE

     PRINT *, 'Enter the name of output file #1 in quotes w/extension'
```

```
      READ *, OUTPUT
      OPEN (UNIT=3,FILE=OUTPUT,STATUS='NEW')
      IF (NFILES.NE.2) THEN
       PRINT *, 'Enter name of 2nd output file in quotes w/extension'
       READ *, OUT2
       OPEN (UNIT=4,FILE=OUT2,STATUS='NEW')
      END IF

      K=1

   66  SUM=0
       SVALUE=0

       DO 6 M=2,4001
        SUM=SUM+1
        SVALUE=DATA(M,K)+SVALUE
    6  CONTINUE
       MEAN=SVALUE/SUM
       N=1

       DO 7 J=3,3000

        VALUE = DATA(J,K) - MEAN
        PREV = DATA(J-1,K) - MEAN
        NEXT = DATA(J+1,K) - MEAN
        TPREV = VALUE - PREV
        TNEXT = VALUE - NEXT

        IF (TPREV.GE.0.AND.TNEXT.GE.0) THEN
         PEAK(N,2*K-1)=VALUE
```

```
      PEAK(N,2*K)=J-1
      N=N+1
     END IF
7    CONTINUE
     K=K+1
    IF (K.LE.NFILES) THEN
     GOTO 66
    END IF

    IF (NFILES.EQ.2) THEN
     DO 91 A=1,1000
      WRITE (3,81) (PEAK(A,B),B=1,4)
81     FORMAT (2(F6.1,1X,F5.0,1X))
91    CONTINUE
    END IF

    IF (NFILES.EQ.9) THEN
     DO 92 A=1,1000
      WRITE (3,82) (PEAK(A,B),B=1,10)
      WRITE (4,83) (PEAK(A,B),B=11,18)
82     FORMAT (5(F6.1,1X,F5.0,1X))
83     FORMAT (4(F6.1,1X,F5.0,1X))
92    CONTINUE
    END IF

    IF (NFILES.EQ.10) THEN
     DO 93 A=1,1000
      WRITE (3,84) (PEAK(A,B),B=1,10)
      WRITE (4,85) (PEAK(A,B),B=11,20)
84     FORMAT (5(F6.1,1X,F5.0,1X))
```

```
85    FORMAT (5(F6.1,1X,F5.0,1X))
93    CONTINUE
      END IF

      END
```

Appendix B
Free Vibration Responses

Appendix B
Section 1
1 m/s - 30 degrees

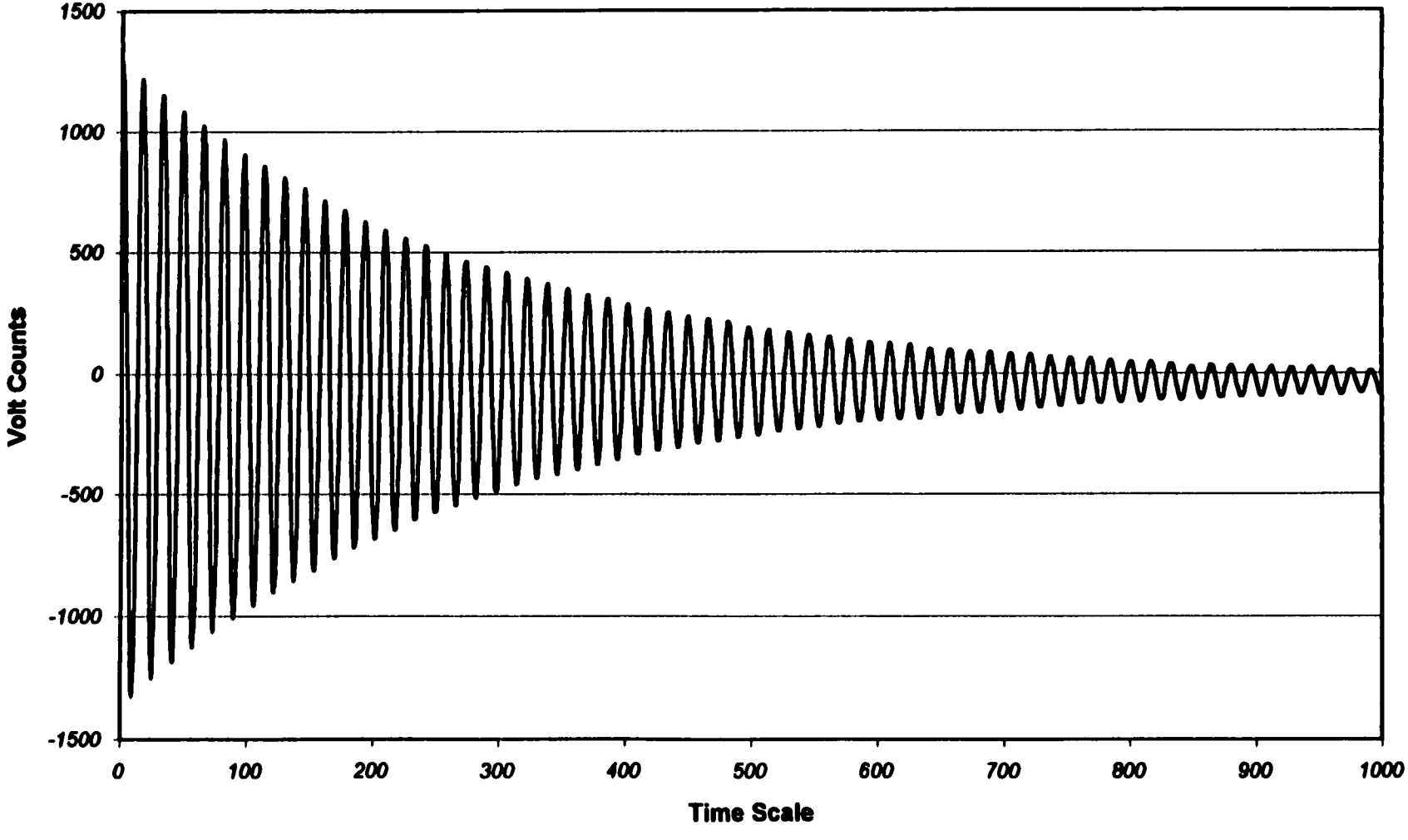

Appendix B
Section 2
5 m/s - 50 degrees

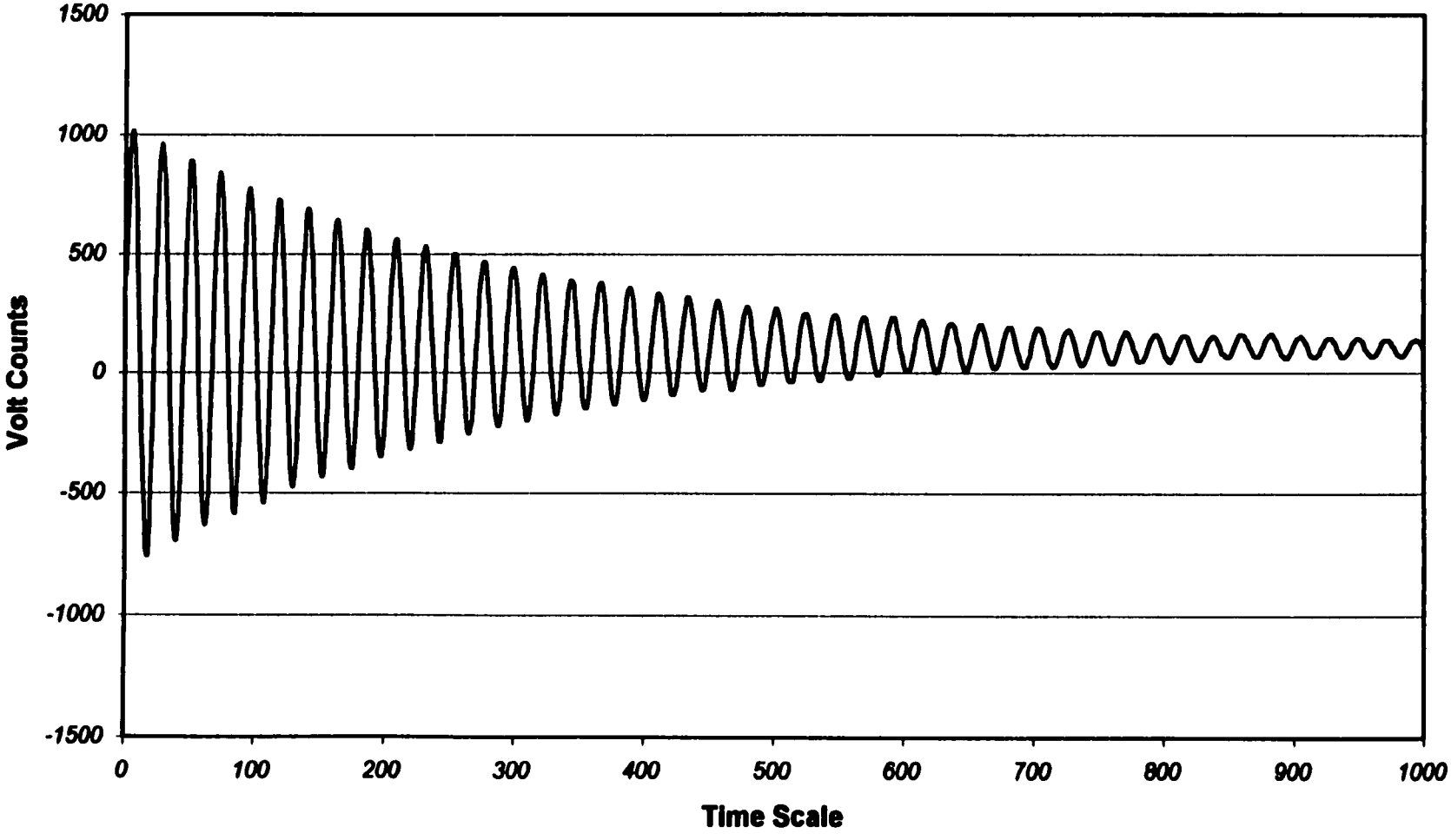

Appendix B
Section 3
2 m/s - 80 degrees

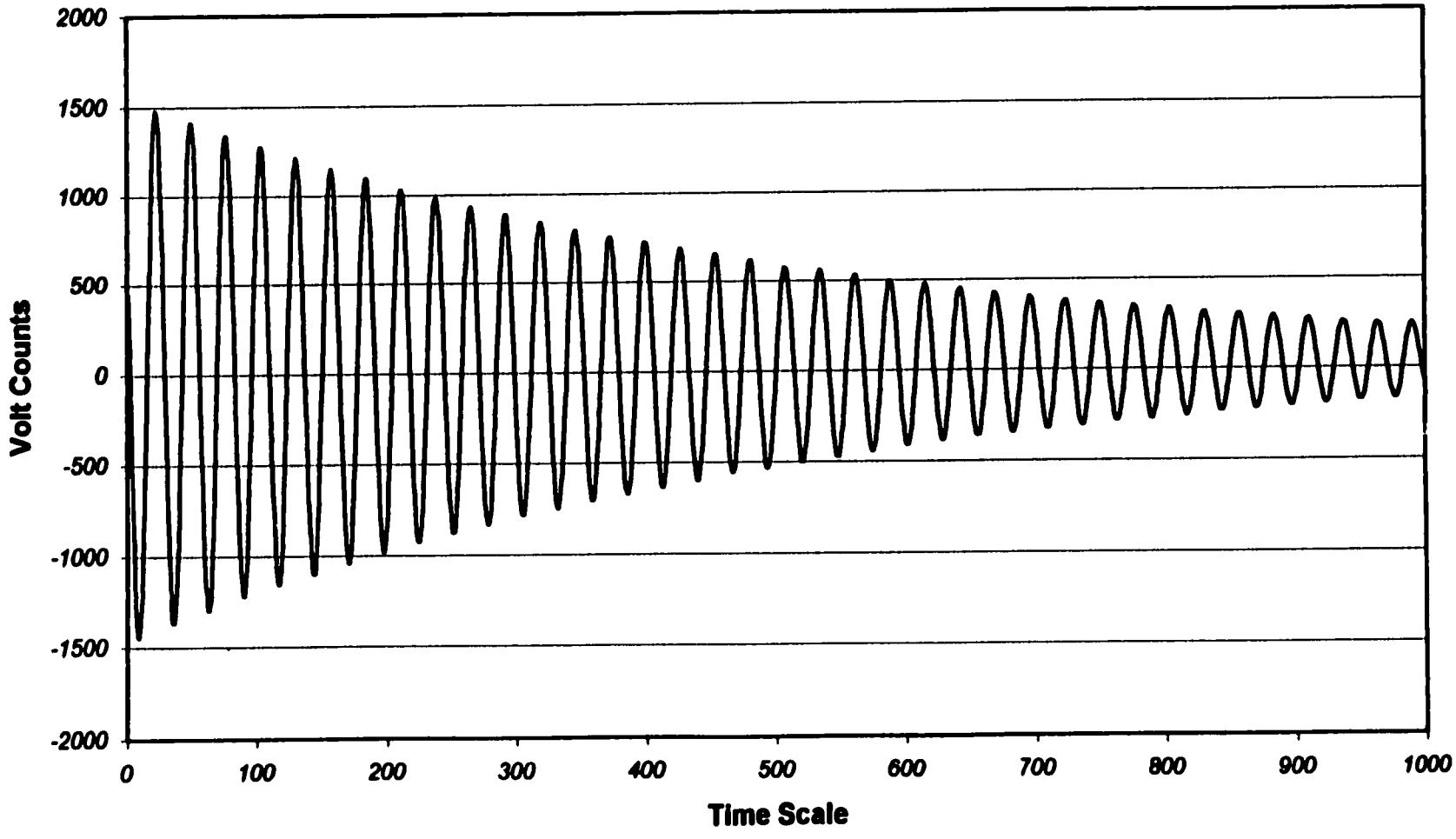

Appendix B
Section 4
4 m/s - 10 degrees

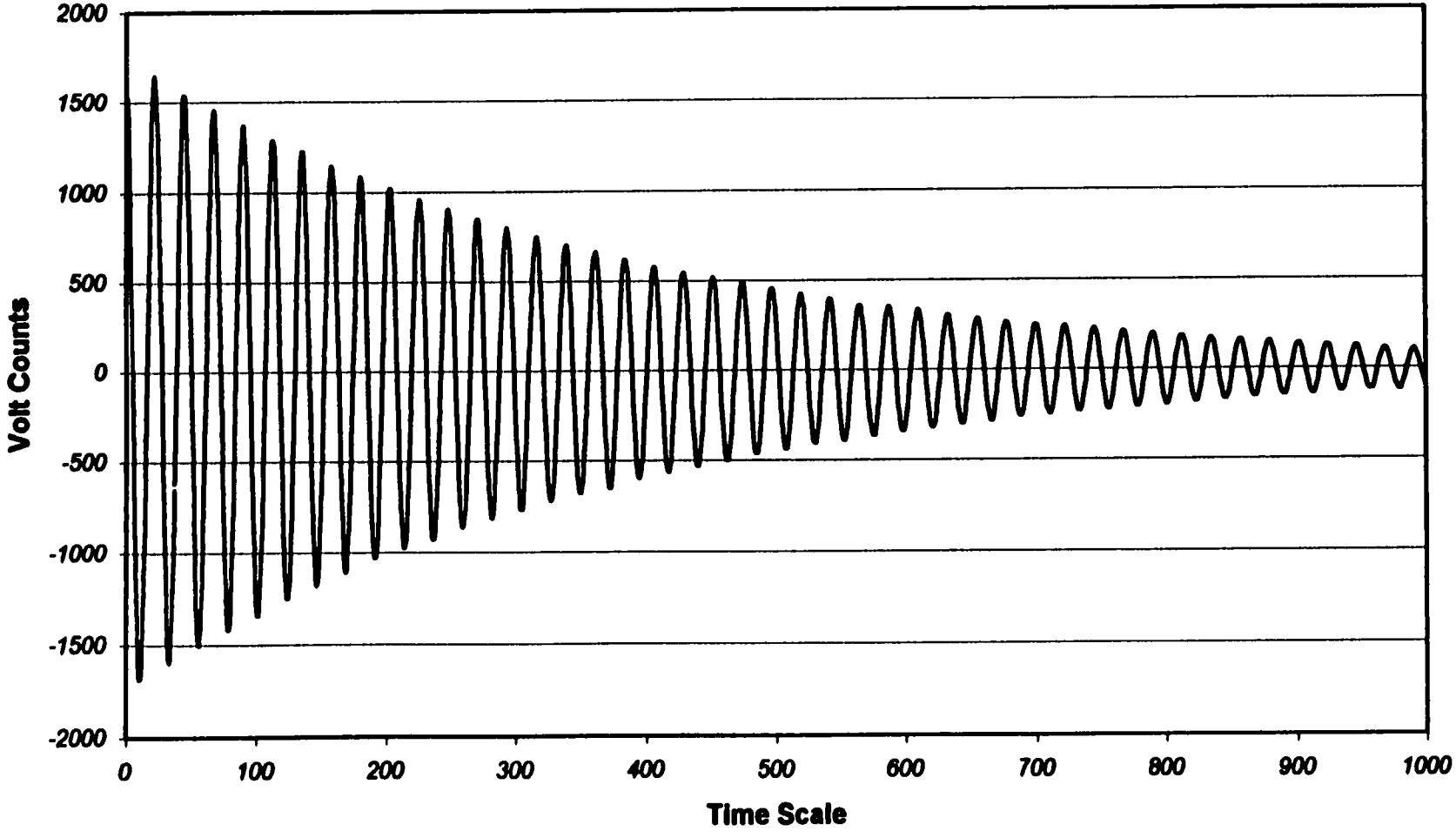

Appendix B
Section 5
3 m/s - 60 degrees

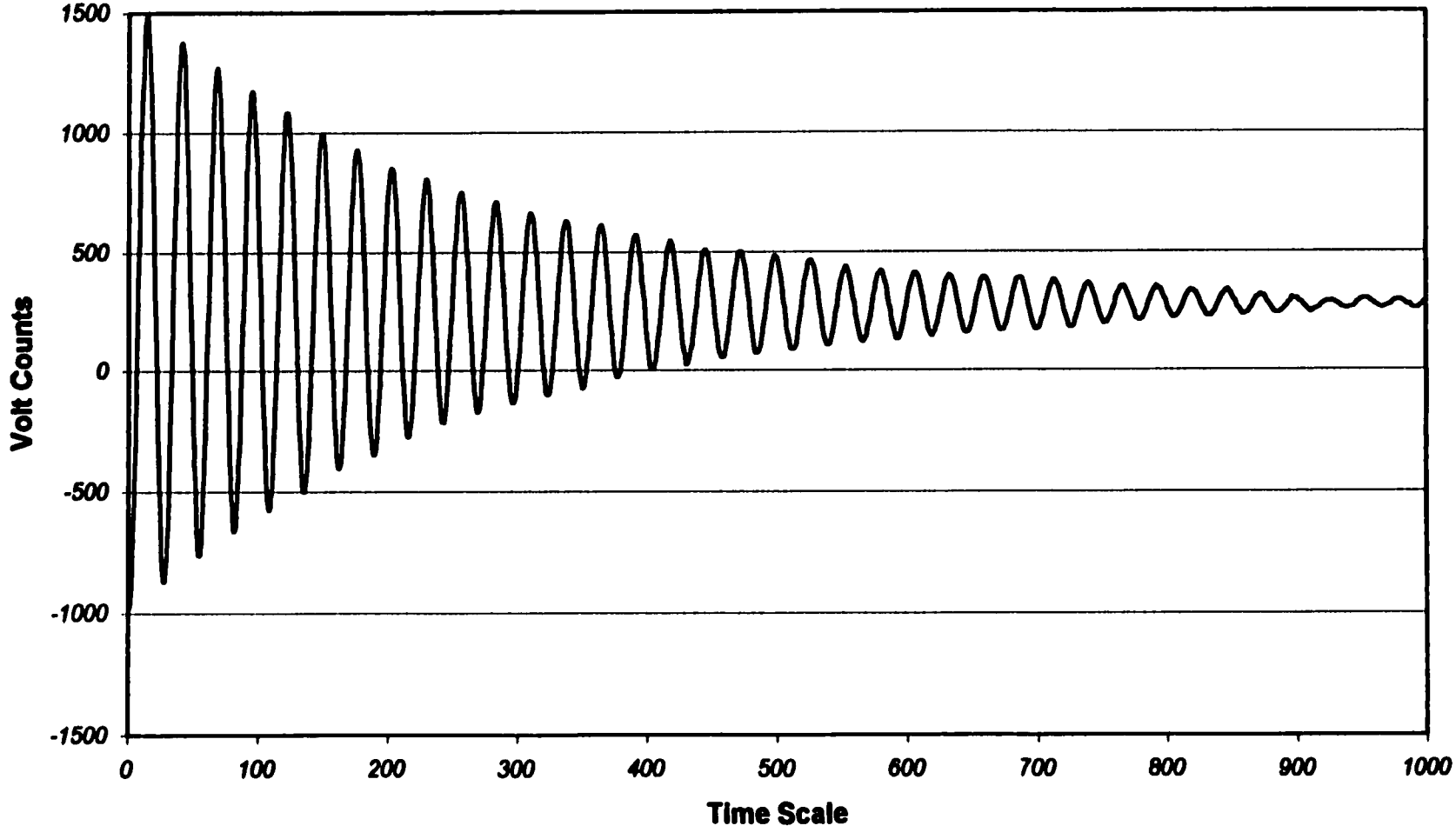

Appendix C

Buffeting Analysis used for the Parametric Study

Appendix C

Buffeting Analysis used for the Parametric Study

C.1 Turbulence Length Scales

The along-wind turbulence length scales were set to be approximately 5%, 10%, and 15% of the model length. With the along-wind scales set, the other scales were determined from ESDU (1975), using the following empirical relationships:

$$L_u^x = 25 z^{0.35} / z_o^{0.063} \tag{C.1}$$

$$L_u^y = 10 z^{0.38} / z_o^{0.068} \tag{C.2}$$

$$L_v^x = 5.1 z^{0.48} / z_o^{0.086} \tag{C.3}$$

$$L_v^z = 3.1 z^{0.55} / z_o^{0.099} \tag{C.4}$$

In the above expression, z is the model height above ground and was taken to be the height of the support stand, 0.305 m. z_o is the roughness length of the surface and was first calculated from C.1 using the set value for L_u^x. The other length scales were then calculated using this roughness length. The lateral length scale L_v^y was taken to equal L_v^z from C.4 because no other formula was available. These equations and assumptions were similar to those used by Kimura et al. (1998).

C.2 Turbulence Intensities

The along-wind turbulence intensity was selected as $I_u = 10\%$. Using this set value, the following ratio taken from Panofsky and Dutton (1984), was used in order to calculate the lateral intensity:

$$I_u : I_v = 2.39 : 1.92 \tag{C.5}$$

With the turbulence intensities, the variances σ_u^2 and σ_v^2 could then be calculated from 2.9. The expression in C.5 was also used by Kimura et al. (1998).

C.3 Modified Buffeting Analysis for Torsional Spring Models

The equation of motion for the models used in this study is

$$\ddot{\Theta} + 2\omega_o \xi_t \dot{\Theta} + \omega^2{}_o \Theta = M_t / J \tag{C.6}$$

The damping term on the left hand side will be the sum of the structural and aerodynamic damping. The total torque moment M_t will then be due only to the fluctuating along-wind and lateral components of the incident wind:

$$M_t = \int_0^L y\, dF \tag{C.7}$$

Taking dF from Equation 6.3 and ignoring the self-excited term (which now appears on the left hand side as the aerodynamic damping term), M_t becomes

$$M_t = \rho D U' \int_0^L y\, u'(t) C_n(y, \beta)\, dy + \frac{\rho D U'}{2} \int_0^L y\, v'(t) \frac{dC_n(y, \beta)}{d\beta} dy \tag{C.8}$$

The usual procedure to obtain the spectrum of the generalized torque moment, S_m, is applied here. The procedure involves taking the Fourier transform of C.6 with C.8 replaced for the torque moment. After applying the transform, the spectrum of the torque moment is generalized by accounting for the cross-dependence of the wind velocities at differenct points $y1$ and $y2$ along the model. The general procedure can be found in Kimura (1991) and will not be repeated here. The generalized torque moment will be

$$S_m(n) = (\rho D U')^2 \int_0^L \int_0^L y1\, y2\, S_{uu}(y1, y2; n) C_n(y1, \beta) C_n(y2, \beta)\, dy1\, dy2 + \left(\frac{\rho D U'}{2}\right)^2 \int_0^L \int_0^L y1\, y2\, S_w(y1, y2; n) \frac{dC_n(y1, \beta)}{d\beta} \frac{dC_n(y2, \beta)}{d\beta} dy1\, dy2 \tag{C.9}$$

The response spectrum for the angular displacement will take the form

$$S_\Theta(n) = \frac{1}{\omega^4 J^2} |H_f(n)|^2 |X_a(n)|^2 S_m(n) \tag{C.10}$$

For the models used in the experiment, it is reasonable to assume that they will vibrate only in one mode. Higher mode vibrations would require the stiff leaf spring to be excited by a high energy input at a high frequency. Using this assumption, the response spectrum for each section will be narrow banded, with the majority of the response energy concentrated at the first mode lateral frequency n_r. Using this, the mean square response for the angular displacement can be evaluated discretely as

$$\sigma_\theta^2 = \frac{\pi n_r}{4\xi_t \omega^4{}_o J^2} |\chi_a(n_r)|^2 S_m(n_r) \tag{C.11}$$

In C.11, the aerodynamic admittance function is used from the modified expressions presented by Irwin (1977).

C.4 Evaluation of $S_m(n)$

The evaluation of the generalized torqure moment in C.9 requires the evaluation of two complicated double integral expressions. The double integral expressions can be simplified by making some assumptions outlined below.

The expression for the along-wind and cross-wind cross-spectrums S_{uu} and S_{vv}, respectively, can be reduced using Xie et al. (1989) to the following expressions:

$$S_{uu}(y_1, y_2, n) = S'_u \cos^2\beta R_{uu}(y_1, y_2, n) + S'_v \sin^2\beta R_{vv}(y_1, y_2, n) \tag{C.12}$$

and

$$S_{vv}(y_1, y_2, n) = S'_u \sin^2\beta R_{uu}(y_1, y_2, n) + S'_v \cos^2\beta R_{vv}(y_1, y_2, n) \tag{C.13}$$

The expressions for the along-wind and cross-wind coherences R_{uu} and R_{vv}, respectively, are taken to be represented here by the exponential forms:

$$R_{uu}(y_1, y_2, n) = e^{-c_1 \Delta y n / U' \cos\beta} \tag{C.14}$$

and

$$R_{vv}(y_1, y_2, n) = e^{-c_1 \Delta y n / U' \cos\beta} \tag{C.15}$$

where c_1 is taken as 7, c_2 is taken as 14, and $\Delta y = |y_1 - y_2|$ is the along-span separation distance.

These forms of coherence are not as accurate as the von Karman forms (see Section 2.3), and at lower n values, the above expressions tend to infinity. To solve this problem, a method is employed similar to Irwin (1977):

If we assume that over the spanwise region of significant velocity correlation, the mode shape, force coefficient, and force coefficient slope with respect to the yaw angle, are all relatively constant, then their correlations become unity and can be removed from the integrand in C.9 leaving

$$S_m(n) = (\rho D U')^2 \int_0^L \int_0^L S_{mm}(y_1, y_2; n)\, dy_1\, dy_2 \left(\frac{\rho D U'}{2}\right)^2 \int_0^L \int_0^L S_{ww}(y_1, y_2; n)\, dy_1\, dy_2 \tag{C.16}$$

Substituting C.14 and C.15 into C.12 and C.13, respectively, equation C.16 will be reduced to an expression having four integral expressions of the form

$$\int_0^L \int_0^L e^{-C\Delta y}\, dy_1\, dy_2 \tag{C.17}$$

where C equals $c_1 n / U' \cos\beta$ or $c_2 n / U' \cos\beta$.

The double integal in C.17 will lead to a good approximation of the mean square response from C.11 when the frequency n is not close to zero. As n approaches zero, a useful expression for C.17 needs to be found.

The integrand in C.17 can be rewritten as

$$\int_0^L \left(\int_0^L e^{-C\Delta y}\, dy_2 \right) dy_1 \tag{C.18}$$

The term inside the brackets can be further reduced to

$$\int_0^{y_1} e^{-C\Delta y} dy_2 + \int_{y_1}^{L-y_1} e^{-C\Delta y} dy_2 \tag{C.19}$$

The first term in C.19 applies when $y_1 > y_2$. Here, $\Delta y = y_1 - y_2$ and $dy_2 = -d\Delta$, so the first term reduces to

$$-\int_{y_1}^{0} e^{-C\Delta y} d\Delta = \int_0^{y_1} e^{-C\Delta} d\Delta \tag{C.20}$$

The second term in C.19 applies when $y_1 < y_2$. Here, $\Delta y = y_2 - y_1$ and $dy_2 = d\Delta$, reducing the second term to

$$\int_0^{L-y_1} e^{-C\Delta y} d\Delta \tag{C.21}$$

Adding C.20 and C.21 leaves

$$\int_0^{L} e^{-C\Delta y} d\Delta = \frac{1-e^{-CL}}{C} \tag{C.22}$$

This expression is independent of y_1, and when integrated in C.18 with respect to y_1 becomes equal to

$$\frac{L}{C}\left(1-e^{-CL}\right) \tag{C.23}$$

As n approaches 0, C approaches zero in C.23. Taking this limit results in C.23 becoming equal to L^2.

In the analysis, the integral in C.18 was evaluated discretely for various values of n. As n approached zero, the integral increased significantly from zero. For these cases, the integral was taken to be equal to the limit L^2, which in turn resulted in more accurate values for the overall buffeting response σ_θ^2.

Appendix D
Parametric Study Results

Section	1		Wind Case	1		
U =	1.23	m/s	Lux	0.01	m	
			Iu	10	%	
Yaw	Aerod (cos)	Aerod (theory)	Aerod (avg)	RMS (cos)	RMS (theory)	RMS (avg)
0	2.364E-03	4.651E-03	2.534E-03	0.028	0.021	0.027
10	2.329E-03	4.580E-03	2.394E-03	0.0024	0.0018	0.0024
20	2.222E-03	4.370E-03	2.360E-03	0.0012	0.0009	0.0012
30	2.048E-03	4.028E-03	2.255E-03	0.00072	0.00055	0.0007
40	1.811E-03	3.563E-03	1.584E-03	0.00048	0.00037	0.00049
50	1.520E-03	2.989E-03	1.481E-03	0.00033	0.00026	0.00033
60	1.182E-03	2.325E-03	9.116E-04	0.00022	0.00019	0.00023
70	8.087E-04	1.591E-03	6.126E-04	0.00013	0.00012	0.00014
80	4.106E-04	8.080E-04	3.332E-04	0.000074	0.000069	0.000075
90	0.000E+00	0.000E+00	1.783E-04	0.000025	0.000025	0.000024

Section	1		Wind Case	1		
U =	2.074	m/s	Lux	0.01	m	
			Iu	10	%	
Yaw	Aerod (cos)	Aerod (theory)	Aerod (avg)	RMS (cos)	RMS (theory)	RMS (avg)
0	3.931E-03	7.842E-03	4.086E-03	0.067	0.044	0.066
10	3.871E-03	7.723E-03	3.779E-03	0.0055	0.0037	0.0056
20	3.693E-03	7.369E-03	3.999E-03	0.0027	0.0018	0.0026
30	3.404E-03	6.791E-03	3.196E-03	0.0015	0.001	0.0015
40	3.011E-03	6.007E-03	3.003E-03	0.0092	0.00064	0.00092
50	2.526E-03	5.041E-03	2.731E-03	0.0006	0.00044	0.00058
60	1.965E-03	3.921E-03	1.893E-03	0.0004	0.00031	0.00041
70	1.344E-03	2.682E-03	1.305E-03	0.00027	0.00022	0.00027
80	6.825E-04	1.362E-03	8.788E-04	0.00018	0.00017	0.00018
90	0.000E+00	0.000E+00	2.254E-04	0.000069	0.000069	0.000066

Section	1		Wind Case	1		
U =	3.227	m/s	Lux	0.01	m	
			Iu	10	%	
Yaw	Aerod (cos)	Aerod (theory)	Aerod (avg)	RMS (cos)	RMS (theory)	RMS (avg)
0	5.803E-03	1.220E-02	5.484E-03	0.2	0.11	0.22
10	5.714E-03	1.202E-02	6.619E-03	0.016	0.0068	0.015
20	5.453E-03	1.147E-02	5.602E-03	0.0074	0.0041	0.0073
30	5.025E-03	1.058E-02	5.097E-03	0.0039	0.0022	0.0039
40	4.445E-03	9.347E-03	4.416E-03	0.0022	0.0013	0.002
50	3.730E-03	7.843E-03	3.741E-03	0.0013	0.0008	0.0013
60	2.901E-03	6.101E-03	2.978E-03	0.00087	0.00057	0.00087
70	1.985E-03	4.173E-03	2.091E-03	0.00068	0.00049	0.00065
80	1.008E-03	2.119E-03	9.032E-04	0.00058	0.00048	0.0006
90	0.000E+00	0.000E+00	2.028E-04	0.00026	0.00026	0.00025

Section	1		Wind Case	1		
U =	4.047	m/s	Lux	0.01	m	
			Iu	10	%	
Yaw	Aerod (cos)	Aerod (theory)	Aerod (avg)	RMS (cos)	RMS (theory)	RMS (avg)
0	7.553E-03	1.530E-02	6.904E-03	0.2	0.11	0.22
10	7.438E-03	1.507E-02	8.037E-03	0.016	0.0068	0.015
20	7.098E-03	1.438E-02	7.231E-03	0.0074	0.0041	0.0073
30	6.541E-03	1.325E-02	6.411E-03	0.0039	0.0022	0.0039
40	5.786E-03	1.172E-02	6.458E-03	0.0022	0.0013	0.002
50	4.855E-03	9.836E-03	4.850E-03	0.0013	0.0008	0.0013
60	3.777E-03	7.651E-03	3.811E-03	0.00087	0.00057	0.00087
70	2.583E-03	5.234E-03	2.908E-03	0.00068	0.00049	0.00065
80	1.312E-03	2.657E-03	1.152E-03	0.00058	0.00048	0.0006
90	0.000E+00	0.000E+00	1.371E-04	0.00026	0.00026	0.00025

Section	1		Wind Case	1		
U =	4.947	m/s	Lux	0.01	m	
			Iu	10	%	
Yaw	Aerod (cos)	Aerod (theory)	Aerod (avg)	RMS (cos)	RMS (theory)	RMS (avg)
0	9.071E-03	1.870E-02	1.007E-02	0.28	0.15	0.26
10	8.933E-03	1.842E-02	8.776E-03	0.022	0.011	0.022
20	8.524E-03	1.758E-02	7.042E-03	0.01	0.0053	0.012
30	7.856E-03	1.620E-02	7.550E-03	0.0053	0.0028	0.0054
40	6.949E-03	1.433E-02	7.360E-03	0.0028	0.0017	0.0027
50	5.831E-03	1.202E-02	5.519E-03	0.0016	0.00094	0.0017
60	4.535E-03	9.353E-03	5.136E-03	0.0011	0.00068	0.001
70	3.102E-03	6.398E-03	4.194E-03	0.00088	0.0006	0.00078
80	1.575E-03	3.248E-03	1.383E-03	0.00061	0.00054	0.00054
90	0.000E+00	0.000E+00	6.477E-04	0.00038	0.00038	0.00034

Section	2		Wind Case	1		
U =	1.212	m/s	Lux	0.01	m	
			Iu	10	%	
Yaw	Aerod (cos)	Aerod (theory)	Aerod (avg)	RMS (cos)	RMS (theory)	RMS (avg)
0	1.386E-03	2.426E-03	1.523E-03	0.018	0.015	0.017
10	1.364E-03	2.389E-03	1.409E-03	0.0011	0.00096	0.0011
20	1.302E-03	2.280E-03	1.364E-03	0.00055	0.00047	0.00054
30	1.200E-03	2.101E-03	1.283E-03	0.00032	0.00028	0.00032
40	1.061E-03	1.859E-03	9.399E-04	0.00021	0.00018	0.00021
50	8.906E-04	1.560E-03	5.432E-04	0.00014	0.00013	0.00015
60	6.927E-04	1.213E-03	3.743E-04	0.000099	0.00009	0.0001
70	4.739E-04	8.300E-04	3.561E-04	0.000063	0.000059	0.000064
80	2.406E-04	4.210E-04	2.102E-04	0.000038	0.000037	0.000038
90	0.000E+00	0.000E+00	1.153E-04	0.000013	0.000013	0.000013

Section	2		Wind Case	1		
U =	1.987	m/s	Lux	0.01	m	
			Iu	10	%	
Yaw	Aerod (cos)	Aerod (theory)	Aerod (avg)	RMS (cos)	RMS (theory)	RMS (avg)
0	2.122E-03	3.978E-03	2.304E-03	0.045	0.035	0.044
10	2.090E-03	3.917E-03	1.885E-03	0.0028	0.0022	0.0028
20	1.994E-03	3.738E-03	2.093E-03	0.0013	0.001	0.0013
30	1.838E-03	3.445E-03	1.850E-03	0.00069	0.00055	0.00069
40	1.626E-03	3.047E-03	1.770E-03	0.00041	0.00033	0.0004
50	1.364E-03	2.557E-03	1.238E-03	0.00026	0.00022	0.00027
60	1.061E-03	1.989E-03	7.955E-04	0.00018	0.00016	0.00019
70	7.258E-04	1.360E-03	6.629E-04	0.00013	0.00012	0.00013
80	3.685E-04	6.910E-04	1.247E-04	0.000094	0.000089	0.000098
90	0.000E+00	0.000E+00	1.225E-04	0.000034	0.000034	0.000033

Section	2		Wind Case	1		
U =	2.95	m/s	Lux	0.01	m	
			Iu	10	%	
Yaw	Aerod (cos)	Aerod (theory)	Aerod (avg)	RMS (cos)	RMS (theory)	RMS (avg)
0	3.181E-03	5.906E-03	3.270E-03	0.095	0.069	0.094
10	3.133E-03	5.816E-03	3.043E-03	0.0057	0.0041	0.0058
20	2.989E-03	5.549E-03	3.258E-03	0.0026	0.0019	0.0025
30	2.755E-03	5.114E-03	2.808E-03	0.0013	0.00098	0.0013
40	2.437E-03	4.524E-03	2.358E-03	0.00072	0.00055	0.00073
50	2.045E-03	3.796E-03	1.798E-03	0.00044	0.00034	0.00045
60	1.591E-03	2.953E-03	1.316E-03	0.0003	0.00025	0.00032
70	1.088E-03	2.020E-03	1.132E-03	0.00029	0.0002	0.00023
80	5.524E-04	1.025E-03	7.608E-04	0.00019	0.00018	0.00018
90	0.000E+00	0.000E+00	-1.520E-05	0.000074	0.000074	0.000075

Section	2		Wind Case	1		
U =	3.951	m/s	Lux	0.01	m	
			Iu	10	%	
Yaw	Aerod (cos)	Aerod (theory)	Aerod (avg)	RMS (cos)	RMS (theory)	RMS (avg)
0	4.508E-03	7.909E-03	4.326E-03	0.16	0.11	0.16
10	4.439E-03	7.789E-03	4.465E-03	0.0095	0.0066	0.0094
20	4.236E-03	7.432E-03	4.672E-03	0.0042	0.003	0.0039
30	3.904E-03	6.850E-03	4.129E-03	0.0021	0.0015	0.0021
40	3.453E-03	6.059E-03	3.183E-03	0.0011	0.00081	0.0011
50	2.898E-03	5.084E-03	2.468E-03	0.00062	0.00047	0.00066
60	2.254E-03	3.955E-03	1.936E-03	0.00041	0.00034	0.00045
70	1.542E-03	2.705E-03	1.599E-03	0.00035	0.0003	0.00035
80	7.828E-04	1.373E-03	7.920E-04	0.00031	0.00028	0.00031
90	0.000E+00	0.000E+00	-1.387E-04	0.00013	0.00013	0.00014

Section	2		Wind Case	1		
U =	4.942	m/s	Lux	0.01	m	
			Iu	10	%	
Yaw	Aerod (cos)	Aerod (theory)	Aerod (avg)	RMS (cos)	RMS (theory)	RMS (avg)
0	5.431E-03	9.893E-03	5.168E-03	0.25	0.16	0.25
10	5.349E-03	9.743E-03	5.439E-03	0.014	0.0094	0.014
20	5.104E-03	9.297E-03	5.205E-03	0.0064	0.0042	0.0064
30	4.704E-03	8.568E-03	4.525E-03	0.0032	0.0021	0.0032
40	4.161E-03	7.579E-03	4.451E-03	0.0016	0.0011	0.0015
50	3.491E-03	6.359E-03	3.268E-03	0.00084	0.0006	0.00087
60	2.716E-03	4.947E-03	2.965E-03	0.00057	0.00043	0.00055
70	1.858E-03	3.384E-03	2.353E-03	0.00049	0.00039	0.00045
80	9.431E-04	1.718E-03	9.411E-04	0.00045	0.0004	0.00045
90	0.000E+00	0.000E+00	2.579E-04	0.00021	0.00021	0.0002

Section	3		Wind Case	1		
U =	1.195	m/s	Lux	0.01	m	
			Iu	10	%	
Yaw	Aerod (cos)	Aerod (theory)	Aerod (avg)	RMS (cos)	RMS (theory)	RMS (avg)
0	7.716E-04	1.538E-03	8.079E-04	0.012	0.01	0.012
10	7.599E-04	1.515E-03	6.392E-04	0.00067	0.00059	0.00068
20	7.250E-04	1.445E-03	7.149E-04	0.00032	0.00028	0.00032
30	6.682E-04	1.332E-03	7.903E-04	0.00019	0.00017	0.00018
40	5.911E-04	1.178E-03	4.292E-04	0.00012	0.00011	0.00012
50	4.960E-04	9.890E-04	5.649E-04	0.000083	0.000076	0.000082
60	3.858E-04	7.690E-04	3.843E-04	0.000057	0.000054	0.000057
70	2.639E-04	5.260E-04	4.365E-04	0.000036	0.000036	0.000037
80	1.340E-04	2.670E-04	1.186E-04	0.000024	0.000024	0.000024
90	0.000E+00	0.000E+00	5.396E-05	0.0000081	0.0000081	0.000008

Section	3		Wind Case	1		
U =	2.064	m/s	Lux	0.01	m	
			Iu	10	%	
Yaw	Aerod (cos)	Aerod (theory)	Aerod (avg)	RMS (cos)	RMS (theory)	RMS (avg)
0	1.454E-03	2.656E-03	1.367E-03	0.034	0.028	0.034
10	1.432E-03	2.616E-03	1.158E-03	0.0018	0.0015	0.0019
20	1.366E-03	2.496E-03	1.185E-03	0.00083	0.0007	0.00077
30	1.259E-03	2.300E-03	1.282E-03	0.00044	0.00037	0.00044
40	1.114E-03	2.035E-03	1.196E-03	0.00025	0.00022	0.00025
50	9.344E-04	1.707E-03	9.562E-04	0.00016	0.00014	0.00016
60	7.268E-04	1.328E-03	8.698E-04	0.00012	0.0001	0.00011
70	4.972E-04	9.090E-04	5.901E-04	0.000087	0.000081	0.000086
80	2.524E-04	4.610E-04	4.839E-04	0.000065	0.000063	0.000062
90	0.000E+00	0.000E+00	2.150E-04	0.000024	0.000024	0.000023

Section	3		Wind Case	1		
U =	2.99	m/s	Lux	0.01	m	
			Iu	10	%	
Yaw	Aerod (cos)	Aerod (theory)	Aerod (avg)	RMS (cos)	RMS (theory)	RMS (avg)
0	2.225E-03	3.848E-03	2.408E-03	0.07	0.056	0.068
10	2.191E-03	3.790E-03	1.894E-03	0.0037	0.003	0.0039
20	2.091E-03	3.616E-03	1.960E-03	0.0017	0.0013	0.0017
30	1.927E-03	3.333E-03	1.842E-03	0.00084	0.00068	0.00085
40	1.705E-03	2.948E-03	1.658E-03	0.00044	0.00037	0.00045
50	1.430E-03	2.474E-03	1.384E-03	0.00026	0.00022	0.00027
60	1.113E-03	1.924E-03	1.202E-03	0.00019	0.00016	0.00019
70	7.610E-04	1.316E-03	1.067E-03	0.00015	0.00014	0.00014
80	3.864E-04	6.680E-04	4.717E-04	0.00013	0.00012	0.00012
90	0.000E+00	0.000E+00	3.368E-04	0.000049	0.000049	0.000046

Section	3		Wind Case	1		
U =	4.009	m/s	Lux	0.01	m	
			Iu	10	%	
Yaw	Aerod (cos)	Aerod (theory)	Aerod (avg)	RMS (cos)	RMS (theory)	RMS (avg)
0	2.847E-03	5.160E-03	3.068E-03	0.13	0.096	0.12
10	2.804E-03	5.081E-03	2.732E-03	0.0068	0.0051	0.0069
20	2.675E-03	4.848E-03	2.406E-03	0.003	0.0022	0.0031
30	3.465E-03	4.469E-03	2.336E-03	0.0013	0.0011	0.0015
40	2.181E-03	3.952E-03	2.210E-03	0.00073	0.00057	0.00073
50	1.830E-03	3.316E-03	1.616E-03	0.0004	0.00032	0.00041
60	1.423E-03	2.580E-03	1.225E-03	0.00028	0.00024	0.00029
70	9.736E-04	1.765E-03	1.587E-03	0.00024	0.00021	0.00022
80	4.943E-04	8.960E-04	6.243E-04	0.00021	0.0002	0.0002
90	0.000E+00	0.000E+00	6.208E-05	0.000088	0.000088	0.000087

Section	3		Wind Case	1		
U =	4.899	m/s	Lux	0.01	m	
			Iu	10	%	
Yaw	Aerod (cos)	Aerod (theory)	Aerod (avg)	RMS (cos)	RMS (theory)	RMS (avg)
0	3.503E-03	6.305E-03	3.202E-03	0.19	0.14	0.2
10	3.450E-03	6.209E-03	3.626E-03	0.01	0.0072	0.0096
20	3.292E-03	5.925E-03	3.313E-03	0.0044	0.0032	0.0044
30	3.034E-03	5.460E-03	2.821E-03	0.0021	0.0016	0.0022
40	2.683E-03	4.830E-03	2.276E-03	0.001	0.00078	0.0011
50	2.252E-03	4.053E-03	2.197E-03	0.00053	0.00041	0.00054
60	1.751E-03	3.152E-03	1.700E-03	0.00036	0.0003	0.00048
70	1.198E-03	2.156E-03	2.149E-03	0.00032	0.00027	0.00027
80	6.083E-04	1.095E-03	9.717E-04	0.00029	0.00027	0.00028
90	0.000E+00	0.000E+00	6.618E-05	0.00013	0.00013	0.00013

Section	4		Wind Case	1		
U =	1.19	m/s	Lux	0.01	m	
			Iu	10	%	
Yaw	Aerod (cos)	Aerod (theory)	Aerod (avg)	RMS (cos)	RMS (theory)	RMS (avg)
0	3.653E-03	5.328E-03	3.592E-03	0.04	0.032	0.04
10	3.597E-03	5.247E-03	3.429E-03	0.0033	0.0027	0.0034
20	3.433E-03	5.008E-03	3.421E-03	0.0017	0.0014	0.0017
30	3.163E-03	4.614E-03	3.155E-03	0.001	0.00083	0.001
40	2.798E-03	4.081E-03	3.025E-03	0.00067	0.00057	0.00065
50	2.348E-03	3.424E-03	2.355E-03	0.00048	0.00041	0.00048
60	1.826E-03	2.664E-03	2.012E-03	0.00034	0.0003	0.00033
70	1.249E-03	1.822E-03	1.098E-03	0.00022	0.0002	0.00022
80	6.343E-04	9.250E-04	2.693E-04	0.00014	0.00013	0.00014
90	0.000E+00	0.000E+00	2.185E-04	0.000049	0.000049	0.000047

Section	4		Wind Case	1		
U =	2.068	m/s	Lux	0.01	m	
			Iu	10	%	
Yaw	Aerod (cos)	Aerod (theory)	Aerod (avg)	RMS (cos)	RMS (theory)	RMS (avg)
0	5.650E-03	9.258E-03	5.083E-03	0.099	0.071	0.11
10	5.762E-03	9.118E-03	5.618E-03	0.008	0.0058	0.0081
20	5.498E-03	8.700E-03	5.366E-03	0.0038	0.0028	0.0038
30	5.067E-03	8.016E-03	5.381E-03	0.0021	0.0016	0.002
40	4.482E-03	7.092E-03	5.011E-03	0.0013	0.00096	0.0012
50	3.761E-03	5.951E-03	4.203E-03	0.00085	0.00065	0.0008
60	2.925E-03	4.629E-03	3.455E-03	0.00061	0.00049	0.00056
70	2.001E-03	3.166E-03	2.473E-03	0.00045	0.00038	0.00042
80	1.016E-03	1.608E-03	9.058E-04	0.00035	0.00032	0.00036
90	0.000E+00	0.000E+00	1.349E-04	0.00014	0.00014	0.00014

Section	4		Wind Case	1		
U =	2.986	m/s	Lux	0.01	m	
			Iu	10	%	
Yaw	Aerod (cos)	Aerod (theory)	Aerod (avg)	RMS (cos)	RMS (theory)	RMS (avg)
0	8.346E-03	3.368E-02	7.546E-03	0.18	0.044	0.19
10	8.219E-03	1.317E-02	7.214E-03	0.014	0.0094	0.016
20	7.842E-03	1.256E-02	7.604E-03	0.0066	0.0044	0.0067
30	7.228E-03	1.158E-02	7.559E-03	0.0035	0.0024	0.0034
40	6.393E-03	1.024E-02	7.489E-03	0.002	0.0014	0.0018
50	5.365E-03	8.593E-03	6.167E-03	0.0012	0.00088	0.0011
60	4.173E-03	6.684E-03	5.246E-03	0.00068	0.00067	0.00078
70	2.854E-03	4.572E-03	3.599E-03	0.00073	0.00058	0.00066
80	1.449E-03	2.321E-03	1.485E-03	0.00064	0.00056	0.00064
90	0.000E+00	0.000E+00	1.410E-04	0.0003	0.0003	0.00029

Section	4		Wind Case	1		
U =	3.939	m/s	Lux	0.01	m	
			Iu	10	%	
Yaw	Aerod (cos)	Aerod (theory)	Aerod (avg)	RMS (cos)	RMS (theory)	RMS (avg)
0	1.109E-02	1.763E-02	9.430E-03	0.27	0.17	0.31
10	1.092E-02	1.737E-02	9.086E-03	0.021	0.014	0.025
20	1.042E-02	1.657E-02	9.749E-03	0.0097	0.0063	0.01
30	9.604E-03	1.527E-02	1.019E-02	0.0051	0.0033	0.0048
40	8.496E-03	1.351E-02	9.479E-03	0.0027	0.0018	0.0025
50	7.129E-03	1.134E-02	8.394E-03	0.0016	0.0011	0.0014
60	5.545E-03	8.817E-03	7.049E-03	0.0012	0.00083	0.00098
70	3.793E-03	6.031E-03	5.429E-03	0.001	0.00078	0.00083
80	1.926E-03	3.062E-03	2.274E-03	0.00099	0.00084	0.00094
90	0.000E+00	0.000E+00	4.245E-04	0.00051	0.00051	0.00047

Section	4		Wind Case	1		
U =	4.943	m/s	Lux	0.01	m	
			Iu	10	%	
Yaw	Aerod (cos)	Aerod (theory)	Aerod (avg)	RMS (cos)	RMS (theory)	RMS (avg)
0	1.335E-02	2.213E-02	1.327E-02	0.4	0.24	0.4
10	1.315E-02	2.197E-02	1.111E-02	0.031	0.018	0.036
20	1.254E-02	2.080E-02	1.228E-02	0.014	0.0084	0.014
30	1.156E-02	1.917E-02	1.241E-02	0.0072	0.0044	0.0067
40	1.028E-02	1.695E-02	1.160E-02	0.0037	0.0023	0.0034
50	8.581E-03	1.422E-02	1.099E-02	0.0021	0.0013	0.0017
60	6.675E-03	1.107E-02	1.000E-02	0.0014	0.00098	0.0011
70	4.566E-03	7.569E-03	6.749E-03	0.0013	0.00096	0.001
80	2.318E-03	3.843E-03	3.121E-03	0.0014	0.0011	0.0013
90	0.000E+00	0.000E+00	6.279E-04	0.0008	0.0008	0.0007

Section	5		Wind Case	1		
U =	1.22	m/s	Lux	0.01	m	
			Iu	10	%	
Yaw	Aerod (cos)	Aerod (theory)	Aerod (avg)	RMS (cos)	RMS (theory)	RMS (avg)
0	4.773E-03	5.489E-03	4.851E-03	0.046	0.042	0.046
10	4.701E-03	5.405E-03	4.196E-03	0.0038	0.0035	0.0041
20	4.486E-03	5.158E-03	4.553E-03	0.0019	0.0018	0.0019
30	4.134E-03	4.753E-03	4.374E-03	0.0011	0.0011	0.0011
40	3.657E-03	4.205E-03	3.766E-03	0.00077	0.00071	0.00076
50	3.068E-03	3.528E-03	3.421E-03	0.00055	0.00052	0.00053
60	2.387E-03	2.744E-03	2.890E-03	0.00041	0.00039	0.00038
70	1.633E-03	1.877E-03	2.230E-03	0.00029	0.00028	0.00026
80	8.269E-04	9.530E-04	9.396E-04	0.0002	0.00019	0.00019
90	0.000E+00	0.000E+00	-3.240E-05	0.000075	0.000075	0.000075

Section	5		Wind Case	1		
U =	2.061	m/s	Lux	0.01	m	
			Iu	10	%	
Yaw	Aerod (cos)	Aerod (theory)	Aerod (avg)	RMS (cos)	RMS (theory)	RMS (avg)
0	7.830E-03	9.362E-03	7.028E-03	0.11	0.092	0.12
10	7.711E-03	9.220E-03	6.602E-03	0.0084	0.0073	0.0094
20	7.358E-03	8.798E-03	7.131E-03	0.004	0.0035	0.0041
30	6.781E-03	8.108E-03	6.650E-03	0.0022	0.0019	0.0022
40	5.998E-03	7.172E-03	6.610E-03	0.0013	0.0012	0.0012
50	5.033E-03	6.018E-03	6.475E-03	0.0009	0.00081	0.00077
60	3.915E-03	4.681E-03	5.076E-03	0.00068	0.00062	0.00059
70	2.678E-03	3.202E-03	3.675E-03	0.00056	0.00052	0.00049
80	1.360E-03	1.626E-03	1.751E-03	0.00048	0.00046	0.00045
90	0.000E+00	0.000E+00	2.406E-04	0.00021	0.00021	0.0002

Section	5		Wind Case	1		
U =	2.999	m/s	Lux	0.01	m	
			Iu	10	%	
Yaw	Aerod (cos)	Aerod (theory)	Aerod (avg)	RMS (cos)	RMS (theory)	RMS (avg)
0	1.067E-02	1.349E-02	9.117E-03	0.19	0.16	0.22
10	1.050E-02	1.329E-02	9.434E-03	0.015	0.012	0.016
20	1.002E-02	1.268E-02	9.337E-03	0.007	0.0057	0.0074
30	9.238E-03	1.168E-02	9.511E-03	0.0037	0.0013	0.0036
40	8.171E-03	1.034E-02	9.399E-03	0.0021	0.0017	0.0018
50	6.856E-03	8.673E-03	9.234E-03	0.0013	0.0011	0.001
60	5.333E-03	6.746E-03	7.986E-03	0.00099	0.00085	0.00075
70	3.648E-03	4.615E-03	5.707E-03	0.00089	0.00079	0.0007
80	1.852E-03	2.343E-03	2.871E-03	0.00087	0.00081	0.00075
90	0.000E+00	0.000E+00	2.183E-04	0.00044	0.00044	0.00042

Section	5		Wind Case	1		
U =	4.074	m/s	Lux	0.01	m	
			Iu	10	%	
Yaw	Aerod (cos)	Aerod (theory)	Aerod (avg)	RMS (cos)	RMS (theory)	RMS (avg)
0	1.393E-02	1.833E-02	1.266E-02	0.31	0.24	0.34
10	1.372E-02	1.805E-02	1.199E-02	0.024	0.018	0.027
20	1.309E-02	1.722E-02	1.017E-02	0.011	0.0085	0.014
30	1.206E-02	1.587E-02	9.716E-03	0.0057	0.0044	0.0069
40	1.067E-02	1.404E-02	1.280E-02	0.003	0.0024	0.0026
50	8.953E-03	1.178E-02	1.290E-02	0.0019	0.0014	0.0013
60	6.964E-03	9.164E-03	1.413E-02	0.0013	0.0011	0.00073
70	4.764E-03	6.269E-03	8.184E-03	0.0013	0.0011	0.00089
80	2.419E-03	3.183E-03	4.651E-03	0.0014	0.0012	0.001
90	0.000E+00	0.000E+00	3.379E-04	0.0008	0.0008	0.00075

Section	5		Wind Case	1		
U =	4.939	m/s	Lux	0.01	m	
			Iu	10	%	
Yaw	Aerod (cos)	Aerod (theory)	Aerod (avg)	RMS (cos)	RMS (theory)	RMS (avg)
0	1.544E-02	2.222E-02	1.321E-02	0.45	0.31	0.53
10	1.520E-02	2.188E-02	1.307E-02	0.035	0.024	0.04
20	1.451E-02	2.088E-02	9.623E-03	0.016	0.011	0.023
30	1.337E-02	1.924E-02	1.088E-02	0.0081	0.0056	0.0098
40	1.183E-02	1.702E-02	1.421E-02	0.0042	0.0029	0.0035
50	9.924E-03	1.428E-02	1.561E-02	0.0023	0.0016	0.0015
60	7.720E-03	1.111E-02	1.461E-02	0.0017	0.0012	0.00096
70	5.281E-03	7.600E-03	1.057E-02	0.0016	0.0013	0.00099
80	2.681E-03	3.858E-03	5.730E-03	0.0019	0.0016	0.0013
90	0.000E+00	0.000E+00	6.272E-04	0.0012	0.0012	0.001

Section	1		Wind Case	2		
U =	1.23	m/s	Lux	0.02	m	
			lu	10	%	
Yaw	Aerod (cos)	Aerod (theory)	Aerod (avg)	RMS (cos)	RMS (theory)	RMS (avg)
0	2.364E-03	4.651E-03	2.534E-03	0.049	0.036	0.048
10	2.329E-03	4.580E-03	2.394E-03	0.0079	0.0059	0.0079
20	2.222E-03	4.370E-03	2.360E-03	0.0042	0.0032	0.0042
30	2.048E-03	4.028E-03	2.255E-03	0.0027	0.002	0.0026
40	1.811E-03	3.563E-03	1.564E-03	0.0018	0.0014	0.0019
50	1.520E-03	2.989E-03	1.481E-03	0.0013	0.001	0.0013
60	1.182E-03	2.325E-03	9.116E-04	0.00068	0.00074	0.00092
70	8.087E-04	1.591E-03	6.126E-04	0.00052	0.00046	0.00054
80	4.106E-04	8.080E-04	3.332E-04	0.00027	0.00026	0.00028
90	0.000E+00	0.000E+00	1.783E-04	0.000086	0.000086	0.000083

Section	1		Wind Case	2		
U =	2.074	m/s	Lux	0.02	m	
			lu	10	%	
Yaw	Aerod (cos)	Aerod (theory)	Aerod (avg)	RMS (cos)	RMS (theory)	RMS (avg)
0	3.931E-03	7.842E-03	4.066E-03	0.12	0.08	0.12
10	3.871E-03	7.723E-03	3.779E-03	0.019	0.012	0.019
20	3.693E-03	7.369E-03	3.999E-03	0.0096	0.0064	0.0092
30	3.404E-03	6.791E-03	3.196E-03	0.0056	0.0038	0.0057
40	3.011E-03	6.007E-03	3.003E-03	0.0035	0.0024	0.0035
50	2.526E-03	5.041E-03	2.731E-03	0.0023	0.0017	0.0022
60	1.965E-03	3.921E-03	1.893E-03	0.0016	0.0012	0.0016
70	1.344E-03	2.682E-03	1.305E-03	0.001	0.00086	0.001
80	6.825E-04	1.362E-03	8.788E-04	0.0007	0.00062	0.00067
90	0.000E+00	0.000E+00	2.254E-04	0.00025	0.00025	0.00024

Section	1		Wind Case	2		
U =	3.227	m/s	Lux	0.02	m	
			lu	10	%	
Yaw	Aerod (cos)	Aerod (theory)	Aerod (avg)	RMS (cos)	RMS (theory)	RMS (avg)
0	5.803E-03	1.220E-02	5.484E-03	0.26	0.15	0.27
10	5.714E-03	1.202E-02	6.619E-03	0.04	0.022	0.036
20	5.453E-03	1.147E-02	5.602E-03	0.02	0.011	0.019
30	5.025E-03	1.058E-02	5.097E-03	0.011	0.0063	0.011
40	4.445E-03	9.347E-03	4.416E-03	0.0062	0.0038	0.0063
50	3.730E-03	7.843E-03	3.741E-03	0.0039	0.0025	0.0039
60	2.901E-03	6.101E-03	2.978E-03	0.0026	0.0018	0.0026
70	1.985E-03	4.173E-03	2.091E-03	0.0019	0.0014	0.0019
80	1.008E-03	2.119E-03	9.032E-04	0.0015	0.0013	0.0015
90	0.000E+00	0.000E+00	2.028E-04	0.00061	0.00061	0.00059

Section	1		Wind Case	2		
U =	4.047	m/s	Lux	0.02	m	
			lu	10	%	
Yaw	Aerod (cos)	Aerod (theory)	Aerod (avg)	RMS (cos)	RMS (theory)	RMS (avg)
0	7.553E-03	1.530E-02	6.904E-03	0.37	0.2	0.4
10	7.438E-03	1.507E-02	8.037E-03	0.055	0.03	0.052
20	7.098E-03	1.438E-02	7.231E-03	0.027	0.015	0.027
30	6.541E-03	1.325E-02	6.411E-03	0.014	0.0083	0.015
40	5.786E-03	1.172E-02	6.456E-03	0.0082	0.0048	0.0076
50	4.855E-03	9.836E-03	4.850E-03	0.0049	0.003	0.0049
60	3.777E-03	7.651E-03	3.811E-03	0.0034	0.0022	0.0033
70	2.583E-03	5.234E-03	2.908E-03	0.0026	0.002	0.0025
80	1.312E-03	2.657E-03	1.152E-03	0.0022	0.0018	0.0023
90	0.000E+00	0.000E+00	1.371E-04	0.00096	0.00096	0.00094

Section	1		Wind Case	2		
U =	4.947	m/s	Lux	0.02	m	
			lu	10	%	
Yaw	Aerod (cos)	Aerod (theory)	Aerod (avg)	RMS (cos)	RMS (theory)	RMS (avg)
0	9.071E-03	1.870E-02	1.007E-02	0.52	0.27	0.48
10	8.933E-03	1.842E-02	8.776E-03	0.076	0.039	0.077
20	8.524E-03	1.758E-02	7.042E-03	0.037	0.019	0.043
30	7.856E-03	1.620E-02	7.550E-03	0.02	0.01	0.02
40	6.949E-03	1.433E-02	7.360E-03	0.011	0.0059	0.01
50	5.831E-03	1.202E-02	5.519E-03	0.0062	0.0036	0.0064
60	4.535E-03	9.353E-03	5.136E-03	0.0042	0.0026	0.0039
70	3.102E-03	6.398E-03	4.194E-03	0.0034	0.0023	0.0029
80	1.575E-03	3.248E-03	1.383E-03	0.0031	0.0024	0.0032
90	0.000E+00	0.000E+00	6.477E-04	0.0014	0.0014	0.0013

Section	2		Wind Case	2		
U =	1.212	m/s	Lux	0.02	m	
			Iu	10	%	
Yaw	Aerod (cos)	Aerod (theory)	Aerod (avg)	RMS (cos)	RMS (theory)	RMS (avg)
0	1.386E-03	2.426E-03	1.523E-03	0.037	0.031	0.036
10	1.364E-03	2.389E-03	1.409E-03	0.0041	0.0035	0.004
20	1.302E-03	2.280E-03	1.364E-03	0.002	0.0018	0.002
30	1.200E-03	2.101E-03	1.283E-03	0.0012	0.0011	0.0013
40	1.061E-03	1.859E-03	9.399E-04	0.00083	0.00073	0.00084
50	8.906E-04	1.560E-03	5.432E-04	0.00058	0.00052	0.00062
60	6.927E-04	1.213E-03	3.743E-04	0.0004	0.00036	0.00042
70	4.739E-04	8.300E-04	3.561E-04	0.00025	0.00024	0.00026
80	2.406E-04	4.210E-04	2.102E-04	0.00014	0.00014	0.00015
90	0.000E+00	0.000E+00	1.153E-04	0.000047	0.000047	0.000046

Section	2		Wind Case	2		
U =	1.987	m/s	Lux	0.02	m	
			Iu	10	%	
Yaw	Aerod (cos)	Aerod (theory)	Aerod (avg)	RMS (cos)	RMS (theory)	RMS (avg)
0	2.122E-03	3.978E-03	2.304E-03	0.095	0.074	0.093
10	2.090E-03	3.917E-03	1.885E-03	0.01	0.0078	0.01
20	1.994E-03	3.738E-03	2.093E-03	0.0048	0.0038	0.0047
30	1.838E-03	3.445E-03	1.850E-03	0.0027	0.0021	0.0026
40	1.626E-03	3.047E-03	1.770E-03	0.0016	0.0013	0.0016
50	1.364E-03	2.557E-03	1.238E-03	0.001	0.00067	0.0011
60	1.061E-03	1.989E-03	7.955E-04	0.00072	0.00062	0.00076
70	7.258E-04	1.360E-03	6.829E-04	0.00051	0.00046	0.00051
80	3.685E-04	6.910E-04	1.247E-04	0.00036	0.00034	0.00037
90	0.000E+00	0.000E+00	1.225E-04	0.00013	0.00013	0.00012

Section	2		Wind Case	2		
U =	2.95	m/s	Lux	0.02	m	
			Iu	10	%	
Yaw	Aerod (cos)	Aerod (theory)	Aerod (avg)	RMS (cos)	RMS (theory)	RMS (avg)
0	3.181E-03	5.906E-03	3.270E-03	0.2	0.15	0.2
10	3.133E-03	5.816E-03	3.043E-03	0.021	0.015	0.021
20	2.989E-03	5.549E-03	3.258E-03	0.0096	0.007	0.0093
30	2.755E-03	5.114E-03	2.808E-03	0.005	0.0037	0.005
40	2.437E-03	4.524E-03	2.358E-03	0.0028	0.0022	0.0028
50	2.045E-03	3.796E-03	1.798E-03	0.0017	0.0013	0.0018
60	1.591E-03	2.953E-03	1.316E-03	0.0012	0.00096	0.0012
70	1.088E-03	2.020E-03	1.132E-03	0.00091	0.00078	0.0009
80	5.524E-04	1.025E-03	7.608E-04	0.00072	0.00067	0.0007
90	0.000E+00	0.000E+00	-1.520E-05	0.00028	0.00028	0.00028

Section	2		Wind Case	2		
U =	3.951	m/s	Lux	0.02	m	
			Iu	10	%	
Yaw	Aerod (cos)	Aerod (theory)	Aerod (avg)	RMS (cos)	RMS (theory)	RMS (avg)
0	4.508E-03	7.909E-03	4.326E-03	0.34	0.24	0.35
10	4.439E-03	7.789E-03	4.465E-03	0.034	0.024	0.034
20	4.236E-03	7.432E-03	4.872E-03	0.016	0.011	0.015
30	3.904E-03	6.850E-03	4.129E-03	0.0081	0.0058	0.0078
40	3.453E-03	6.059E-03	3.183E-03	0.0042	0.0031	0.0044
50	2.898E-03	5.084E-03	2.468E-03	0.0024	0.0018	0.0025
60	2.254E-03	3.955E-03	1.936E-03	0.0017	0.0013	0.0017
70	1.542E-03	2.705E-03	1.599E-03	0.0014	0.0012	0.0014
80	7.828E-04	1.373E-03	7.920E-04	0.0012	0.0011	0.0012
90	0.000E+00	0.000E+00	-1.387E-04	0.0005	0.0005	0.00052

Section	2		Wind Case	2		
U =	4.942	m/s	Lux	0.02	m	
			Iu	10	%	
Yaw	Aerod (cos)	Aerod (theory)	Aerod (avg)	RMS (cos)	RMS (theory)	RMS (avg)
0	5.431E-03	9.893E-03	5.168E-03	0.53	0.34	0.54
10	5.349E-03	9.743E-03	5.439E-03	0.053	0.034	0.052
20	5.104E-03	9.297E-03	5.205E-03	0.024	0.016	0.024
30	4.704E-03	8.568E-03	4.525E-03	0.012	0.0081	0.012
40	4.161E-03	7.579E-03	4.451E-03	0.0061	0.0042	0.006
50	3.491E-03	6.359E-03	3.268E-03	0.0032	0.0023	0.0033
60	2.716E-03	4.947E-03	2.965E-03	0.0022	0.0016	0.0021
70	1.858E-03	3.384E-03	2.353E-03	0.0019	0.0015	0.0017
80	9.431E-04	1.718E-03	9.411E-04	0.0017	0.0015	0.0017
90	0.000E+00	0.000E+00	2.579E-04	0.00079	0.00079	0.00075

Section	3		Wind Case	2		
U =	1.195	m/s	Lux	0.02	m	
			Iu	10	%	
Yaw	Aerod (cos)	Aerod (theory)	Aerod (avg)	RMS (cos)	RMS (theory)	RMS (avg)
0	7.716E-04	1.538E-03	8.079E-04	0.027	0.023	0.026
10	7.599E-04	1.515E-03	6.392E-04	0.0025	0.0022	0.0025
20	7.250E-04	1.445E-03	7.149E-04	0.0012	0.0011	0.0012
30	6.682E-04	1.332E-03	7.903E-04	0.00073	0.00065	0.00071
40	5.911E-04	1.178E-03	4.292E-04	0.00048	0.00043	0.0005
50	4.960E-04	9.890E-04	5.649E-04	0.00034	0.00031	0.00033
60	3.856E-04	7.690E-04	3.843E-04	0.00023	0.00022	0.00023
70	2.639E-04	5.260E-04	4.365E-04	0.00015	0.0014	0.00014
80	1.340E-04	2.670E-04	1.186E-04	0.000092	0.00009	0.000092
90	0.000E+00	0.000E+00	5.396E-05	0.00003	0.00003	0.000029

Section	3		Wind Case	2		
U =	2.084	m/s	Lux	0.02	m	
			Iu	10	%	
Yaw	Aerod (cos)	Aerod (theory)	Aerod (avg)	RMS (cos)	RMS (theory)	RMS (avg)
0	1.454E-03	2.656E-03	1.387E-03	0.078	0.064	0.079
10	1.432E-03	2.616E-03	1.158E-03	0.0068	0.0056	0.0071
20	1.366E-03	2.496E-03	1.185E-03	0.0032	0.0026	0.0032
30	1.259E-03	2.300E-03	1.282E-03	0.0017	0.0014	0.0017
40	1.114E-03	2.035E-03	1.198E-03	0.00099	0.00085	0.00098
50	9.344E-04	1.707E-03	9.562E-04	0.00064	0.00056	0.00064
60	7.268E-04	1.328E-03	8.698E-04	0.00046	0.00041	0.00045
70	4.972E-04	9.090E-04	5.901E-04	0.00034	0.00032	0.00033
80	2.524E-04	4.610E-04	4.839E-04	0.00025	0.00024	0.00024
90	0.000E+00	0.000E+00	2.150E-04	0.000089	0.000089	0.000086

Section	3		Wind Case	2		
U =	2.99	m/s	Lux	0.02	m	
			Iu	10	%	
Yaw	Aerod (cos)	Aerod (theory)	Aerod (avg)	RMS (cos)	RMS (theory)	RMS (avg)
0	2.225E-03	3.848E-03	2.408E-03	0.16	0.13	0.16
10	2.191E-03	3.790E-03	1.894E-03	0.014	0.011	0.015
20	2.091E-03	3.616E-03	1.960E-03	0.0063	0.0051	0.0064
30	1.927E-03	3.333E-03	1.842E-03	0.0032	0.0026	0.0032
40	1.705E-03	2.948E-03	1.658E-03	0.0017	0.0014	0.0017
50	1.430E-03	2.474E-03	1.384E-03	0.001	0.00087	0.001
60	1.113E-03	1.924E-03	1.202E-03	0.00074	0.00064	0.00072
70	7.610E-04	1.316E-03	1.067E-03	0.00059	0.00054	0.00056
80	3.864E-04	6.680E-04	4.717E-04	0.00048	0.00046	0.00047
90	0.000E+00	0.000E+00	3.368E-04	0.00019	0.00019	0.00018

Section	3		Wind Case	2		
U =	4.009	m/s	Lux	0.02	m	
			Iu	10	%	
Yaw	Aerod (cos)	Aerod (theory)	Aerod (avg)	RMS (cos)	RMS (theory)	RMS (avg)
0	2.847E-03	5.160E-03	3.068E-03	0.3	0.22	0.29
10	2.804E-03	5.081E-03	2.732E-03	0.025	0.019	0.025
20	2.675E-03	4.848E-03	2.406E-03	0.011	0.0085	0.012
30	3.465E-03	4.468E-03	2.336E-03	0.0049	0.0043	0.0057
40	2.181E-03	3.952E-03	2.210E-03	0.0028	0.0022	0.0028
50	1.830E-03	3.316E-03	1.616E-03	0.0016	0.0012	0.0016
60	1.423E-03	2.580E-03	1.225E-03	0.0011	0.00091	0.0011
70	9.736E-04	1.765E-03	1.587E-03	0.00092	0.00081	0.00083
80	4.943E-04	8.960E-04	6.243E-04	0.0008	0.00075	0.00078
90	0.000E+00	0.000E+00	6.208E-05	0.00034	0.00034	0.00033

Section	3		Wind Case	2		
U =	4.899	m/s	Lux	0.02	m	
			Iu	10	%	
Yaw	Aerod (cos)	Aerod (theory)	Aerod (avg)	RMS (cos)	RMS (theory)	RMS (avg)
0	3.503E-03	6.305E-03	3.202E-03	0.44	0.32	0.46
10	3.450E-03	6.209E-03	3.626E-03	0.037	0.027	0.036
20	3.292E-03	5.925E-03	3.313E-03	0.017	0.012	0.017
30	3.034E-03	5.460E-03	2.821E-03	0.0082	0.006	0.0094
40	2.683E-03	4.830E-03	2.276E-03	0.004	0.003	0.0042
50	2.252E-03	4.053E-03	2.197E-03	0.002	0.0016	0.0021
60	1.751E-03	3.152E-03	1.700E-03	0.0014	0.0012	0.0014
70	1.198E-03	2.156E-03	2.149E-03	0.0012	0.0011	0.0011
80	6.083E-04	1.095E-03	9.717E-04	0.0011	0.001	0.001
90	0.000E+00	0.000E+00	6.618E-05	0.0005	0.0005	0.00049

Section	4		Wind Case	2		
U =	1.19	m/s	Lux	0.02	m	
			Iu	10	%	
Yaw	Aerod (cos)	Aerod (theory)	Aerod (avg)	RMS (cos)	RMS (theory)	RMS (avg)
0	3.653E-03	5.328E-03	3.592E-03	0.071	0.058	0.072
10	3.597E-03	5.247E-03	3.429E-03	0.011	0.0093	0.012
20	3.433E-03	5.006E-03	3.421E-03	0.006	0.005	0.006
30	3.163E-03	4.614E-03	3.155E-03	0.0038	0.0032	0.0038
40	2.798E-03	4.081E-03	3.025E-03	0.0026	0.0022	0.0025
50	2.348E-03	3.424E-03	2.355E-03	0.0019	0.0016	0.0019
60	1.826E-03	2.664E-03	2.012E-03	0.0014	0.0012	0.0013
70	1.249E-03	1.822E-03	1.098E-03	0.00087	0.00079	0.00089
80	6.343E-04	9.250E-04	2.693E-04	0.00051	0.00046	0.00054
90	0.000E+00	0.000E+00	2.185E-04	0.00018	0.00018	0.00017

Section	4		Wind Case	2		
U =	2.068	m/s	Lux	0.02	m	
			Iu	10	%	
Yaw	Aerod (cos)	Aerod (theory)	Aerod (avg)	RMS (cos)	RMS (theory)	RMS (avg)
0	5.650E-03	9.258E-03	5.083E-03	0.18	0.13	0.2
10	5.762E-03	9.118E-03	5.618E-03	0.027	0.02	0.026
20	5.498E-03	8.700E-03	5.366E-03	0.014	0.01	0.014
30	5.067E-03	8.018E-03	5.381E-03	0.0079	0.0058	0.0076
40	4.482E-03	7.092E-03	5.011E-03	0.0049	0.0037	0.0046
50	3.761E-03	5.951E-03	4.203E-03	0.0033	0.0026	0.0031
60	2.925E-03	4.629E-03	3.455E-03	0.0024	0.0019	0.0022
70	2.001E-03	3.166E-03	2.473E-03	0.0018	0.0015	0.0016
80	1.016E-03	1.608E-03	9.058E-04	0.0013	0.0012	0.0014
90	0.000E+00	0.000E+00	1.349E-04	0.00053	0.00053	0.00052

Section	4		Wind Case	2		
U =	2.986	m/s	Lux	0.02	m	
			Iu	10	%	
Yaw	Aerod (cos)	Aerod (theory)	Aerod (avg)	RMS (cos)	RMS (theory)	RMS (avg)
0	8.346E-03	3.368E-02	7.546E-03	0.33	0.034	0.35
10	8.219E-03	1.317E-02	7.214E-03	0.048	0.032	0.053
20	7.842E-03	1.256E-02	7.604E-03	0.024	0.016	0.024
30	7.228E-03	1.158E-02	7.559E-03	0.013	0.0089	0.013
40	6.393E-03	1.024E-02	7.489E-03	0.0075	0.0052	0.0067
50	5.365E-03	8.593E-03	6.167E-03	0.0047	0.0034	0.0043
60	4.173E-03	6.684E-03	5.246E-03	0.0034	0.0026	0.003
70	2.854E-03	4.572E-03	3.599E-03	0.0028	0.0022	0.0025
80	1.449E-03	2.321E-03	1.485E-03	0.0024	0.0021	0.0024
90	0.000E+00	0.000E+00	1.410E-04	0.0011	0.0011	0.0011

Section	4		Wind Case	2		
U =	3.939	m/s	Lux	0.02	m	
			Iu	10	%	
Yaw	Aerod (cos)	Aerod (theory)	Aerod (avg)	RMS (cos)	RMS (theory)	RMS (avg)
0	1.109E-02	1.763E-02	9.430E-03	0.5	0.32	0.57
10	1.092E-02	1.737E-02	9.066E-03	0.073	0.047	0.085
20	1.042E-02	1.657E-02	9.749E-03	0.036	0.023	0.038
30	9.604E-03	1.527E-02	1.019E-02	0.019	0.012	0.018
40	8.496E-03	1.351E-02	9.479E-03	0.01	0.0069	0.0094
50	7.129E-03	1.134E-02	8.394E-03	0.0061	0.0042	0.0054
60	5.545E-03	8.817E-03	7.049E-03	0.0044	0.0032	0.0038
70	3.793E-03	6.031E-03	5.429E-03	0.004	0.003	0.0032
80	1.926E-03	3.062E-03	2.274E-03	0.0038	0.0032	0.0036
90	0.000E+00	0.000E+00	4.245E-04	0.0019	0.0019	0.0018

Section	4		Wind Case	2		
U =	4.943	m/s	Lux	0.02	m	
			Iu	10	%	
Yaw	Aerod (cos)	Aerod (theory)	Aerod (avg)	RMS (cos)	RMS (theory)	RMS (avg)
0	1.335E-02	2.213E-02	1.327E-02	0.73	0.43	0.73
10	1.315E-02	2.197E-02	1.111E-02	0.1	0.062	0.12
20	1.254E-02	2.080E-02	1.228E-02	0.051	0.031	0.052
30	1.156E-02	1.917E-02	1.241E-02	0.027	0.016	0.025
40	1.028E-02	1.695E-02	1.160E-02	0.014	0.0088	0.013
50	8.581E-03	1.422E-02	1.099E-02	0.0078	0.005	0.0064
60	6.675E-03	1.107E-02	1.000E-02	0.0056	0.0037	0.0041
70	4.566E-03	7.569E-03	6.749E-03	0.0051	0.0037	0.004
80	2.318E-03	3.843E-03	3.121E-03	0.0053	0.0043	0.0048
90	0.000E+00	0.000E+00	6.279E-04	0.003	0.003	0.0027

Section	5		Wind Case	2		
U =	1.22	m/s	Lux	0.02	m	
			Iu	10	%	
Yaw	Aerod (cos)	Aerod (theory)	Aerod (avg)	RMS (cos)	RMS (theory)	RMS (avg)
0	4.773E-03	5.489E-03	4.851E-03	0.084	0.077	0.083
10	4.701E-03	5.405E-03	4.198E-03	0.013	0.012	0.014
20	4.486E-03	5.158E-03	4.553E-03	0.007	0.0064	0.0069
30	4.134E-03	4.753E-03	4.374E-03	0.0043	0.004	0.0042
40	3.657E-03	4.205E-03	3.766E-03	0.003	0.0028	0.003
50	3.068E-03	3.528E-03	3.421E-03	0.0022	0.0021	0.0021
60	2.387E-03	2.744E-03	2.690E-03	0.0016	0.0016	0.0015
70	1.633E-03	1.877E-03	2.230E-03	0.0011	0.0011	0.001
80	8.269E-04	9.530E-04	9.398E-04	0.00074	0.00072	0.00073
90	0.000E+00	0.000E+00	-3.240E-05	0.00027	0.00027	0.00028

Section	5		Wind Case	2		
U =	2.061	m/s	Lux	0.02	m	
			Iu	10	%	
Yaw	Aerod (cos)	Aerod (theory)	Aerod (avg)	RMS (cos)	RMS (theory)	RMS (avg)
0	7.830E-03	9.362E-03	7.028E-03	0.19	0.17	0.21
10	7.711E-03	9.220E-03	6.602E-03	0.029	0.025	0.032
20	7.358E-03	8.798E-03	7.131E-03	0.015	0.013	0.015
30	6.781E-03	8.108E-03	6.650E-03	0.0083	0.0072	0.0084
40	5.998E-03	7.172E-03	6.610E-03	0.0051	0.0045	0.0049
50	5.033E-03	6.018E-03	6.475E-03	0.0035	0.0031	0.003
60	3.915E-03	4.681E-03	5.076E-03	0.0027	0.0024	0.0023
70	2.678E-03	3.202E-03	3.675E-03	0.0022	0.002	0.0019
80	1.360E-03	1.626E-03	1.751E-03	0.0018	0.0017	0.0017
90	0.000E+00	0.000E+00	2.406E-04	0.0008	0.0008	0.00076

Section	5		Wind Case	2		
U =	2.999	m/s	Lux	0.02	m	
			Iu	10	%	
Yaw	Aerod (cos)	Aerod (theory)	Aerod (avg)	RMS (cos)	RMS (theory)	RMS (avg)
0	1.067E-02	1.349E-02	9.117E-03	0.35	0.29	0.4
10	1.050E-02	1.329E-02	9.434E-03	0.052	0.042	0.057
20	1.002E-02	1.268E-02	9.337E-03	0.026	0.021	0.027
30	9.238E-03	1.168E-02	9.511E-03	0.014	0.011	0.013
40	8.171E-03	1.034E-02	9.399E-03	0.0078	0.0064	0.007
50	6.856E-03	8.673E-03	9.234E-03	0.005	0.0042	0.004
60	5.333E-03	6.746E-03	7.986E-03	0.0038	0.0033	0.0029
70	3.648E-03	4.615E-03	5.707E-03	0.0034	0.003	0.0027
80	1.852E-03	2.343E-03	2.871E-03	0.0033	0.0031	0.0028
90	0.000E+00	0.000E+00	2.183E-04	0.0016	0.0016	0.0016

Section	5		Wind Case	2		
U =	4.074	m/s	Lux	0.02	m	
			Iu	10	%	
Yaw	Aerod (cos)	Aerod (theory)	Aerod (avg)	RMS (cos)	RMS (theory)	RMS (avg)
0	1.393E-02	1.833E-02	1.266E-02	0.58	0.44	0.63
10	1.372E-02	1.805E-02	1.199E-02	0.083	0.063	0.095
20	1.309E-02	1.722E-02	1.017E-02	0.041	0.031	0.051
30	1.206E-02	1.587E-02	9.716E-03	0.021	0.016	0.026
40	1.067E-02	1.404E-02	1.260E-02	0.011	0.0089	0.0097
50	8.953E-03	1.178E-02	1.290E-02	0.0073	0.0053	0.0049
60	6.964E-03	9.164E-03	1.413E-02	0.0051	0.0041	0.0028
70	4.764E-03	6.269E-03	8.184E-03	0.0049	0.0041	0.0034
80	2.419E-03	3.183E-03	4.651E-03	0.0053	0.0047	0.0039
90	0.000E+00	0.000E+00	3.379E-04	0.003	0.003	0.0028

Section	5		Wind Case	2		
U =	4.939	m/s	Lux	0.02	m	
			Iu	10	%	
Yaw	Aerod (cos)	Aerod (theory)	Aerod (avg)	RMS (cos)	RMS (theory)	RMS (avg)
0	1.544E-02	2.222E-02	1.321E-02	0.83	0.57	0.97
10	1.520E-02	2.188E-02	1.307E-02	0.12	0.082	0.14
20	1.451E-02	2.088E-02	9.623E-03	0.058	0.04	0.064
30	1.337E-02	1.924E-02	1.088E-02	0.03	0.021	0.036
40	1.183E-02	1.702E-02	1.421E-02	0.016	0.011	0.013
50	9.924E-03	1.428E-02	1.561E-02	0.0086	0.0062	0.0056
60	7.720E-03	1.111E-02	1.461E-02	0.0063	0.0047	0.0036
70	5.281E-03	7.600E-03	1.057E-02	0.0063	0.0049	0.0038
80	2.681E-03	3.858E-03	5.730E-03	0.0071	0.0061	0.0048
90	0.000E+00	0.000E+00	6.272E-04	0.0044	0.0044	0.0039

Section	1		Wind Case	3		
U =	1.23	m/s	Lux	0.03	m	
			Iu	10	%	
Yaw	Aerod (cos)	Aerod (theory)	Aerod (avg)	RMS (cos)	RMS (theory)	RMS (avg)
0	2.364E-03	4.651E-03	2.534E-03	0.061	0.046	0.06
10	2.329E-03	4.580E-03	2.394E-03	0.015	0.011	0.014
20	2.222E-03	4.370E-03	2.360E-03	0.0084	0.0063	0.0082
30	2.048E-03	4.028E-03	2.255E-03	0.0055	0.0042	0.0054
40	1.811E-03	3.563E-03	1.564E-03	0.0039	0.0031	0.0041
50	1.520E-03	2.989E-03	1.481E-03	0.0028	0.0023	0.0029
60	1.182E-03	2.325E-03	9.116E-04	0.002	0.0017	0.0021
70	8.067E-04	1.591E-03	6.126E-04	0.0012	0.001	0.0012
80	4.106E-04	8.080E-04	3.332E-04	0.00057	0.00054	0.00058
90	0.000E+00	0.000E+00	1.783E-04	0.00016	0.00016	0.00015

Section	1		Wind Case	3		
U =	2.074	m/s	Lux	0.03	m	
			Iu	10	%	
Yaw	Aerod (cos)	Aerod (theory)	Aerod (avg)	RMS (cos)	RMS (theory)	RMS (avg)
0	3.931E-03	7.842E-03	4.066E-03	0.16	0.1	0.16
10	3.871E-03	7.723E-03	3.779E-03	0.036	0.024	0.036
20	3.693E-03	7.369E-03	3.999E-03	0.019	0.013	0.019
30	3.404E-03	6.791E-03	3.196E-03	0.012	0.0079	0.012
40	3.011E-03	6.007E-03	3.003E-03	0.0074	0.0052	0.0074
50	2.526E-03	5.041E-03	2.731E-03	0.005	0.0037	0.0049
60	1.965E-03	3.921E-03	1.893E-03	0.0035	0.0024	0.0035
70	1.344E-03	2.682E-03	1.305E-03	0.0026	0.0019	0.0023
80	6.825E-04	1.362E-03	8.788E-04	0.0015	0.0013	0.0014
90	0.000E+00	0.000E+00	2.254E-04	0.0005	0.0005	0.00048

Section	1		Wind Case	3		
U =	3.227	m/s	Lux	0.03	m	
			Iu	10	%	
Yaw	Aerod (cos)	Aerod (theory)	Aerod (avg)	RMS (cos)	RMS (theory)	RMS (avg)
0	5.803E-03	1.220E-02	5.484E-03	0.35	0.2	0.36
10	5.714E-03	1.202E-02	6.619E-03	0.076	0.044	0.069
20	5.453E-03	1.147E-02	5.602E-03	0.04	0.023	0.039
30	5.025E-03	1.058E-02	5.097E-03	0.023	0.013	0.022
40	4.445E-03	9.347E-03	4.416E-03	0.013	0.0082	0.013
50	3.730E-03	7.843E-03	3.741E-03	0.0084	0.0054	0.0084
60	2.901E-03	6.101E-03	2.978E-03	0.0058	0.004	0.0057
70	1.985E-03	4.173E-03	2.091E-03	0.0042	0.0031	0.0041
80	1.008E-03	2.119E-03	9.032E-04	0.0033	0.0028	0.0033
90	0.000E+00	0.000E+00	2.026E-04	0.0013	0.0013	0.0012

Section	1		Wind Case	3		
U =	4.047	m/s	Lux	0.03	m	
			Iu	10	%	
Yaw	Aerod (cos)	Aerod (theory)	Aerod (avg)	RMS (cos)	RMS (theory)	RMS (avg)
0	7.553E-03	1.530E-02	6.904E-03	0.5	0.27	0.53
10	7.438E-03	1.507E-02	8.037E-03	0.11	0.059	0.1
20	7.098E-03	1.438E-02	7.231E-03	0.056	0.031	0.055
30	6.541E-03	1.325E-02	6.411E-03	0.031	0.017	0.031
40	5.786E-03	1.172E-02	6.458E-03	0.017	0.01	0.016
50	4.855E-03	9.836E-03	4.850E-03	0.011	0.0066	0.011
60	3.777E-03	7.651E-03	3.811E-03	0.0073	0.0048	0.0073
70	2.583E-03	5.234E-03	2.908E-03	0.0056	0.004	0.0054
80	1.312E-03	2.657E-03	1.152E-03	0.0048	0.0039	0.0049
90	0.000E+00	0.000E+00	1.371E-04	0.002	0.002	0.002

Section	1		Wind Case	3		
U =	4.947	m/s	Lux	0.03	m	
			Iu	10	%	
Yaw	Aerod (cos)	Aerod (theory)	Aerod (avg)	RMS (cos)	RMS (theory)	RMS (avg)
0	9.071E-03	1.870E-02	1.007E-02	0.7	0.36	0.64
10	8.933E-03	1.842E-02	8.776E-03	0.15	0.076	0.15
20	8.524E-03	1.758E-02	7.042E-03	0.076	0.04	0.088
30	7.856E-03	1.620E-02	7.550E-03	0.041	0.022	0.043
40	6.949E-03	1.433E-02	7.360E-03	0.023	0.013	0.022
50	5.831E-03	1.202E-02	5.519E-03	0.013	0.0077	0.014
60	4.535E-03	9.353E-03	5.136E-03	0.0091	0.0056	0.0085
70	3.102E-03	6.398E-03	4.194E-03	0.0073	0.005	0.0064
80	1.575E-03	3.248E-03	1.383E-03	0.0066	0.0052	0.0068
90	0.000E+00	0.000E+00	6.477E-04	0.0031	0.0031	0.0027

Section	2		Wind Case	3		
U =	1.212	m/s	Lux	0.03	m	
			Iu	10	%	
Yaw	Aerod (cos)	Aerod (theory)	Aerod (avg)	RMS (cos)	RMS (theory)	RMS (avg)
0	1.386E-03	2.426E-03	1.523E-03	0.051	0.044	0.05
10	1.364E-03	2.389E-03	1.409E-03	0.0082	0.007	0.0082
20	1.302E-03	2.280E-03	1.364E-03	0.0043	0.0037	0.0043
30	1.200E-03	2.101E-03	1.283E-03	0.0027	0.0023	0.0027
40	1.061E-03	1.858E-03	9.399E-04	0.0018	0.0016	0.0019
50	8.906E-04	1.560E-03	5.432E-04	0.0013	0.0012	0.0014
60	6.927E-04	1.213E-03	3.743E-04	0.0009	0.00083	0.00096
70	4.739E-04	8.300E-04	3.561E-04	0.00056	0.00052	0.00057
80	2.406E-04	4.210E-04	2.102E-04	0.00031	0.0003	0.00031
90	0.000E+00	0.000E+00	1.153E-04	0.000092	0.000092	0.00009

Section	2		Wind Case	3		
U =	1.987	m/s	Lux	0.03	m	
			Iu	10	%	
Yaw	Aerod (cos)	Aerod (theory)	Aerod (avg)	RMS (cos)	RMS (theory)	RMS (avg)
0	2.122E-03	3.978E-03	2.304E-03	0.14	0.1	0.13
10	2.090E-03	3.917E-03	1.885E-03	0.02	0.016	0.021
20	1.994E-03	3.738E-03	2.093E-03	0.01	0.008	0.01
30	1.838E-03	3.445E-03	1.850E-03	0.0057	0.0046	0.0057
40	1.626E-03	3.047E-03	1.770E-03	0.0035	0.0028	0.0034
50	1.364E-03	2.557E-03	1.238E-03	0.0023	0.0019	0.0024
60	1.061E-03	1.989E-03	7.955E-04	0.0016	0.0014	0.0017
70	7.258E-04	1.360E-03	6.829E-04	0.0011	0.001	0.0011
80	3.685E-04	6.910E-04	1.247E-04	0.00078	0.00073	0.00081
90	0.000E+00	0.000E+00	1.225E-04	0.000027	0.00027	0.00026

Section	2		Wind Case	3		
U =	2.95	m/s	Lux	0.03	m	
			Iu	10	%	
Yaw	Aerod (cos)	Aerod (theory)	Aerod (avg)	RMS (cos)	RMS (theory)	RMS (avg)
0	3.181E-03	5.908E-03	3.270E-03	0.29	0.21	0.29
10	3.133E-03	5.816E-03	3.043E-03	0.043	0.031	0.043
20	2.989E-03	5.549E-03	3.258E-03	0.021	0.015	0.02
30	2.755E-03	5.114E-03	2.808E-03	0.011	0.0081	0.011
40	2.437E-03	4.524E-03	2.358E-03	0.0061	0.0046	0.0062
50	2.045E-03	3.796E-03	1.798E-03	0.0037	0.0029	0.0039
60	1.591E-03	2.953E-03	1.316E-03	0.0026	0.0021	0.0027
70	1.088E-03	2.020E-03	1.132E-03	0.002	0.0017	0.002
80	5.524E-04	1.025E-03	7.608E-04	0.0016	0.0015	0.0015
90	0.000E+00	0.000E+00	-1.520E-05	0.0006	0.0006	0.0006

Section	2		Wind Case	3		
U =	3.951	m/s	Lux	0.03	m	
			Iu	10	%	
Yaw	Aerod (cos)	Aerod (theory)	Aerod (avg)	RMS (cos)	RMS (theory)	RMS (avg)
0	4.508E-03	7.909E-03	4.326E-03	0.49	0.34	0.5
10	4.439E-03	7.789E-03	4.465E-03	0.071	0.05	0.071
20	4.236E-03	7.432E-03	4.672E-03	0.034	0.024	0.031
30	3.904E-03	6.850E-03	4.129E-03	0.018	0.012	0.017
40	3.453E-03	6.059E-03	3.183E-03	0.0092	0.0068	0.0096
50	2.898E-03	5.084E-03	2.468E-03	0.0053	0.004	0.0056
60	2.254E-03	3.955E-03	1.936E-03	0.0037	0.0029	0.0038
70	1.542E-03	2.705E-03	1.599E-03	0.003	0.0025	0.003
80	7.828E-04	1.373E-03	7.920E-04	0.0026	0.0024	0.0026
90	0.000E+00	0.000E+00	-1.387E-04	0.0011	0.0011	0.0011

Section	2		Wind Case	3		
U =	4.942	m/s	Lux	0.03	m	
			Iu	10	%	
Yaw	Aerod (cos)	Aerod (theory)	Aerod (avg)	RMS (cos)	RMS (theory)	RMS (avg)
0	5.431E-03	9.893E-03	5.168E-03	0.76	0.46	0.78
10	5.349E-03	9.743E-03	5.439E-03	0.11	0.071	0.11
20	5.104E-03	9.297E-03	5.205E-03	0.052	0.034	0.051
30	4.704E-03	8.568E-03	4.525E-03	0.026	0.018	0.027
40	4.161E-03	7.579E-03	4.451E-03	0.013	0.0091	0.013
50	3.491E-03	6.359E-03	3.268E-03	0.0071	0.0051	0.0073
60	2.716E-03	4.947E-03	2.965E-03	0.0048	0.0036	0.0047
70	1.858E-03	3.384E-03	2.353E-03	0.0041	0.0033	0.0038
80	9.431E-04	1.718E-03	9.411E-04	0.0038	0.0033	0.0038
90	0.000E+00	0.000E+00	2.579E-04	0.0017	0.0017	0.0016

Section	3		Wind Case	3		
U =	1.195	m/s	Lux	0.03	m	
			lu	10	%	
Yaw	Aerod (cos)	Aerod (theory)	Aerod (avg)	RMS (cos)	RMS (theory)	RMS (avg)
0	7.716E-04	1.538E-03	8.079E-04	0.04	0.035	0.039
10	7.599E-04	1.515E-03	6.392E-04	0.0052	0.0045	0.053
20	7.250E-04	1.445E-03	7.149E-04	0.0026	0.0023	0.0026
30	6.682E-04	1.332E-03	7.903E-04	0.0016	0.0014	0.0016
40	5.911E-04	1.178E-03	4.292E-04	0.0011	0.00098	0.0011
50	4.960E-04	9.890E-04	5.649E-04	0.00076	0.0007	0.00075
60	3.858E-04	7.690E-04	3.843E-04	0.00053	0.00049	0.00053
70	2.639E-04	5.260E-04	4.365E-04	0.00034	0.00032	0.00032
80	1.340E-04	2.670E-04	1.186E-04	0.0002	0.00019	0.0002
90	0.000E+00	0.000E+00	5.396E-05	0.000059	0.000059	0.000059

Section	3		Wind Case	3		
U =	2.064	m/s	Lux	0.03	m	
			lu	10	%	
Yaw	Aerod (cos)	Aerod (theory)	Aerod (avg)	RMS (cos)	RMS (theory)	RMS (avg)
0	1.454E-03	2.656E-03	1.367E-03	0.12	0.097	0.12
10	1.432E-03	2.616E-03	1.158E-03	0.014	0.012	0.015
20	1.366E-03	2.496E-03	1.185E-03	0.0068	0.0057	0.007
30	1.259E-03	2.300E-03	1.282E-03	0.0037	0.0031	0.0037
40	1.114E-03	2.035E-03	1.196E-03	0.0022	0.0019	0.0022
50	9.344E-04	1.707E-03	9.562E-04	0.0014	0.0013	0.0014
60	7.268E-04	1.328E-03	8.698E-04	0.001	0.00092	0.001
70	4.972E-04	9.090E-04	5.901E-04	0.00075	0.0007	0.00074
80	2.524E-04	4.610E-04	4.839E-04	0.00054	0.00052	0.00052
90	0.000E+00	0.000E+00	2.150E-04	0.00019	0.00019	0.00018

Section	3		Wind Case	3		
U =	2.99	m/s	Lux	0.03	m	
			lu	10	%	
Yaw	Aerod (cos)	Aerod (theory)	Aerod (avg)	RMS (cos)	RMS (theory)	RMS (avg)
0	2.225E-03	3.848E-03	2.408E-03	0.25	0.2	0.24
10	2.191E-03	3.790E-03	1.894E-03	0.029	0.023	0.03
20	2.091E-03	3.616E-03	1.960E-03	0.014	0.011	0.014
30	1.927E-03	3.333E-03	1.842E-03	0.007	0.0057	0.0071
40	1.705E-03	2.948E-03	1.658E-03	0.0038	0.0032	0.0038
50	1.430E-03	2.474E-03	1.384E-03	0.0023	0.0019	0.0023
60	1.113E-03	1.924E-03	1.202E-03	0.0016	0.0014	0.0016
70	7.610E-04	1.316E-03	1.067E-03	0.0013	0.0012	0.0012
80	3.864E-04	6.680E-04	4.717E-04	0.0011	0.001	0.001
90	0.000E+00	0.000E+00	3.368E-04	0.00041	0.00041	0.00038

Section	3		Wind Case	3		
U =	4.009	m/s	Lux	0.03	m	
			lu	10	%	
Yaw	Aerod (cos)	Aerod (theory)	Aerod (avg)	RMS (cos)	RMS (theory)	RMS (avg)
0	2.847E-03	5.160E-03	3.068E-03	0.45	0.34	0.44
10	2.804E-03	5.081E-03	2.732E-03	0.053	0.04	0.054
20	2.675E-03	4.848E-03	2.406E-03	0.024	0.018	0.026
30	3.465E-03	4.468E-03	2.336E-03	0.011	0.0093	0.012
40	2.181E-03	3.952E-03	2.210E-03	0.0062	0.0048	0.0062
50	1.830E-03	3.316E-03	1.616E-03	0.0034	0.0028	0.0036
60	1.423E-03	2.580E-03	1.225E-03	0.0024	0.002	0.0025
70	9.736E-04	1.765E-03	1.587E-03	0.002	0.0018	0.0018
80	4.943E-04	8.960E-04	6.243E-04	0.0018	0.0016	0.0017
90	0.000E+00	0.000E+00	6.208E-05	0.00073	0.00073	0.00072

Section	3		Wind Case	3		
U =	4.899	m/s	Lux	0.03	m	
			lu	10	%	
Yaw	Aerod (cos)	Aerod (theory)	Aerod (avg)	RMS (cos)	RMS (theory)	RMS (avg)
0	3.503E-03	6.305E-03	3.202E-03	0.67	0.48	0.7
10	3.450E-03	6.209E-03	3.626E-03	0.079	0.056	0.078
20	3.292E-03	5.925E-03	3.313E-03	0.036	0.026	0.036
30	3.034E-03	5.460E-03	2.821E-03	0.018	0.013	0.018
40	2.683E-03	4.830E-03	2.276E-03	0.0087	0.0066	0.0093
50	2.252E-03	4.053E-03	2.197E-03	0.0045	0.0035	0.0046
60	1.751E-03	3.152E-03	1.700E-03	0.0031	0.0025	0.0032
70	1.198E-03	2.156E-03	2.149E-03	0.0027	0.0023	0.0023
80	6.083E-04	1.095E-03	9.717E-04	0.0025	0.0023	0.0023
90	0.000E+00	0.000E+00	6.618E-05	0.0011	0.0011	0.0011

Section	4		Wind Case	3		
U =	1.19	m/s	Lux	0.03	m	
			Iu	10	%	
Yaw	Aerod (cos)	Aerod (theory)	Aerod (avg)	RMS (cos)	RMS (theory)	RMS (avg)
0	3.653E-03	5.328E-03	3.592E-03	0.092	0.075	0.093
10	3.597E-03	5.247E-03	3.429E-03	0.022	0.018	0.022
20	3.433E-03	5.006E-03	3.421E-03	0.012	0.01	0.012
30	3.163E-03	4.614E-03	3.155E-03	0.008	0.0067	0.008
40	2.798E-03	4.081E-03	3.025E-03	0.0057	0.0048	0.0056
50	2.348E-03	3.424E-03	2.355E-03	0.0042	0.0036	0.0042
60	1.826E-03	2.664E-03	2.012E-03	0.003	0.0027	0.003
70	1.249E-03	1.822E-03	1.098E-03	0.0019	0.0018	0.002
80	6.343E-04	9.250E-04	2.693E-04	0.0011	0.001	0.0012
90	0.000E+00	0.000E+00	2.185E-04	0.00034	0.00034	0.00038

Section	4		Wind Case	3		
U =	2.068	m/s	Lux	0.03	m	
			Iu	10	%	
Yaw	Aerod (cos)	Aerod (theory)	Aerod (avg)	RMS (cos)	RMS (theory)	RMS (avg)
0	5.850E-03	9.258E-03	5.083E-03	0.24	0.17	0.26
10	5.762E-03	9.118E-03	5.618E-03	0.053	0.038	0.054
20	5.498E-03	8.700E-03	5.366E-03	0.028	0.021	0.029
30	5.067E-03	8.018E-03	5.381E-03	0.017	0.012	0.016
40	4.482E-03	7.092E-03	5.011E-03	0.01	0.0079	0.0099
50	3.761E-03	5.951E-03	4.203E-03	0.0072	0.0056	0.0068
60	2.925E-03	4.629E-03	3.455E-03	0.0053	0.0042	0.0049
70	2.001E-03	3.166E-03	2.473E-03	0.0038	0.0032	0.0036
80	1.016E-03	1.608E-03	9.058E-04	0.0026	0.0026	0.0029
90	0.000E+00	0.000E+00	1.349E-04	0.0011	0.0011	0.0011

Section	4		Wind Case	3		
U =	2.986	m/s	Lux	0.03	m	
			Iu	10	%	
Yaw	Aerod (cos)	Aerod (theory)	Aerod (avg)	RMS (cos)	RMS (theory)	RMS (avg)
0	8.346E-03	3.368E-02	7.546E-03	0.44	0.11	0.47
10	8.219E-03	1.317E-02	7.214E-03	0.094	0.063	0.1
20	7.842E-03	1.256E-02	7.604E-03	0.049	0.033	0.05
30	7.228E-03	1.158E-02	7.559E-03	0.027	0.019	0.027
40	6.393E-03	1.024E-02	7.489E-03	0.016	0.011	0.014
50	5.365E-03	8.593E-03	6.167E-03	0.01	0.0074	0.0094
60	4.173E-03	6.684E-03	5.246E-03	0.0075	0.0057	0.0066
70	2.854E-03	4.572E-03	3.599E-03	0.0061	0.0049	0.0055
80	1.449E-03	2.321E-03	1.485E-03	0.0053	0.0046	0.0052
90	0.000E+00	0.000E+00	1.410E-04	0.0023	0.0023	0.0023

Section	4		Wind Case	3		
U =	3.939	m/s	Lux	0.03	m	
			Iu	10	%	
Yaw	Aerod (cos)	Aerod (theory)	Aerod (avg)	RMS (cos)	RMS (theory)	RMS (avg)
0	1.109E-02	1.763E-02	9.430E-03	0.67	0.43	0.77
10	1.092E-02	1.737E-02	9.086E-03	0.14	0.091	0.16
20	1.042E-02	1.657E-02	9.749E-03	0.073	0.048	0.078
30	9.604E-03	1.527E-02	1.019E-02	0.04	0.026	0.038
40	8.498E-03	1.351E-02	9.479E-03	0.022	0.015	0.02
50	7.129E-03	1.134E-02	8.394E-03	0.013	0.0092	0.012
60	5.545E-03	8.817E-03	7.049E-03	0.0096	0.007	0.0082
70	3.793E-03	6.031E-03	5.429E-03	0.0084	0.0064	0.0069
80	1.926E-03	3.062E-03	2.274E-03	0.0081	0.0069	0.0077
90	0.000E+00	0.000E+00	4.245E-04	0.0041	0.0041	0.0038

Section	4		Wind Case	3		
U =	4.943	m/s	Lux	0.03	m	
			Iu	10	%	
Yaw	Aerod (cos)	Aerod (theory)	Aerod (avg)	RMS (cos)	RMS (theory)	RMS (avg)
0	1.335E-02	2.213E-02	1.327E-02	0.98	0.58	0.99
10	1.315E-02	2.197E-02	1.111E-02	0.2	0.12	0.24
20	1.254E-02	2.080E-02	1.228E-02	0.11	0.064	0.11
30	1.156E-02	1.917E-02	1.241E-02	0.056	0.034	0.053
40	1.028E-02	1.695E-02	1.160E-02	0.03	0.019	0.027
50	8.581E-03	1.422E-02	1.099E-02	0.017	0.011	0.014
60	6.675E-03	1.107E-02	1.000E-02	0.012	0.0081	0.0089
70	4.566E-03	7.569E-03	6.749E-03	0.011	0.008	0.0086
80	2.318E-03	3.843E-03	3.121E-03	0.012	0.0094	0.01
90	0.000E+00	0.000E+00	6.279E-04	0.0065	0.0065	0.0058

Section	5		Wind Case	3		
U =	1.22	m/s	Lux	0.03	m	
			Iu	10	%	
Yaw	Aerod (cos)	Aerod (theory)	Aerod (avg)	RMS (cos)	RMS (theory)	RMS (avg)
0	4.773E-03	5.489E-03	4.851E-03	0.11	0.1	0.11
10	4.701E-03	5.405E-03	4.198E-03	0.025	0.023	0.027
20	4.486E-03	5.158E-03	4.553E-03	0.014	0.013	0.014
30	4.134E-03	4.753E-03	4.374E-03	0.0093	0.0086	0.009
40	3.657E-03	4.205E-03	3.766E-03	0.0066	0.0061	0.0065
50	3.068E-03	3.528E-03	3.421E-03	0.0049	0.0046	0.0047
60	2.387E-03	2.744E-03	2.690E-03	0.0037	0.0035	0.0034
70	1.633E-03	1.877E-03	2.230E-03	0.0025	0.0024	0.0023
80	8.269E-04	9.530E-04	9.396E-04	0.0016	0.0016	0.0016
90	0.000E+00	0.000E+00	-3.240E-05	0.00055	0.00055	0.00055

Section	5		Wind Case	3		
U =	2.061	m/s	Lux	0.03	m	
			Iu	10	%	
Yaw	Aerod (cos)	Aerod (theory)	Aerod (avg)	RMS (cos)	RMS (theory)	RMS (avg)
0	7.830E-03	9.362E-03	7.026E-03	0.36	0.22	0.28
10	7.711E-03	9.220E-03	6.602E-03	0.056	0.049	0.063
20	7.358E-03	8.798E-03	7.131E-03	0.03	0.026	0.031
30	6.781E-03	8.106E-03	6.650E-03	0.018	0.015	0.018
40	5.998E-03	7.172E-03	6.610E-03	0.011	0.0098	0.01
50	5.033E-03	6.018E-03	6.475E-03	0.0077	0.0069	0.0066
60	3.915E-03	4.681E-03	5.076E-03	0.0059	0.0054	0.0052
70	2.678E-03	3.202E-03	3.675E-03	0.0048	0.0044	0.0042
80	1.360E-03	1.626E-03	1.751E-03	0.0039	0.0038	0.0037
90	0.000E+00	0.000E+00	2.406E-04	0.0017	0.0017	0.0016

Section	5		Wind Case	3		
U =	2.999	m/s	Lux	0.03	m	
			Iu	10	%	
Yaw	Aerod (cos)	Aerod (theory)	Aerod (avg)	RMS (cos)	RMS (theory)	RMS (avg)
0	1.067E-02	1.349E-02	9.117E-03	0.48	0.38	0.54
10	1.050E-02	1.329E-02	9.434E-03	0.1	0.081	0.11
20	1.002E-02	1.268E-02	9.337E-03	0.053	0.043	0.056
30	9.238E-03	1.168E-02	9.511E-03	0.029	0.024	0.028
40	8.171E-03	1.034E-02	9.399E-03	0.017	0.014	0.015
50	6.856E-03	8.673E-03	9.234E-03	0.011	0.0091	0.0086
60	5.333E-03	6.746E-03	7.986E-03	0.0084	0.0072	0.0064
70	3.648E-03	4.615E-03	5.707E-03	0.0074	0.0066	0.0058
80	1.852E-03	2.343E-03	2.871E-03	0.0071	0.0066	0.0061
90	0.000E+00	0.000E+00	2.183E-04	0.0035	0.0035	0.0034

Section	5		Wind Case	3		
U =	4.074	m/s	Lux	0.03	m	
			Iu	10	%	
Yaw	Aerod (cos)	Aerod (theory)	Aerod (avg)	RMS (cos)	RMS (theory)	RMS (avg)
0	1.393E-02	1.933E-02	1.266E-02	0.78	0.59	0.85
10	1.372E-02	1.805E-02	1.199E-02	0.16	0.12	0.18
20	1.309E-02	1.722E-02	1.017E-02	0.084	0.064	0.1
30	1.206E-02	1.587E-02	9.716E-03	0.045	0.035	0.055
40	1.067E-02	1.404E-02	1.280E-02	0.025	0.019	0.021
50	8.953E-03	1.178E-02	1.290E-02	0.016	0.012	0.011
60	6.964E-03	9.164E-03	1.413E-02	0.011	0.009	0.0061
70	4.764E-03	6.269E-03	8.184E-03	0.011	0.009	0.0074
80	2.419E-03	3.183E-03	4.651E-03	0.011	0.01	0.0084
90	0.000E+00	0.000E+00	3.379E-04	0.0065	0.0065	0.0061

Section	5		Wind Case	3		
U =	4.939	m/s	Lux	0.03	m	
			Iu	10	%	
Yaw	Aerod (cos)	Aerod (theory)	Aerod (avg)	RMS (cos)	RMS (theory)	RMS (avg)
0	1.544E-02	2.222E-02	1.321E-02	1.12	0.76	1.3
10	1.520E-02	2.188E-02	1.307E-02	0.23	0.16	0.27
20	1.451E-02	2.088E-02	9.623E-03	0.12	0.082	0.17
30	1.337E-02	1.924E-02	1.088E-02	0.064	0.044	0.077
40	1.183E-02	1.702E-02	1.421E-02	0.034	0.024	0.028
50	9.924E-03	1.428E-02	1.561E-02	0.019	0.013	0.012
60	7.720E-03	1.111E-02	1.461E-02	0.014	0.01	0.0079
70	5.281E-03	7.600E-03	1.057E-02	0.014	0.011	0.0082
80	2.681E-03	3.858E-03	5.730E-03	0.015	0.013	0.01
90	0.000E+00	0.000E+00	6.272E-04	0.0096	0.0096	0.0065